論文 / 著書情報
Article / Book Information

題目(和文)	高難度選択酸化反応用Fe含有ゼオライト触媒に関する研究
Title(English)	Study on Fe-containing zeolite catalysts for extremely difficult selective oxidation reactions
著者(和文)	XiaoPeipei
Author(English)	PEIPEI XIAO
出典(和文)	学位:博士(工学), 学位授与機関:東京工業大学, 報告番号:甲第10979号, 授与年月日:2018年9月20日, 学位の種別:課程博士, 審査員:野村 淳子,鎌田 慶吾,本倉 健,庄子 良晃,横井 俊之
Citation(English)	Degree:Doctor (Engineering), Conferring organization: Tokyo Institute of Technology, Report number:甲第10979号, Conferred date:2018/9/20, Degree Type:Course doctor, Examiner:,,,,
学位種別(和文)	博士論文
Type(English)	Doctoral Thesis

Doctor thesis 2018

Study on Fe-containing zeolite catalysts for extremely difficult selective oxidation reactions

（高難度選択酸化反応用 Fe 含有ゼオライト触媒に関する研究）

This thesis was submitted to Tokyo Institute of Technology for the degree of Doctor of Engineering.

Xiao Peipei

Department of Electronic Chemistry

Interdisciplinary Graduate School of Science and Engineering

Tokyo Institute of Technology

Contents

Chapter 1

Introduction

1.1. Zeolites

1.1.1 Structure and composition

The term zeolite was originally created in 1756 by Swedish mineralogist Axel Fredrik Cronstedt. They are also called molecular sieves, regarding to the ability to discriminate molecules on the basis of their micropore size (< 2 nm). Zeolites occur naturally but are also produced industrially on a large scale. The first synthesis of zeolite in laboratory was performed by Saint Clair Deville in the middle of 18th century.

Zeolites consist of the primary building unit tetrahedral [TO_4], typically [SiO_4] and [AlO_4], which are linked to each other by corner-sharing oxygen bridges to form the secondary building units (SBUs) (**Figure 1.1(a)**). More complex composite building units (CBUs) can be formed by linking the groups of SBUs (**Figure 1.1(b)**). These CBUs units are further combined to form a specific structure in the presence of channels and cavities of different shapes, which finally determine the framework types of the zeolite.

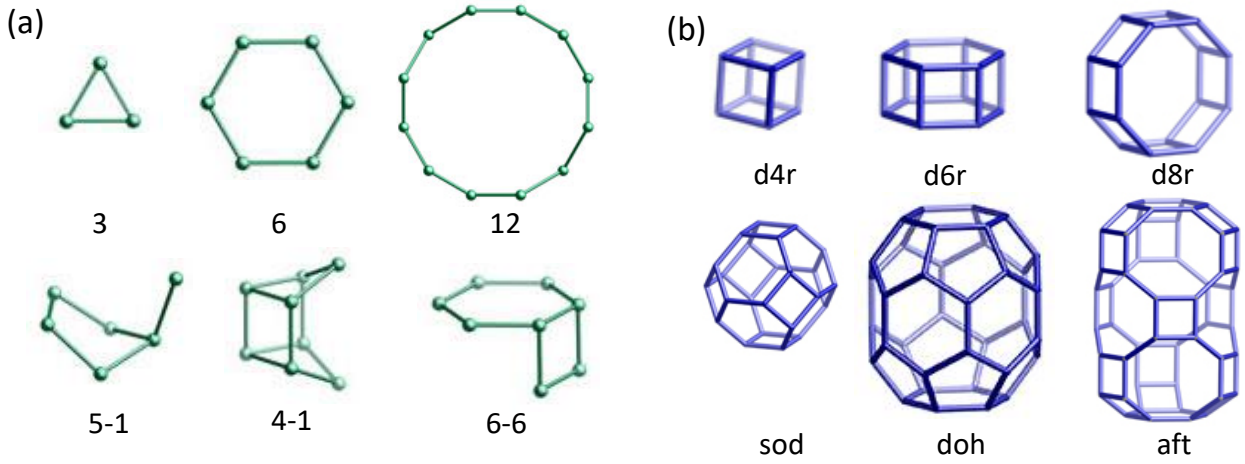

Figure 1.1 (a) example of SBUs and (b) CBUs [1].

The introduction of aluminum atom in the silica lattice results in the formation of negative charges on the framework, i.e. AlO_4^-, which is compensated by the extra framework cations, such as $Na^+$and K^+, located in the channels [2]. When proton is the compensating cation, zeolites possess strong Brønsted acid sites **(Figure 1.2**). The strength of the Brønsted acid site depends significantly on the type of next nearest neighbor substitutions. The metallosilicates containing trivalent elements in the

framework other than Al (B, Ga, Fe, In) are of interest in designing the acid strength and active. The heteroatoms reach weaker acid sites upon framework substitution than Al. The ranking in the acid strength displays as the following order: B(OH)Si < In(OH)Si < Fe(OH)Si < Ga(OH)Si< Al(OH)Si [3-5].

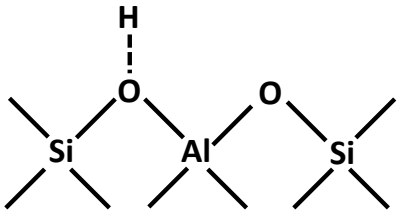

Figure 1.2 Schematic representation of the Brønsted acid site associated with the presence of framework Al substitution.

Normally, zeolites possess the advantages of favorable textural properties, high surface area, high connectivity of uniformly-sized micropores, high thermal stability and tunable surface acidity [6-8]. Thus they are commonly used as commercial adsorbents and catalysts in industry such as arsenic control, water purification, construction, detergents, and conversion of crude oil into gasoline and other fuels and so on [9-14].

232 unique zeolite frameworks have been identified and over 40 naturally occurring zeolite frameworks have been known until September 2016. Among them, the most popular ones in industrial applications are **MFI**, **FAU**, **MWW**, **MOR**, **BEA** and **CHA-type** zeolites.

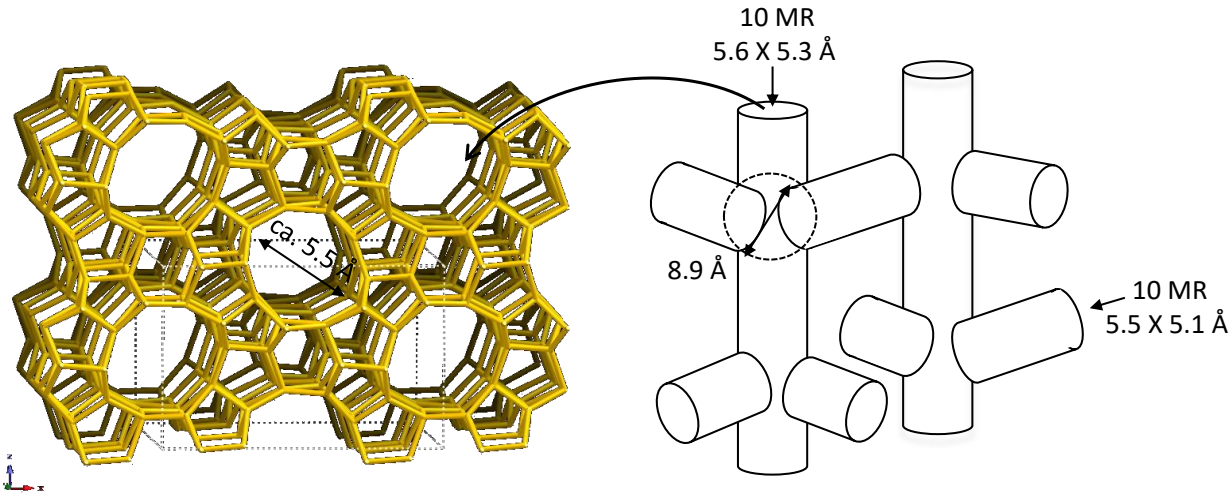

Figure 1.3 (Left) Skeletal diagram of the [010] face of MFI zeolite. (Right) Channel structure of MFI.

The structure of MFI zeolite has 10-membered-ring and two types of channel systems with

straight channels about 5.3 × 5.6 Å and sinusoidal channels about 5.1 × 5.5 Å (**Figure 1.3**) [15]. The two different channels are perpendicular to each other, generating intersections with diameters of 8.9 Å. ZSM-5, Zeolite Socony Mobil-5, is one of the most typical aluminosilicate MFI structure zeolite, belonging to the pentasil family of zeolites [16]. The crystallographic unit cell of ZSM-5 has 96 T sites (Si or Al), 192 O sites, and a number of compensating cations depending on the Si/Al ratio, which ranges from 12 to infinity [17, 18]. Patented by Mobil Oil Company in 1975, it is widely applied in petrochemical chemistry [19, 20], environmental protection [21, 22] and adsorption [23] because of the high surface area, special channel structure, abundant acid sites, and thermal and hydrothermal stability [24]. Catalytic cracking of hydrocarbon is significant for industrial manufacture, due to the advantages of high cracking conversion efficiency, high light alkene selectivity and less carbon deposition compared with thermal cracking [25]. When it was applied in n-hexane cracking under high pressure, good catalytic activity and stability are achieved [26].

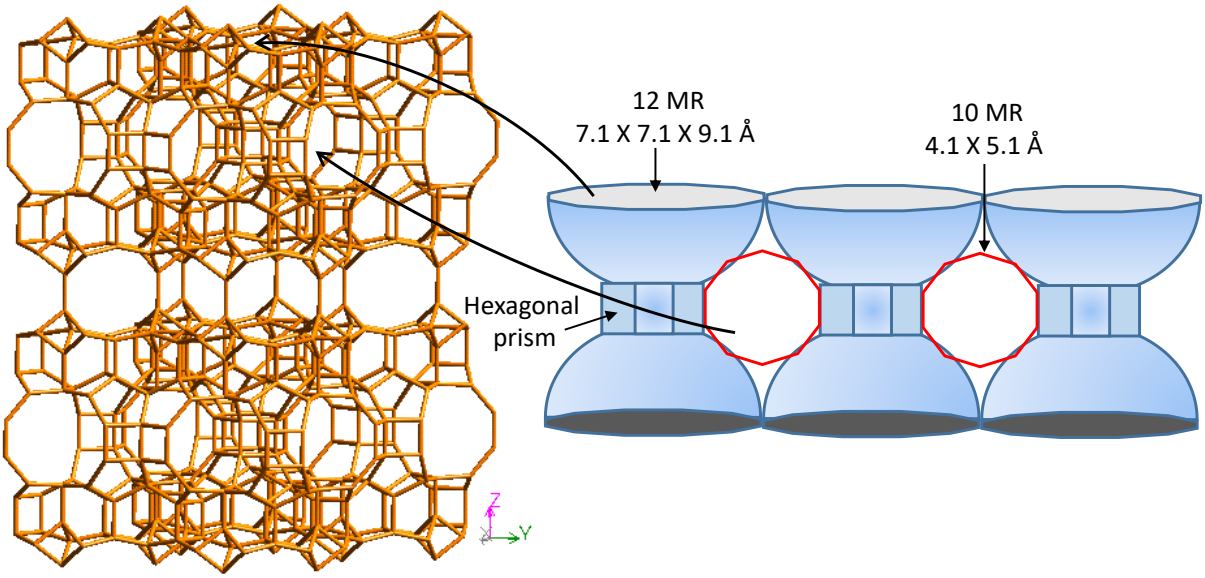

Figure 1.4 (Left) Skeletal diagram of the [001] face of MWW zeolite. (Right) Channel structure of MWW.

MWW structure zeolite is a kind of layered zeolite with high surface area, complex porosity and containing both medium and large pores [27, 28]. The structural complexity derives from the presence of two independent pore systems accessible through 10-ring openings. One of these systems is defined by two-dimensional sinusoidal channels, maintaining an effective 10-ring diameter throughout the structure [15]. The second one includes large supercages with 12-ring openings defined by inner diameter of 7.1 Å and inner length of 18.2 Å (**Figure 1.4**) [27, 29]. MWW such as MCM-22 zeolite has been studied extensively as shape selective catalyst for many hydrocarbon conversions such as

isomerization [30, 31], etherification [32], disproportionation [33], and alkylation [34]. Good catalytic performance for fluid catalytic cracking (FCC) process in petro-chemistry industry using MCM-22 has been achieved [35].

BEA zeolite adopts large 12-membered-ring with three-dimensional interconnection with 6.6 × 6.7 Å channels running straight along the a (or b) axis and 5.6 × 5.6 Å channels running tortuously along the c axis (**Figure 1.5**) [36]. Among several types of natural and artificial synthetic zeolites, BEA has received special attention from the scientific community regarding its high Si/Al ratio, high surface area, strong acidity and hydrothermal stability [15]. Thus, BEA, normally Beta zeolite catalysts are widely applied in catalytic cracking reactions, alkane hydroisomerization, and alkylation and acylation of aromatic hydrocarbons [37].

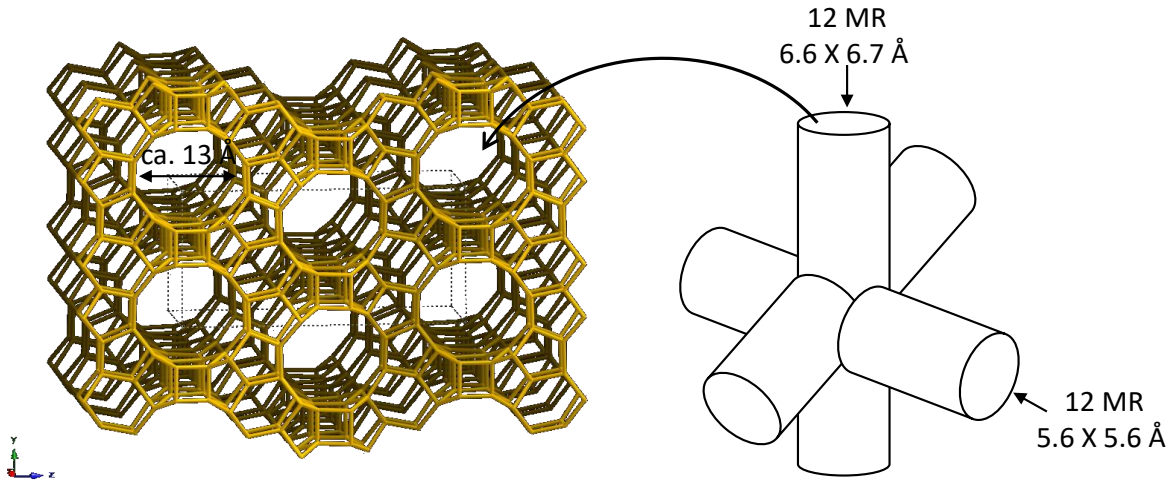

Figure 1.5 (Left) Skeletal diagram of the [100] face of BEA zeolite. (Right) Channel structure of BEA.

1.1.2 Fe-containing zeolites

Al-containing zeolite catalysts, such as ZSM-5, Beta, MCM-22, SSZ-13, are widely applied in catalytic cracking reaction. While zeolites containing other heteroatoms, such as Fe, Cu, Ti and Sn, present excellent performance in oxidation reactions [5]. Fe-containing zeolites have been widely used and revealed outstanding performance in various catalytic conversions related to environmental applications, such as direct N_2O decomposition [38-40], selective catalytic reduction of N_2O and NO_x [41, 42], selective oxidation of NH_3 to N_2 [43] and so on; and in extremely difficult selective oxidation reactions, for instance hydroxylation of benzene and phenol [44-46], propane oxidative dehydrogenation [39, 47-49], and hydroxylation of methane to methanol [50-52].

The preparation method of Fe-containing zeolites strongly influences the nature and distribution

of the resulting Fe species, which basically determines the catalytic performance. Extensive efforts have been dedicated to establishing reliable procedures for iron incorporation, including direct synthesis [41, 53, 54], ion exchange [55], impregnation [56, 57], chemical vapor deposition (CVD) [58, 59] and so on. Incorporation of heteroatoms into zeolites can adjust the surface properties to obtain highly dispersed active sites and to improve the catalytic activity. Compared to the post-synthesis approaches, the direct synthetic method is more feasible and has industrial potential [60].

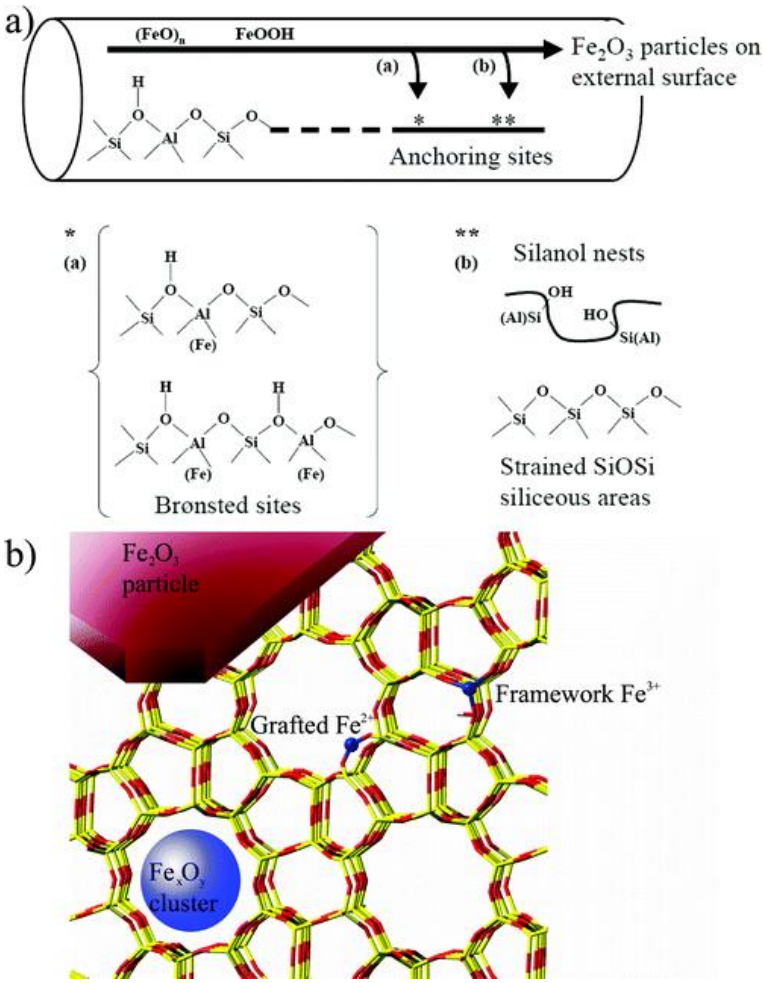

Figure 1.6 Schematic representation of (a) possible mechanisms leading to the Fe migration from framework to extra framework positions ([61]) and (b) diagrammatic sketch of the Fe species: Fe_2O_3 particles, Fe_xO_y clusters, grafted Fe^{2+} ions and Fe^{3+} in framework position [62].

Figure 1.6 displays a general scheme involving migration, grafting and clustering, and gives a pictorial representation of the structure of the Fe species formed by migration from the framework to the extra framework positions and successive grafting on the walls of the zeolite channels. As for the anchoring sites, two different structures have been considered: Brønsted sites (structure a) associated with residual M^{3+} in the lattice (M stands for Al or Fe in Fe-ZSM-5, M stands for Fe in Fe-silicalite-1)

and silanol nests (structure b) [61, 62]. Generally, the Fe species on the zeolite can be divided into several categories: framework Fe, isolated Fe cations, oligomeric cationic Fe complexes, and neutral iron oxide clusters (Fe_xO_y) as well as larger Fe-oxide aggregates [44], which play different activity.

1.2. Conversion of methane to methanol (MTM)

Methane is the main component of natural gas, including unconventional sources like coalbed methane and shale gas, landfill gas, and a by-product of oil refining and chemical processing [63, 64]. It has been suggested that natural gas can be a potential energy source to replace the more polluting coal and oil until carbon-free energy sources become mature and deployed. However, to store and transport natural gas from the remote sites undertake great challenge, making it difficult to competitive with the fossil oil [65]. Therefore methane is often required to convert to other transportable products with high-density energy and high value-added [66]. Based on that, the conversion of methane into liquid methanol is much more economical and energy-efficiency [63]. In addition, methanol is a major carbon chemical feedstock and important building blocks for a wide range of commodities such as cosmetics, lubricants, detergents, and polymers [66]. A methanol economy is generally regarded as one of the most promising alternative energy platforms that can be employed to replace fossil fuels in the near future [67, 68]. Methane is recognized as one of the most stable hydrocarbon due to its perfectly symmetrical tetrahedron structure [69]. The dissociation energy of the methane C-H bond is 440 $kJ \cdot mol^{-1}$, hence its activation requires harsh conditions [69].

1.2.1 Two-step method (industrial route)

So far, the industrial route to conversion of methane to methanol is indirect. Firstly, methane reacts with steam to convert to CO and H_2 (synthesis gas) under high temperature using Ni-containing catalysts (Reaction 1) [70]. The catalysts are usually prepared by impregnation Ni salt solution on MgO, α-Al_2O_3 or the mixture of these supports. Typical operating conditions are 1073 K and 15-20 bar with a H_2O/CH_4 stoichiometric ratio of 3.0-3.5. Usually the excess steam is added to suppress the carbon formation on the catalyst, and promote the reforming reaction [64, 71]. The second stage for methanol production is carried out by passing synthesis gas on the $Cu/ZnO/Al_2O_3$ catalyst at around 523 K and high pressure in the range of 50-100 bar (Reaction 2) [52, 72]. In practice CO_2 is added to the feed, which produces advantageous effects, $H_2/CO/CO_2$ reaction ratios are usually 80-86/8-10/6-10. The $Cu/ZnO/Al_2O_3$ catalyst produces highly methanol selectively, generally greater than 99% [73]. The stream in the exit of the reactor usually contains methanol with the content of 4-7 vol. %, which can be removed and recycled the gas stream. The two separate steps method has been applied to

produce nearly 100% of methanol worldwide [73].

$$CH_4\,(g) + H_2O\,(g) \xrightarrow[\text{Heat}]{\text{Ni}} CO\,(g) + H_2\,(g) \qquad (1)$$

$$\triangle H = 49.3 \text{ kcal}$$

$$CO\,(g) + H_2\,(g) \xrightarrow[\text{Pressure + Heat}]{\text{Cat.}} CH_3OH\,(g) \qquad (2)$$

$$\triangle H = -30.7 \text{ kcal}$$

1.2.2 Enzymatic activation of methane

Even so, the highly selective method to oxidize methane to methanol at low temperature in aqueous phase has already existed in nature. Methanotrophic bacteria can transfer methane to methanol under aerobic conditions due to the methane monooxygenase (MMO) enzymes contained. There are two types of MMOs: soluble MMO (sMMO) and particulate MMO (pMMO). sMMO has been found to be a multi-enzyme complex composed of hydroxylase unit, reductase unit, and regulatory protein. The oxidation of methane by molecular oxygen occurs at the active site, diiron μ-oxo species in sMMO (**Figure 1.7(a)**) and dicopper center in pMMO (**Figure 1.7(b)**) are found to be the active sites [74].

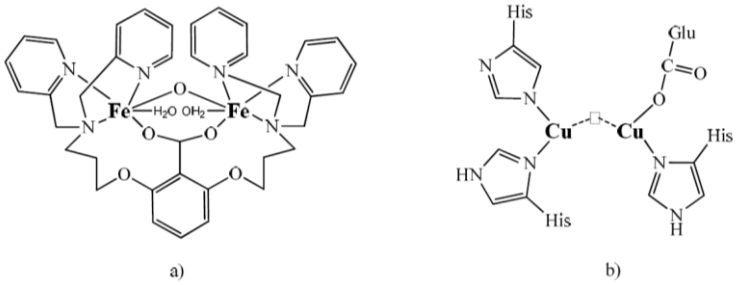

Figure 1.7 Structure of the active centers in the methane monooxygenase enzymes: (a) the diiron center in soluble MMO and (b) the dicopper center in particulate MMO [74].

1.2.3 Homogeneous catalytic system in liquid phase

The enzymatic systems inspired researchers to develop homogeneous catalysts for low temperature partial oxidation of methane. The organometallic approach to methane conversion became an intense research area [74]. Periana *et al.* described the oxidation of methane to methanol through methyl bisulfate catalyzed by mercuric bisulfate. Methanol was recovered by hydrolysis of methyl bisulfate. An unprecedented 85% selectivity of methyl bisulfate at 50% methane conversion was reported [75]. Besides, a subsequent publication showed platinum bipyrimidine complexes to be more efficient in oleum, resulting in 90% methane conversion and methyl bisulfate at 81% selectivity [76].

Note that, the homogeneous liquid phase system usually accompanies by high acid and high pollution, and that methanol is not the direct product. Thus relative research and application are limited.

1.2.4 Direct gas phase system

In the gas phase, generally transition metals (Fe [77, 78], Co [79] and Cu [80-85]) exchanged zeolites are used as catalysts to form highly active metal-oxygen species with O_2 [83, 86-90] or N_2O [91-93] (in the case of Fe-containing zeolites). Until now, there are two means for partial oxidation of methane: high temperature route based on radical gas phase reaction and low temperature route involving heterogeneous catalysis [94]. High temperature partial oxidation reaction works under temperature higher than 773K, involving fuel-rich feed to minimize combustion, and inert reactor walls for high selectivity to methanol. Under these conditions the desired oxygenated products are more active than methane. A few report addressed outstanding yields to methanol and formaldehyde (7-10%), a large number of studies agreed on the level of CH_3OH selectivity of 30-40% with methane conversion of 5-10% [95]. Nevertheless, the over oxidation still exists and limits the selectivity of the system to partial oxygenates. Decreasing the methane partial pressure reduced the concentration of methyl radicals thus diminished competition with coupling reactions. A number of studies have adopted this high temperature and low pressure approach, however it was found that methanol was only selectively produced when methane conversion was <1% [96]. In order to overcome these disadvantages, more recent works have focused on low temperature system. The low temperature approach (< 523K) requires the high active catalytic system. Isothermal step-wise CH_3OH formation has been reported at 423K and 473K using NO [84] or O_2 [97] as the oxidant, but the CH_3OH produced amount of 0.6 mmol $CH_3OH\ g_{zeolite}^{-1}$ on Cu-ZSM-5 [80] and 5.4 mmol $CH_3OH\ g_{zeolite}^{-1}$ on Cu-MOR [97] were much lower than those obtained by O_2 activation at 723K, 8.1 mmol $CH_3OH\ g_{zeolite}^{-1}$ on Cu-ZSM-5 [84] and 45.3 mmol CH_3OH on Cu-MOR [97].

1.2.5 Heterogeneous approaches in the liquid phase

It is preferable that the direct conversion of methane to methanol takes place on the heterogeneous catalysts owing to the advantages of separation and reusability when compared with the homogenous system. With this in mind heterogeneous analogues of the Periana catalyst (Pt-bipyrimidine complex) were produced by Palkovits *et al*.[98, 99]. This kinds of catalyst consisted of polymer frameworks

coordinated to a Pt centre, where the Pt was coordinated to a covalent triazine-based framework. These catalysts were reusable and more active than the homogeneous system. However they still required a highly acidic solvent. Cationic gold was used as the heterogeneous catalyst to selective methane to methanol in strong acid solvents such as sulfuric acid by Periana and co-workers [100]. In their research gold cations was consider as the uniquely efficient electrophilic catalyst for methane conversion. The highest methanol yield of 94% and methane conversion of 28% were achieved under 453K.

In addition, transition metal exchanged zeolites are widely used as heterogeneous catalysts in liquid phase. Hammond *et al*. used iron- and/or copper-containing zeolites for oxidation of methane selectively to methanol in an aqueous medium with hydrogen peroxide [50-52, 101, 102]. The active iron site is identified as the extra framework binuclear core, which forms a Fe-OOH intermediate upon activation with H_2O_2 while copper acts as a modulator to ensure high methanol selectivity [103]. Besides, supported gold-palladium alloy nanoparticles [104] and titania supported gold palladium copper catalysts [105] were both applied in direct conversion of methane to methanol with H_2O_2, achieving selectivity of 90.3% and 82.7% to methanol, respectively. In the above mention conditions, normally water is used as the solvent, thus the conversion of methane is not satisfactory.

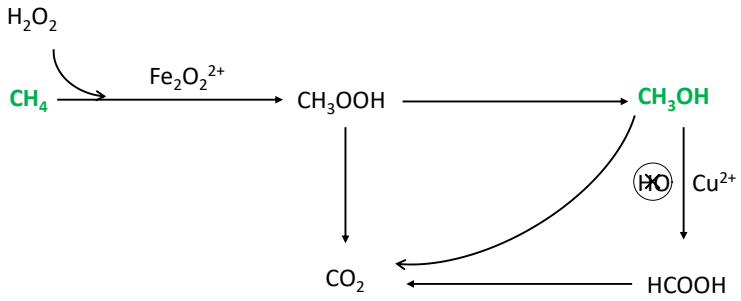

Figure 1.8 A potential reaction scheme for the oxidation of methane based on the time-on-line profile. Methanol is formed through the conversion of the methyl hydrogen peroxide intermediate over the Fe sites present in the catalyst. HO· radicals produced during the reaction are later responsible for the over-oxidation of methanol [52].

The reaction pathway that is determined for the oxidation of methane with H_2O_2 on copper-promoted Fe-ZSM-5 is shown in **Figure 1.8** [52]. Methyl hydroperoxide (CH_3OOH) was found to be the primary product of the reaction which underwent subsequent reactions to consecutively form methanol, formic acid and carbon dioxide. CH_3OOH was found to decompose to methanol without the presence of catalyst. It seems that control of the product distribution could be achieved by the addition

of extra framework copper to the zeolite [52, 102]. The Fe-ZSM-5 catalyst achieved a selectivity of 12% to methanol without affecting the overall conversion of the reaction (0.7%). EPR spectroscopy studies found that Cu^{2+} did not play a direct role in methane activation but scavenged OH· radicals to play a role in oxidation of methanol to HCOOH and CO_2 [52]. Thus the presence of Cu to Fe-ZSM-5 can improve the selectivity of methanol due to a decrease in concentration of hydroxyl radicals [52].

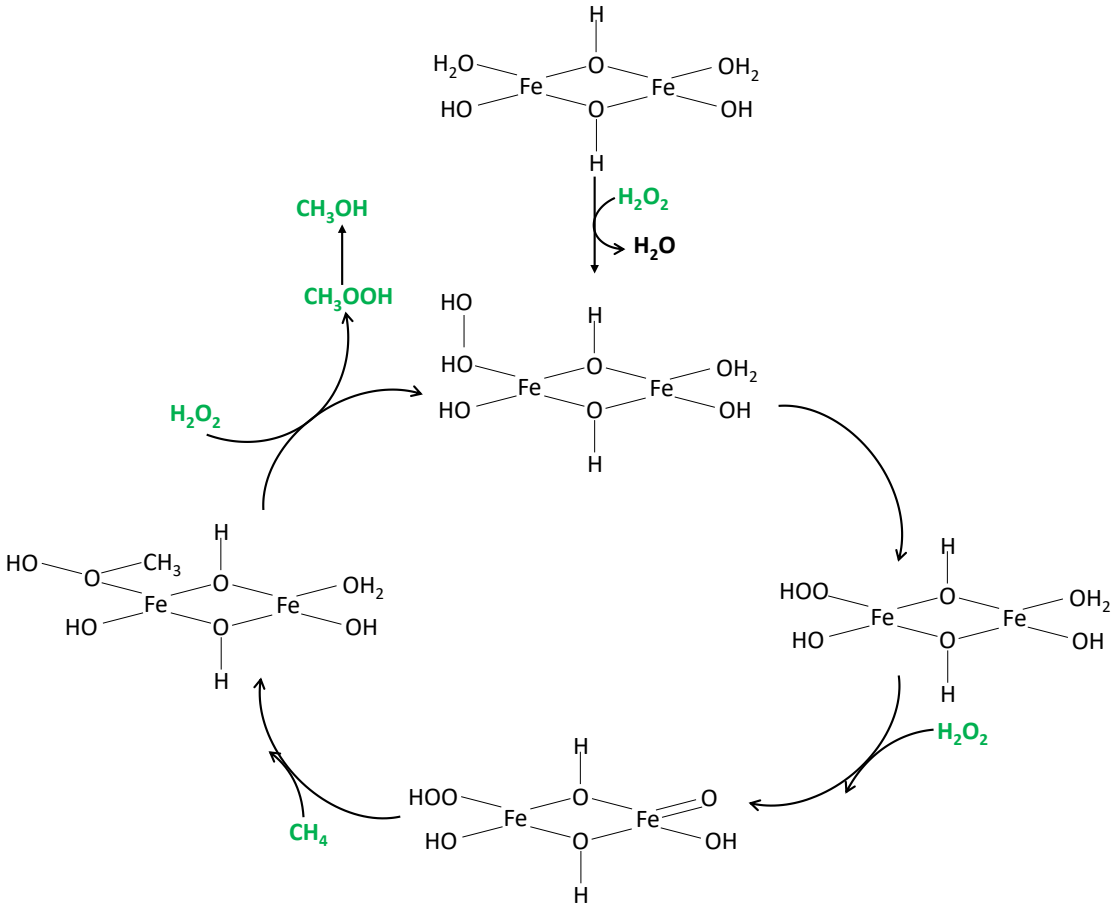

Figure 1.9 Catalytic cycle for the oxidation of methane to CH_3OOH using H_2O_2 catalyzed by a binuclear Fe species in ZSM-5 [52].

Moreover, the ctalytic cycle for the oxidation of methane to CH_3OOH using H_2O_2 catalyzed by a binuclear Fe species is presented in **Figure 1.9**. The mechanism which is distinguished from Fenton's chemistry, α-oxygen, and a MMO-type rebound mechanism was put forward. Hydrogen peroxide reacts at the iron centers to produce species capable of the activation of the carbon-hydrogen bond, forming methyl hydroperoxide as the primary product [101].

Besides, Chadwick *et al.* [106] set forth a slightly different reaction scheme over Fe-containing zeolites from Hammond [52], as shown in **Figure 1.10**. Formaldehyde was identified as an

intermediate in the oxidation reaction pathway from MeOOH to formic acid and ultimately CO_2. The relationship between methanol and formaldehyde is competitive, not formaldehyde is oxidated by H_2O_2 from methanol.

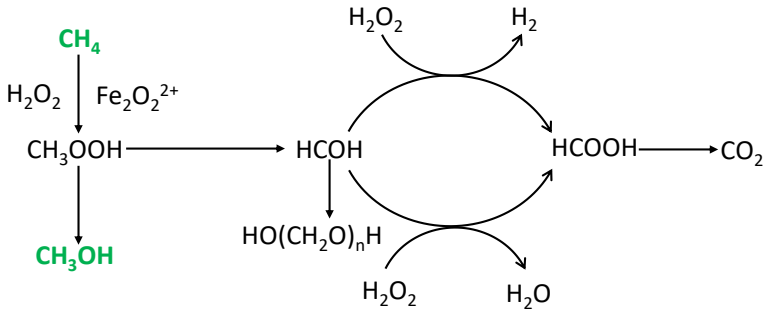

Figure 1.10 A simplified methane oxidation reaction scheme over Fe-containing catalysts [106].

1.3. Conversion of benzene to phenol (BTP)

Phenol is an important intermediate for synthesis of petrochemicals, agrochemicals, and plastics. The conversion of benzene to phenol, is one of the most active topics in applied and fundamental catalytic research [107].

1.3.1 Three-step method (industrial route)

In industry, phenol is obtained by the so-called "three-step cumene process". Firstly, cumene is made from benzene and propene using solid pelletised phosphoric acid as catalyst in vapor gas phase or aluminium chloride as catalyst in liquid phase. Second, cumene is oxidated with oxygen at temperatures in the range 363-403 K and pressures of 1-10 atm. Thirdly, the hydroperoxide is mixed with dilute sulphuric acid at 333-343 K to produce both phenol and acetone as products [108, 109]. This process has drawbacks such as high pollution, high-energy consumption, fussy process and relatively low selectivity towards phenol.

1.3.2 Direct gas phase system

The researches aimed at studying the possibility of direct converting benzene to phenol using molecular oxygen as an oxidant have shown low phenol yield. Cu/ZSM-5 zeolites were used as catalysts for oxidation of benzene to phenol with oxygen in gas phase at 673K, achieving the highest phenol yield of 5% [110]. Cu-containing zeolite catalysts were also researched by Ichihashi and co-workers in direct conversion of benzene to phenol with oxygen, attaining phenol yield of 4% and selectivity of 88% under a low O_2 partial pressure [111]. Iwasawa *et al.* innovatively applied the Re/zeolites for selective oxidation of benzene with molecular oxygen at 573K in the presence of

ammonia, achieving the best results benzene conversion of 10% with phenol selectivity of 91% [112, 113]. However, the catalytic performance was very poor under the condition of none ammonia.

Besides, the most commonly used oxidant is N_2O. Because it contains 36 wt.% oxygen and the by-product is N_2 for hydroxylation of benzene to phenol. The disadvantage of using N_2O is the high cost. The processes using metal modified zeolite catalysts, such as V_2O_5/ MoO_5/ ZSM-5 and Fe_2O_3/ MoO_3/ ZSM-5, transfer atomic oxygen from the decomposition of the N_2O on the catalyst surface to benzene, which active catalyst appears to be the metal species occupying the pores in the zeolite structure [44, 46, 114-119].

Panov and co-workers found that Fe-containing zeolites were useful in the oxidation of benzene to phenol using N_2O as oxidant [120-122]. The mechanism of oxidation benzene to phenol with N_2O on Fe-containing zeolites involves two steps [44]. N_2O decomposition conducts on the active iron centers to form a surface oxygen species that is often called "α-oxygen", which is able to oxidize benzene to phenol [44].

$$N_2O + ()_\alpha \longrightarrow (O)_\alpha + N_2 \qquad (3)$$

$$C_6H_6 + (O)_\alpha \longrightarrow ()_\alpha + C_6H_6O \qquad (4)$$

Many references reported direct oxidation of benzene to phenol with N_2O. Hensen *et al.* researched on many kinds of hierarchical and nanosheet Fe/ZSM-5 zeolites for conversion of benzene to phenol with N_2O at 523K, the sheet-like and hierarchical structure present slowly deactivation properties [44, 123-127]. Xiao's group synthesized the hierarchical Fe-ZSM-5 for conversion of benzene to phenol with N_2O, achieving more than 20% in benzene conversion [46]. Sheldon and co-workers prepared Fe-ZSM-5 for hydroxylation of benzene with N_2O, resulting in high selectivity (>99%) and phenol yields (up to 27%) [114]. Sachtler *et al.* has been studied a variety of Fe/MFI catalysts at 673 and 723K for conversion of benzene to phenol with N_2O, they identified three types of Fe species in Fe/MFI catalysts: (1) mononuclear Fe, catalyzing phenol formation, (2) dinuclear Fe, catalyzing NO_x reduction, and (3) iron oxide nanoparticles, catalyzing deep oxidation [128].

1.3.3 Homogeneous catalytic system in liquid phase

The direct oxidation of benzene to phenol using homogeneous catalysts has been less explored. Homogeneous catalysts based on transition metal complexes with organic ligands offer the advantage of chemoselectivity. Fukuzumi and co-workers used 3-cyano-1-methylquinolinium ($QuCN^+$) as photocatalyst for selective oxygenation of benzene to phenol with oxygen and water under homogeneous and ambient conditions, achieving the highest phenol yield of 26% [129]. The vanadyl (IV), iron (III) and several first row transition metals acetylacetonate complexes with N_2O_2 and N_4

Schiff base ligands were studied as homogeneous catalysts. The results show that the most selective and active transition metal complex is the Fe(II) complex with the N_4 Schiff base ligand with a selectivity of 98% to phenol and 64% conversion of benzene with a turnover number (TON) of 89 in just 3 hours of reaction [130].

1.3.4 Heterogeneous catalytic system in liquid phase

The homogenous catalysts can provide good catalytic performance, but the disadvantages of difficult separation from the reaction media and the non-reusable limit its application in industry. From the sustainable point of view, heterogeneous catalysts are the focus of research. The anchoring of transition metal complexes with Schiff base ligands can be complicated as it often involves a change of the ligand structure in order to allow the efficient covalent attachment onto a support, which is the most effective strategy against active phase leaching. Amine-functionalized activated carbon (AC) and hexagonal mesoporous silica (HMS) are widely used as the supports due to the rich hydroxyl on the large surface to incorporate vanadyl and iron acetylacetonate complexes [130]. According to Silva *et al.*, [$Fe(acac)_2$]APTES@HMS achieved the highest phenol yield of 68% with hydrogen peroxide at 323K [130]. Mesoporous graphitic carbon nitride (g-CN) was utilized as a new support to immobilize vanadyl acetylacetonate ([$VO(acac)_2$]), affording a maximum phenol yield of ca. 20% [131].

Another common way is to build a transition metal complex on the porous supports, such as activated carbon [132-135], carbon nanotubes [136], zeolites [111, 137-139], mesoporous materials [45, 140], metal organic frameworks (MOF) [141, 142], graphene oxide (GO) [143], nanoparticles [144] and so on. There are many investigations using titanium-containing molecular sieves as heterogeneous catalysts for the hydroxylation of benzene to phenol. Pinnavaia *et al.* obtained a benzene conversion of 31% with phenol selectivity of 95% in TS-1 catalyzed benzene hydroxylation with hydrogen peroxide [145]. Amorphous titanosilicates showed the selectivity to phenol almost 100% at a conversion of benzene of 13% [146]. Balducci *et al.* observed a dramatic improvement of selectivity by using sulfolane as a cosolvent in the oxidation of benzene with hydrogen peroxide using a NH_4HF_2 modified TS-1 catalyst (TS-1B), limiting the formation of multiple-oxidation products probably due to the formation of complexes with phenolic compounds [147].

Molecular sieves such as MCM-48 and MCM-41 take high surface area, rich pores and silanol groups providing the superiority to graft active species on the surface of mesopores materials or to incorporate the metal ions in the mesoporous system directly by substitution of Si atoms in regular tetrahedral positions. The incorporation of two different metals into the framework of MCM-41 can create new properties such as redox activity and acidity. The V-MCM-41 catalysts incorporated with titanium increased the activity significantly in the oxidation of benzene, achieving the highest

conversion of 78% [148]. Cubic KIT-6 and mesoporous hexagonal SBA-15 supported CuO were synthesized, achieving the phenol yield of 11% with 85% phenol selectivity and phenol yield of 19% with 92% phenol selectivity, respectively [149]. VO_x/SBA-16 with 7.3 wt.% vanadium showed excellent activity for the hydroxylation of benzene to phenol with hydrogen peroxide, affording phenol yield of 14% with selectivity of 98% [150]. Fe/SBA-16 was used as catalyst, under the optimized conditions, 12% phenol yield with 96% selectivity to phenol were obtained [45]. Metal oxides Fe_2O_3 and Co_3O_4 were stabilized in the mesopores of MCM-41 molecular sieve, the total conversion of benzene could not exceed 11% at 348K [151].

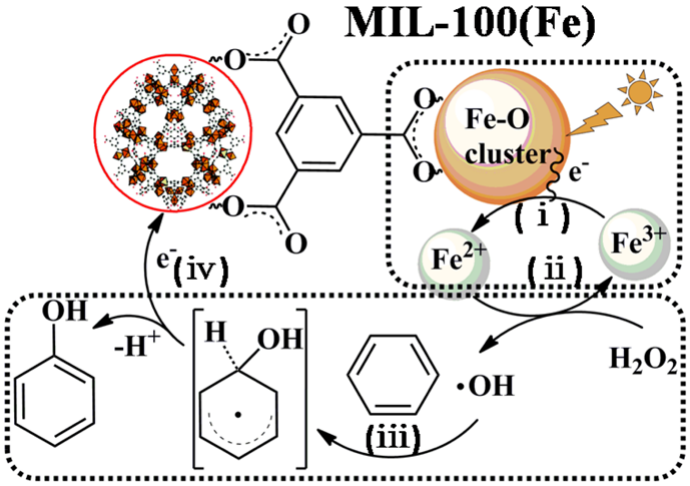

Figure 1.11 Free-radical mechanism of photo-catalytic benzene hydroxylation over MIL-100(Fe)[141].

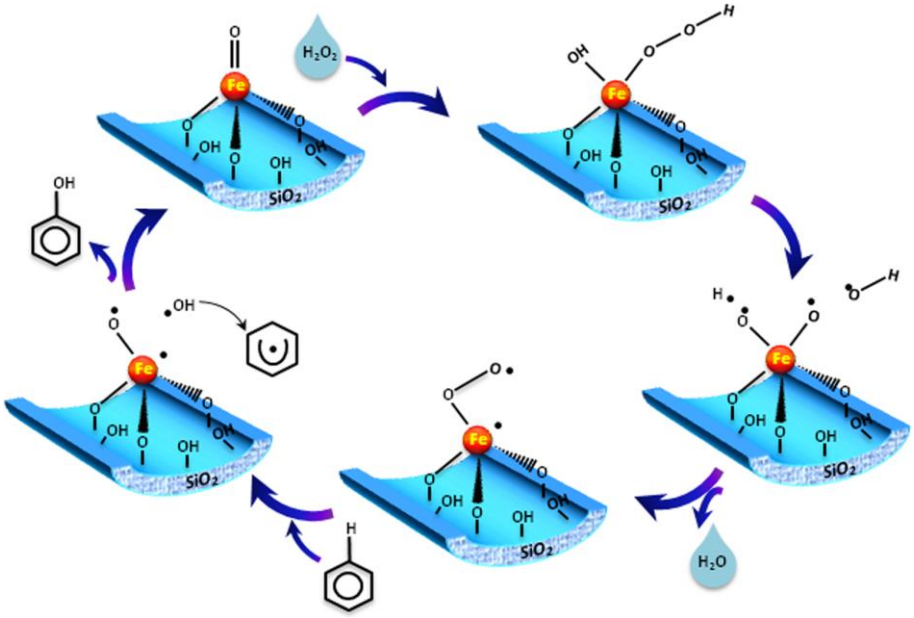

Figure 1.12 Free-radical and nonradical mechanisms of the catalytic benzene hydroxylation by H_2O_2 in the presence of Fe/SBA-16[45].

As for the reaction mechanism using Fe-containing catalysts for hydroxylation of benzene to

phenol with H_2O_2, it is still a matter for debate, radical mechanism (**Figure 1.11**) [141, 152-154] and/or non-radical mechanism (**Figure 1.12**) [45, 130, 155] are the mainstreams.

In addition, heterogeneous catalysts are used in the liquid phase, oxygen (gas) can be applied as oxidant [156-158]. Interstitial-N/Re Cluster/Zeolite as catalysts were used in conversion of benzene to phenol, attaining benzene conversion of 10% and phenol selectivity of 91% at 553 K [113]. Besides, yield of 4% and selectivity of 88% to phenol were achieved over Cu/Ti/HZSM-5 under the O_2 partial pressure of 2.5 kPa and 673 K [111]. Note that, under this kind of condition, high reaction temperature is normally required.

1.4. Relationship between MTM and BTP

Extremely difficult selective oxidation reactions take hydrocarbon containing stable C-H bond as reactant to produce the product with higher value-added, including hydroxylation of methane, selective oxidation of propane, direct oxidation of aromatic compounds and so on. In this thesis, only MTM and BTP reaction were involved. Studies have shown that the reaction intermediates and the transition states in the reaction pathway of benzene to phenol are quite similar to those in the methane to methanol conversion pathway with respect to essential bonding characters [159]. Benzene and methane, especially methane is recognized as one of the most stable hydrocarbon due to its perfectly symmetrical tetrahedron structure [69]. The dissociation energy of the methane C-H bond is 440 $kJ \cdot mol^{-1}$ and hence its activation may require harsh conditions [69]. Typically, the products of direct conversion methane to methanol are trace and high requirement on the analysis equipment [52]. It seems that the benzene to phenol process is slightly easier compared to the methane to methanol process, judging from the published papers concerning the methane hydroxylation and benzene hydroxylation [160]. Besides, the products of benzene to phenol process are easier to detect [161]. When Fe-containing zeolites are used as catalysts with H_2O_2, the processes of hydroxylation of benzene to phenol and methane to methanol possess the similar mechanism. Hence, benzene to phenol process can be selected as the screening reaction to investigate the catalytic performance firstly. The catalysts with good performance are then applied in the conversion of methane to methanol process.

1.5. Aim of the thesis

Selective oxidation of methane in a stirred autoclave and selective oxidation of benzene in a stirred reflux setup were studied using hydrogen peroxide as oxidant and Fe-containing zeolites,

mainly including **MFI**, **MWW** and **BEA** topological structure, as catalysts. High activity Fe-containing zeolite catalysts were prepared and the reaction parameters based on the catalyst were optimized for both MTM and BTP reaction in order to obtain an efficient and environmentally friendly reaction system.

1.6. Scope of the thesis

Chapter 2 explored Fe-containing MFI zeolite catalysts including Fe-silicalite-1 and Fe-ZSM-5 by direct or post-synthesized method and post-modification by acid or alkaline treatment. The reaction conditions were investigated in detail. The relationship between the states of Fe species and catalytic performance was established. The formation of isolated and oligomeric extra framework Fe species in MFI zeolite played a key role for achieving high yield of phenol.

Chapter 3 investigated the Fe-silicalite-1 zeolites by direct method using TPAOH as OSDA with or without Na cations in the synthesis gel. The physicochemical properties, especially the states of Fe species were characterized. The impact of solvent on the reaction performance was mainly investigated. The use of aqueous sulfolane with an appropriate proportion led to an extremely high methanol production with a high selectivity. The influence of distribution of Fe species for the Fe-silicalite-1 zeolites on the catalytic performance in direct conversion of methane to methanol with H_2O_2 have been studied.

Chapter 4 discussed the Fe-ZSM-5 zeolites by direct method using TPAOH as OSDA with or without Na cations. The physicochemical properties, especially the states of Fe species were characterized. Fe-ZSM-5 zeolites synthesized without Na cations displayed more uniform distribution for each kind of Fe species and higher proportion of framework Fe than those synthesized with Na cations. Thus synthesized Fe-ZSM-5 zeolites were applied in direct oxidation of benzene to phenol and methane to methanol with H_2O_2. Meanwhile, the catalytic performance in the two reactions were compared with the Fe-silicalite-1 zeolites to explore the function of aluminum.

Chapter 5 researched the influence of desilication on as-synthesized and calcined Fe-ZSM-5 and Fe-silicate-1 zeolites. The textural properties and the states of Fe species were thoroughly discussed. The function of OSDA and metals, including Fe and Al, in the process of desilication were researched. Finally, the thus prepared zeolites were used in hydroxylation of benzene to phenol with H_2O_2.

Chapter 6 discovered Fe-containing MWW zeolites, including Fe-MWW and Fe,Al-MWW, by direct method. Extensively characterization, especially the states of Fe species and the acidity of catalysts were researched. The effects of calcination temperature in different steps on the catalytic performance have been studied in detail. The influence of aluminum in the Fe-containing MWW zeolites on the formation of Fe species and catalytic performance for both hydroxylation of benzene to phenol and methane to methanol with H_2O_2 have been researched.

Chapter 7 included Fe and/ or Cu exchanged Beta catalysts with varying metal contents for hydroxylation of benzene to phenol and methane to methanol with H_2O_2. The states of Fe and Cu species were characterized by UV-vis, NO adsorbed FT-IR and NH_3-TPD in detail. The influence of the reaction conditions in BTP reaction on Fe and/ or Cu-containing Beta zeolite catalysts have been investigated. The reusability of the Fe and/ or Cu-containing Beta zeolite catalysts and the effects of different metallic states of the bimetallic Beta zeolite catalysts on the catalytic performance in BTP reaction were studied. The catalysts with noble performance in each serial were applied in conversion of methane to methanol with H_2O_2.

References

[1] International Zeolite Association, Structure Commission, http://www.iza-structure.org/databases/.
[2] V. S. Marakatti, A. B. Halgeri, G.V. Shanbhag, Catal. Sci. Technol., 4 (2014) 4065.
[3] S. P. Yuan, J. G. Wang, Y. W. Li, H. Jiao, J. Phys. Chem. A, 106 (2002) 8167.
[4] C. T. W. Chu, C. D. Chang, J. Phys. Chem. C, 89 (1985) 1569.
[5] J. Čejka, B. Wichterlová, Catal. Rev., 44 (2002) 375.
[6] T. Prasomsri, W. Jiao, S. Z. Weng, M. J. Garcia, Chem. Commun. (Camb), 51 (2015) 8900.
[7] W. J. Roth, P. Nachtigall, R. E. Morris, J. Cejka, Chem. Rev., 114 (2014) 4807.
[8] M. E. Davis, Nature, 417 (2002) 813.
[9] K. Li, J. Valla, J. Garcia-Martinez, ChemCatChem, 6 (2014) 46.
[10] V. K. Gupta, Suhas, J. Environ. Manage, 90 (2009) 2313.
[11] J. Li, H. Chang, L. Ma, J. Hao, R. T. Yang, Catal. Today, 175 (2011) 147.
[12] K. Pirkanniemi, M. Sillanp€a, Chemosphere 48 (2002) 1047.
[13] M. W. Ackley, S. U. Rege, H. Saxena, Micropor. Mesopor. Mater., 61 (2003) 25.
[14] K. H. Goh, T. T Lim, Z. Dong, Water Res., 42 (2008) 1343.
[15] R. Xu, W. Pang, J. Yu, Chemistry of zeolites and related porous materials: synthesis and structure, 2009.
[16] Y. He, T. C. Hoff, L. Emdadi, Y. Wu, J. Bouraima, D. Liu, Catal. Sci. Technol., 4 (2014) 3064.
[17] D. G. Hay, H. Jaeger, G. W. Wes, J. Phys. Chem. C, 89 (1985) 1070.
[18] R. Grau-Crespo, E. Acuay, A. R. Ruiz-Salvador, Chem. Commun., 21 (2002) 2544.
[19] E. Y. Emori, F. H. Hirashima, C. A. Zandonai, C. A. Ortiz-Bravo, N. R. C. Fernandes-Machado, M. H. N. Olsen-Scaliante, Catal. Today, 279 (2017) 168.
[20] Q. Zhang, G. Liu, L. Wang, X. Zhang, G. Li, Energ. Fuel., 28 (2014) 4431.
[21] A. Aziz, K. S. Kim, J. Porous. Mater., 22 (2015) 1401.
[22] W. Li, Gang Li, C. Jin, X. Liu, J. Wang, J. Mater. Chem. A, 3 (2015) 14786.
[23] D. Xu, G. R. Swindlehurst, H. Wu, D. H. Olson, X. Zhang, M. Tsapatsis, Adv. Funct. Mater., 24 (2014) 201.
[24] S. C. Cundy, P. A. Cox, Chem. Rev., 103 (2003) 663.
[25] S. M. Sadrameli, Fuel, 173 (2016) 285.
[26] J. Luo, B. V. Bhaskar, Y. H. Yeh, R. J. Gorte, Appl. Catal. A: Gen, 478 (2014) 228.
[27] G. Berlier, M. Pourny, S. Bordiga, G. Spoto, A. Zecchina, C. Lamberti, J. Catal., 229 (2005) 45.
[28] M. Rutkowska, U. Díaz, A. E. Palomares, L. Chmielarz, Appl. Catal. B: Environ, 168-169 (2015) 531.
[29] Y. Wang, T. Yokoi, S. Namba, J. N. Kondo, T. Tatsumi, J. Catal., 333 (2016) 17.
[30] A. Corma, C. Corell, F. Llopisb, A. Martinez, J. Pbrez-Pariente, Appl. Catal. A: Gen, 115 (1994) 121.
[31] K. J. D. Rossi, A. Huss, Zeolte MCM-22 Catalysts For Olefn Somerization, United States Patent, 1992.
[32] E. J. Creyghton, M. J. Verhoef, J. A. Peters, H. van Bekkum, Chem. Commun., 20 (1997) 1989.
[33] P. Wu, T. Komatsu, T. Yashima, Micropor. Mesopor. Mater., 22 (1998) 343.
[34] A. Huss, G. W. Kirker, K. M. Keville, R. T. Thomson, Soparaffin-olefin Alkylation Process, 1992.
[35] J. Mart´ınez-Triguero, A. Corma, J. Catal., 165 (1997) 102.
[36] T. Cao, T. Pham, H. S. Kim, K. B. Yoon, Science, 334 (2011) 1533.
[37] A. R. do Nascimento, G. P. de Figueredo, E. M. F. Silva, M. A. F. Melo, D. M. A. Melo, M. J. B.

de Souza, Revista Virtual de Quimica, 9 (2017) 1570.
[38] P. Sazama, B. Wichterlová, E. Tábor, P. Šťastný, K. S. Naveen, Z. Sobalík, J. Dědeček, S. Sklenák, P. Klein, A. Vondrová, J. Catal., 312 (2014) 123.
[39] P. Sazama, N. K. Sathu, E. Tabor, B. Wichterlová, S. Sklenák, Z. Sobalík, J. Catal., 299 (2013) 188.
[40] H. Xia, K. Sun, Z. Liu, Z. Feng, P. Ying, C. Li, J. Catal., 270 (2010) 103.
[41] E. Yuan, G. Wu, W. Dai, N. Guana, L. Li, Catal. Sci. Technol., 7 (2017) 3036.
[42] L. Xu, C. Shi, B. Chen, Q. Zhao, Y. Zhu, H. Gies, F. S. Xiao, D. De Vos, T. Yokoi, X. H. Bao, U. Kolb, M. Feyen, S. Maurer, A. Moini, U. Müller, W. Zhang, Micropor. Mesopor. Mater., 236 (2016) 211.
[43] G. Qi, R. T. Yang, Appl. Catal. A: Gen, 287 (2005) 25.
[44] L. Meng, X. Zhu, E. J. M. Hensen, ACS Catal., 7 (2017) 2709.
[45] M. Jourshabani, A. Badiei, Z. Shariatinia, N. Lashgari, G. M. Ziarani, Ind Eng Chem Res, 55 (2016) 3900.
[46] L. Li, Q. Meng, J. Wen, J. Wang, G. Tu, C. Xu, F. Zhang, Y. Zhong, W. Zhu, Q. Xiao, Micropor. Mesopor. Mater., 227 (2016) 252.
[47] V. Peneau, R. D. Armstrong, G. Shaw, J. Xu, R. L. Jenkins, D. J. Morgan, N. Dimitratos, S. H. Taylor, H. W. Zanthoff, S. Peitz, G. Stochniol, Q. He, C. J. Kiely, G. J. Hutchings, ChemCatChem, 9 (2017) 642.
[48] G. Wu, F. Hei, N. Zhang, N. Guan, L. Li, W. Grünert, Appl. Catal., A, 468 (2013) 230.
[49] G. Wu, F. Hei, N. Guan, L. Li, Catal. Sci. Technol., 3 (2013) 1333.
[50] C. Hammond, I. Hermans, N. Dimitratos, N. Dimitratos, J. A. Lopez-Sanchez, R. L. Jenkins, G. Whiting, S. A. Kondrat, M. H. ab Rahim, M. M. Forde, A. Thetford, H. Hagen, E. E. Stangland, J. M. Moulijn, S. H. Taylor, D. J. Willock, G. J. Hutchings, ACS Catal., 3 (2013) 1835.
[51] C. Hammond, N. Dimitratos, R. L. Jenkins, J. A. Lopez-Sanchez, S. A. Kondrat, M. H. ab Rahim, M. M. Forde, A. Thetford, S. H. Taylor, H. Hagen, E. E. Stangland, J. H. Kang, J. M. Moulijn, D. J. Willock, G. J. Hutchings, ACS Catal., 3 (2013) 689.
[52] C. Hammond, M. M. Forde, R. Rahim, A. Thetford, Q. He, R. L. Jenkins, N. Dimitratos, J. A. Lopez-Sanchez, N. F. Dummer, D. M. Murphy, A. F. Carley, S. H. Taylor, D. J. Willock, E. E. Stangland, H. Hagen J. Kang, C. J. Kiely, G. J. Hutchings, Angew. Chem. Int. Ed., 51 (2012) 5129.
[53] H. Zhang, L. Chu, Q. Xiao, L. Zhu, C. Yang, X. Meng, F. S. Xiao, J. Mater. Chem. A, 1 (2013) 3254.
[54] Y. Yue, H. Liu, P. Yuan, C. Yu, X. Bao, Scientific Reports, 5 (2015) 9270.
[55] F. Gao, J. Szanyi, J. H. Kwak, M. Kollar, Y. Wang, C. H. Peden, Phys. Chem. Chem. Phys., 18 (2016) 10473.
[56] D. Zhang, R. T. Yang, Energ. Fuel., 32 (2018) 2170.
[57] A. Zhang, C. Dai, L. Luo, Z. Zhang, M. Liu, J. Wang, X. Guo, C. Song, Catal. Today, 297 (2017) 335.
[58] E. J. M. Hensen, Q. Zhu, M. M. R. M. Hendrix, A. R. Overweg, P. J. Kooyman, M. V. Sychev, R.A. van Santena, J. Catal., 221 (2004) 560.
[59] Q. Zhu, R. M. V. Teeffelen, R. A. V. Santen, E. J. M. Hensen, J. Catal., 221 (2004) 575.
[60] T. Jiang, W. Wang, B. Han, New J. Chem., 37 (2013) 1654.
[61] G. Berlier, A. Zecchina, G. Spoto, G. Ricchiardi, S. Bordiga, C. Lambert, J. Catal., 215 (2003) 264.

[62] A. Zecchina, M. Rivallan, G. Berlier, C. Lamberti, G. Ricchiardi, Phys. Chem. Chem. Phys., 9 (2007) 3483.
[63] V. C. Wang, S. Maji, P. P. Chen, H. K. Lee, S. S. Yu, S. I. Chan, Chem. Rev., 117 (2017) 8574.
[64] K. Aasberg-Petersen, I. Dybkjær, C. V. Ovesen, N. C. Schjødt, J. Sehested, S. G. Thomsen, J. Nat, Gas, Sci. Eng., 3 (2011) 423.
[65] M. J. da Silva, Fuel Process Technol., 145 (2016) 42.
[66] P. Schwach, X. Pan, X. Bao, Chem. Rev., 117 (2017) 8497.
[67] G. A. Olah, Angew. Chem. Int. Ed. Engl., 52 (2013) 104.
[68] G. A. Olah, Angew. Chem. Int. Ed. Engl., 44 (2005) 2636.
[69] M. Ravi, M. Ranocchiari, J. A. van Bokhoven, Angew. Chem. Int. Ed., (2017).
[70] A. P. E. York, T. Xiao, M. L. H. Green, Top Catal., 22 (2003) 345.
[71] M. H. A. Rahim, Heterogeneous gold, palladium and copper based catalysts for liquid phase oxidation of methane, Cardiff University, 2011.
[72] H. D. Gesser, N. R. Hunter, C. B. Prakash, Chem. Rev., 85 (1985) 235.
[73] D. Palagin, V. L. Sushkevich, M. Ranocchiari, J. A. van Bokhoven, Science, 356 (2017) 523.
[74] V. C. Wang, S. Maji, P. P. Chen, H.K. Lee, S. S. Yu, S. I. Chan, Chem. Rev., 117 (2017) 8574.
[75] R. A. Periana, D. J. Taube, E. R. Evitt, D. G. Loffler, P. R. Wentrcek, G.Voss, T. Masuda, Science, 259 (1993) 340.
[76] R. A. Periana, D. J. Taube, S. Gamble, H. Taube, T. Satoh, H. Fuji, Science, 280 (1998) 560.
[77] B. R. Wood, J. A. Reimer, M. T. Janicke, K. C. Ott, A. T. Bell, J. Catal., 225 (2004) 300.
[78] K. A. Dubkov, V. I. Sobolev, E. P. Talsi, M. A. Rodkin, N. H. Watkins, A. A. Shteinman, G. I. Panov, J. Mol. Catal. A: Chem,123 (1997) 155.
[79] N. V. Beznis, A. N. C. van Laak, B. M. Weckhuysen, B. H. Johannes, Micropor. Mesopor. Mater., 138 (2011) 176.
[80] M. H. Groothaert, P. J. Smeets, B. F. Sels, B. A. Jacobs, R. A. Schoonheydt, J. Am. Chem. Soc., 127 (2005) 1394.
[81] V. B. Nadzeya, B. M. Weckhuysen, J. H. Bitter, Catal. Lett., 138 (2010) 14.
[82] M. A. C. Markovits, S. Grundner, G. Li, M. Tromp, E. A. Pidko, E. J. M. Hensen, A. Jentys, M. Sanchez-Sanchez, J. A. Lercher, Nat. Commun., 6 (2015) 7546.
[83] P. Vanelderen, R. G. Hadt, P. J. Smeets, E. I. Solomon, R. A. Schoonheydt, B. F. Sels, J. Catal., 284 (2011) 157.
[84] T. Sheppard, C. D. Hamill, A. Goguet, D. W. Rooney, J. M. Thompson, Chem. Commun., 50 (2014) 11053.
[85] P. J. Smeets, R. G. Hadt, J. S. Woertink, J. Am. Chem. Soc., 132 (2010) 14736.
[86] P. Vanelderen, J. Vancauwenbergh, B. F. Sels, R. A. Schoonheydt, Chem. Rev., 257 (2013) 483.
[87] P. Vanelderen, B. E. Snyder, M. L. Tsai, R. G. Hadt, J. Vancauwenbergh, O. Coussens, R. A. choonheydt, B. F. Sels, E. I. Solomon, J. Am. Chem. Soc., 137 (2015) 6383.
[88] J. S. Woertink, P. J. Smeets, M. A. Vance, M. H. Groothaert, B. F. Sels, R. A. Schoonheydt, E.I. Solomon, Proc. Natl. Acad. Sci., USA, 106 (2009) 18908.
[89] M. C. A. Evalyn, M. Nachtegaal, E. Kleymenov, J. A. van Bokhoven, Micropor. Mesopor. Mater., 166 (2013) 131.
[90] P. Vanelderen, J. Vancauwenbergh, M. L. Tsai, R. G. Hadt, E. I. Solomon, R. A. Schoonheydt, B.F. Sels, Chemphyschem, 15 (2014) 91.
[91] V. I. Sobolev, A. S. Kharitonov, A. Paukshtis, G. I. Panov, J. Mol. Catal., 84 (1993) 117.

[92] L. V. Pirutko, V. S. Chernyavsky, E. V. Starokon, A. A. Ivanov, A. S. Kharitonov, G. I. Panov, Appl. Catal. B: Environ, 91 (2009) 174.
[93] D. Schröder, H. Schwarz, Angew. Chem. Int. Edit., 29 (1990) 1433.
[94] O. V. Krylov, Catal. Today, 18 (1993) 209.
[95] K. Otsuka, Y. Wang, Appl. Catal. A: Gen, 222 (2001) 145.
[96] Y. Wang, K. Otsuka, J. Chem. Soc., Chem. Commun., 19 (1994) 2209.
[97] P. Tomkins, A. Mansouri, S. E. Bozbag, F. Krumeich, M. B. Park, E. M. Alayon, M. Ranocchiari, J. A. an Bokhoven, Angew. Chem. Int. Ed. Engl., 55 (2016) 5467.
[98] R. Palkovits, C. von Malotki, M. Baumgarten, K. Mullen, C. Baltes, M. Antonietti, P. Kuhn, J. Weber, A. Thomas, F. Schuth, ChemSusChem, 3 (2010) 277.
[99] R. Palkovits, M. Antonietti, P. Kuhn, A. Thomas, F. Schuth, Angew. Chem. Int. Ed. Engl., 48 (2009) 6909.
[100] C. J. Jones, D. Taube, V. R. Ziatdinov, R. A Periana, R. J. Nielsen, J. Oxgaard, W. A. Goddard, Angew. Chem., 116 (2004) 4726.
[101] M. M. Forde, R. D. Armstrong, C. Hammond, Q. He, R. L. Jenkins, S. A. Kondrat, N. Dimitratos, J. A. Lopez-Sanchez, S. H. Taylor, D. Willock, C. J. Kiely, G. J. Hutchings, J. Am. Chem. Soc., 135 (2013) 11087.
[102] C. Hammond, R. L. Jenkins, N. Dimitratos, J. A. Lopez-Sanchez, A. H. ab Rahim, M. M. Forde, A. Thetford, D. M. Murphy, H. Hagen, E. E. Stangland, J. M. Moulijn, S. H. Taylor, D. J. Willock, G. J. Hutchings, Chemistry, 18 (2012) 15735.
[103] C. Hammond, I. Hermans, N. Dimitratos, ChemCatChem, 7 (2015) 434.
[104] M. H. A. Rahim, M. M. Forde, R. L. Jenkins, C. Hammond, Q. He, N. Dimitratos, J. A. Sopez-Sanchez, A. F. Carley, S. H. Taylor, D. J. Willock, D. M. Murphy, C. J. Kiely, G. J. Hutchings, Angew. Chem., 52 (2013) 1280.
[105] M. H. A. Rahim, B. D. Armstrong, C. Hammond, N. Dimitratos, S. J. Freakley, M. M. Forde, D. J. Morgan, G. Lalev, R. L. Jenkins, J. A. Lopez-Sanchez, S. H. Taylor, G. J. Hutchings, Catal. Sci. Technol., 6 (2016) 3410.
[106] S. Al-Shihri, C. J. Richard, D. Chadwick, ChemCatChem, 9 (2017) 1276.
[107] S. Niwa, M. Eswaramoorthy, J. Nair, A. Raj, N. Itoh, H. Shoji, T. Namba, F. Mizukami, Science, 295 (2002) 105.
[108] M. H. Sayyar, R. J. Wakeman, Chem Eng Res Des, 86 (2008) 517.
[109] B. Laurent, Direct hydroxylation of benzene to phenol in a microstructured Pd-Based membrane reactor, KIT Scientific Publishing, 2011.
[110] R. Hamada, Y. Shibata, S. Nishiyama, S. Tsuruya, Phys. Chem. Chem. Phys., 5 (2003) 956.
[111] A. Okemoto, Y. Tsukano, A. Utsunomiya, K. Taniya, Y. Ichihashi, S. Nishiyama, J Mol Catal A: Chem, 411 (2016) 372.
[112] T. Kusakari, T. Sasaki, Y. Iwasawa, Chem. Commun. (Camb), 8 (2004) 992.
[113] R. Bal, M. Tada, T. Sasaki, Y. Iwasawa, Angew. Chem. Int. Ed. Engl., 45 (2006) 448.
[114] A. Ribera, I. W. C. E. Arends, S. de Vries, J. Pérez-Ramírez, R. A. Sheldon, J. Catal., 195 (2000) 287.
[115] D. Meloni, R. Monaci, V. Solinas, C. Oliva, G. Berlier, L. Forni, J. Catal., 214 (2003) 169.
[116] S. Perathoner, F. Pinoa, G. Centi, G. Giordano, A. Katovic, J. B. Nagy, Top Catal., 23 (2003) 125.
[117] G. Centi, S. Perathoner, R. Arrigo, G. Giordano, A. Katovic, V. Pedulà, Appl. Catal. A: Gen, 307

(2006) 30.
[118] I. Yuranov, D. A. Bulushev, A. Renken, L. Kiwi-Minsker, Appl. Catal., A, 319 (2007) 128.
[119] F. Zhang, X. Chen, J. Zhuang, Q. Xiao, Y. Zhong, W. Zhu, Catal. Sci. Technol., 1 (2011) 1250.
[120] N. S. Ovanesyan, K. A. Dubkov, A. A. Shteinman, E. V. Starokon, E. V. Starokon, G. I. Panov, J. Catal., 207 (2002) 341.
[121] G. A. Sheveleva, G. I. Panov, A. S. Kharitonov, V. N. Romannikov, L. A. Vostrikova, Appl. Catal. A: Gen, 82 (1992) 31.
[122] L.V. Pirutko, V. S. Chernyavsky, A. K. Uriarte, G. I. Panov, Appl. Catal. A: Gen, 227 (2002) 143.
[123] A. J. J. Koekkoek, W. Kim, V. Degirmenci, H. Xin, R. Ryoo, E. J. M. Hensen, J. Catal., 299 (2013) 81.
[124] H. Xin, A. Koekkoek, Q. Yang, R. van Santen, C. Li, E. J. M. Hensen, Chem. Commun. (Camb), 48 (2009) 7590.
[125] A. J. J. Koekkoek, H. Xin, Q. Yang, C. Li, E. J. M. Hensen, Micropor. Mesopor. Mater., 145 (2011) 172.
[126] E. J. M. Hensen, Q. Zhu, R. A. J. Janssen, P. C. M. M. Magusin, P. J. Kooyman, R. A. van Santen, J. Catal., 233 (2005) 123.
[127] E. J. M. Hensen, Q. Zhu, R. A. vanSanten, J. Catal., 233 (2005) 136.
[128] J. Jia, K. S. Pillai, W. M. H. Sachtler, J. Catal., 221 (2004) 119.
[129] K. Ohkubo, T. Kobayashi, S. Fukuzumi, Angew. Chem. Int. Ed. Engl., 50 (2011) 8652.
[130] L. Carneiro, A. R. Silva, Catal. Sci. Technol., 6 (2016) 8166.
[131] J. Xu, Q. Jiang, J. K. Shang, Y. Wang, Y. X. Li, RSC Adv., 5 (2015) 92526.
[132] K. Tian, W. J. Liu, S. Zhang, H. Jiang, Green Chemistry, 18 (2016) 5643.
[133] Y. Ma, X. Ren, W. Wang, P. Lu, L. Shi, Reaction Kinetics, Mechanisms and Catalysis, 117 (2015) 693.
[134] M. Jin, R. Yang, M. Zhao, G. Li, C. Hu, Ind. Eng. Chem. Res., 53 (2014) 2932.
[135] Y. Zhong, G. Li, L. Zhu, Y. Yan, G. Wu, C. Hu, J Mol Catal A: Chem, 272 (2007) 169.
[136] S. Song, H. Yang, R. Rao, H. Liu, A. Zhang, Appl. Catal. A: Gen, 375 (2010) 265.
[137] X. Ye, Y. Cui, X. Qiu, X. Wang, Appl. Catal. B: Environ, 152-153 (2014) 383.
[138] R. Dimitrova, M. Spassova, Catal. Commun., 8 (2007) 693.
[139] B. Daniele, B. Luigi, B. Rossella, D. Rino, R. Marco, S. Guido, T. Roberto, T. Cristina, U. Raffaele, Adv. Synth. Catal., 349 (2007) 979.
[140] M. Yamada, K.D. Karlin, S. Fukuzumi, Chem Sci, 7 (2016) 2856.
[141] D. Wang, M. Wang, Z. Li, ACS Catal., 5 (2015) 6852.
[142] H. Yang, J. Li, L. Wang, W. Dai, Y. Lv, S. Gao, Catal. Commun., 35 (2013) 101.
[143] C. Wang, L. Hu, Y. Hu, Y. Ren, X. Chen, B. Yue, H. He, Catal. Commun., 68 (2015) 1.
[144] B. Xu, Z. Chen, B. Han, C. Li, Catal. Commun., 98 (2017) 112.
[145] P. T. Tanev, M. Chibwe, T. J. Pinnavaia, Nature, 368 (1994) 321.
[146] A. Keshavaraja, V. Ramaswamy, H. S. Soni, J. Catal., 157 (1995) 501.
[147] D. Bianchi, L. Balducci, R. Bortolo, R. D'Aloisio, M. Ricci, R. Tassinari, R. Ungarelli, Angew. Chem. Int. Ed., 115 (2003) 5087
[148] V. I. Parvulescu, D. Dumitriu, G. Poncelet, J. Mol. Catal. A: Chem, 140 (1999) 91.
[149] A. G. Kong, H. W. Wang, X. Yang, Y. W. Hou, Y. K. Shan, Micropor. Mesopor. Mater., 118 (2009) 348.
[150] Y. Zhu, Y. Dong, L. Zhao, F. Yuan, J. Mol. Catal. A: Chem, 315 (2010) 205.

[151] S. V. Sirotin, I. F. Moskovskaya, Petrol. Chem. 49 (2009) 99.
[152] X. Fu, X. Gu, S. Lu, V. K. Sharma, M. L. Brusseau, Y. Xue, M. Danish, G. Y. Fu, Z.Qiu, Q. Sui, Chem. Eng. J., 309 (2017) 22.
[153] K. A. Sashkina, E. V. Parkhomchuk, N. A. Rudina, V. N. Parmon, Micropor. Mesopor. Mater., 189 (2014) 181.
[154] K. Chellal, K. Bachari, F. Sadi, Kinet. Catal., 55 (2014) 467.
[155] Y. Shiota, K. Suzuki, K. Yoshizawa, Organometallics, 24 (2005) 3532.
[156] K. Hirose, K. Ohkubo, S. Fukuzumi, Chemistry, 22 (2016) 12904.
[157] G. Luo, X. Lv, X. Wang, S. Yan, X. Gao, J. Xu, H. Ma, Y. Jiao, J. Chen F. Li, RSC Advances, 5 (2015) 94164.
[158] V. Chernyavsky, L. Pirutko, A. Uriarte, A. Kharitonov, G. Panov, J. Catal., 245 (2007) 466.
[159] K. Yoshizawa, Y. Shiota, Y. Kagawa,T. Yamabe, J. Phys. Chem. A, 104 (2000) 2552.
[160] K. Yoshizawa, Y. Shiota, T. Yumura, T. Yamabe, J. Phys. Chem. B, 104 (2000) 734.
[161] M. Sasaki, Y. Sato, Y. Tsuboi, S. Inagaki, Y. Kubota, ACS Catal., 4 (2014) 2653.

Chapter 2

Direct synthesis of phenol by hydroxylation of benzene with hydrogen peroxide over Fe-containing MFI zeolite catalysts

Abstract

Fe-containing **MFI** zeolite catalysts, including Fe-silicalite-1 and Fe-ZSM-5, with different states of Fe species were prepared by the direct and post synthesis method. The states of Fe species and acidic property were characterized by UV-vis, NO adsorbed FT-IR, and NH_3-TPD in details. The prepared catalysts have been investigated in the hydroxylation of benzene to phenol with H_2O_2. The effects of various reaction parameters on the catalytic performance and the reusability of the catalyst have been studied. The phenol yield of the directly synthesized Fe-silicalite-1 zeolites were increased with the Fe content due to the increasing of isolated and oligomeric Fe species on the extra framework, while for the post synthesized Fe-silicalite-1 and Fe-ZSM-5 zeolites, phenol yield were not proportional to the Fe content. Under optimized reaction conditions, directly synthesized Fe-silicalite-1 showed the highest phenol yield of 5.7 %, which was higher than the post-synthesized Fe-silicalite-1 and Fe-ZSM-5. Furthermore, the phenol yield can be improved to 7.6 % by the post-treatment under alkaline conditions. Combination of the catalytic performance and the characterization results, we have considered that the isolated and oligomeric Fe species on the extra framework play an essential role in direct hydroxylation of benzene to phenol with H_2O_2.

2.1. Introduction

The conversion of benzene to oxygen-containing aromatic compounds, such as phenol, is one of the most active topics in applied and fundamental catalytic research. In industry, phenol is obtained by the "three-step cumene process" [1-3]. This process has drawbacks such as high pollution, high-energy consumption, fussy process and relatively low selectivity towards phenol. Thus, much effort has been devoted to the one-step hydroxylation of benzene to phenol (hereinafter called "BTP") using different oxidants such as N_2O [4], O_2 [5], air [6], H_2/O_2 [7], and H_2O_2 [8]. However, the direct introduction of hydroxyl functionality into benzene is challenging. Almost all the developed catalytic systems in the gas phase require an elevated temperature and suffer from low conversion because of the notoriously low reactivity of aromatic C-H bonds [9,10]. Moreover, phenol is easily over-oxidized to produce by-products such as catechol (CL), hydroquinone (HQ), benzoquinones (p-BQ), and tar in the liquid phase, which makes the selective oxidation of benzene to phenol very difficult [11].

Fe-containing **MFI** zeolite has been recognized as a potential catalyst in the BTP reaction, but almost all the related reports were about acting in concert with N_2O in the gas phase under 500-700 K [4,12,13]. Round 20-30% initial benzene conversion were achieved by Fe-MFI zeolites under the high temperature [14]. However, the common problem was the rapid deactivation of the catalysts due to the coke formation [4,15]. In general, the activity can be reduced by 50% in the first three hours [15]. Meanwhile, more than one literatures reported that the catalytic activity required the participation of aluminum besides iron, but aluminum on the extra framework could result in a faster catalyst deactivation [14,16,17], which was difficult to get a good balance.

Among the oxidants for the BTP reaction, H_2O_2 has a clear advantage from the viewpoint of an environmentally benign green process and economical efficiency because of relatively mild reaction conditions and environmental friendly product [18]. Although few reports were about Fe-MFI zeolites with H_2O_2 to directly convert of benzene to phenol. Other metal-based heterogeneous catalysts including amorphous microporous mixed oxides [19], mesoporous silica and silica-alumina [20,21], activated carbon [22,23], graphitic carbon nitride [24] and metal-organic framework [9] were often reported with H_2O_2 in liquid phase [22,25]. Bianchi *et al.* used titanium silicalite (TS-1) as catalyst, 4.5% of benzene conversion with 43% of phenol selectivity in acetonitrile was obtained;[26] when they applied TS-1B, which modified with NH_4HF_2 and H_2O_2, the benzene conversion and phenol selectivity were up to 8.6% and 94% in sulfolane [27]. CuAPO-5 zeolite was applied in the BTP reaction, 5.9% benzene conversion with 68% phenol selectivity was achieved [28,29]. Besides, the BTP reaction was performed by Fe/TS-1 mixture, a moderate phenol yield of 7.6% with selectivity of 15% was obtained [30]. Hu and co-workers reported the stability of different vanadium species existing on vanadium silicalite-1 (VS-1) zeolite catalysts during the hydroxylation conditions, vanadium incorporation in the framework showed a stable phenol yield of 11% with above 90% selectivity [31].

It is well known that the reaction mechanism in hydroxylation of benzene was related to the oxidants and catalysts. The published literatures showed that the activation of H_2O_2 to radicals (HO·) via a Fenton-like route over Fe-containing catalysts can be conceived for the oxidation of benzene [9,20,32]. Moreover, it was normally accepted that the isolated or oligomeric Fe species on the Fe-containing zeolite catalysts are active for the BTP reaction [33,34]. But the differences in activity of the Fe species have not been fully investigated in BTP reaction with H_2O_2. The preparation method of Fe-containing zeolites strongly influences the nature and states of the resulting Fe species, which basically determine the catalyst performance. Extensive efforts have been dedicated to establishing reliable procedures for iron incorporation, including isomorphous substitution [35], ion exchange [36], impregnation [37], chemical vapor deposition (CVD) [38] and so on. Incorporation of heteroatoms

into zeolites can modify the surface properties to obtain highly dispersed Fe species so as to improve the catalytic activity. Compared to the post-synthetic modification, the direct synthetic method is more feasible and has industrial potential [18].

To our best knowledge, no open literature has been reported the direct synthesis of phenol from benzene using Fe-containing **MFI** zeolite catalysts with H_2O_2 to date. In this study, Fe-containing **MFI**-type zeolite catalysts were prepared by different methods, modified with acid or alkaline treatment, and applied in the BTP reaction. The effects of solvent and the reaction conditions on the BTP reaction and the reuse of the catalyst were investigated. In addition, the catalytic performance was considered based on the states and species of iron in the catalysts.

2.2. Experiments

2.2.1. Materials

Tetraethyl orthosilicate (TEOS), tetrapropylammonium hydroxide (TPAOH) (20-25% in water) and tert-butanol were purchased from Tokyo Chemical Industry. NaOH, $Fe(NO_3)_3{\cdot}9H_2O$, α-Fe_2O_3, NH_4NO_3, H_2O_2 (30%), benzene, acetone, acetonitrile, sulfolane and anisole were purchased from Wako. All of the reagents were used as received, without further purification.

2.2.2. Catalysts preparation

Fe-containing **MFI**-type zeolites were synthesized by directly hydrothermal or post-synthesis method. In the direct synthesis method, TEOS was added to the solution containing water, TPAOH, NaOH and $Fe(NO_3)_3{\cdot}9H_2O$. The gels with molar composition of 1 Si: (0.01-0.067) Fe: 0.25 TPA: 0.25 Na: 30 H_2O were crystallized at 443 K for 24 h (40 rpm) after aging 24 h at 353 K. The solid products were filtered, washed, and dried to get the as-synthesized ones. The as-made samples were calcined at 823 K for 10 h to remove TPA^+, and then ion-exchanged with 1 M NH_4NO_3 aqueous solution at 353 K for 3 h twice to obtain the NH_4^+-type ones. H-type samples were made from the NH_4^+-ones by calcination at 823 K for 5 h. Thus obtained products were denoted as "FMD*x*", where *x* was the Si/Fe molar ratio in the mother gel. In the post-synthesis method, silicalite-1, which has a siliceous framework with the **MFI** topology, was synthesized by the similar procedure to that of FMD*x*.

Fe-silicalite-1 catalysts were also prepared by incipient wetness impregnation. A certain amount of $Fe(NO_3)_3$ aqueous solution was added to the silicalite-1, and then the mixture was dried at 373 K overnight and calcined at 823 K for 5 h in air. The obtained products were denoted as "FMP*y*", where *y* was the inputting Fe content (wt.%) (based on the zeolite).

The as-synthesized FMD15 sample was representatively treated in acidic or alkaline aqueous

solution using 6 M HNO_3 at 373 K refluxed for 20 h or 0.2 M NaOH at 353 K for 2 h, respectively. The resultant samples were NH_4^+ exchanged and calcined to obtain the H-type ones. The final products were designated as "ACT-FMD15" and "ALT-FMD15", respectively.

In order to study the influence of aluminum in the post-synthesized Fe-containing **MFI** zeolites, Fe-ZSM-5 zeolites were prepared by incipient wetness impregnation using NH_4-type ZSM-5 (Si/Al=40, Zeolyst) as parent. The preparation procedure was similar to that of FMP*y*. The final products were designated as "FZP*z*", where *z* was the inputting Fe content (wt.%) (based on the zeolite).

2.2.3. Characterization of catalysts

XRD patterns were collected on a Rint-Ultima III (Rigaku) using a Cu Kα X-ray source (40 kV, 20 mA). Field-emission scanning electron microscopic (FE-SEM) images of the powder samples were obtained on S-5200 (Hitachi) microscope operating at 1 kV. Elemental analyses of the samples were performed on an inductively coupled plasma-atomic emission spectrometer (ICP-AES, Shimadzu ICPE-9000). Nitrogen adsorption and desorption measurements to obtain information on the micro- and meso-porosities were conducted at 77 K on a Belsorp-mini II (MicrotracBEL).

UV-vis diffuse reflectance spectra were recorded on a V-650DS spectrometer (JASCO). The diffuse reflectance spectra were converted into the absorption spectra using the Kubelka-Munk function. Fourier Transform Infrared (FT-IR) spectra were obtained by a JASCO FT-IR 4100 spectrometer equipped with a triglycine sulfate (TGS) detector. For FT-IR observation, the sample was pressed into a self-supporting disk (20 mm diameter, ca. 30 mg) and placed in an IR cell attached to a closed gas-circulation system. The sample was pretreated by evacuation at 773 K for 2 h, then adsorbed 5-1000 Pa NO at ambient temperature. The IR spectra resulting from the subtraction of the background spectra from those with NO adsorbed are shown unless otherwise noted.

Temperature-programmed ammonia desorption (NH_3-TPD) profiles were noted down on a Multitrack TPD equipment (Japan BEL). Normally, 25 mg catalyst was pretreated at 773 K for 1 h in a He flow of 50 mL min^{-1} and then cooled down to 423 K. The sample was evacuated at 423 K for 1 h prior to the adsorption of NH_3. Approximately 2500 Pa of NH_3 contacted with the sample at 423 K for 10 min. Subsequently, the sample was evacuated to remove the weakly adsorbed NH_3 at the same temperature for 30 min. Finally, the sample was heated from 423 to 873 K at a ramping rate of 10 K min^{-1} in a He flow of 50 mL min^{-1}.

2.2.4. Catalytic tests

The BTP reaction was carried out in a 25 mL round-bottom flask equipped with a reflux condenser and a magnetic stirrer. In a typical run, the mixture containing 50 mg catalyst, 10 mL acetonitrile, 5 mmol benzene, and 10 mmol H_2O_2 was stirred at 333 K for 6 h. After the mixture was cooled down, a certain amount of anisole as internal standard was added. Then the catalyst was removed and the products were fixed by exhaustive acetylation with excess $(CH_3CO)_2O$-K_2CO_3, the derivative products were analyzed by GC [39]. The amount of unconverted H_2O_2 was quantified by standard titration method with 0.1 mol/L $Ce(SO_4)_2$ solution. The phenol yield was based on the amount of phenol produced per the initial amount of benzene. The product selectivity was based on phenol, hydroquinone and catechol. As for the reusability tests, the catalyst was recovered by filtering and washing with water and ethanol, and drying at 373 K overnight.

2.3. Results and discussion

2.3.1 Characterization of catalysts

2.3.1.1 Physicochemical properties

Figure 2.1 shows the XRD patterns of the samples with the typical **MFI** structure. The diffraction peaks ascribed to large bulk iron oxide were not observed, suggesting that the Fe ions were well dispersed. The FMD15 showed a relatively lower crystallinity compared to other FMD*x* samples, probably due to the formation of amorphous silica and/or Fe species under the high Fe content. After acid or alkaline modification (ACT-FMD15 and ALT-FMD15), the crystallinity was slightly increased owing to the removing of the amorphous silica and/or Fe species on the surface. In addition, the **MFI** structure and crystallinity remained, and the peaks ascribed to large bulk iron oxide were not observed for the post-synthesized FMP*y* and FZP*z*. The post-synthesized samples showed similar morphology and crystal size to the parent silicalite-1 and ZSM-5, respectively.

The FE-SEM images of the samples are shown in **Figure 2.2**. The FMD*x* catalysts possess a typical coffin-shaped crystal with the crystal size increasing from ca. 0.5 to 2.4 μm (Figs. 2(a-d)). Some small particles, probably silica and/or Fe species were observed on the surface of FMD15, which was consistent with the results of XRD (**Figure 2.1**). After acid treatment, the morphology was unchanged, and the floccule on the surface of ACL-FMD15 still exist, may be the amorphous silica (**Figure 2.2(e)**). However, most of the floccule species disappeared and lots of tiny holes appeared on the surface of ALT-FMD15 (**Figure 2.2(f)**). Combination the characters of demetalization by acid treatment and desiliconization by alkaline treatment, the floccule can be inferred to contain most of amorphous silica and small amount of amorphous Fe species. The morphology and particle size of

silicalite-1 was similar to FMD100 (**Figure 2.2(g)**). The parent zeolite of FZP*z*, *i.e.* NH_4^+-ZMS-5, showed the irregular shape with tiny particle size but reunion (**Figure 2.2(h)**).

BET surface area (S_{BET}) and external surface area (S_{EXT}) of FMD*x* zeolites determined by N_2 adsorption isotherms were deceased from 378 m^2g^{-1} to 234 m^2g^{-1} and 103 m^2g^{-1} to 81 m^2g^{-1}, respectively, along with the Fe content increase (**Table 2.1** and **Figure 2.3**). The possible reasons were the increased particle size and the increased Fe species on the surface and channels. The micropore volume of FMD*x* zeolites maintained at 0.17-0.13 cm^3g^{-1} and the total pore volume were 0.42-0.49 cm^3g^{-1}. The S_{BET} of ACT-FMD15 and ALT-FMD15 were drastically increased from 234 m^2g^{-1} to 491 m^2g^{-1} and 452 m^2g^{-1}, respectively. For ACT-FMD15, the formation of considerable amount micropores (0.30 cm^3g^{-1}) contributed to the increase of S_{EXT} from 81 to 121 m^2g^{-1}. In contrast, the significantly incremental S_{EXT} of ALT-FMD15 from 81 to 245 m^2g^{-1} was owing to the formation of considerable amount mesopores (0.58 cm^3g^{-1}) [40]. The S_{BET} of FMP*y* and FZP*z* were decreased comparison with the parents. The compositions of the catalysts are listed in **Table 2.1**. The Si/Fe ratios in the FMD*x* were higher than those in the synthesis gels, meaning that only a part of Fe species was introduced into the zeolite. After acid treatment of FMD15, the Si/Fe ratio was drastically increased from 22 to 184. Contrarily, the Si/Fe ratio was slightly decreased from 22 to 20 after the alkaline treatment.

2.3.1.2 Fe states

According to the references [41,42], different types of Fe species exist in Fe-containing zeolites. The possible Fe species are illustrated in Scheme 1. UV-vis spectroscopy is a facile technique to characterize the Fe species in Fe-containing zeolites. The oxygen-to-metal charge transfer bands can give useful information on the coordination states and aggregation extent of Fe species [36]. Generally, the bands below 250 nm are assigned to framework Fe species, the bands between 250-350 nm are ascribed to isolated and oligomeric Fe species on the extra framework within the zeolite channels (*e.g.*, dimeric, trimeric, and tetrameric Fe species), the bands between 350-450 nm are ascribed to iron oxide clusters, and the bands above 450 nm are ascribed to bulk iron oxide particles smaller or larger than 2 nm [43].

Figure 2.4 shows the UV-vis spectra of the Fe-containing **MFI** zeolite catalysts, which were deconvoluted into several bands by applying Gauss functions. The amount and proportion of different Fe species based on the relative peak areas are listed in **Table 2.2**. For FMD100, ca. 68% of Fe ions in the zeolite were in the framework. The extra framework Fe species were only in the form of isolated and oligomeric types. When the Fe content was increased (FMD50), the proportion of framework Fe

species was decreased, and the iron oxide clusters were newly formed. Further increasing Fe content (FMD25), the proportion of isolated and oligomeric extra framework Fe species were further increased. Moreover, iron oxide species including clusters and bulk particles were also formed. The distribution of Fe species in FMD15 was similar to that of FMD25, while obtained much higher content in each kind of Fe species due to the high total Fe content. For ACT-FMD15, only ca. 14% of Fe species were in the form of isolated and oligomeric Fe species on the extra framework. The fact meant that most of Fe species including in the framework and extra framework were removed by the acid treatment. On the other hand, the alkaline treatment caused an increase in the proportions of iron oxide clusters and bulk iron oxide particles (ALT-FMD15), while those of framework Fe species were greatly decreased from 45 to 30%, the isolated and oligomeric Fe species were slightly decreased from 39 to 36%. Because acid treatment was demetallization and alkali treatment was desiliconization. Unlike the directly synthesized FMD*x* samples, the post-synthesized FMP*y* and FZP*z* catalysts showed broad bands at 250-450 nm. Around 80% Fe species were on the extra framework, and most of them were in the forms of iron oxide species including clusters and bulk particles (**Table 2.2**). The UV-vis spectra of FMP*y* zeolites showed the shoulders on high wavenumbers (550 nm), while FZP*z* samples displayed the corresponding on the low wavenumbers (210 nm). The FZP*z* samples showed similar amount of isolated and oligomeric Fe species to the FMP*y*, but less iron oxide under the similar Fe content.

Even though there was no references to report the fitting and classification based on the bands position for catalysts with high Fe content. It was not suitable to deconvolute for FMP*y* and FZP*z* zeolites. Because no matter there were tetra and hexa-coordinated Fe species, or isolated and oligomeric Fe species, the intensity of bands from 190 to 350 nm were higher than zero, which also has been proved by the spectrum of α-Fe_2O_3. Besides, it was hard to distinguish the FMP*y* and FZP*z* zeolites based on the spectra of UV-vis. Thus the *in-situ* FT-IR spectroscopy using NO as probe molecule was required.

According to the references [44-46], NO adsorbed FT-IR technology would characterize the coordination unsaturated Fe species on the extra framework. **Figure 2.5** shows the FT-IR spectra collected from the annealed Fe-containing **MFI** zeolites during stepwise adsorbed NO at 298 K. For FMD*x* zeolites, the main bands centered at 1867 cm^{-1} have been assigned to Fe^{2+}(NO) complexes formed on oligomeric Fe species [45,47]. Further increasing NO pressure, new bands at 1915 and 1809 cm^{-1} assigned to $Fe^{2+}(NO)_3$ complexes, 1840 and 1765 cm^{-1} assigned to $Fe^{2+}(NO)_2$ complexes on the isolated Fe species appeared [45]. These bands were gradually increased along with the NO pressure until saturated. For ACT-FMD15, the intensities of all the bands were decreased compared to the parent FMD15, indicating that both the isolated and oligomeric Fe cations were removed by the acid

treatment. In contrast, for ALT-FMD15, the intensities were slightly higher than those of FMD15, suggesting the possibility of higher amount of isolated and oligomeric Fe species after desilication.

No remarkable bands were observed for FMP2.5, FMP5.0, the mixture of α-Fe_2O_3 and silicalite-1, indicating that iron oxide species including aggregated clusters and bulk particles were dominant in the FMP2.5 and FMP5.0, which were silent in NO adsorbed FT-IR [45,48]. While for FZP2.5 and FZP5.0, both the bands at 1810 cm^{-1} assigned to $Fe^{2+}(NO)_3$ complexes and the shoulder at 1850 cm^{-1} attributed to the $Fe^{2+}(NO)_2$ complexes on the isolated Fe species were weak, indicating the low content of isolated Fe species [44,49]. The main bands at 1880 cm^{-1} assigned to $Fe^{2+}(NO)$ complexes formed on the surface of the iron oxide clusters or Fe^{2+}-O-Al particles [50]. The Fe content of FZP5.0 was twice that of FZP2.5, but the intensity of NO adsorbed FT-IR was similar, suggesting that the content of coordination unsaturated Fe species was approximative.

2.3.1.3 Acidity

Figure 2.6 shows the NH_3-TPD profiles of the Fe-containing **MFI** zeolite catalysts. All the profiles can be deconvoluted into three peaks at low, medium, and high temperatures (designated as LT, MT, and HT). The amounts of NH_3 adsorbed and the temperature of the maximum peak (T_{max}) are listed in **Table 2.3**. According to the references [51,52], the LT peak, which corresponds to NH_3 adsorbed on the non-acidic OH groups and NH_4^+ by hydrogen bonding, was not related to the true acid site and excluded in the discussion. The MT and HT peaks were corresponded to NH_3 adsorbed on the extra framework Fe species (Lewis acid site), and on the bridged Si-O(H)-Fe species (Brønsted acid site), respectively [53].

When *x* was decreased from 100 to 25, the amounts of NH_3 adsorbed for both the MT and the HT peaks were increased, meaning that both the extra framework and framework Fe species were increased. Meanwhile, the MT peak was shifted to lower temperature, suggesting the decrease in the acid strength. It may be related to the different fractions of extra framework Fe species in these samples. Further decrease the Si/Fe ratio, FMD15 showed slightly low acid amounts for both the MT and the HT peaks due to the severely aggregated Fe species. After acid treatment, ACT-FMD15 showed a lower amount of NH_3 adsorbed for the HT peak, meaning that the framework Fe was easily removed during the acid treatment. However, the amount of NH_3 adsorbed for the MT peak was increased and the peak was shifted to high temperature. On the other hand, after alkaline treatment, ALT-FMD15 showed a high amount of NH_3 adsorbed for MT peak. Of particular note is that the MT for ALT-FMD15 was lower than that for ACT-FMD15. These facts suggested that the extra framework Fe species were different in the two samples; more isolated Fe species existed in ACT-FMD15 and more

clustered Fe species were formed in ALT-FMD15. In addition, NH_3 was hardly adsorbed on the post-synthesized FMP*y* samples, so as to the pure α-Fe_2O_3, suggesting that iron oxide species including severe aggregated clusters and bulk particles were dominant in the FMP*y* samples once more. Note that, although the total Fe content of ACL-FMD15 and FMD100 were only 0.5 wt.%, the acid amount at both MT and HT were much higher than FMP2.5. It implied that it was the states of Fe species, not the content, that affected the acidity. For the H-ZSM-5, the HT was higher than that of the FMD samples, meaning the acidity of H-ZSM-5 zeolite was stronger than Fe-silicalite-1 [54]. Compared to H-ZSM-5, FZP2.5 and FZP5.0 showed an increased NH_3 adsorbed amount on the MT due to the introduction of Fe species on the extra framework (**Table 2.3**). Meanwhile, the HT for FZP2.5 and FZP5.0 were reduced to 614 and 619 K from 752 K, but the acid amount were maintained, probably due to the affected states of aluminum by the incorporation of Fe species [52].

2.3.2 Benzene to phenol reaction with H_2O_2 (BTP)

2.3.2.1 BTP reaction over Fe-containing MFI catalysts

The catalytic results in BTP reaction of the thus prepared catalysts are summarized in **Table 2.4**. When *x* was decreased from 100 to 15, the phenol yield was increased from 1.5 to 5.7%. Meanwhile, the H_2O_2 conversion was also increased along with Fe content. The selectivity of phenol was sustained at 95-97%. The phenol yield for ACT-FMD15 was decreased to 1.3% due to the removed iron. In contrast, the phenol yield for ALT-FMD15 was improved to 7.6% owing to the increased Fe content, surface area and pore size. Compared to FMD*x*, the post-synthesized FMP*y* catalysts exhibited extremely low phenol yields regardless of the Fe content, so as to the silicalite-1. In contrast, the FZP2.5 achieved 3.8% of phenol yield, which was comparable to FMD25. Further increasing the Fe content, FZP5.0 resulted in a decrease to 3.0% in the phenol yield. It was noteworthy that the catalytic performance of FMDx zeolites were increased with Fe content, while high Fe content of the post-synthetic zeolites were not beneficial to improve the reaction performance.

2.3.2.2 The influence of the reaction conditions on the reaction performance

The influences of reaction temperature, the molar ratio of H_2O_2/benzene, reaction time and catalyst amount on the BTP performance were investigated by using FMD15 as catalyst. As shown in **Figure 2.7(a)**, the phenol yield was firstly increased with temperature increasing from 313 to 333 K, and then decreased with the temperature increasing from 333 to 373 K. Meanwhile, the H_2O_2 conversion was gradually increased from 43 to 93% along with the temperature. The increased H_2O_2 conversion was partly to produce HO· and HO_2·, and another part was consumed due to the self-

decomposition.[55] Although the phenol selectivity was almost remained above 98%, the darker colors of the liquid phase after reaction indicated the production of undetectable by-products with reaction temperature increasing.

As for the influence of the molar ratio of H_2O_2/benzene on the catalytic performance, the results are showed in **Figure 2.7(b)**. When the molar ratio of H_2O_2/benzene was increased from 0.5 to 8, the phenol yield was firstly increased from 1.9 to 6.9% and then slightly decreased to 5.9% with the selectivity of phenol decreasing from 100 to 93%. Although the H_2O_2 conversion was decreased from 90 to 50, the consumed molar amount of H_2O_2 was increased. Theoretically, more H_2O_2 can provide more HO· and HO_2· when the catalyst activity was high enough [20], thus more products including the undetectable ones were produced. The increased benzene conversion from 6.6 to 57% was advantageous to prove. On the other hand, the increased H_2O_2 amount diluted the reaction system on a certain degree, this may be a reason to reduce the phenol yield when the molar ratio of H_2O_2/benzene was up to 8.

Thirdly, the effects of reaction time on the catalytic performance were investigated (**Figure 2.7(c)**). When the reaction time was prolonged from 2 to 6 h, both of the benzene and H_2O_2 conversions were increased, leading to the increase of the phenol yield from 2.6 to 5.7% with the phenol selectivity stabled above 98%. The H_2O_2 conversion reached above 72% at 6 h; most of the H_2O_2 was consumed by the self-decomposition as well as the reaction. Further prolonging the reaction time from 6 to 10 h, the benzene conversion and phenol selectivity were slightly increased or maintained, resulting in the slight increase in the phenol yield to 5.8%. It was possible explained by the fact that no more active HO· was provided by H_2O_2 [20].

The effect of catalyst dosage was evaluated on the direct production of phenol from benzene in the range of 10 to 100 mg (**Figure 2.7(d)**). The phenol yield was increased from 1.5% to 7.2% with the catalyst amount increasing due to the presence of more catalytic active sites. Both the conversion of H_2O_2 and benzene were rapidly growth from 50 to 80% and 15 to 25%, respectively, with the catalyst amount increasing from 10 to 50 mg. The conversion of H_2O_2 and conversion were slowly increased from 80 to 88% and 25 to 29%, respectively, with further increasing the catalyst dosage from 50 to 100 mg, possibly due to the limitation of other reactants. The phenol selectivity was maintained above 95% with catalyst amount increasing.

Besides, solvent is vitally important for the BTP reaction [19]. Several solvents such as acetone, acetonitrile, sulfolane and *tert*-butanol were investigated in the study (**Figure 2.8**). When acetonitrile was used as solvent, the highest phenol yield, high phenol selectivity and H_2O_2 conversion were achieved. In the open literature, sulfolane has been used as a decent solvent in BTP reaction with TS-

1 as catalyst due to its good solubility, giving high phenol selectivity [26]. However, in our case, the phenol yield was very low in the cases of acetone, sulfolane and *tert*-butanol, which was consistent with the report by Bianchi *et al.*[55]. Because the compatibility of metal active centers and reaction solvents are critical factor to influence the reaction performance. Basically, TS-1 catalysts achieved better performance in sulfolane [25,26], while Fe- and Cu- containing catalysts were suitable in acetonitrile [9,28].

2.3.2.3 Reusability of FMD15 catalyst

The reusability of FMD15 in the BTP reaction with H_2O_2 was investigated. **Figure 2.9** shows the changes in the phenol yield, phenol selectivity, and H_2O_2 conversion in the 6 times reactions, indicating that the phenol selectivity was fairly constant above 95% and that the phenol yield and H_2O_2 conversion were gradually decreased by 10-15%. The fresh catalyst showed 5.7% of phenol yield and 88% of H_2O_2 conversion (the first-run). The used catalyst was simply washed with water and ethanol and dried at 373 K overnight after each run. Thus regenerated catalyst gave 5.1% of phenol yield and 69% of H_2O_2 conversion after the 5th run. The reduced phenol yield and H_2O_2 conversion would be partly related to the leaching of the Fe content, which decreased from 4.0 to 3.3 wt.% after the 5th run (**Table 2.5**). Moreover we found that the phenol yield was restored to the level of slightly less than the fresh catalyst by calcination at 823 K for 5 h in air of the 5th run catalyst. The fact suggested that the formation of heavy carbonaceous by-products, which were difficult to remove by washing, resulting the decrease of the activity. In addition, calcination can not only remove the coke but also rearrange the Fe species so as to improve the activity, even though the total Fe content was reduced [56].

Besides, the leaching Fe species during the BTP reaction was curtly researched. Firstly, the liquid phase after BTP reaction (noted as LA) was separated with the catalyst and re-reacted in the same condition, the results are listed in **Table 2.6**. 0.5% phenol yield and 0.4% HQ yield were achieved, indicating that the lost Fe species contained a part of active Fe species. Considering 72% H_2O_2 has been already consumed in the first run, 1 g additional H_2O_2 was added to eliminate the effect of insufficient H_2O_2 (noted as LA+H_2O_2). Surprisingly, 3.8% phenol yield and 0.3% CL yield were achieved in the system of LA+H_2O_2, with extra 16% H_2O_2 conversion. The results once again confirmed the presence of active Fe species in the leaching ones. The catalytic performance of α-Fe_2O_3 and $Fe(NO_3)_3{\cdot}9H_2O$ were investigated in the typical reaction conditions to explore the leaching Fe species, results showed that $Fe(NO_3)_3{\cdot}\ 9H_2O$, i.e. Fe^{3+} was active while α-Fe_2O_3 was not active in the BTP reaction. 50 mg $Fe(NO_3)_3{\cdot}\ 9H_2O$ contained about 6.9 mg Fe^{3+}, achieved 104 μmol phenol (1.7% phenol yield) and 101 μmol CL (1.7% CL yield). The produced phenol amount of $Fe(NO_3)_3{\cdot}\ 9H_2O$

was equivalent to that in the system of LA+H_2O_2, but the system of LA+H_2O_2 only contained 0.15 mg Fe species, which was calculated based on the loss of Fe content after the first run. It implied that the leaching Fe species included active Fe^{3+} or more active Fe species.

2.3.3 Discussion on the active sites in the BTP reaction

In this section, we will discuss the active sites for the BTP reaction with H_2O_2 as oxidant in liquid phase, by correlating the catalytic performance with the characterization results.

2.3.3.1 Fe content and state

Figure 2.10 summaries the phenol yield as a function of Fe content for all the catalysts used in this study. Fe-containing **MFI** zeolites achieved 0.1-7.6% of phenol yield dependent on the Fe content. Considering that silicalite-1 did not show any activity in the BTP reaction, the introduction of Fe species was indispensable for the reaction. It was observed that the phenol yield was dependent on the Fe content for the directly synthesized FMD*x* zeolites, which was increased from 1.5 to 5.7% with Fe content increasing from 0.6 to 4.0 wt.%. ACT-FMD15 showed 1.3% phenol yield, which was similar to FMD100 with comparable low Fe content (0.5-0.6 wt.%). Contrarily, ALT-FMD15 displayed 7.6% phenol yield, achieving the highest value among the catalysts investigated in the research. On one hand, the desilication made the increase of Fe content from 4.0 to 4.5 wt.%, thus increased in the isolated and oligomeric Fe species. On the other hand, the increased pore size and surface area reduced the mass transfer resistance [14]. The catalytic performance of the post-synthesized FMP*y* and FZP*z* illustrated the importance of the Fe states besides the Fe content in the BTP reaction.

As mentioned above, the states and the extent of aggregation of the Fe species on the extra framework were affected by several factors, such as preparation method, post-treatment, and the absence or presence of Al in the parent zeolite. According to the reference [57], the extra framework Fe species played an essential role in the BTP reaction with N_2O in gas phase, though the exact structure of active Fe centers (α-sites) remained unclear. In our case, iron oxide species (α-Fe_2O_3) were inactive for the BTP reaction. The post-synthesized FMP*y* samples, which mainly contained iron oxide clusters and bulk iron oxides, showed very low phenol yield (0.1-0.2%). Thus, the isolated and oligomeric Fe species on the extra framework were discussed in the next part.

2.3.3.2 The importance of isolated and oligomeric Fe species on the extra framework

Figure 2.11(a) shows the change in the content of isolated and oligomeric extra framework Fe species as a function of the total Fe content for the FMD*x* samples, indicating that the content of

isolated and oligomeric Fe species was increased along with the total Fe content both at low Fe content (< 1.5 wt.%) and high Fe content (> 3.1 wt.%). Actually, the degree of aggregation of Fe species was increased with Fe content. It was reasonable that the fraction of oligomeric Fe species in the FMD*x* with high Fe content was higher than that in the samples with low Fe content. Although the band ascribed to the isolated or oligomeric Fe species cannot be separated accurately in the UV-vis spectrum, it can be confirmed that the proportion of coordination unsaturated oligomeric Fe species was increased at high Fe content from the NO adsorbed FT-IR results. For ACT-FMD15, the content of isolated and oligomeric Fe species was lower than FMD100 although the Fe content was similar, which was in consistent with the NO adsorbed FT-IR result. Contrarily, for ALT-FMD15, the content of isolated and oligomeric Fe species was almost similar to FMD15, although the Fe content was increased by ca. 10%. On one hand, the degree of aggregation of Fe species was increased after alkali treatment, leading to the formation of mesopores, large Fe clusters and iron oxide particles. On the other hand, the content of highly coordination unsaturated oligomeric Fe species were increased while that of isolated Fe species was decreased, which can be proved by the NO adsorbed FT-IR and NH_3-TPD results (Figs. 4 and 5).

The change in the phenol yield as a function of the isolated and oligomeric extra framework Fe species in the FMD*x* catalysts is shown in **Figure 2.11(b)**, clearly indicating that the phenol yield was correlated with the content of isolated and oligomeric extra framework Fe species. Thus, the formation of isolated and oligomeric extra framework Fe species in the **MFI** zeolite is vital for achieving a high yield of phenol. FMD50 showed slightly higher phenol yield than FMD100, although it had more than two times isolated and oligomeric Fe species, which may be due to the difference in the extent of increased isolated or oligomeric Fe species. With further increasing Fe content, FMD25 showed the phenol yield about two times higher than FMD50, due to the significant increase in the isolated and oligomeric Fe species from 30 to 40%. Further increasing the Fe content, FMD15 showed the phenol yield about 1.5 times higher than FMD25, although the content of isolated and oligomeric Fe species was increased by ca. 1.3 times. It was also suggests the essential role of the oligomeric Fe species. After alkali treatment, ALT-FMD15 showed the phenol yield about 1.3 times higher than FMD15, although they had similar isolated and oligomeric Fe content. Considering that ALT-FMD15 contained more oligomeric Fe species rather than isolated ones, it can be concluded that oligomeric Fe species would be more active than isolated ones.

2.3.3.3 The impact of the framework Al

Finally, the impact of aluminum in the zeolites on the catalytic performance was considered. FZP*z*

attained higher phenol yield than FMP*y*, though the content of isolated and oligomeric Fe species were similar in the UV-vis spectra. Significant differences were displayed in the NO adsorbed FT-IR spectra and NH_3-TPD profiles between FMP*y* and FZP*z*. FZP*z* exhibited stronger NO adsorptions and more acid amount, indicating the abounding coordination unsaturated Fe species. We can estimate that the oligomeric Fe species with low nuclearity (such as dimeric Fe) was formed in FZP*z*, while those with a high nuclearity (such as trimeric and tetrameric Fe) existed in FMP*y*. The function of aluminum was to provide location site and disperse the Fe species, which has been reported in the reference [43]. Therefore, completely different catalytic performances were displayed when silicalite-1 and ZSM-5 were used as parents. It was concluded that the isolated and oligomeric Fe species with low nuclearity were the active sites in the BTP reaction with H_2O_2.

2.4. Conclusions

Fe-containing **MFI**-type zeolite catalysts including Fe-silicalite-1 and Fe-ZSM-5 were prepared by direct or post-synthesized method and post-modification by acid or alkaline treatment. In the BTP reaction with H_2O_2, direct-synthesized Fe-silicalite-1 achieved much higher phenol yield than the post-synthesized ones at similar Fe content. Based on the specific characterizations, we successfully clarified that the formation of isolated and oligomeric Fe species on the extra framework in **MFI** zeolites were critical for achieving high phenol yield. Among isolated and oligomeric extra framework Fe species, low nuclear oligomeric Fe species would be more active. Moreover, alkaline treatment was found to be advantageous to the formation of oligomeric Fe species, and as a result, 7.6% of phenol yield with 92% selectivity was attained. Our findings would contribute to the improvement of catalytic activity of Fe-containing zeolite catalysts, and also the development of the catalytic process for direct production of phenol from benzene.

References

[1] M. H. Sayyar, R. J. Wakeman, Chem. Eng. Res. Des., 86 (2008) 517.
[2] B. Laurent, Direct hydroxylation of benzene to phenol in a microstructured Pd-Based membrane reactor, KIT Scientific Publishing, 2011.
[3] R. J. Schmidt, Appl. Catal., A, 280 (2005) 89.
[4] L. Li, Q. Meng, J. Wen, J. Wang, G. Tu, C. Xu, F. Zhang, Y. Zhong, W. Zhu, Q. Xiao, Micropor. Mesopor. Mater., 227 (2016) 252.
[5] N. Hansen, A. Heyden, A. T. Bell, F. J. Keil, J. Phys. Chem. C, 111 (2007) 2092.
[6] N. B. Castagnola, A. Kropf, C. Marshall, Appl. Catal., A, 290 (2005) 110.
[7] S. Niwa, M. Eswaramoorthy, J. Nair, A. Raj, N. Itoh, H. Shoji, T. Namba, F. Mizukami, Science, 295 (2002) 105.
[8] J. Yang, G. Sun, Y. Gao, H. Zhao, P. Tang, J. Tan, A. Lu, D. Ma, Energ. Environ. Sci., 6 (2013) 793.
[9] M. Wang, D. Wang, Z. Li, ACS Catal., 5 (2015) 6852.
[10] C. I. Herrerı´as, X. Yao, Z. Li, C. J. Li, Chem. Rev., 107 (2007) 2546.
[11] J. Piera, J. E. Backvall, Angew. Chem. Int. Ed. Engl., 47 (2008) 3506.
[12] A. Ribera, I. W. C. E. Arends, S. de Vries, J. Pérez-Ramírez, R. A. Sheldon, J. Catal., 195 (2000) 287.
[13] D. Meloni, R. Monaci, V. Solinas, C. Oliva, G. Berlier, L. Forni, J. Catal., 214 (2003) 169.
[14] F. Zhang, X. Chen, J. Zhuang, Q. Xiao, Y. Zhong, W. Zhu, Catal. Sci. Technol., 1 (2011) 1250.
[15] S. Gopalakrishnan, A. Zampieri, W. Schwieger, J. Catal., 260 (2008) 193.
[16] E. J. M. Hensen, Q. Zhu, R.A. van Santen, J. Catal., 233 (2005) 136.
[17] E. J. M. Hensen, Q. Zhu, R. A. van Santen, J. Catal., 220 (2003) 260.
[18] T. Jiang, W. Wang, B. Han, New J. Chem., 37 (2013) 1654.
[19] M. Stöckmann, F. Konietzni, J. U. Notheis, J. Voss ,W. Keune, W. F. Maie, Appl. Catal., A, 208 (2001) 343.
[20] M. Jourshabani, A. Badiei, Z. Shariatinia, N. Lashgari and G. M. Ziarani, Ind. Eng. Chem. Res., 55 (2016) 3900.
[21] M. Yamada, K. D. Karlin, S. Fukuzumi, Chem. Sci., 7 (2016) 2856.
[22] Y. Zhong, G. Li, L. Zhu, Y. Yan, G. Wu, C. Hu, J. Mol. Catal. A: Chem, 272 (2007) 169.
[23] J. S. Choi, T. H. Kimb, K. Y. Choo, J. S. Sung, M. B. Saidutta, S. O. Ryu, S. D. Song, B. Ramachandra, Y. W. Rhee, Appl. Catal., A, 290 (2005) 1.
[24] L. Muniandy, F. Adam, A. R. Mohamed, A. Iqbal, N. R .A. Rahman, Appl. Surf. Sci., 398 (2017) 43.
[25] M. Ahlquist, R. J. Nielsen, R. A. Periana, W. A. Goddard, J. Am. Chem. Soc., 131 (2009) 17110.
[26] D. Bianchi, M. Ricci, L. Balducci, G. Span, R. Ungarellia, Adv. Synth. Catal., 349 (2007) 979.
[27] D. Yuan, W. P. Deng, Q. H. Zhang, Y. Wang, Adv. Synth. Catal., 349 (2007) 1199.
[28] X. Qi, J. Li, T. Ji, Y. Wang, L. Feng, Y. Zhu, X. Fan, C. Zhang, Micropor. Mesopor. Mater., 2009, 122, 36.
[29] B. Chou, J. Tsai, S. Cheng, Micropor. Mesopor. Mater., 48 (2001) 309.
[30] X. Ye, Y. Cui, X. Qiu, X. Wang, Appl. Catal., B, 152-153 (2014) 383.
[31] B. Guo, L. Zhu, X. Hu, Q. Zhang, D. Tong, G. Li, C. Hu, Catal. Sci. Technol., 1 (2011) 1060.
[32] X. Fu, X. Gu, S. Lu, V. K. Sharma, M. L. Brusseau, Y. Xue, M. Danish, G. Y. Fu, Z. Qiu, Q. Sui, Chem. Eng. J., 309 (2017) 22.
[33] K. Sun, H. Xia, Z. Feng, R. Vansanten, E. J. M. Hensen, C. Li, J. Catal., 254 (2008) 383.

[34] L. Meng, X. Zhu, E. J. M. Hensen, ACS Catal., 7 (2017) 2709.
[35] E. Yuan, G. Wu, W. Dai, N. Guana, L. Li, Catal. Sci. Technol., 7 (2017) 3036.
[36] J. Szanyi, F. Gao, J. H. Kwak, M. Kollar, Y. Wang, C. H. Peden, Phys. Chem. Chem. Phys., 18 (2016) 10473.
[37] D. Zhang, R. T. Yang, Energ. Fuel, 32 (2018) 2170.
[38] E. J. M. Hensen, Q. Zhu, P. Liu, K. Chao, R. Vansanten, J. Catal., 226 (2004) 466.
[39] M. Sasaki, Y. Sato, Y. Tsuboi, S. Inagaki, Y. Kubota, ACS Catal., 4 (2014) 2653.
[40] A. Zecchina, M. Rivallan, G. Berlier, C. Lamberti, G. Ricchiardi, Phys. Chem. Chem. Phys., 9 (2007) 3483.
[41] P. Sazama, R. Pilar, L. Mokrzycki, A. Vondrova, D. Kaucky, J. Plsek, S. Sklenak, P. Stastny, P. Klein, Appl. Catal., B, 189 (2016) 65.
[42] M. S. Kumar, M. Schwidder, W. Grünert, A. Brückner, J. Catal., 227 (2004) 384.
[43] C. Hammond, I. Hermans, N. Dimitratos, J. A. Lopez-Sanchez, R. L. Jenkins, G. Whiting, S. A. Kondrat, M. H. ab Rahim, M. M. Forde, A. Thetford, H. Hagen, E. E. Stangland, J. M. Moulijn, S. H. Taylor, D. J. Willock, G. J. Hutchings, ACS Catal., 3 (2013) 1835.
[44] G. Berlier, C. Lamberti, M. Rivallan, G. Mul, Phys. Chem. Chem. Phys., 12 (2010) 358.
[45] G. Berlier, G. Spoto, P. Fisicaro, S. Bordigaa, A. Zecchinaa, E. Giamello, C. Lamberti, Microchem. J., 71 (2002) 101.
[46] K. Hadjiivanov, H. Knözinger, B. Tsyntsarski, Catal. Lett., 62 (1999) 35.
[47] G. Berlier, C. Lamberti, M. Rivallan, G. Mul, G. Spoto, S. Bordiga, G. Ricchiardi, P. Fisicaro, A. Zecchina, I. Rossetti, E. Selli, L. Forni, E. Giamello, C. Lamberti, J. Catal., 208 (2002) 64.
[48] G. Mul, J. P. Ramírez, F. Kapteijn, J. A. Moulijn, Catal. Lett., 80 (2002) 129.
[49] A. Ayten, H. Christopher, G. Alexandre, Appl. Catal., A, 441-442 (2012) 30.
[50] G. Wu, F. Hei, N. Guan, L. Li, Catal. Sci. Technol., 3 (2013) 1333.
[51] L. J. Lobree, I. Hwang, J. A. Reimer, A. T. Bell, J. Catal., 186 (1999) 242.
[52] G. Wu, F. Hei, N. Zhang, N. Guan, L. Li, W. Grünert, Appl. Catal., A, 468 (2013) 230.
[53] R. Mohammad, Y. Fereydoon, Fuel, 181 (2016) 537.
[54] J. Luo, F. Gao, K. Kamasamudram, N. Currier, C. H. F. Peden, A. Yezerets, J. Catal., 348 (2017) 291.
[55] L. Balducci, D. Bianchi, R. Bortolo, R. D'Aloisio, M. Ricci, R. Tassinari, R. Ungarelli, Angew. Chem. Int. Ed., 115 (2003) 5087.
[56] E. A. Pidko, E. J. M. Hensen, R. A. Van Santen, In: Proc. R. Soc. A., 468 (2012) 2070.
[57] M. Schwidder, M. Kumar, K. Klementiev, M. Pohl, A. Bruckner, W. Grunert, J. Catal., 231 (2005) 314.

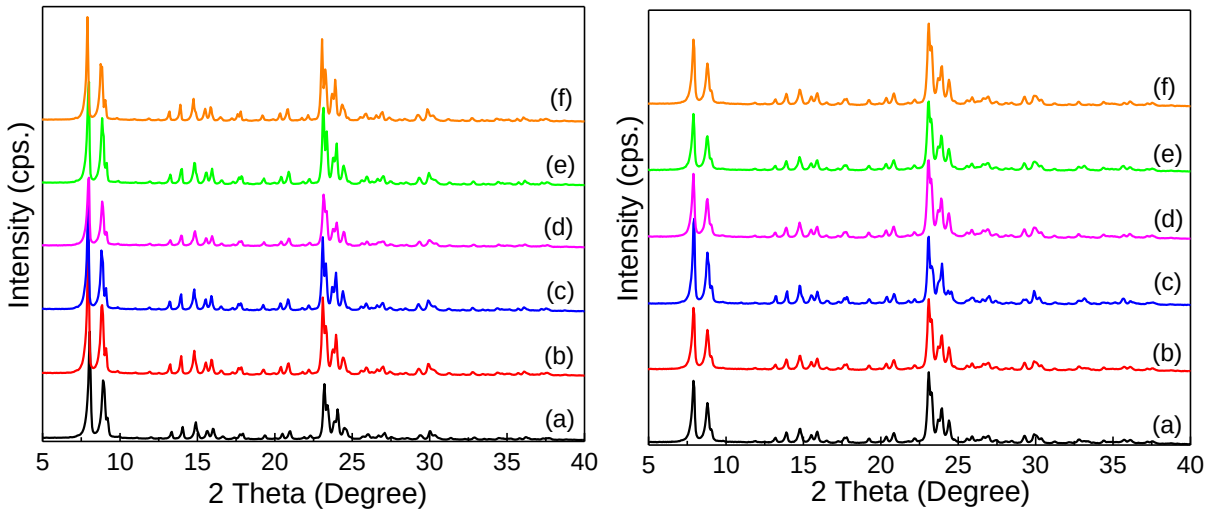

Figure 2.1 XRD patterns of left: (a) FMD100, (b) FMD50, (c) FMD25, (d) FMD15, (e) ACT-FMD15 and (f) ALT-FMD15; and right: (a) FMP2.5, (b) FMP5.0, (c) silicalite-1, (d) H-ZSM-5, (e) FZP2.5 and (f) FZP5.0.

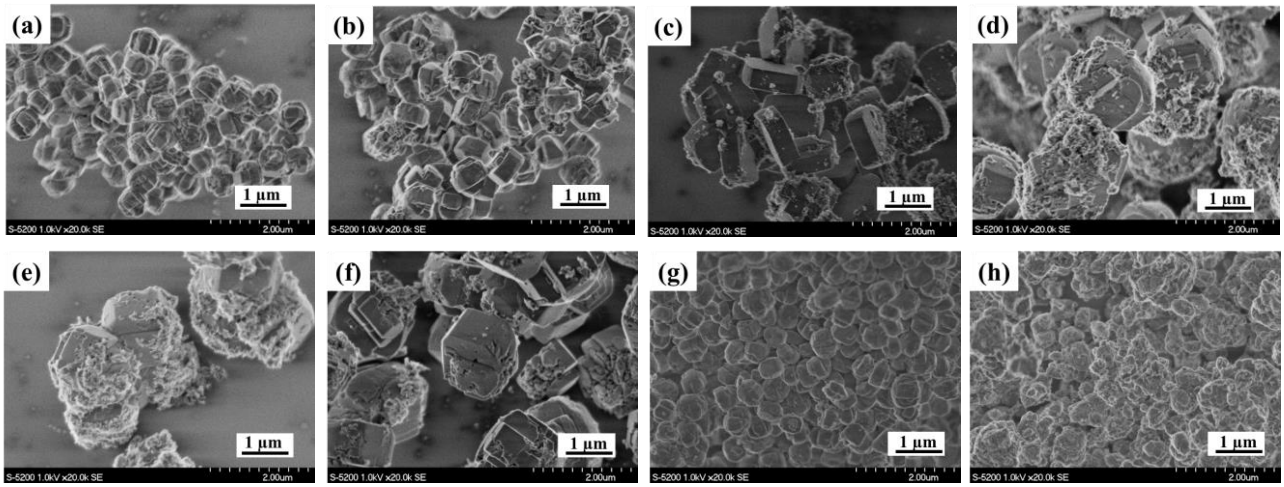

Figure 2.2 FE-SEM images of (a) FMD100, (b) FMD50, (c) FMD25, (d) FMD15, (e) ACT-FMD15 and (f) ALT-FMD15, (g) silicalite-1 and (h) H-ZSM-5 catalysts.

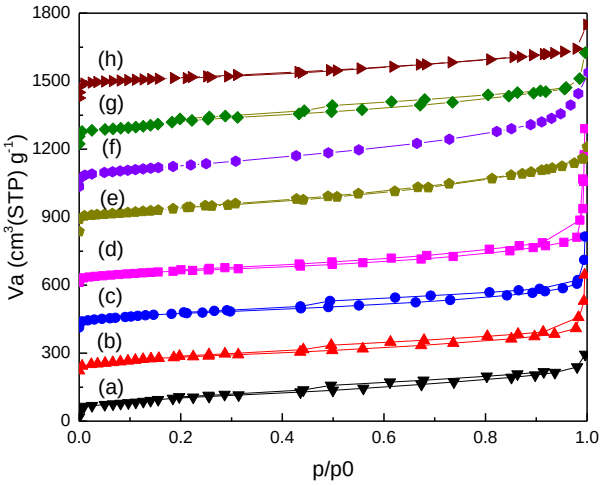

Figure 2.3 N_2 adsorption desorption isotherms of (a) FMD100, (b) FMD50, (c) FMD25, (d) FMD15, (e) ACT-FMD15, (f) ALT-FMD15, (g) FMP2.5 and (h) FZP2.5.

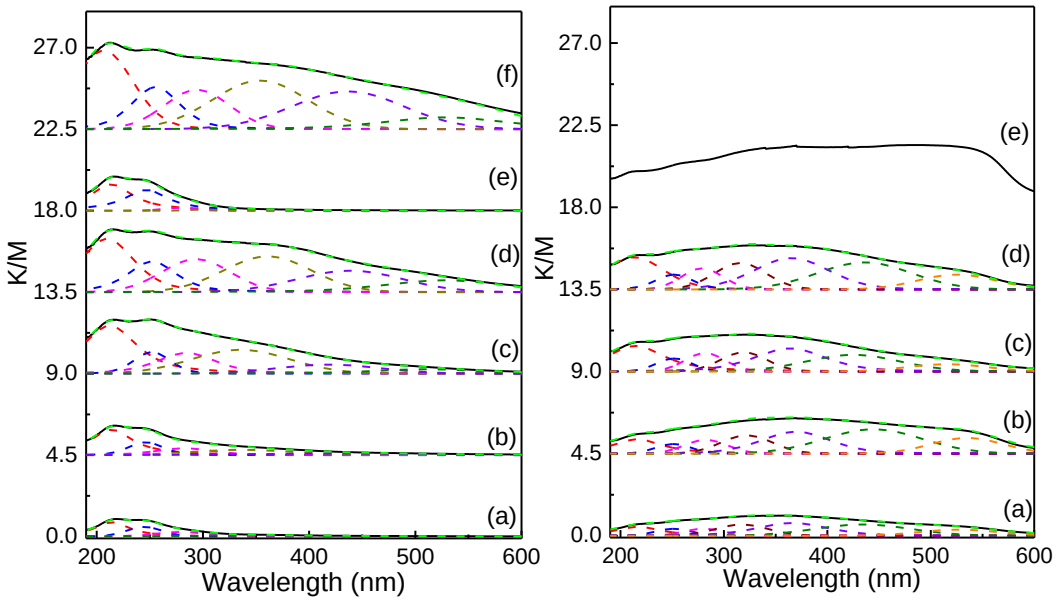

Figure 2.4 UV-vis spectra of left: (a) FMD100, (b) FMD50, (c) FMD25, (d) FMD15, (e) ACT-FMD15 and (f) ALT-FMD15; and right: (a) FMP2.5, (b) FMP5.0, (c) FZP2.5, (d) FZP5.0 and (e) α-Fe_2O_3.

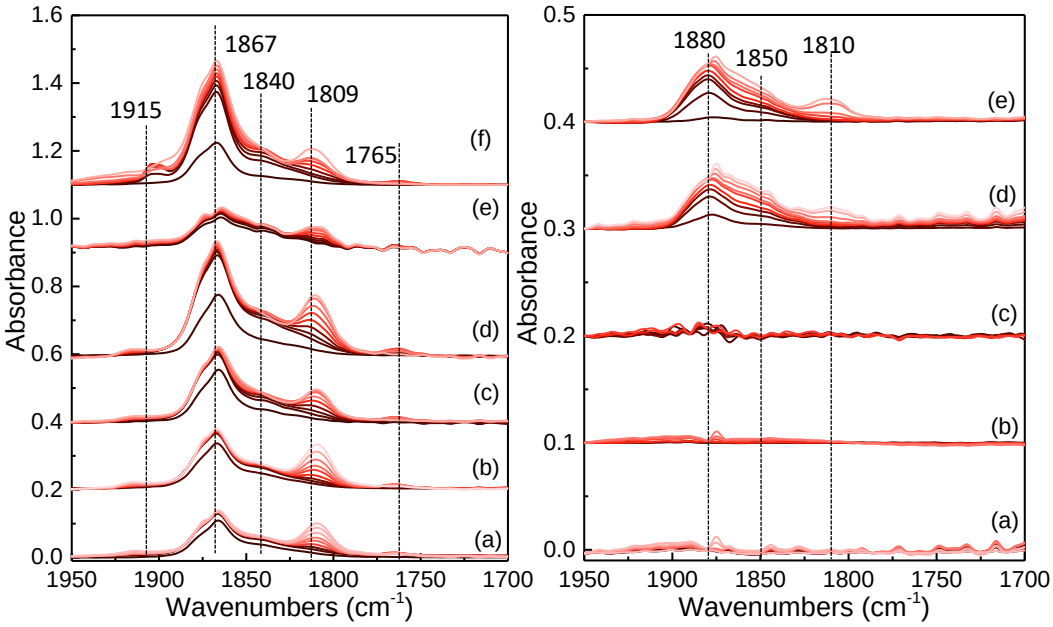

Figure 2.5 FT-IR spectra of NO adsorbed on left: (a) FMD100, (b) FMD50, (c) FMD25, (d) FMD15, (e) ACT-FMD15, and (f) ALT-FMD15 and right: (a) FMP2.5, (b) FMP5.0, (c) mixture of silicalite-1 and α-Fe_2O_3, (d) FZP2.5, (e) FZP5.0.

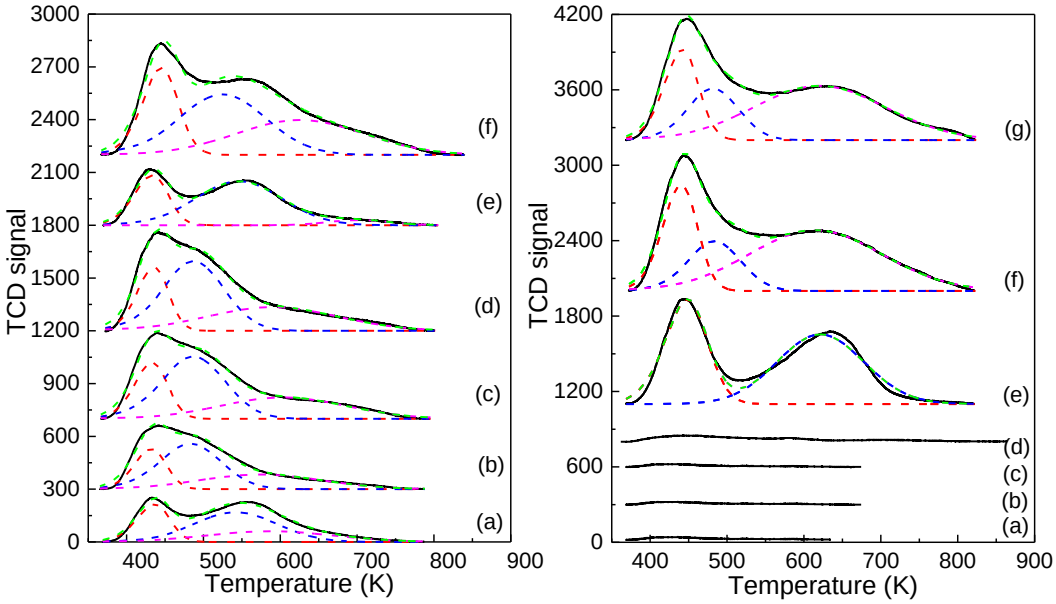

Figure 2.6 NH_3-TPD profiles of left: (a) FMD100, (b) FMD50, (c) FMD25, (d) FMD15, (e) ACT-FMD15 and (f) ALT-FMD15; right: (a) silicalite-1, (b) FMP2.5, (c) FMP5.0, (d) α-Fe_2O_3, (e) H-ZSM-5, (f) FZP2.5, (g)FZP5.0.

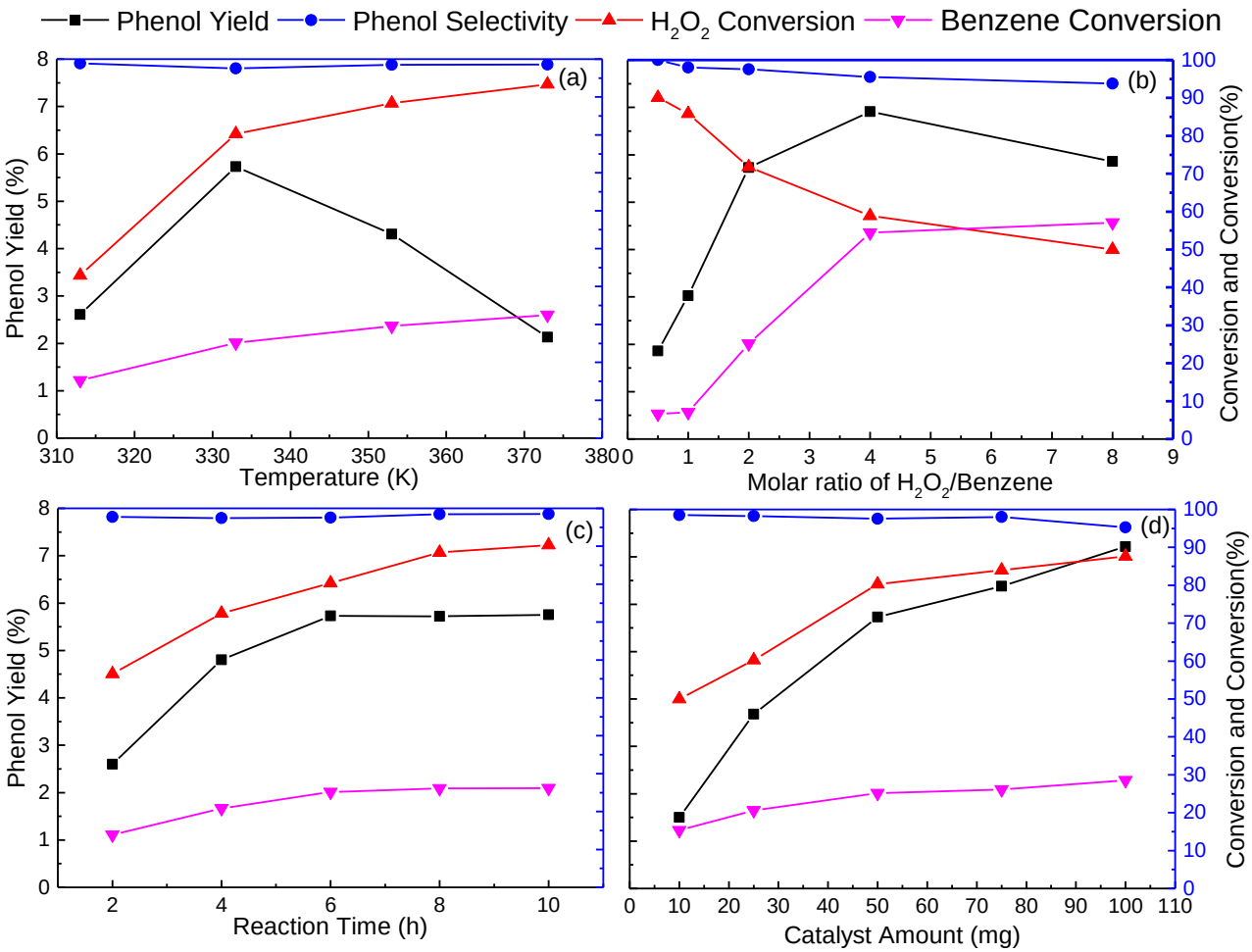

Figure 2.7 Changes of phenol yield, selectivity, and H_2O_2 conversion over FMD15 catalyst as a function of (a) temperature, (b) molar ratio of H_2O_2/benzene, (c) reaction time and (d) catalyst amount. Reaction conditions: (a) 50 mg catalyst, 10 ml CH_3CN, 5 mmol Benzene, H_2O_2/Benzene=2, 6 h. (b) 50 mg catalyst, 10 ml CH_3CN, 5 mmol Benzene, 333 K, 6 h. (c) 50 mg catalyst, 10 ml CH_3CN, 5 mmol Benzene, H_2O_2/Benzene=2, 333 K. (d) 10 ml CH_3CN, 5 mmol Benzene, H_2O_2/Benzene=2, 333 K, 6 h.

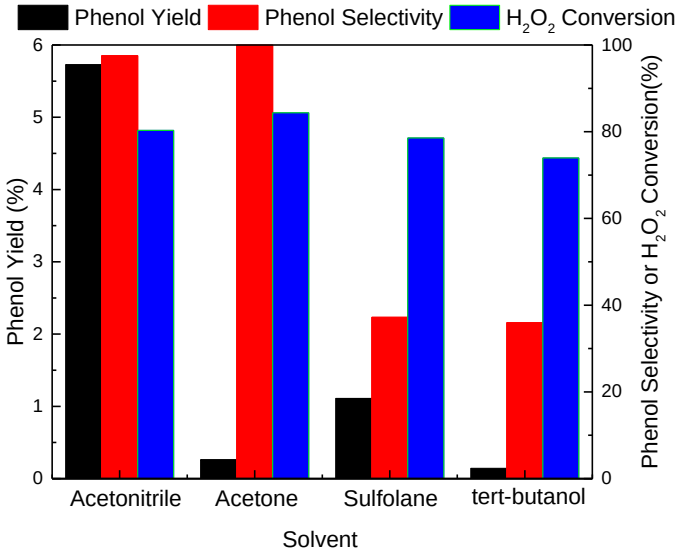

Figure 2.8 Changes of phenol yield, selectivity, and H_2O_2 conversion over the FMD15 catalyst with different solvents. Reaction conditions: 50 mg catalyst, 10 ml solvent, 5 mmol Benzene, H_2O_2/Benzene=2, 333 K, 6 h.

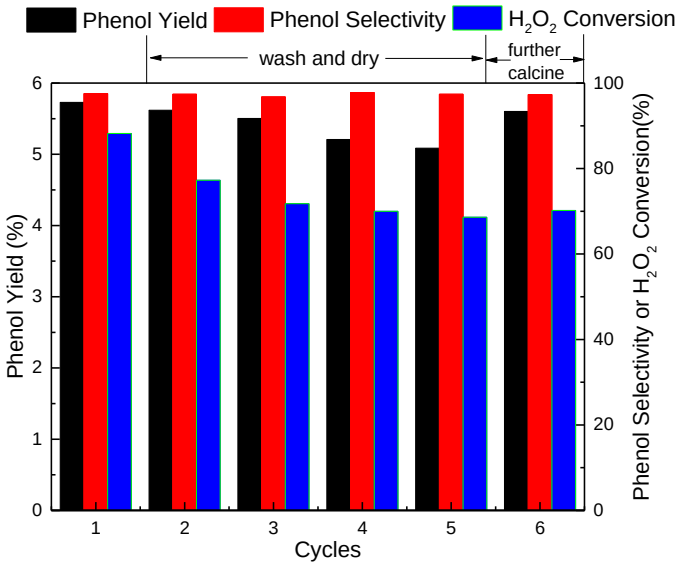

Figure 2.9 Reuse and regeneration of the FMD15 catalyst. Reaction conditions: 50 mg catalyst, 10 ml CH_3CN, 5 mmol Benzene, H_2O_2/Benzene=2, 333 K, 6 h.

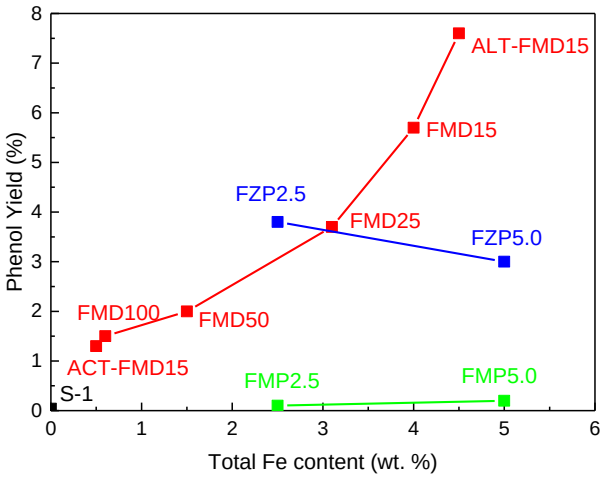

Figure 2.10 Change of phenol yield as a function of Fe content for different catalysts. Reaction conditions: 50 mg catalyst, 10 ml CH_3CN, 5 mmol Benzene, H_2O_2/Benzene=2, 333 K, 6 h.

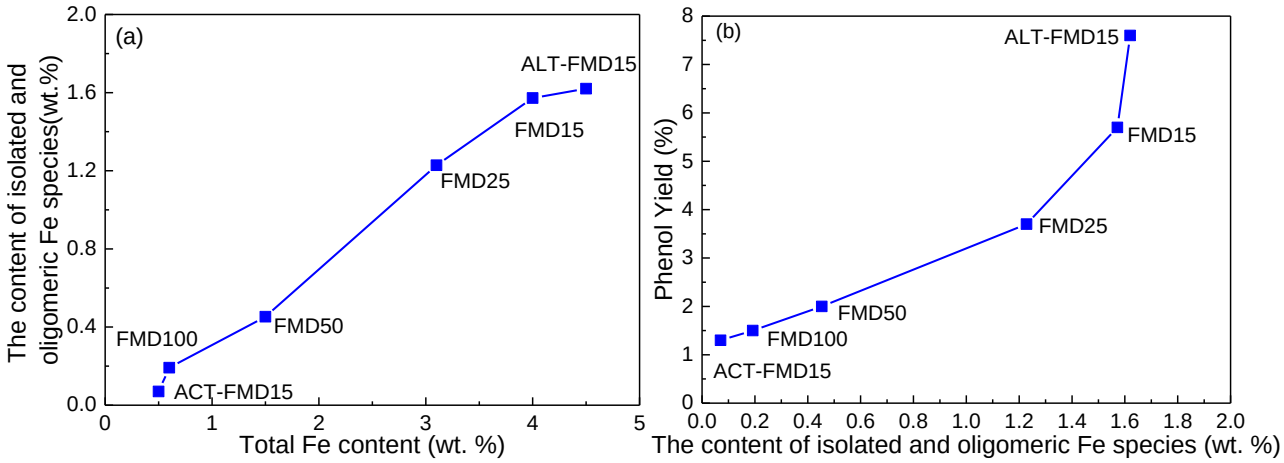

Figure 2.11 (a) change of isolated and oligomeric extra framework Fe species content as a function of Fe content for FMD catalysts, and (b) change in the phenol yield as a function of isolated and oligomeric extra framework Fe species content for the FMD*x* catalysts. Reaction conditions: 50 mg catalyst, 10 ml CH_3CN, 5 mmol Benzene, H_2O_2/Benzene=2, 333 K, 6 h.

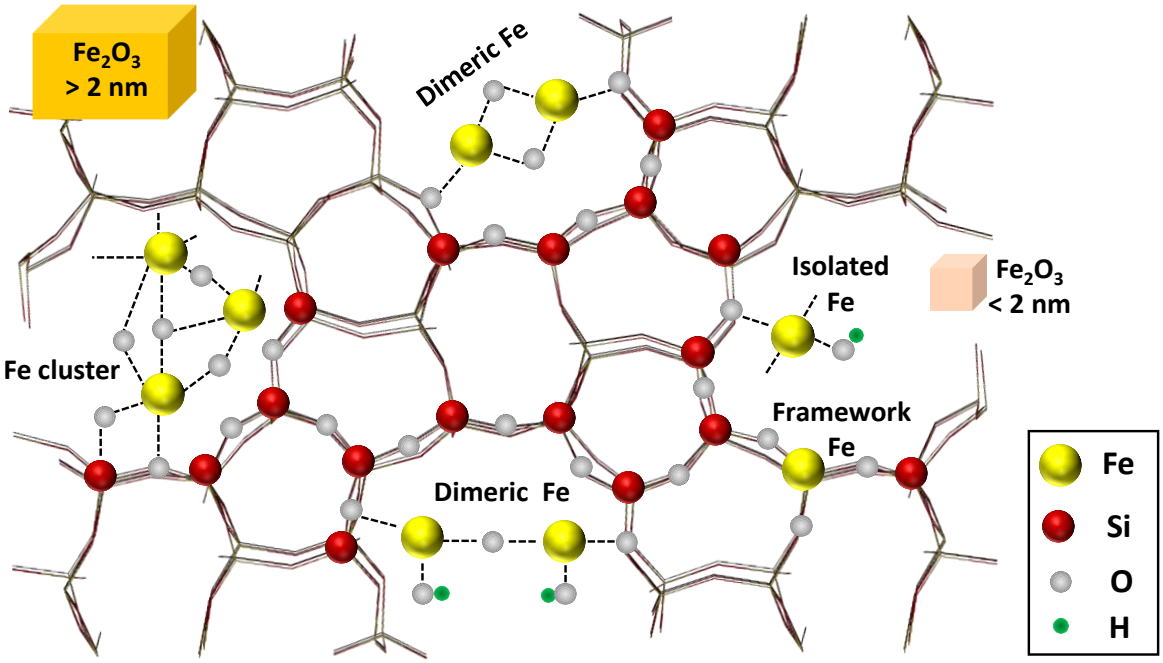

Scheme 2.1 Possible Fe species in the Fe-silicalite-1 zeolite.

Table 2.1 Composition and textural property of the Fe-containing **MFI** zeolites catalysts.

Catalyst	Si/Fe (gel)	Si/Fe (product) [a]	Fe content (wt.%) [a]	S_{BET} ($m^2\ g^{-1}$) [b]	S_{EXT} ($m^2\ g^{-1}$) [c]	V_{Total} ($cm^3\ g^{-1}$) [d]	V_{Micro} ($cm^3\ g^{-1}$) [e]
FMD100	100	167	0.6	378	103	0.42	0.17
FMD50	50	60	1.5	314	98	0.46	0.17
FMD25	25	29	3.1	278	94	0.43	0.13
FMD15	15	22	4.0	234	81	0.49	0.15
ACT-FMD15	15	184	0.5	491	121	0.55	0.30
ALT-FMD15	15	20	4.5	452	245	0.74	0.16
silicalite-1	-	-	-	415	146	0.35	0.13
FMP2.5	-	-	2.5	407	235	0.50	0.12
FMP5.0	-	-	5.0	403	203	0.47	0.12
H-ZSM-5	-	-	-	485	87	0.43	0.23
FZP2.5	-	-	2.5	410	118	0.46	0.18
FZP5.0	-	-	5.0	399	115	0.44	0.15

[a] Si/Fe was determined by ICP-AES analysis, Fe content was calculated by Si/Fe.
[b] Specific surface areas of the catalysts were calculated using the Brunauer-Emmett-Teller (BET) equation on the N_2 adsorption isotherms.
[c] External surface area (S_{EXT}) of the catalysts were calculated by the *t*-plot method based on the adsorption isotherms.
[d] Total pore volumes of the catalysts were calculated based on BET equation on the N_2 adsorption isotherms.
[e] Micropore volumes of the catalysts were calculated by the *t*-plot method based on the adsorption isotherms.

Table 2.2 Percentage of sub-band areas (I_1:λ< 250 nm, I_2: 250 <λ< 350 nm, I_3: 350 <λ< 450 nm, and I_4:λ>450 nm) based on the UV-vis spectra and contents of corresponding Fe species.

Catalyst	Framework Fe		Isolated and oligomeric Fe		Iron oxide cluster		Bulk iron oxide	
	I_1(%)	wt.%	I_2(%)	wt.(%)	I_3(%)	wt.%	I_4(%)	wt.%
FMD100	68.0	0.4	32.0	0.2	-	-	-	-
FMD50	60.5	0.9	30.2	0.5	9.3	0.1	-	-
FMD25	46.3	1.4	39.6	1.2	8.8	0.3	5.3	0.2
FMD15	45.4	1.8	39.3	1.6	9.4	0.4	5.9	0.2
ACT-FMD15	86.0	0.4	14.0	0.1	-	-	-	-
ALT-FMD15	29.7	1.3	36.0	1.6	20.2	0.9	14.1	0.6
FMP2.5	20.2	0.5	19.8	0.5	49.1	1.2	10.9	0.3
FMP5.0	17.0	0.9	18.7	0.9	50.4	2.5	13.8	0.7
FZP2.5	30.3	0.8	19.6	0.5	43.0	1.1	7.0	0.2
FZP5.0	24.2	1.2	20.2	1.0	45.3	23	10.3	0.5

Table 2.3 NH_3 adsorbed amount on the samples used in this study.

Catalyst	NH_3 adsorbed amount (mmol/g) / T_{max} (K)		
	LT	**MT**	**HT**
FMD100	0.04/ 436	0.08/ 541	0.05/ 578
FMD50	0.04/ 423	0.10/ 482	0.06/ 574
FMD25	0.06/ 433	0.14/ 486	0.10/ 602
FMD15	0.05/ 434	0.10/ 512	0.08/ 607
ACT-FMD15	0.05/ 433	0.13/ 545	0.01/ 701
ALT-FMD15	0.06/ 435	0.15/ 487	0.11/ 589
silicalite-1	-	0	0
FMP2.5	-	0	0
FMP5.0	-	0	0
α-Fe_2O_3	-	0	0
H-ZSM-5	0.21/ 448	0	0.32/ 752
FZP2.5	0.17/ 440	0.13/ 481	0.39/ 614
FZP5.0	0.14/ 445	0.13/ 486	0.34/ 619

Table 2.4 Catalytic results of the FMD*x*, modified ALT-FMD15 and ALT-FMD15, post-synthesized FMP*y* and FZP*z* samples in hydroxylation of benzene to phenol with H_2O_2.

Catalyst	Phenol Yield (%) [a]	Product Selectivity (%) [b]			H_2O_2 Conv. (%)[c]
		Phenol	HQ	CL	
FMD100	1.5	97	2	1	46
FMD50	2.0	97	1	2	59
FMD25	3.7	97	2	1	76
FMD15	5.7	95	4	1	72
ACT-FMD15	1.3	99	1	0	49
ALT-FMD15	7.6	92	7	1	82
silicalite-1	0.0	-	-	-	0.2
FMP2.5	0.1	100	0	0	8
FMP5.0	0.2	100	0	0	2
H-ZSM-5	0.1	100	0	0	1
FZP2.5	3.8	99	1	0	47
FZP5.0	3.0	99	1	0	44

Reaction conditions: 333 K, 10 mmol H_2O_2, 50 mg catalyst, 10 ml CH_3CN, 5 mmol Benzene, 6 h.

[a] Phenol yield = (moles of phenol produced)*100/(initial moles of benzene).

[b] Product selectivity = (moles of each liquid product)*100/(moles of phenol + moles of HQ + moles of CL).

[c] H_2O_2 conversion = (moles of H_2O_2 consumed)*100/(initial moles of H_2O_2).

Table 2.5 Chemical composition of FMD15 catalyst after each run of benzene to phenol reaction.

Run	Si/Fe [a]	Fe (wt.%) [b]
0	22	4.0
1	24	3.7
2	25	3.6
3	26	3.4
4	27	3.3

[a] Si/Fe was determined by ICP
[b] Fe content was calculated according to Si/Fe ratio.

Table 2.6 Reaction results of hydroxylation of benzene to phenol.

Sample	Yield (%)/ (μmol) [d]			Selectivity (%) [e]			H_2O_2 Conv. (%) [f]
	Phenol	HQ	CL	Phenol	HQ	CL	
FMD15 [a]	5.7/ 340	0.2/ 13	0.1/ 4	95	4	1	72
LA [b]	0.5/ 17	0.4/ 13	0/ 0	56	44	0	4
LA+H_2O_2 [c]	3.8/ 111	0/ 0	0.3/ 9	93	0	7	16
α-Fe_2O_3 [a]	0.1/ 7	0/ 0	0/ 0	100	0	0	2
$Fe(NO_3)_3 \cdot 9H_2O$ [a]	1.7/ 104	0.6/ 35	1.7/ 101	43	15	42	77

[a] 333 K, 10 mmol H_2O_2, 50 mg catalyst, 10 ml CH_3CN, 5 mmol Benzene, 6 h.
[b] Liquid phase after BTP reaction separated with catalyst.
[c] Liquid phase after BTP reaction separated with catalyst was mixed with 1 g H_2O_2 (30 wt.%).
[d] Phenol yield = (moles of phenol produced)*100/(initial moles of benzene).
[e] Product selectivity = (moles of each liquid product)*100/(moles of phenol + moles of HQ + moles of CL).
[f] H_2O_2 conversion = (moles of H_2O_2 consumed)*100/(initial moles of H_2O_2).

Chapter 3

Dramatic impacts of the distribution of Fe species in Fe-silicalite-1 zeolites and solvent on liquid-phase methane conversion to methanol with H_2O_2

Abstract

The conversion of methane to methanol over Fe-containing MFI zeolites under mild conditions has been investigated. Fe-silicalite-1 zeolites were directly synthesized using TPAOH as OSDA with and without Na cations. The physicochemical properties, especially the states of Fe species was characterized. The impact of solvent on the performance was investigated. We firstly found that sulfolane was the best one among the solvents used in terms of the improvement in the production of methanol and its stability during the reaction. Finally, the effects of various reaction parameters, such as reaction temperature, CH_4 pressure, reaction time, catalyst amount and the amount of H_2O_2 were optimized. Furthermore, the use of mixture of sulfolane-water solvent with an appropriate proportion led to an extremely high CH_3OH production with a high selectivity.

3.1. Introduction

Methane, as the main component of natural gas, is a highly abundant and inexpensive source of fuel and chemicals [1, 2]. So far, two approaches to conversion of CH_4 to CH_3OH have been implemented. The first route is CH_4 reaction with steam conversion to synthesis gas under 723-823 K [3] and then the synthesis gas is converted into CH_3OH under high temperate and high pressure [4, 5]. The two separate steps method has been applied to produce nearly 100% of methanol worldwide [6]. Another approach is a direct conversion, including gas-phase using O_2 [7, 8], N_2O [9, 10] or H_2O [6] as oxidant. For example, Bokhoven and co-workers introduced a direct stepwise method for converting of CH_4 into CH_3OH over Cu-MOR with water under 473 K and 7 bars of CH_4 [6]. Krisnandi *et al.* achieved 79% methane yield from CH_4 with O_2 over Co-modified mesoporous H-ZSM-5 catalyst under 423 K [11]. However, gas-phase oxidation of CH_4 require high temperatures (473 to 773 K) to activate the oxidant and desorb products [2, 6, 12-14]. The liquid-phase oxidation of CH_4 over homogenous and heterogeneous catalysts with H_2O_2 have been researched [2, 15-17]. Nevertheless the reaction results have not been satisfactory. Recently, Hutchings and co-workers have made great

achievements in the field of direct catalytic conversion of CH_4 to CH_3OH in an aqueous medium with H_2O_2 and various kinds of catalysts, including Cu and/or Fe-ZSM-5 [1, 4, 18, 19], Au-Pd/TiO_2 [20], AuPdCu/TiO_2 [21] and Au-Pd colloids [22]. Among of these catalysts, they achieved the highest 92% of selectivity to CH_3OH at 0.5% of CH_4 conversion [18]. It is still a challenging issue in terms of conversion and selectivity, and the development of novel catalyst and catalytic process have strongly been desired.

As described above, Fe-containing **MFI**-type zeolites have been found to be valid in the liquid-phase oxidation of CH_4 to CH_3OH (MTM) reaction with H_2O_2; a part of the extra framework Fe species are the active component for this reaction [1, 4, 19]. The extra framework Fe specie consist of isolated Fe cations, oligomeric Fe complexes, and neutral iron oxide clusters (Fe_xO_y) as well as larger iron oxide aggregates [23, 24]. Among various states of Fe species, isolated and oligomeric Fe species are involved in the MTM reaction over Fe/ZSM-5 catalyst [25]. Fe-containing **MFI**-type zeolites can be prepared by several methods. In the post-synthesis method, ion-exchange and impregnation techniques have been applied but accordingly prepared catalysts exhibited poor activity [24, 26]. On the other hand, a method for one-pot construction of Fe-containing **MFI**-type zeolite catalyst has been established by adding Fe source into the synthesis gel for the **MFI**-type zeolite, the isolated and oligomer Fe species are formed by calcination in air [24, 27]. It is expected that the fine-tuning of the state of Fe species must be a key factor for improving the catalytic activity.

Meanwhile, the distribution of hetero atoms in zeolite framework has been recognized as an important factor for catalytic activity and selectivity. In aluminosilicate zeolites, to balance the charge, Al^{3+} atoms in silica framework, AlO_4^-, are located near cations including inorganic cations, such as Na^+ and K^+, and organic ones. We have reported the control of the Al distribution in the **MFI** framework based on the rational choice of inorganic and/or organic cations [28, 29], and the use of alcohols as pore-filling agent [30]. However, the distribution and state of Fe species in ferrosilicate zeolites has not been achieved, and their impact on the catalytic activity has also been reported to date.

In addition to the inertia C-H bond of CH_4 molecule [2, 31-33], the difficulty in conversion of CH_4 under the liquid-phase system is related to the solubility of CH_4, which is a kind of non-polar molecule with very symmetrical tetrahedron structure and is extremely difficult to dissolve in H_2O [34]. According to Weare and co-worker's results, only 1.9 mg of CH_4 dissolves in 100 g water at 303

K and 0.1 Mpa [34]. Besides, the solubility of CH_4 is dependent on the temperature and pressure of CH_4. When the pressure increase to 5 Mpa, the solubility of CH_4 is increased to 87.5 mg / 100 g water at the same temperature [34]. In addition, ionic liquid has been employed as solvent in the MTM reaction over nano-Au/SiO_2 catalyst system, 25 % of CH_4 conversion with 72 % of CH_3OH selectivity was achieved [35]. However, the use of ionic liquid hinder a facile operation because it contains other kinds of chemicals like potassium persulfate, trifluoroacetic acid and trifluoroacetic anhydride.

In this work, Fe-silicatelite-1 zeolites were synthesized directly using TPAOH as OSDA with or without Na cations in the synthesis gel. Different organic solvents were used in the MTM reaction to enhance the solubility and the conversion of methane. Finally, the effects of various reaction parameters, such as reaction temperature, CH_4 pressure, reaction time, catalyst amount, H_2O_2 amount were optimized. Besides, we reported the control of the distribution of the Fe species in the **MFI**-type zeolite, and its impact on the activity for liquid-phase MTM reaction with H_2O_2.

3.2. Experiments

3.2.1. Materials

Colloid silica (HS-40) and tetrapropylammonium hydroxide (TPAOH) (20-25% in water) were purchased from Tokyo Chemical Industry. NaOH, $Fe(NO_3)_3{\cdot}9H_2O$, NH_4NO_3, H_2O_2 (30 wt.%), ethanol, acetonitrile, sulfolane, mesitylene, 1,4-dioxane, tetramethylsilane (TMS), 2,2,3,3-d(4)-3-(Trimethylsilyl)propionic acid sodium (TMSP-D4), CD_3CN and D_2O were purchased from Wako. Methane (99.99%) gas was provided by Taiyo Nippon Sanso Co., Ltd.. All of the reagents were used as received, without further purification.

3.2.2. Catalysts preparation

The Fe-silicalite-1 zeolites were directly synthesized with TPAOH as OSDA in the absence of Na cation. First, colloid silica was added to the solution containing water, TPAOH and Fe $(NO_3)_3{\cdot}9H_2O$. The gel with the molar composition of 1 Si: 0.01-0.067 Fe: 0.25 TPA: 20 H_2O was crystallized at 443 K for 7 days with 40 rpm before aged at 353 K for 24 h. Then, the solid product was collected after filtering, rinsing and drying. The as-synthesized material was calcined at 823 K for 10 h to remove TPA^+ species. The calcined samples were treated with 1 M NH_4NO_3 aq. at 353 K for 3 h twice, and

filtered, washed, dry and calcined at 823 K for 5 h to obtain the H-type samples. Thus obtained catalyst was designated as "FS(T)*x*", where *x* is the atomic ratio of Si/Fe in the gel ranging from 15 to 100.

The Fe-silicalite-1 zeolites were also directly prepared with TPA cation in the presence of Na cation. The gel was aged at 353 K for 24 h and then crystallized at 443 K for 3 days. The final molar composition was 1 Si: 0.01-0.067 Fe: 0.25 TPA: 0.25 Na: 20 H_2O. The calcined Na-type samples were treated with 1 M NH_4NO_3 aq. at 353 K for 3 h twice, and filtered, washed, dry and calcined at 823 K for 5 h to obtain the H-type samples. Thus obtained catalyst was designated as "FS(TN)*y* ", where *y* is the atomic ratio of Si/Fe in the gel ranging from 15 to 100.

3.2.3. Characterization of catalysts

XRD patterns were collected on a Rint-Ultima III (Rigaku) using a Cu Kα X-ray source (40 kV, 20 mA). Field-emission scanning electron microscopic (FE-SEM) images of the powder samples were obtained on S-5200 (Hitachi) microscope operating at 1 kV. Elemental analyses of the samples were performed on an inductively coupled plasma-atomic emission spectrometer (ICP-AES, Shimadzu ICPE-9000). Nitrogen adsorption and desorption measurements to obtain information on the micro- and meso-porosities were conducted at 77 K on a Belsorp-mini II (MicrotracBEL).

UV-vis diffuse reflectance spectra were recorded on a V-650DS spectrometer (JASCO). The diffuse reflectance spectra were converted into the absorption spectra using the Kubelka-Munk function. Fourier Transform Infrared (FT-IR) spectra were obtained by a JASCO FT-IR 4100 spectrometer equipped with a triglycine sulfate (TGS) detector. For FT-IR observation, the sample was pressed into a self-supporting disk (20 mm diameter, ca. 30 mg) and placed in an IR cell attached to a closed gas-circulation system. After the sample was pretreated by evacuation at 773 K for 2 h, then adsorbed 5-1000 Pa NO at ambient temperature. The IR spectra resulting from the subtraction of the background spectra from those with NO adsorbed are shown unless otherwise noted.

Temperature-programmed ammonia desorption (NH_3-TPD) profiles were noted down on a Multitrack TPD equipment (Japan BEL). Normally, 25 mg catalyst was pretreated at 773 K for 1 h in a He flow of 50 mL min^{-1} and then cooled down to 423 K. The sample was evacuated at 423 K for 1 h prior to the adsorption of NH_3. Approximately 2500 Pa of NH_3 contacted with the sample at 423 K for 10 min. Subsequently, the sample was evacuated to remove the weakly adsorbed NH_3 at the same

temperature for 30 min. Finally, the sample was heated from 423 to 873 K at a ramping rate of 10 K min^{-1} in a He flow of 50 mL min^{-1}.

3.2.4. Catalytic tests

The liquid-phase MTM reactions were carried out in a 100 ml PTFE autoclave. The CH_4 pressure was controlled by the pressure gage ranging from 0.5 to 3 MPa. The reactants were stirred vigorously by an agitator blade. Aqueous hydrogen peroxide (30 wt.%) was used as oxidant. In a typical standard CH_4 oxidation experiment, deionized water (10 ml) or sulfolane (10 ml) was exploited as solvent, 50 mg catalyst and 27 mmol H_2O_2 were added to the autoclave and heated to 323 K. The sealed reactor was then purged with CH_4 to achieve the desired pressure, typically 3 Mpa. After the desired reaction time, usually 2 h, the autoclave was cooled rapidly to 278 K in an ice bath to minimize any further chemical reaction and reduce loss of volatile products.

Liquid-phase products were analyzed by ^1H NMR spectroscopy on JEOL ECA-600 spectrometer (14.1 T) equipped with an additional 1 kW power amplifier. Mesitylene and 1.4-dioxane were took as the internal standard when the reaction solvent were sulfolane and water, respectively. TMS/CD_3CN and TMSP-D4/D_2O were took as the chemical shift calibrator when sulfolane and water using as solvent, respectively. The detectable products in the liquid-phase were CH_3OH, HCOH and HCOOH. The amount of unconverted H_2O_2 was quantified by standard titration method with 0.1 mol/L $Ce(SO_4)_2$ solution.

3.3. Results and discussion

3.3.1 Characterization

3.3.1.1 Structure and composition

Figure 3.1 shows the XRD patterns of the as-synthesized FS(T)*x* and FS(TN)*y* catalysts. All the directly synthesized Fe-MFI samples had the typical **MFI** structure, and the crystallinity were decreased with the Fe content increasing for both the FS(T)*x* and FS(TN)*y* samples. No features belonging to large iron oxide particles were observed, which was indicative for the high Fe dispersion in the as-synthesized zeolites.

Figure 3.2 shows the FE-SEM images of FS(T)*x* and FS(TN)*y* samples. **Figure 3.2(a-d)** reveal the spherical morphology for FS(T)*x* samples with the particle size varying from 0.5 to 1.2 μm. The

surface of FS(T)*x* zeolites changed from smooth to coarse with the Si/Fe ratio varying from 100 to 15. However, the particle size of FS(TN)*y* catalysts with irregular shape, about 100-200 nm, were similar from each other and smaller than the FS(T)*x* ones, displayed in **Figure 3.2(e-h)**.

The chemical composition and textural properties of the catalysts are listed in **Table 3.1**. For both FS(T)*x* and FS(TN)*y* zeolites, the actual Si/Fe ratios in the products were higher than those in the synthesis gels, meaning that only part of iron was introduced into the zeolite. Meanwhile, the actual Si/Fe ratios of FS(T)*x* samples were higher than those of FS(TN)*y* samples, possibly due to the less amount of positive charge provided by TPA^+ for FS(T)*x* than that provided by TPA^+ and Na^+ for FS(TN)*y*.

The corresponding textural properties of these zeolites are also listed in **Table 3.1**. The BET surface area (S_{BET}), external surface area (S_{EXT}), the total pore volume (V_{total}), and the micropore volume (V_{micro}) of the zeolites were similar to each other for FS(T)*x* and FS(TN)*y* samples at different Si/Fe ratios. In addition, the S_{BET} of all the catalysts were higher than 400 cm^2g^{-1} due to the small particle size, which was verified by SEM images in **Figure 3.2**.

3.3.1.2 Fe states

According to the references [36, 37], the coordination state and extent aggregation of Fe in the Fe-containing MFI zeolites were investigated by UV-vis spectroscopy. **Figure 3.3** show the UV-vis spectra of FS(T)*x* and FS(TN)*y* catalysts, respectively, which were deconvoluted into sub-bands by applying Gauss functions. The amount and proportion of different Fe species based on the relative peak areas are listed in **Table 3.2**. Generally, the bands below 250 nm were assigned to framework Fe species, the bands between 250-350 nm were ascribed to isolated and oligomeric Fe species on the extra framework (e.g., dimeric, trimeric, and tetrameric Fe species), the bands between 350-450 nm were ascribed to iron oxide clusters, and the bands above 450 nm were ascribed to bulk iron oxide particles less or larger than 2 nm [38]. One of the most obvious difference between FS(T)*x* and FS(TN)*y* was the distribution of different Fe species. For FS(T)*x*, no matter the samples with high or low Fe content, the Fe species were evenly distributed as framework Fe, isolate and oligomer Fe, iron oxide clusters, and bulk iron oxide, only the content of each kind of Fe species changed. However, FS(TN)100 and FS(TN)50 samples contained higher Fe content than FS(T)100 and FS(T)50, respectively, but only framework Fe, isolate and oligomer Fe species were detected. When the Si/Fe ratio was decreased to 25 and 15, the Fe species of iron oxide clusters and bulk iron oxide for FS(TN)25 and FS(TN)15 appeared and the corresponding amount were directly increased to a high value. As for the reason, it may be related to the charge position and amount. As mentioned before, only TPA^+ can

balance the negative charge in FS(T)*x* samples which produced by coordinated Fe species, like FeO_4^-, and the location was concentrated at the intersection, as shown in **Scheme 3.1**. Influenced by the charge amount and position, negative coordinated Fe species preferentially were distributed in the intersection at the low Fe content. Increase Fe content, no more TPA^+ balanced the Fe species, which only overlay on the formed ones. As a result, Fe species for FS(T)*x* samples showed no significant change at both low and high Fe content. While for FS(TN)*y*, TPA^+ coupled with Na^+, more positive charge can be provided and the location expand to the channels due to the tiny particle size of Na^+ (**Scheme 3.1)**. Consequently, iron in FS(TN)*y* existed as isolated species at low Fe content, like FS(TN)100 and FS(TN)50. And iron oxide clusters and bulk iron oxide species appeared when the Fe content reached a certain high degree.

In addition to UV-vis spectroscopy, *in-situ* FT-IR spectroscopy using NO as probe molecule was also applied to investigate the state of Fe species [39, 40]. **Figure 3.4** shows the FT-IR spectra collected from the annealed FS(T)*x* and FS(TN)*y* zeolites during stepwise NO adsorption at 298 K. The main band centered at 1867 cm^{-1} assigned to $Fe^{2+}(NO)$ with a shoulder at 1843 cm^{-1} attributed to $Fe^{2+}(NO)_2$ complexes formed on Fe clusters [40-42]. The intensities of these bands were increased along with NO pressure increasing until saturated. Further increasing NO pressure, new bands at 1810 cm^{-1} assigned to $Fe^{2+}(NO)_3$ appeared, which was related to the highly coordination unsaturated Fe species [43]. The weak bands at 1915 and 1902 cm^{-1} were also attributed to $Fe^{2+}(NO)_3$ on isolated Fe species [40, 41]. It was clear to see that the intensity of bands at 1810 cm^{-1} for FS(T)*x* zeolites were increased with Fe content and basically higher than FS(TN)*y* zeolites. But the intensity of bands at 1810 cm^{-1} for FS(TN)*y* zeolites showed no obvious regularity with Fe content changing. The intensity of the main band at 1867 cm^{-1} for FS(TN)*y* were higher than FS(T)*x*, possibly due to the higher Fe amount for the former ones. The differences in the proportion of isolated Fe and Fe clusters between FS(T)*x* and FS(TN)*y* samples specified the influence of the present of Na cation in the synthesis gel.

3.3.1.3 Acidity

The situation of the ammonia adsorbed amount for the Fe-silicalite-1 zeolites measured by NH_3-TPD revealed the Fe environment to a certain degree. **Figure 3.5** show the NH_3-TPD profiles of the FS(T)*x* and FS(TN)*y* samples, respectively. Most of the profiles can be deconvoluted into three kinds of peaks at low (373-473 K), medium (473-573 k), and high temperature (573-773 K) (designated as LT, MT and HT). The amounts of NH_3 adsorbed and the temperature of the maximum peak (T_{max}) are listed in **Table 3.3**. According to the references [44, 45], the LT peak corresponds to NH_3 adsorbed on the non-acidic-OH groups and NH_4^+ by hydrogen bonding, which was not related to the true acid site

and excluded in the discussion. The MT peak corresponds to NH_3 adsorbed on the extra framework Fe species (Lewis acid site), and the HT peak corresponds to NH_3 adsorbed on the bridged Si-O(H)-Fe and Fe-O(H)-Fe species (Brønsted acid site) [45].

For FS(T)*x*, the amounts of NH_3 adsorbed on both the MT and HT peaks were increased along with the Si/Fe ratios, indicating the evenly distribution of each kinds of Fe species, which was consistent with the results of UV-vis. Similarly, the amounts of NH_3 adsorbed on both the MT and HT peaks of FS(TN)*y* samples were increased along with the Si/Fe ratio decreasing under the condition of low Fe content, including FS(TN)100 and FS(TN)50. However, for FS(TN)15 and FS(TN)25, a part of adsorbed NH_3 amount for the MT peak shift to the LT peak, leading to the decrease of the counterpart for the MT. The difference involved more bridged hydroxyl for the FS(TN) samples with high Fe content. Moreover, the amount of each kind of Fe species is not proportional to the total Fe content of FS(TN)*y* catalysts and the ability of adsorbed NH_3 for each kind of coordinate iron is different, leading to the different NH_3-adsorbed amounts for the MT peaks between FS(TN)50 and FS(TN)25, and the HT peaks between FS(TN)15 and FS(TN)25. At the same time, the NH_3-adsorbed amount of the FS(T)*x* samples were lower than those of the FS(TN)*y* ones under the same Si/Fe ratio in the synthesis gel, which was similar to the ZSM-5 synthesized using TPAOH as OSDA with or without Na cations [28,29]. One of main reasons is the lower Fe content for the FS(T)*x* products than FS(TN)*y* under the same *x* value. Another reason is the different coordinated and aggregated state for the Fe species. These results validate the difference Fe state between FS(T)*x* and FS(TN)*y* samples.

3.3.2 Methane to methanol reaction

3.3.2.1 Solvent selection

H_2O has been widely applied as solvent in the MTM reaction [38, 46]. However, the solubility of CH_4 in H_2O is extremely low, wherefore it limits the reaction performance. Taking this into account, some kinds of organic solvents with higher solubility of CH_4 such as acetonitrile, ethanol and sulfolane were employed. Firstly, the stability of the solvents should be checked. Here, FS(T)15 was representatively took as catalyst and treated in the solvents with H_2O_2 at 323 K in the absence of CH_4 for 2 h, named blank test. After separation the catalyst, the resultant solutions were analyzed by liquid-phase ^{1}H NMR technique.

Although acetonitrile has been took as the solvent in the MTM reaction by homogeneous catalysis [47, 48], the stability has not been checked. First, the blank test for acetonitrile was checked (**Figure 3.6**), several peaks were observed at around 4.9 and 8.1 ppm, which were assigned to the hydrogen of

HCOH and hydroxyl hydrogen of HCOOH, revealing that these products were resultant from the reaction of acetonitrile with H_2O_2. As a result, acetonitrile is not stable in MTM reaction with H_2O_2 in the fundamental research. According to the reference [49], acetonitrile is easily reacted with H_2O_2 thorough chemiluminescence reaction, revealing the unstable characteristics.

Similarly, methyl hydrogen of MeOH (3.4), proton of HCOH (4.9 ppm) and hydroxyl hydrogen of HCOOH (8.1 ppm) were also observed in the blank test using ethanol as solvent (**Figure 3.7**). Thus, ethanol is also not suitable applied as solvent in MTM reaction with H_2O_2.

However, when sulfolane was employed as solvent, no peaks were newly observed after the blank test (**Figure 3.8**), indicating that sulfolane was stable under this reaction condition. According to the reference [50], sulfolane is a dipolar aprotic, very stable and water-soluble industrial solvent. To the best of our knowledge, there has been still no open report on its application in MTM reaction with H_2O_2. The ^{1}H-NMR spectra of liquid phase solution after MTM reaction with H_2O_2 over FS(T)15 are presented in **Figure 3.9**. These signals ascribed to hydrogen of CH_3OH, HCOH and HCOOH proved the reaction between CH_4 and H_2O_2 in both sulfolane and H_2O.

3.3.2.2 The influence of reaction conditions

In the section the effects of reaction conditions such as reaction temperature, methane pressure, reaction time, H_2O_2 amount and catalyst amount on the reaction performance were investigated using sulfolane as solvent and FS(T)15 as catalyst.

3.3.2.1.1 Reaction temperature

The influence of reaction temperature on the performance of MTM reaction was investigated by varying temperature from 303 to 353 K, under the reaction conditions: 10 ml sulfolane, 3 Mpa CH_4, 27 mmol H_2O_2, 50 mg FS(T)15 as catalyst,1000 rpm, 2 h.

As shown in **Figure 3.10(a)**, the total liquid products productivity and HCOOH amount were increased by rising the reaction temperature from 303 to 353 K, indicating that more methane converted to the products. The yield amounts of MeOH and HCOH were firstly increased when the reaction temperature was enhanced from 303 to 323 K. However, part of MeOH and HCOH converted to HCOOH by increasing the temperature from 323 to 353 K, thus the amount of MeOH and HCOH were decreased with the temperature increasing from 323 to 353 K. Similar trends for the selectivity

of liquid products were demonstrated in **Figure 3.11(a)**. Meanwhile the H_2O_2 conversion was increased along with reaction temperature.

Temperature is a "double-edged sword". On one hand, the solubility of methane in sulfolane will be decreased by increasing temperature. According to Mather's research results, the solubility of methane in sulfolane was slightly decreased from 1229 mg/ 100 g sulfolane at 298 K and 3.36 Mpa to 1137 mg/ 100 g sulfolane at 343 K and 3.04 Mpa [51]. On the other hand, high temperature could improve the reaction activity for both catalysts and reactants due to the activation energy change [52], which has been verified by the increased conversions of H_2O_2 and methane. Actually, sulfolane is not stable over 353 K under the 3Mpa high pressure due to the decomposed property.

3.3.2.2.2 CH_4 pressure

A range of CH_4 pressure from 0.5 to 3 Mpa were investigated at the conditions: 10 ml sulfolane, 323 K, 27 mmol H_2O_2, 50 mg catalyst, 1000 rpm, 2 h. As expected, the productivity of total liquid products and each liquid product were increased along with CH_4 pressure. Among the liquid products, MeOH achieved the maximum growth rate, as shown in **Figure 3.10(b)**. Meanwhile **Figure 3.11(b)** displays the selectivity of liquid product and H_2O_2 conversion. MeOH gave the highest selectivity among the liquid products and the selectivity of every liquid product was relatively stable at different CH_4 pressure, except the slightly increase for HCOOH and decrease for MeOH and HCOH by increasing CH_4 pressure from 1.5 to 3 Mpa. In addition, H_2O_2 conversion was increased along with CH_4 pressure. It is clear that the CH_4 pressure mainly influences the solubility of methane, i.e. the reactant amount. According to Mather's paper, the solubility of methane in sulfolane was increased from 917 to 2460 mg/ 100 g sulfolane with increasing methane pressure from 2.37 to 7.44 Mpa at 313 K [51]. Obviously, high CH_4 pressure is beneficial to the reaction, taking into account the maximum pressure that our reaction device can endure, 3 Mpa of CH_4 is better for our research.

3.3.2.2.3 Reaction time

The effect of reaction time variations from 0.5 to 4 h on the reaction performance at a constant reaction condition: 10 ml sulfolane, 3 Mpa CH_4, 323 K, 27 mmol H_2O_2, 50 mg catalyst, 1000 rpm, was depicted in **Figure 3.10(c)** and **Figure 3.11(c)**. It was observed that the productivity of total and each

liquid product were increased by prolonging the reaction time, especially the productivity of HCOH, which was greatly increased by extending reaction time from 2 h to 4 h. Correspondingly, the selectivity of HCOH was increased while MeOH and HCOOH were decreased with the reaction time. The H_2O_2 conversion was relatively stable with reaction time varying. HCOH was reported as the oxidation product of MeOH [53]. But according to the Chadwick, HCOH comes from the intermediate MeOOH [46], which was closer to our research results. As the oxidative production of HCOH [54], HCOOH showed lower selectivity than Hutchings group [1, 4] and Chadwick group [46] due to the solvent effect. The possible reaction pathway in conversion of methane to methanol with H_2O_2 over catalyst in this study is showed in **Scheme 3.2**.

3.3.2.2.4 H_2O_2 amount

The production of the liquid products shows a maximum at 27 mmol with increasing H_2O_2 amount (**Figure 3.10(d)**). The total liquid products amount was decreased by increasing H_2O_2 amount from 27 to 38 mmol due to the total H_2O_2 converted amount reducing from 3.3 to 2.2 mmol. The possible reason is the liquid products converting to CO_2, which reported by Chadwick group in the aqueous system [46]. With the H_2O_2 amount change, methanol achieved the highest selectivity all the time, shown in **Figure 3.11(d)**.

3.3.2.2.5 Catalyst amount

Figure 3.10(e) shows the relationship between the amount of liquid products and catalyst mass under the conditions: 10 ml sulfolane, 3 Mpa CH_4, 323 K, 27 mmol H_2O_2, 1000 rpm, 2 h. As the catalyst amount rose from 10 to 100 mg, the amount of the total and each liquid products, and the hydrogen peroxide conversion were increased. MeOH attained the highest selectivity all the time, the selectivity of MeOH was reduced and the selectivity of HCOH and HCOOH were increased along with the catalyst amount, as shown in **Figure 3.11(e)**. In general, more catalyst can provide more active site, thus produce more products.

3.3.2.2.6 Mixed solvent

According to the Mather's literature, sulfolane is rarely brought into play alone but in admixture

with another solution [55]. The use of mixed solvents is an attractive alternative to either the solvent effect or the economic benefit and environment protection. Sulfolane-water mixed solvent is extensively applied in the lithium batteries [56] and extraction agent in the petrochemical industry [57]. Here, the performance of aqueous sulfolane with the volume content range from 0 to 100 vol.% were investigated. **Figure 3.12(a)** shows the influence of the sulfolane content on the reaction performance. When pure distilled water (0 vol.% of sulfoalne) was individually used as solvent, the lowest MeOH(12.2 μmol) and HCOH (0 μmol), while the highest HCOOH (462.5 μmol) amount were obtained. The productivity of the total liquid products and MeOH were increased by increasing the sulfolane content from 0 to 50 vol.%. Continually increasing the sulfolane content from 50 to 100 vol.%, the productivity of the total liquid products and MeOH were decreased. Interestingly, the productivity of HCOH and HCOOH display obvious and opposite regularity along with the sulfolane content, increase and decrease, respectively. The selectivity of the liquid products were consistent with the productivity. The conversion of H_2O_2 was decreased with the sulfolane content.

The highest H_2O_2 amount was consumed using H_2O as solvent, attained the highest HCOOH amount but the lowest productivity of MeOH and HCOH. In addition, when 50 vol.% sulfolane was used as solvent, the amount of consumed H_2O_2 was reduced a half compared with that of H_2O, and also the productivity of the HCOOH was decrease 3 times, but the productivity of MeOH was extremely increased. Finally, H_2O_2 converted in a minimum amount in sulfolane, but the productivity of HCOH was significantly increased compared with those of in H_2O and 50 vol.% sulfolane. The abovementioned results can be described in **Figure 3.12(b)**, which illustrated the importance of the solvent on the selectivity of product. The interesting phenomenon could be explained with the solvent effect. On the one hand, sulfolane possesses the feature of temporary combination of hydroxyl, which has been reported in other systems [58]. In Balducci's research, the selectivity of phenol in sulfolane is twice than that of other solvents, because the temporary formation of phenol-sulfolane complex prevents the production of by-products [59]. Murata *et al.* also has reported that sulfolane is effective for improving phenol selectivity on oxidation of benzene with oxygen and acetic acid on palladium catalyst [60]. One the other hand, water is a protic solvent, which could provide proton, while sulfolane is an aprotic solvent, which is difficult to provide proton. Hydrogen peroxide has an interesting chemistry because of its ability to function as oxidant as well as a reductant in both acid and alkaline

solutions, indicating that protic solvent is beneficial to H_2O_2 convert. It is the probably reason that H_2O_2 showed the highest conversion in water and the lowest conversion in sulfolane.

Actually, the excellent ability of sulfolane-water solution has been revealed in the literatures. Stewart and co-workers have reported the drastic increase in the effective basicity of hydroxide ion, as a result of the solvents' inability to effectively drastic increase in the hydrate such small ion [61]. In other words, sulfolane is a good solvent for improving methane solubility because of "the law of similar mutual solubility" but bad for H_2O_2 decomposition due to the aprotic nature. However, water has the opposite characteristics: low methane solubility and beneficial for H_2O_2 decomposition because of the protic nature. The aqueous sulfolane solvent combines the advantages and avoids the shortcomings of both water and sulfolane.

3.3.2.3 The catalytic performance over FS(T)*x* and FS(TN)*y* catalysts in MTM reaction

Thus prepared zeolites were applied as catalysts for the MTM reaction under the optimized reaction conditions. The catalytic results of the FS(T)*x* and FS(TN)*y* catalysts are summarized in **Table 3.4**. When *x* was decreased from 100 to 15, the productivity of total liquid products and MeOH were increased for both FS(T)*x* and FS(TN)*y* catalysts, due to the increase of the active Fe species with Fe content. Meanwhile, the H_2O_2 conversion for both FS(T)*x* and FS(TN)*y* catalysts were increased along with Fe content. The selectivity of MeOH for FS(T)*x* and FS(TN)*y* were more than 85% and 83%, respectively. In particular, the selectivity of MeOH for FS(T)100 was high to reach 94% at the expense of the total production. At the same time, the H_2O_2 efficiency was involved and calculated using the molar amount of total liquid products dividing by the molar amount of hydrogen peroxide consumed. Basically the H_2O_2 efficiency for both FS(T)*x* and FS(TN)*y* catalysts were increased with Fe content and the value was lower than 25%, suggesting that byproducts such as CO_2 was produced in the gas phase or useless self-decomposition of H_2O_2. Compared with the reaction performance, it was obvious to see the difference between FS(T)*x* and FS(TN)*y* catalysts. FS(T)*x* zeolites achieved higher productivity of the total liquid products and MeOH than FS(TN)*y* ones under the same Si/Fe molar ratio in the synthesis gel. Meanwhile, the H_2O_2 conversion of FS(T)*x* samples were slightly higher than that of FS(TN)*y*, probably indicating the higher CH_4 conversion of FS(T)*x*.

Association the total Fe content, different Fe species and amount, and the productivity of MeOH and total liquid products, interesting and obvious difference were noticed. As shown in **Figure 3.13(a)**, the change of the different Fe species content was as a function of the total Fe content for FS(T)*x* catalysts. In particular the isolated and oligomeric Fe species, and larger Fe clusters on the extra

framework, corresponding Fe content were proportional to the total Fe content, but the slope of the isolated and oligomeric Fe species was higher than that of the larger Fe clusters. The proportion of the framework Fe was decreased with the total Fe content in the FS(T)*x* catalysts, indicating that the Fe species and content were affected by the Fe distribution. As for the bulk iron oxide in the FS(T)*x* catalysts, it appeared only when *x* reached as low as 15. **Figure 3.13(b)** shows the relationship between the total Fe content and the different Fe species content in the FS(TN)*y* catalysts. At the low total Fe content (0−2.0 wt.%), there were only framework Fe, and isolated and oligomeric Fe species on the extra framework. Because the positive charge like TPA^+ and Na^+ were located in the intersection and the channels, Fe can be separated in and /or around the corresponding position. Positive charge was enough to balance the Fe species on the low Fe content condition. It was not easy to aggregation due to the well separation. While at the high Fe content (3.0−6.0 wt.%), other Fe species, i.e. larger Fe clusters and bulk iron oxide, appeared due to the Fe ions gathered in a more concentrated place in the corresponding as made samples. The proportion of framework Fe was decreased, and the isolated and oligomeric Fe species became the mainstream.

Figure 3.14 summaries the product amount as a function of the total Fe content in both the FS(T)*x* and FS(TN)*y* samples. The amount of both MeOH and the total liquid products for FS(T)*x* samples were higher than those of FS(TN)*y* catalysts under the similar total Fe content, indicating the higher activity for FS(T)*x* samples. As for the FS(T)*x* catalysts, the slope was high in the low Fe content, but decreased with the total Fe content increasing (**Figure 3.14(a)**). It implied that the proportion of Fe species with no or low activity was increase, but the active Fe amount was increased as well due to the increase of total Fe content. While for FS(TN)*y* samples, the slope was basically unchanged with the total Fe content, suggesting that the proportion of active Fe species was low and unchanged, as shown in **Figure 3.14(b)**.

The change in the product amount as a function of the Fe content of the isolated and oligomeric Fe species on the extra framework in the FS(T)*x* and FS(TN)*y* catalysts are shown in **Figure 3.15**, clearly indicating that the product amount was correlated with the content of isolated and oligomeric extra framework Fe species. Thus, the formation of isolated and oligomeric extra framework Fe species in the **MFI** structure is vital for achieving a high yield of methanol. Interestingly, it took more than two times Fe content of the isolated and oligomeric Fe species on the extra framework for FS(TN)*y* samples to achieve the similar product amount than those of FS(T)*x* catalysts. Perhaps it means the Fe species on the channels for FS(TN)*y* samples with low or no activity in the MTM reaction.

3.4. Conclusions

The conversion of methane to methanol over Fe-containing MFI zeolites under mild conditions has been investigated. Fe-silicalite-1 zeolites were directly synthesized using TPAOH as OSDA with or without Na cations in the synthesis gel. The physicochemical properties, especially the states of Fe species was characterized. Fe-silicalite-1 zeolites synthesized without Na cations displayed more uniform distribution for each kinds of Fe species and higher proportion of framework Fe than those synthesized with Na cations. The impact of solvent on the reaction performance was investigated. We firstly found that sulfolane was the best one among the solvents used in terms of the improvement in the production of methanol and its stability during the reaction. Finally, the effects of various reaction parameters, such as reaction temperature, CH_4 pressure, reaction time, catalyst amount and the amount of H_2O_2 were optimized. Furthermore, the use of mixture of sulfolane-water solvent with an appropriate proportion led to an extremely high methanol production with a high selectivity. Generally Fe-silicalite-1 zeolites synthesized using TPAOH as OSDA without Na cations (FS(T)*x*) showed better catalytic performance than those with Na cations (FS(TN)*y*). Under the optimal condition, FS(T)15 zeolite displayed the highest methanol yield of 947.8 μmol with the selectivity of 85% in the aqueous sulfolane solvent.

References

[1] C. Hammond, I. Hermans, N. Dimitratos, N. Dimitratos, J. A. Lopez-Sanchez, R. L. Jenkins, G. Whiting, S. A. Kondrat, M. H. ab Rahim, M. M. Forde, A. Thetford, H. Hagen, E. E. Stangland, J. M. Moulijn, S. H. Taylor, D. J. Willock, G. J. Hutchings, ACS Catal., 3 (2013) 1835.
[2] M. Ranocchiari, M. Ravi, J. A. van Bokhoven, Angew. Chem. Int. Ed., (2017).
[3] T. Xiao, A. P. E. York, M. L. H. Green, Top Catal., 22 (2003) 345.
[4] M. M. Forde, C. Hammond, R. Rahim, A. Thetford, Q. He, R. L. Jenkins, N. Dimitratos, J. A. Lopez-Sanchez, N. F. Dummer, D. M. Murphy, A. F. Carley, S. H. Taylor, D. J. Willock, E. E. Stangland, H. Hagen, J. Kang, C. J. Kiely, G. J. Hutchings, Angew. Chem. Int. Ed., 51 (2012) 5129.
[5] N. R. Hunter, H. D. Gesser, C. B. Prakash Chem. Rev., 85 (1985) 235.
[6] D. Palagin, V. L. Sushkevich, M. Ranocchiari, J. A. van Bokhoven, Science 356 (2017) 523.
[7] M. A. C. Markovits, S. Grundner, G. Li, M. Tromp, E. A. Pidko, E. J. M. Hensen, A. Jentys, M. Sanchez-Sanchez, J. A. Lercher, Nat Commun, 6 (2015) 7546.
[8] Y. Shiota, K. Yoshizawa, J. Am. Chem. Soc., 128 (2006) 9873.
[9] I. Onal, M. F. Fellah, J. Phys. Chem. C, 114 (2010) 3042.
[10] Y. Wang, X. X. Wang, Q. H. Tang, Q. Guo, Q. H. Zhang, H. L. Wan, J. Catal., 217 (2003) 457.
[11] A. S. Bayu, K. K. Yuni, S. Riwandi, F. H. Russell, Indonesian Journal of Chemistry, 15 (2015) 263.
[12] C. D. Hamill, T. Sheppard, A. Goguet, D. W. Rooney, J. M. Thompson, Chem. Commun., 50 (2014) 11053.
[13] P. J. Smeets, M. H. Groothaert, B. F. Sels, B. A. Jacobs, R. A. Schoonheydt, J. Am. Chem. Soc., 127 (2005) 1394.
[14] M. V. Parfenov, E. V. Starokon, S. S. Arzumanov, L.V. Pirutko, A. G. Stepanov, G. I. Panov, J. Catal., 300 (2013) 47.
[15] D. J. Taube, R. A. Periana, S. Gamble, H. Taube, T. Satoh, H. Fujii, Science 28 (1998) 560.
[16] O. Mirinov, R. A. Periana, D. J. Taubeb, S. Gamble, Chem. Commun., 20 (2002) 2376.
[17] W. P. Deng, D. Yuan, Q. H. Zhang, Y. Wang, Adv. Synth. Catal., 349 (2007) 1199.
[18] R. D. Armstrong, J. Xu, G. Shaw, N. F. Dummer, S. J. Freakley, S. H. Taylor, G. J. Hutchings, Catal. Today, 270 (2016) 93.
[19] I. Hermans, C. Hammond, N. Dimitratos, ChemCatChem, 7 (2015) 434.
[20] M. M. Forde, M. H. A. Rahim, R. L. Jenkins, C. Hammond, Q. He, N. Dimitratos, J. A. Sopez-Sanchez, A. F. Carley, S. H. Taylor, D. J. Willock, D. M. Murphy, C. J. Kiely, G. J. Hutchings, Angew Chem, 52 (2013) 1280.
[21] B. D. Armstrong, M. H. A. Rahim, C. Hammond, N. Dimitratos, S. J. Freakley, M. M. Forde, D. J. Morgan, G. Lalev, R. L. Jenkins, J. A. Lopez-Sanchez, S. H. Taylor, G. J. Hutchings, Catal. Sci. Technol., 6 (2016) 3410.
[22] N. Agarwal, S. J. Freakley, R. U. McVicker, S. M. Althahban, N. Dimitratos, Q. He, D. J. Morgan, R. L. Jenkins, D. J. Willock, S. H. Taylor, C. J. Kiely, G. J. Hutchings, Science, 358 (2017) 223.
[23] M. Schwidder, M. S. Kumar, W. Grünert, A. Brückner, W. Grünert, A. Brückner, J. Catal., 227 (2004) 384.
[24] L. Meng, X. Zhu, E. J. M. Hensen, ACS Catal., 7 (2017) 2709.
[25] M. He, J. Zhang, X. L. Sun, B. H. Chen, Y. G. Wang, J. Phys. Chem. C, 120 (2016) 27422.
[26] E. J. M. Hensen, Q. Zhu, M. M. R. M. Hendrix, A. R. Overweg, P. J. Kooyman, M. V. Sychev, R.

A. van Santena, J. Catal., 221 (2004) 560.
[27] A. Zecchina, M. Rivallan, G. Berlier, C. Lamberti, G. Ricchiardi, Phys. Chem. Chem. Phys., 9 (2007) 3483.
[28] H. Mochizuki, T. Yokoi, S. Namba, J. N. Kondo, T. Tatsumi, J. Phys. Chem. C, 119 (2015) 15303.
[29] T. Yokoi, H. Mochizuki, T. Biligetu, Y. Wang, T. Tatsumi, Chem. Lett., 46 (2017) 798.
[30] T. Biligetu, Y. Wang, T. Nishitoba, R. Otomoa, S. Park, H. Mochizuki, J. N. Kondo, T. Tatsumi, T. Yokoi, J. Catal., 353 (2017) 1.
[31] C. Pabitra, Q. Thalia, Molecular Catalysis, 431 (2017) 9.
[32] D. J. Taube, R. A. Periana, E. R. Evitt, Science, 259 (1993) 15.
[33] A. C. Rosenzweig, Nature, 518 (2015) 309.
[34] N. Mølle, Z. H. Duan, J. Greenberg, H. Weare, Geochim Cosmochim Acta, 56 (1992) 1451.
[35] S. J. Wang, T. Li, C. S. Yu, Y. C. Ma, K. L. Li, L. W. Lin, Appl. Catal., A, 398 (2011) 150.
[36] R. Pilar, P. Sazama, L. Mokrzycki, A. Vondrova, D. Kaucky, J. Plsek, S. Sklenak, P. Stastny, P. Klein, Appl. Catal., B, 189 (2016) 65.
[37] D. Bulushev, I. Yuranov, A. Renken, L. Kiwiminsker, J. Catal., 227 (2004) 138.
[38] I. Hermans, C. Hammond, N. Dimitratos, N. Dimitratos, J. A. Lopez-Sanchez, R. L. Jenkins, G. Whiting, S. A. Kondrat, M. H. ab Rahim, M. M. Forde, A. Thetford, H. Hagen, E. E. Stangland, J. M. Moulijn, S. H. Taylor, D. J. Willock, G. J. Hutchings, ACS Catal., 3 (2013) 1835.
[39] C. Lamberti, G. Berlier, M. Rivallan, G. Mul, Phys. Chem. Chem. Phys., 12 (2010) 358.
[40] G. Spoto, G. Berlier, P. Fisicaro, S. Bordigaa, A. Zecchinaa, E. Giamello, C. Lamberti, Microchem J, 71 (2002) 101.
[41] H. Knözinger, K. Hadjiivanov, B. Tsyntsarski, Catal. Lett., 62 (1999) 35.
[42] C. Lamberti, G. Berlier, M. Rivallan, G. Mul, G. Spoto, S. Bordiga, G. Ricchiardi, P. Fisicaro, A. Zecchina, I. Rossetti, E. Selli, L. Forni, E. Giamello, C. Lamberti, J. Catal., 208 (2002) 64.
[43] A. Zecchina, G. Spoto, G. Berlier, S. Bordiga, M. G. Clerici, L. Basini, J. Mol. Catal. A: Chem, 158 (2000) 107.
[44] F. Hei, G. Wu, N. Zhang, N. Guan, L. Li, W. Grünert, Appl. Catal., A, 468 (2013) 230.
[45] Y. Fereydoon, R. Mohammad, Fuel, 181 (2016) 537.
[46] C. J. Richard, S. Al-Shihri, D. Chadwick, ChemCatChem, 9 (2017) 1276.
[47] G. V. Nizova, G. Süss-Fink, S. Stanislas, G. B. Shul'pin, J. Mol. Catal., A: Chem, 130 (1998) 163.
[48] G. V. Nizova, G. B. Shul'pin, Y. N. Kozlov, L. G. Cuervo, G. Süss-Fink, Adv. Synth. Catal., 346 (2004) 317.
[49] J. Z. Lu, C. Lau, M. Morizono, K. Ohta, M. Kai, Anal Chim Acta, 503 (2004) 235.
[50] U. Tilstam, Org. Process. Res. Dev., 16 (2012) 1273.
[51] R. D. Deshmukh, F. Y. Jou, F. D. Otto, A. E. Mather, Fluid Phase Equilibria, 56 (1990) 313.
[52] B. Michalkiewicz, Chem Pap, 59 (2005) 403.
[53] B. Ensing, F. Buda, M. C. M. Gribnau, E. J. Baerends, J. Am. Chem. Soc., 126 (2004) 10236.
[54] J. H. Payne, F. H. Shipley, J. Am. Chem. Soc., 53 (1931) 1973.
[55] F. Y. Jou, R. D. Deshmukh, F. D. Otto, A. E. Mather, Fluid Phase Equilibria, 56 (1990) 313.
[56] T. Ueda, M. Hojo, E. Ueno, T. Hamasaki, D. Fujimura, Bull Chem. Soc. Jpn., 79 (2006) 751.
[57] M. N. Lotfollahi, J. Mahmoudi, Korean J. Chem. Eng., 27 (2010) 214.
[58] W. Bradford, R. S. Drago, R. L. Carlson, J. Am. Chem. Soc., 85 (1963) 3125.
[59] L. Balducci, D. Bianchi, R. Bortolo, R. D'Aloisio, M. Ricci, R. Tassinari, R. Ungarelli, Angew. Chem. Int. Ed., 115 (2003) 5087

[60] Y. Y. Ryu, M. Kazuhisa, I. Megumu, Catal. Lett., 102 (2005) 143.
[61] J. D. V. Dyke, R. Stewart, Can J. Chem., 50 (1972) 1992.

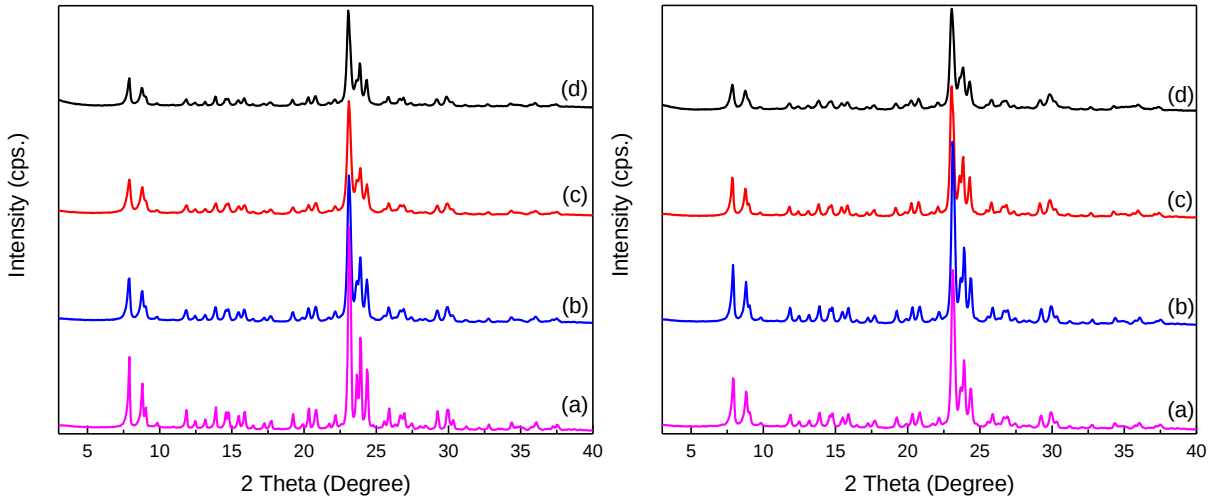

Figure 3.1 XRD patterns of the as-synthesized samples: left: (a) FS(T)100, (b) FS(T)50, (c) FS(T)25, (d) FS(T)15, and right: (a) FS(TN)100, (b) FS(TN)50, (c) FS(TN)25, (d) FS(TN)15.

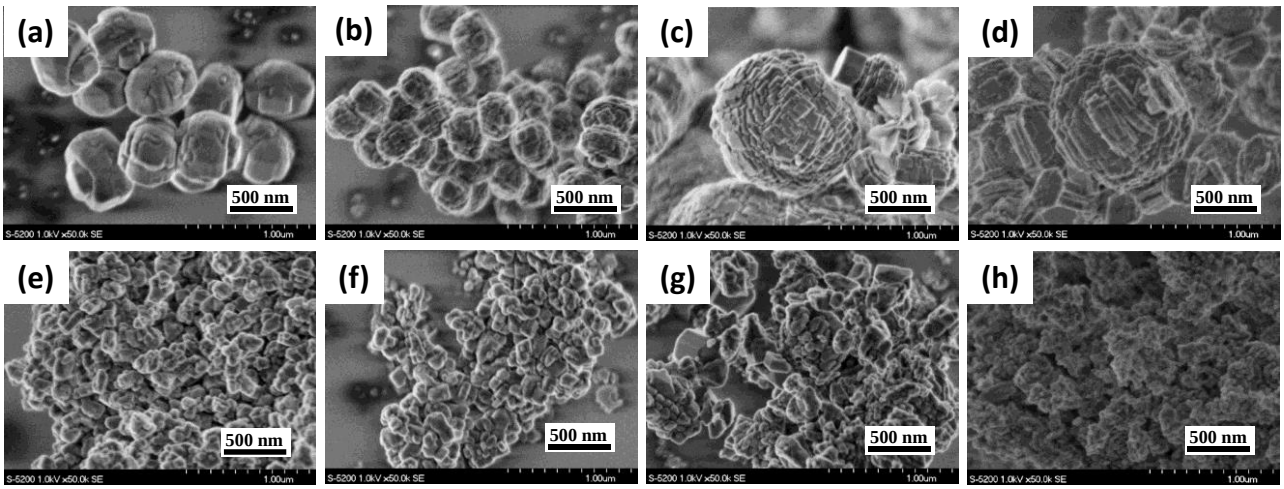

Figure 3.2 FE-SEM images of (a) FS(T)100, (b) FS(T)50, (c) FS(T)25, (d) FS(T)15, (e) FS(TN)100, (f) FS(TN)50, (g) FS(TN)25 and (h) FS(TN)15.

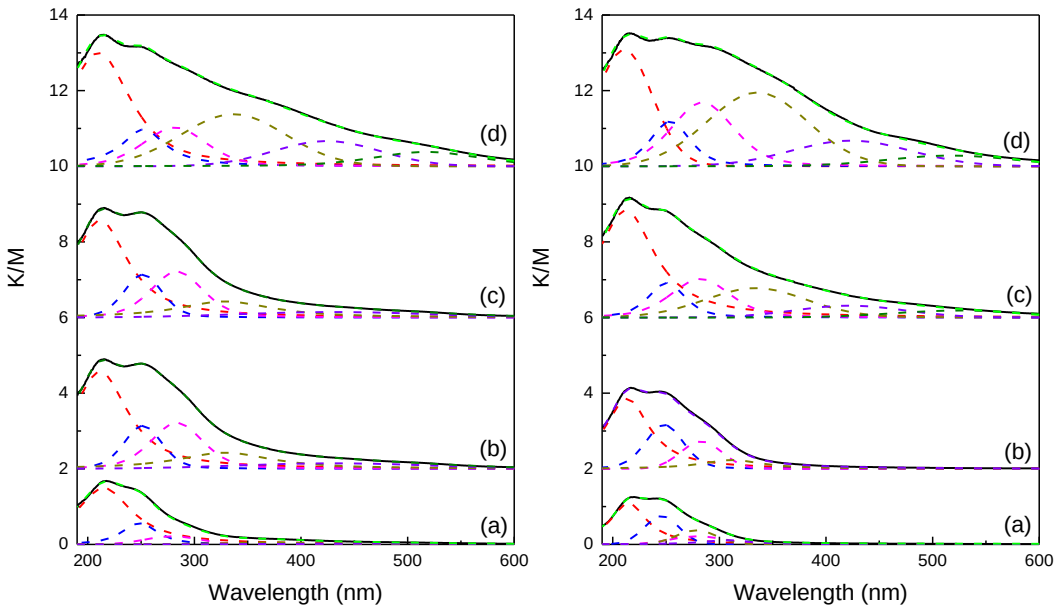

Figure 3.3 UV-vis spectra of left: (a) FS(T)100, (b) FS(T)50, (c) FS(T)25, (d) FS(T)15, and right: (a) FS(TN)100, (b) FS(TN)50, (c) FS(TN)25, (d) FS(TN)15.

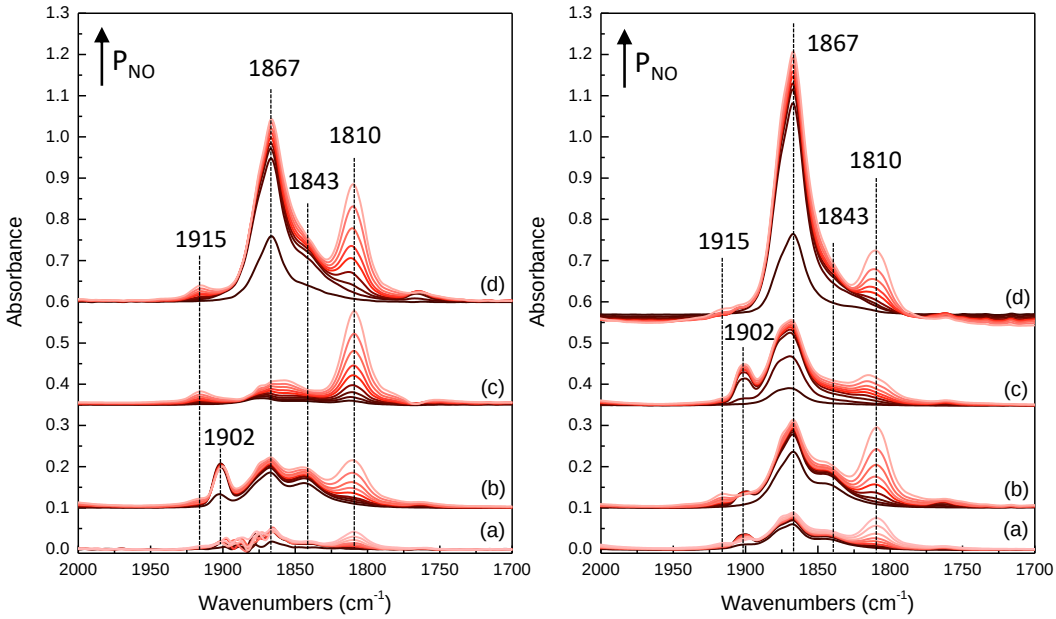

Figure 3.4 NO adsorbed FT-IR spectra of left: (a) FS(T)100, (b) FS(T)50, (c) FS(T)25, (d) FS(T)15, and right: (a) FS(TN)100, (b) FS(TN)50, (c) FS(TN)25, (d) FS(TN)15.

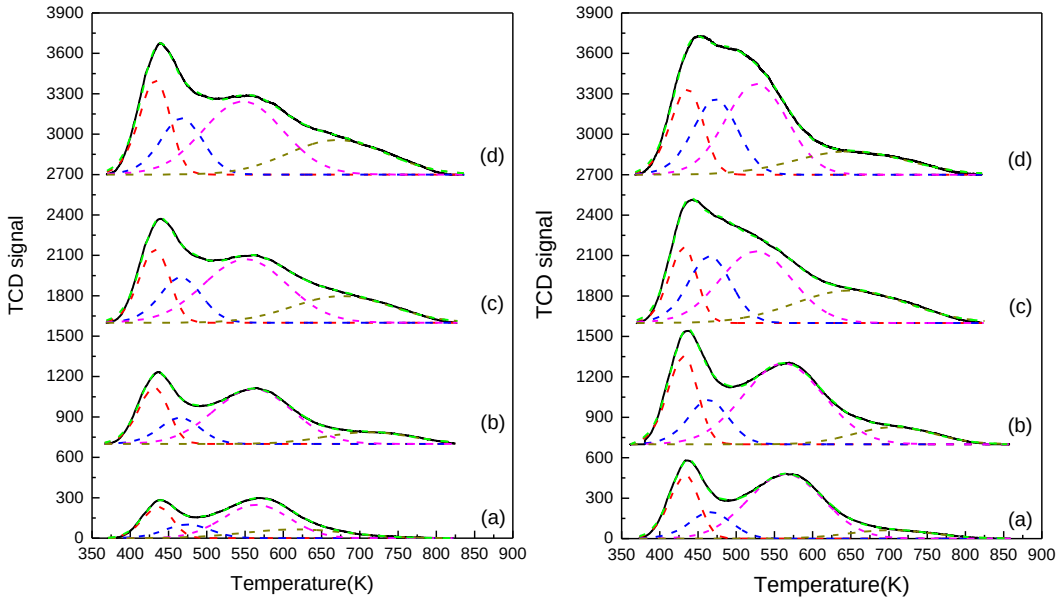

Figure 3.5 NH_3-TPD spectra of left: (a) FS(T)100, (b) FS(T)50, (c) FS(T)25, (d) FS(T)15, and right: (a) FS(TN)100, (b) FS(TN)50, (c) FS(TN)25, (d) FS(TN)15.

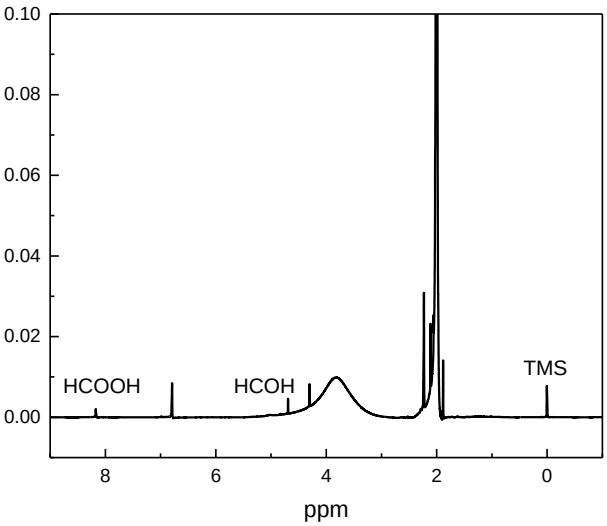

Figure 3.6 ^{1}H-NMR spectrum of blank test using acetonitrile as solvent (no CH_4 as reactant) over FS(T)15 catalyst, mesitylene was used as internal standard and CD_3CN/ TMS mixture was used as chemical shift calibrator.

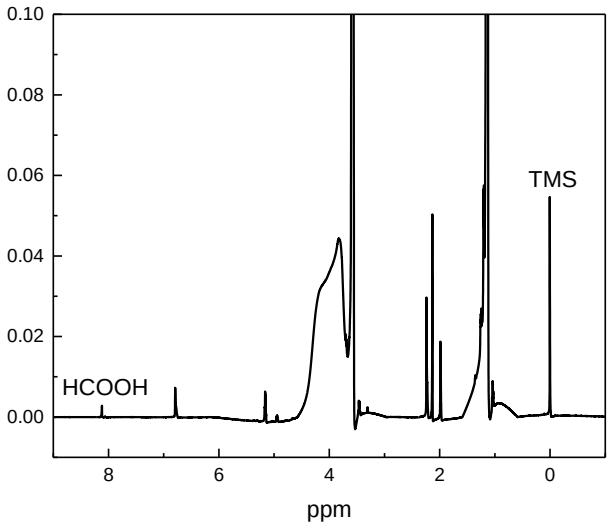

Figure 3.7 ^{1}H-NMR spectrum of blank test using ethanol as solvent (no CH_4 as reactant) over FS(T)15 catalyst, mesitylene was used as internal standard and CD_3CN/ TMS mixture was used as chemical shift calibrator.

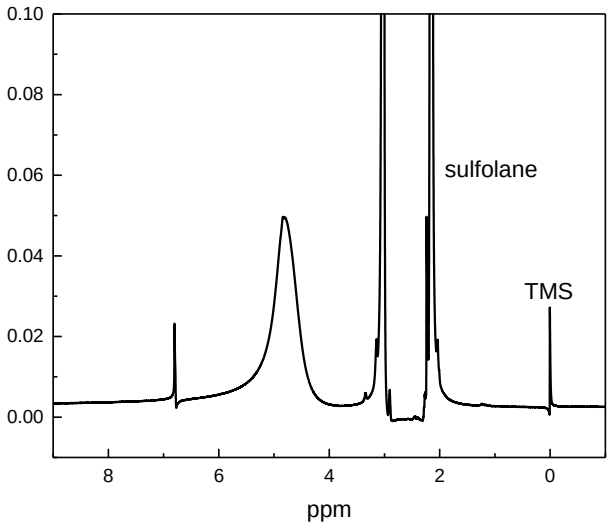

Figure 3.8 ^{1}H-NMR spectrum of blank test using sulfolane as solvent (no CH_4 as reactant) over FS(T)15 catalyst, mesitylene was used as internal standard and CD_3CN/ TMS mixture was used as chemical shift calibrator.

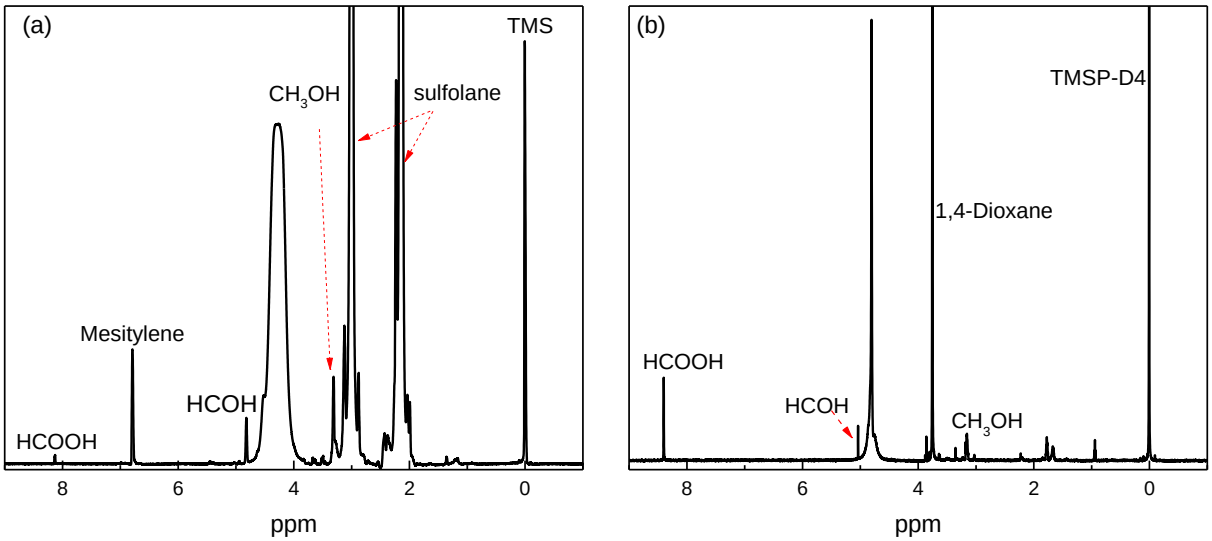

Figure 3.9 (a) ^{1}H-NMR spectrum of methane oxidation over FS(T)15 zeolite catalyst using sulfolane as solvent, mesitylene was used as internal standard and CD_3CN/ TMS mixture was used as chemical shift calibrator. (b) ^{1}H-NMR spectrum of methane oxidation over FS(T)15 zeolite catalyst using H_2O as solvent, 1,4-dioxane was used as internal standard and D_2O/TMSP-D4 mixture was used as chemical shift calibrator.

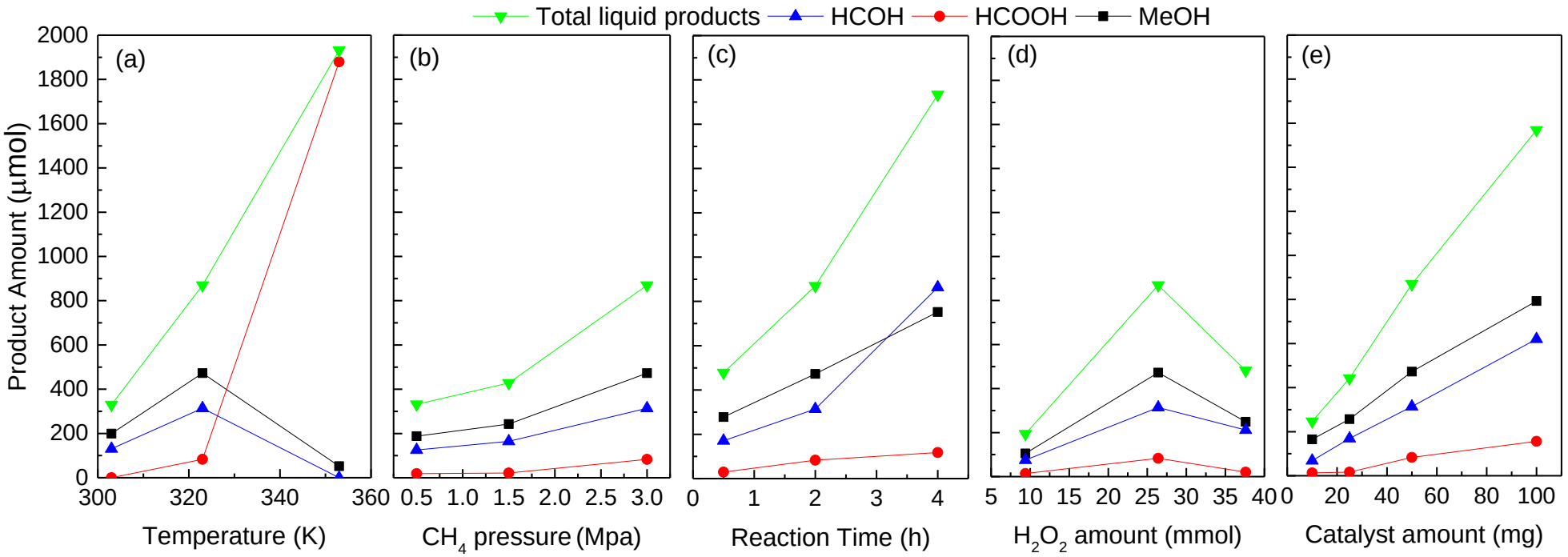

Figure 3.10 Changes of liquid product amount over FMD15 catalyst as a function of (a) temperature, (b) CH_4 pressure, (c) reaction time, (d) H_2O_2 amount, (e) catalyst amount. Reaction conditions: (a) 10 ml sulfolane, 50 mg FS(T)15, 27 mmol H_2O_2, 2 h, 3 Mpa CH_4. (b) 323 K, 10 ml sulfolane, 50 mg FS(T)15, 27 mmol H_2O_2, 2 h. (c) 323 K, 10 ml sulfolane, 50 mg FS(T)15, 27 mmol H_2O_2, 3 Mpa CH_4. (d) 323 K, 10 ml sulfolane, 50 mg FS(T)15, 2 h, 3 Mpa CH_4. (e) 323 K, 10 ml sulfolane, 27 mmol H_2O_2, 2 h, 3 Mpa CH_4.

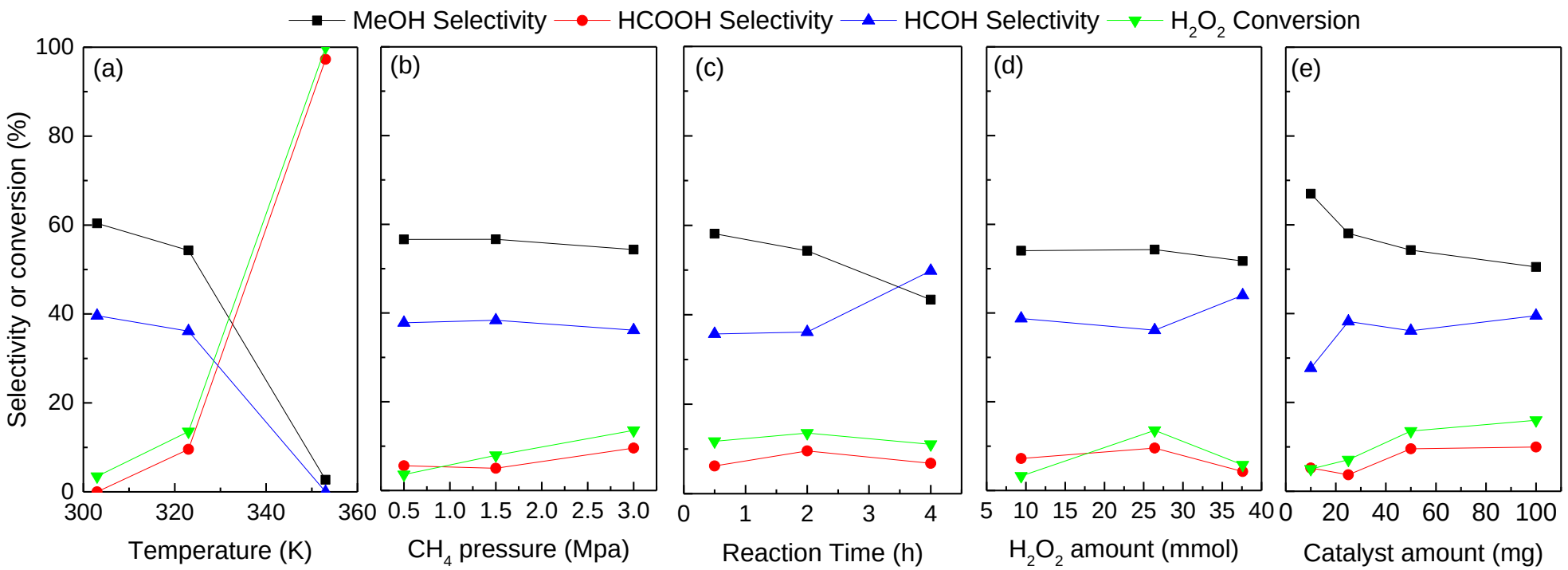

Figure 3.11 Changes of the selectivity of the liquid product and H_2O_2 conversion over FMD15 catalyst as a function of (a) temperature, (b) CH_4 pressure, (c) reaction time, (d) H_2O_2 amount, (e) catalyst amount. Reaction conditions: (a) 10 ml sulfolane, 50 mg FS(T)15, 27 mmol H_2O_2, 2 h, 3 Mpa CH_4. (b) 323 K, 10 ml sulfolane, 50 mg FS(T)15, 27 mmol H_2O_2, 2 h. (c) 323 K, 10 ml sulfolane, 50 mg FS(T)15, 27 mmol H_2O_2, 3 Mpa CH_4. (d) 323 K, 10 ml sulfolane, 50 mg FS(T)15, 2 h, 3 Mpa CH_4. (e) 323 K, 10 ml sulfolane, 27 mmol H_2O_2, 2 h, 3 Mpa CH_4.

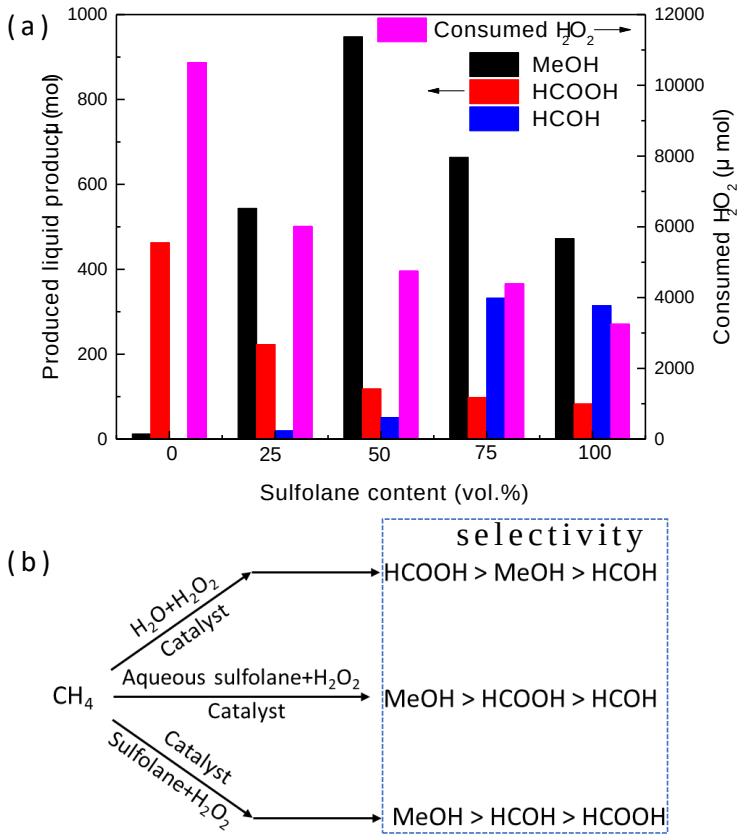

Figure 3.12 (a) The amount of liquid product and consumed H_2O_2 under different sulfolane content (b) possible liquid product species distribution under different sulfolane content. Reaction condition: 323 K, 50 mg FS(T)15, 27 mmol H_2O_2, 2 h, 3 Mpa CH_4.

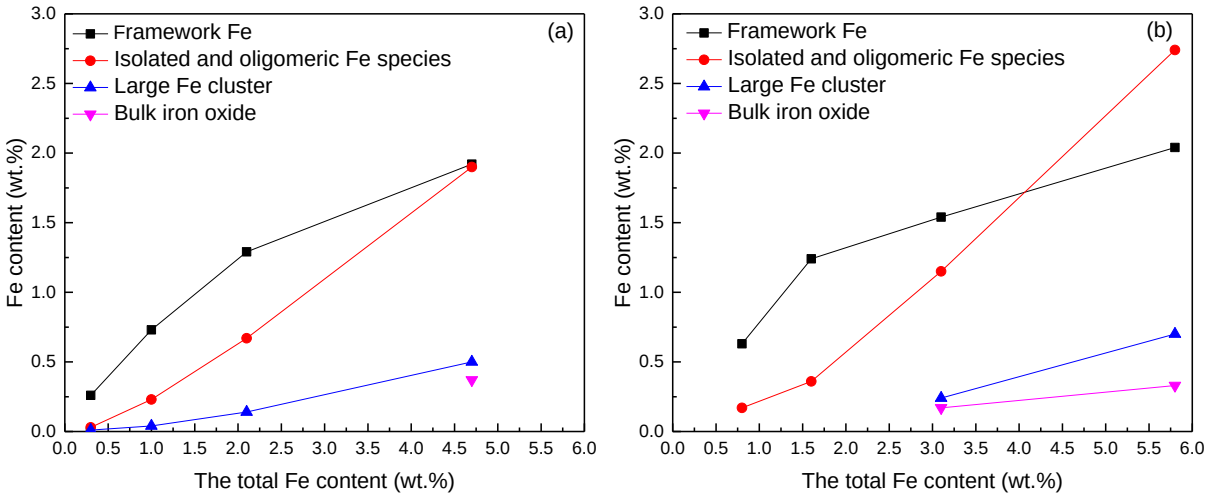

Figure 3.13 Fe content change of different Fe species as a function of the total Fe content for (a) FS(T)*x* and FS(TN)*y* catalysts.

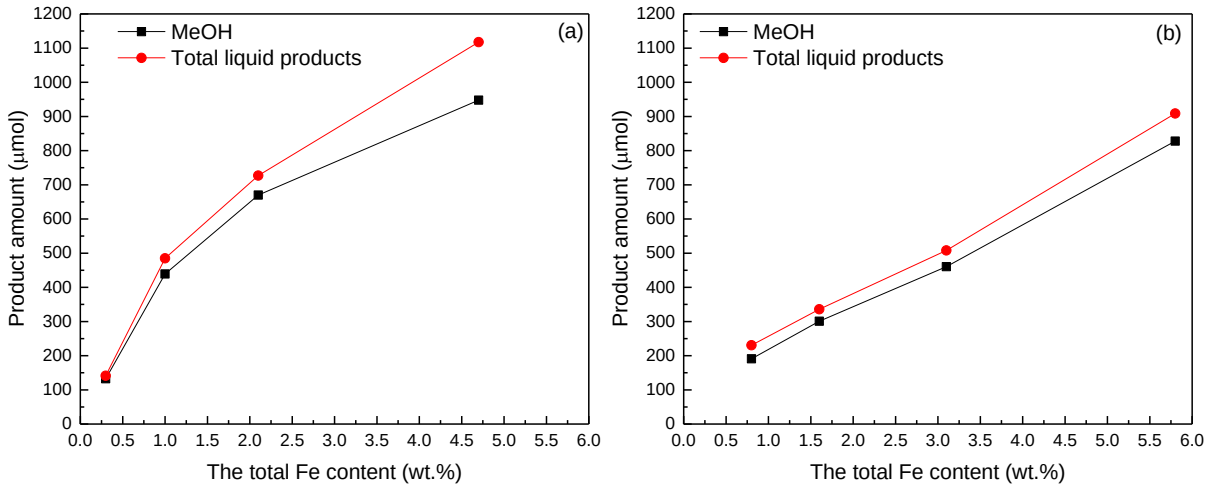

Figure 3.14 Change of the product amount as a function of the total Fe content for (a) FS(T)*x* and (b) FS(TN)*y* catalysts. Reaction conditions: 10 ml 50 vol.% sulfolane, 323 K, 50 mg catalysts, 27 mmol H_2O_2, 2 h, 3 Mpa CH_4.

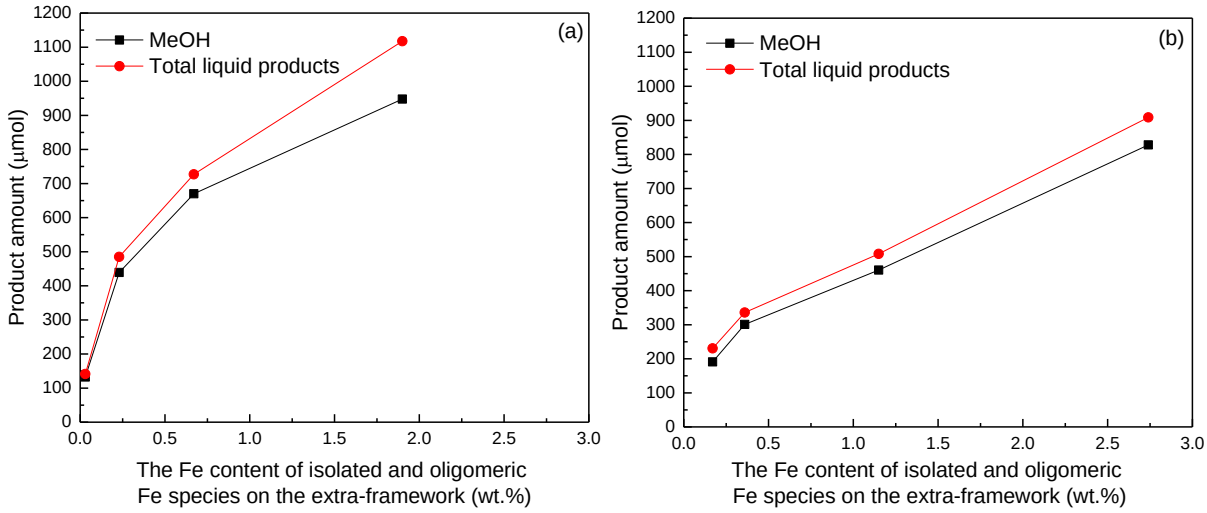

Figure 3.15 Change of the product amount as a function of the Fe content of the isolated and oligomeric Fe species on the extra framework for (a) FS(T)*x* and (b) FS(TN)*y* catalysts. Reaction conditions: 10 ml 50 vol.% sulfolane, 323 K, 50 mg catalysts, 27 mmol H_2O_2, 2 h, 3 Mpa CH_4.

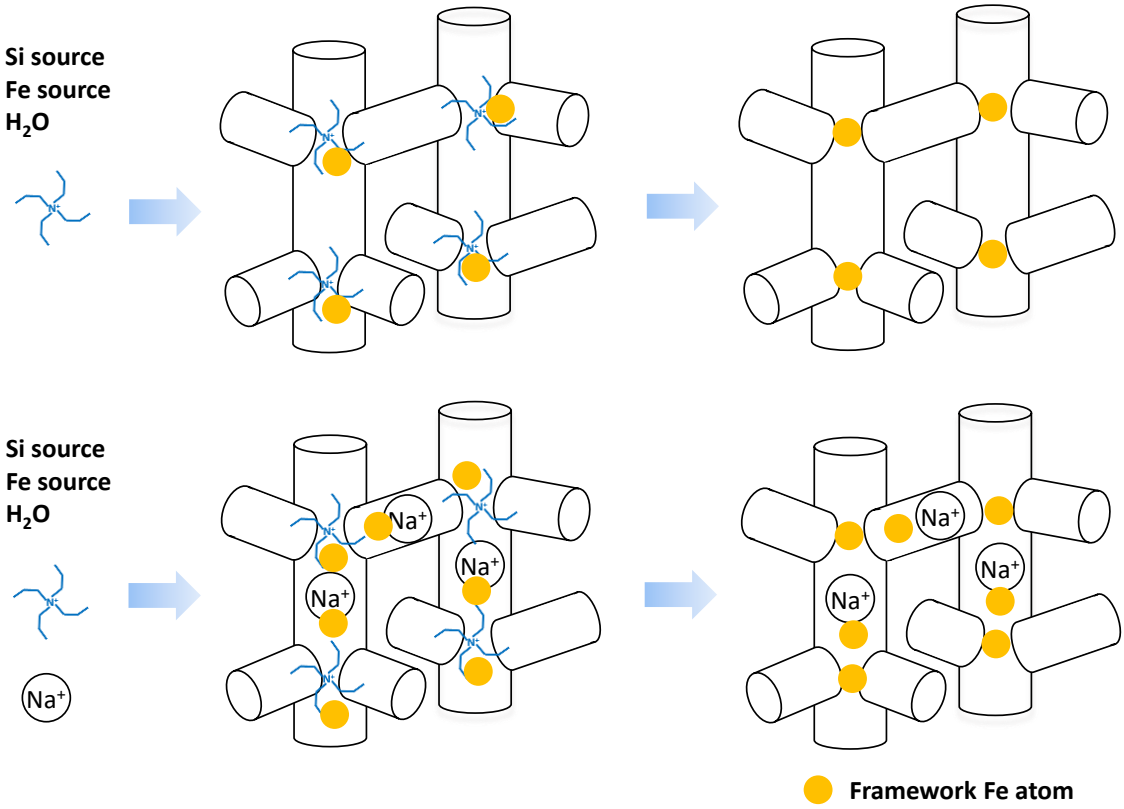

Scheme 3.1 Strategy for preferential distribution of the Fe atoms in intersection and/ or channels of the MFI framework.

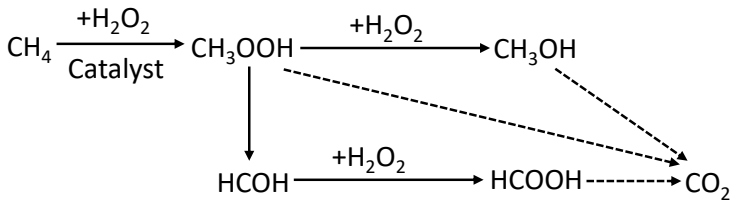

Scheme 3.2 Assumed reaction pathway in conversion of methane to methanol with H_2O_2 over catalyst.

Table 3.1 Physicochemical characteristics of the FS(T)*x* and FS(TN)*y* catalysts.

Samples	In gel	In product [a]		S_{BET}	S_{EXT}	V_{Total}	V_{Micro}
	Si/Fe		Fe (wt.%)	(m^2g^{-1})[b]	(m^2g^{-1})[c]	(cm^3g^{-1})[d]	(cm^3g^{-1})[e]
FS(T)100	100	306	0.3	440	145	0.39	0.16
FS(T)50	50	95	1.0	434	157	0.45	0.16
FS(T)25	25	44	2.1	430	142	0.37	0.17
FS(T)15	15	19	4.7	474	183	0.46	0.18
FS(TN)100	100	114	0.8	455	190	0.61	0.14
FS(TN)50	50	59	1.6	457	196	0.58	0.15
FS(TN)25	25	29	3.1	400	134	0.48	0.15
FS(TN)15	15	15	5.8	406	196	0.76	0.13

[a] Si/Fe was determined by ICP-AES analysis, Fe content was calculated by Si/Fe ratio.
[b] Specific surface areas of the catalysts were calculated using the Brunauer-Emmett-Teller (BET) equation on the N_2 adsorption isotherms.
[c] External surface area (S_{EXT}) of the catalysts were calculated by the *t*-plot method based on the adsorption isotherms.
[d] Total pore volumes of the catalysts were calculated based on BET equation on the N_2 adsorption isotherms.
[e] Micropore volumes of the catalysts were calculated by the *t*-plot method based on the adsorption isotherms.

Table 3.2 Percentage of sub-band areas (I_1: λ< 250 nm, I_2: 250 <λ< 350 nm, I_3: 350 <λ< 450 nm, and I_4: λ>450 nm) derived by deconvoluting UV-vis spectra and corresponding Fe species content for the FS(T)*x* and FS(TN)*y* catalysts.

Samples	Framework Fe		Isolated and oligomeric Fe		Iron oxide clusters		Bulk iron oxides	
	I_1(%)	wt.%	I_2(%)	wt.(%)	I_3(%)	wt.%	I_4(%)	wt.%
FS(T)100	86.7	0.26	10.7	0.03	2.6	0.01	-	-
FS(T)50	73.0	0.73	23.3	0.23	3.6	0.04	-	-
FS(T)25	61.6	1.29	31.7	0.67	6.7	0.14	-	-
FS(T)15	40.9	1.92	40.4	1.90	10.7	0.50	7.9	0.37
FS(TN)100	78.7	0.63	21.3	0.17	-	-	-	-
FS(TN)50	77.3	1.24	22.7	0.36	-	-	-	-
FS(TN)25	49.8	1.54	37.0	1.15	7.8	0.24	5.5	0.17
FS(TN)15	35.1	2.04	47.3	2.74	12.0	0.70	5.6	0.33

Table 3.3 NH_3 adsorbed amount of the FS(T)*x* and FS(TN)*y* catalysts.

Samples	NH_3 adsorbed amount (mmol/g) / T_{max} (K)			
	LT		MT	HT
FS(T)100	0.04/436	0.03/474	0.10/565	0.04/615
FS(T)50	0.07/432	0.05/472	0.20/570	0.05/713
FS(T)25	0.10/433	0.09/470	0.25/568	0.12/683
FS(T)15	0.12/433	0.11/472	0.27/563	0.16/678
FS(TN)100	0.08/433	0.05/467	0.23/564	0.03/702
FS(TN)50	0.12/431	0.09/463	0.31/562	0.06/707
FS(TN)25	0.09/431	0.13/469	0.24/543	0.17/668
FS(TN)15	0.11/436	0.15/472	0.25/548	0.12/669

Table 3.4 Catalytic performance for the FS(T)*x* and FS(TN)*y* catalysts using mixed aqueous sulfolane (50 vol.% sulfolane) as reaction solvent for the direct oxidation of methane to methanol with H_2O_2.

Catalyst	Products(μmol)			Selectivity (%) [a]			H_2O_2	H_2O_2
	MeOH	HCOOH	HCOH	MeOH	HCOOH	HCOH	Conv. (%)[b]	Eff. (%)[c]
FS(T)100	133	9	0	94	6	0	7	8
FS(T)50	439	35	11	91	7	2	10	20
FS(T)25	670	28	29	92	4	4	15	19
FS(T)15	948	119	51	85	11	5	18	24
FS(TN)100	191	31	8	83	14	4	6	16
FS(TN)50	301	25	10	90	7	3	8	17
FS(TN)25	461	22	25	91	4	5	15	13
FS(TN)15	828	42	39	91	5	4	17	21

Reaction conditions: 323K, 10 ml 50 vol.% sulfolane, 50 mg catalyst, 27 mmol H_2O_2, 2 h, 3 Mpa CH_4.

[a] Each product selectivity= (moles of each product)*100/(moles of total liquid products).

[b] H_2O_2 conversion = (moles of H_2O_2 after reaction)*100/(initial moles of H_2O_2).

[c] H_2O_2 efficiency = (moles of total liquid products)*100/(moles of H_2O_2 conversion).

Chapter 4

The influence of iron and aluminum location in MFI zeolites on the catalytic performance in hydroxylation of benzene to phenol and methane to methanol with H_2O_2

Abstract

Fe-ZSM-5 zeolites were directly synthesized using tetrapropylammonium hydroxide (TPAOH) as OSDA with and without Na cations. The physicochemical properties, especially the states of Fe species were characterized. Fe-ZSM-5 zeolites synthesized without Na cations (FZ(T)) displayed more uniform distribution for each kinds of Fe species than the zeolites synthesized with Na cations (FZ(TN)). Generally FZ(T) zeolites showed slightly better catalytic performance than FZ(TN) in both benzene to phenol and methane to methanol reactions with H_2O_2. The introduction of aluminum in FZ(T) and FZ(TN) zeolites decrease the proportion of framework Fe and increased the proportion of isolated and oligomeric Fe species on the extra framework, thus improved the catalytic performance for FZ(T) zeolites in BTP and MTM reactions. But for FZ(TN) zeolites, only the catalytic performance in BTP reaction was improved.

4.1. Introduction

The location and distribution of Al atoms in the zeolite framework is a hot topic in recent years, which have been recognized as an important factor for activity and selectivity, because they would profoundly affect the accessibility of molecules to acid sites and the spatial constraints of the reaction field in the pores [1-4]. It's generally recognized that to balance the charge, AlO_4^- tetrahedra species are located near cations including organic cations, such as quaternary ammonium ions as OSDAs, or inorganic ones, for example, Na^+ and K^+. Hence, the Al content is affected by the number of the cations, and the location of Al atoms may be reliant on their size and type of the cations. A synthetic strategy to control of the distribution of Al in the Ferrierite-type (FER) zeolite by using different OSDAs in the presence or absence of Na cations has been established [5-9]. Recently, the relationship between the size of templates in the synthetic gel and the distribution of acid sites has been reported [7, 8].

Meanwhile, the Al distribution over the RTH-type framework was found to dependent on the type of the cations by the high-resolution ^{27}Al MAS NMR and ^{27}Al MQMAS NMR techniques [10]. In addition, Dedecek and co-workers controlled the distribution of Al in ZSM-5 zeolite by using different Si, Al and Na sources [2]. In our previous reports, the distribution of Al in ZSM-5 could be controlled by using different kinds of alcohols as the pore-forming agent and identified by the ^{27}Al MAS NMR, Co(II) ion UV-vis DRS, and constraint index value [4]. Moreover, the distribution of Al in the CHA-type zeolite can be controlled by varying the starting materials, and be detected by ^{27}Al MAS NMR [11].

Except the distribution of Al in the zeolites, the location of other metals can also be controlled. The most common method is depending on the parent zeolites with different Al location. Sobalik *et al.* used FER-type zeolites with different Si/Al ratios, thus with different amount of Al pairs and single Al atoms, as the parent zeolite to impregnate with the acetyl acetone solution of $FeCl_3$. The prepared Fe-FER zeolite with different Fe locations according to the site of Al in the framework [12]. In addition, Sazama and co-workers applied ZSM-5 with different Al locations as the parent zeolite and the counterpart impregnated with an anhydrous solution of $FeCl_3$ in acetyl acetone [13]. What is more, the formation of Cu-oxo clusters can be controlled by using ZSM-5 with different Al distribution and ion exchanging with $Cu(CH_3COO)_2$ solution [14].

In addition, similar to aluminum, iron as the positive trivalent transition metal possibly possesses the same property by direct introducing Fe source into the synthesis gel, which exist and distribute in the framework according the synthesis conditions. It is possible to form FeO_4^- tetrahedra in the framework rings of high-silica zeolites and the local negative charge to balance by the Na^+, TPA^+ and so on. In the presence of both iron and aluminum, situation will be a little complex than in the presence of only Fe. Both Fe and Al can form the AlO_4^- and FeO_4^- tetrahedra in the framework, and meanwhile Fe in single ions or iron-oxo species can control the negative charge produce by the tetrahedral in the framework as the counter ion species. However, this method has not been published in the open literatures, and the influence of both the Fe and Al in the presence of the synthesis gel on the catalytic morphology and performance has not been involved.

The distribution of AlO_4^- tetrahedra in the framework of aluminosilicate zeolites has contributed to control the structures and contents of the transition metal counter ion species and their activities in,

for example, SCR-NO_x by hydrocarbons or ammonia [15, 16], decomposition of NO [15, 17] and N_2O [18, 19], selective oxidation of benzene to phenol [20, 21] or methane to methanol [22, 23], as well as the local proton density affecting the acid-catalyzed transformations of hydrocarbons [24]. But the relationship between their structures and distribution of the framework Al atoms has not been established so far.

Here we report the synthesis of Fe-ZSM-5 zeolite catalysts with the location of aluminum and iron atoms in the framework controlled by using TPA cations as OSDA with or without Na cations. The distribution of iron and aluminum in the zeolites were estimated by the UV-vis, NH_3-TPD and ^{27}Al MAS NMR techniques. Finally, thus prepared Fe-ZSM-5 catalysts with different iron and aluminum locations were applied in the direct conversion of benzene to phenol and methane to methanol reactions with H_2O_2 to clarify the effects of the distributions of iron and aluminum. Meanwhile, the Fe-silicalite-1 zeolites with different locations of Fe species were applied in the two reactions to investigate the effect of aluminum.

4.2. Experiments

4.2.1. Materials

Colloid silica (HS-40) and tetrapropylammonium hydroxide (TPAOH) (20-25% in water) were purchased from Tokyo Chemical Industry. NaOH, $Fe(NO_3)_3{\cdot}9H_2O$, $Al(NO_3)_3{\cdot}9H_2O$, NH_4NO_3, H_2O_2 (30 wt.%), benzene, acetonitrile, sulfolane, mesitylene, anisole, 1,4-dioxane, tetramethylsilane (TMS), and CD_3CN were purchased from Wako. Methane (99.99%) gas was purchase from Taiyo Nippon Sanso Co., Ltd.. All of the reagents were used as received, without further purification.

4.2.2. Catalysts preparation

Fe-ZSM-5 zeolites were directly prepared using TPAOH as OSDA without Na cations. First, colloid silica was added to the solution containing water, TPAOH and $Fe(NO_3)_3$ and $Al(NO_3)_3$. The gel with the molar composition of 1 Si: 0.01-0.04 Fe: 0.04 Al: 0.25 TPA: 20 H_2O was crystallized at 443 K for 7 days with 40 rpm before aging at 353 K for 24 h. Then, the solid product was collected by filtering, rinsing and drying. The as-synthesized samples were calcined at 823 K for 10 h to remove TPA^+ species. Thus obtained zeolites were designated as "FZ(T)*x*", where *x* means the Si/Fe ratio in

the synthesis gel. The ZSM-5 without Fe source in the condition was denoted as Z(T).

Fe-ZSM-5 zeolites were also directly prepared using TPAOH as OSDA with Na cations. The gel was aging at 353 K for 24 h and then crystallized at 443 K for 3 days. The final molar composition was 1 Si: 0.01-0.04 Fe: 0.04 Al: 0.25 TPA: 0.25 Na: 20 H_2O. The calcined Na-type samples were treated with 1 M NH_4NO_3 aq. at 353 K for 3 h twice, and filtered, washed, dry and calcined at 823 K for 5 h to obtain the H-type samples. Thus obtained catalyst was designated as "FZ(TN)*y* " where *y* means the Si/Fe ratio in the synthesis gel.. The ZSM-5 without Fe source in this condition was denoted as Z(TN).

The specific information of "FS(T)x" and "FS(TN)y" zeolites refer Chapter 3.

4.2.3. Characterization of catalysts

XRD patterns were collected on a Rint-Ultima III (Rigaku) using a Cu Kα X-ray source (40 kV, 20 mA). Field-emission scanning electron microscopic (FE-SEM) images of the powder samples were obtained on S-5200 (Hitachi) microscope operating at 1 kV. Elemental analyses of the samples were performed on an inductively coupled plasma-atomic emission spectrometer (ICP-AES, Shimadzu ICPE-9000). Nitrogen adsorption desorption measurements to obtain information on the micro- and meso-porosities were conducted at 77 K on a Belsorp-mini II (MicrotracBEL).

UV-vis diffuse reflectance spectra were recorded on a V-650DS spectrometer (JASCO). The diffuse reflectance spectra were converted into the absorption spectra using the Kubelka-Munk function.

Temperature-programmed ammonia desorption (NH_3-TPD) profiles were noted down on a Multitrack TPD equipment (Japan BEL). Normally, 25 mg catalyst was pretreated at 773 K for 1 h in a He flow of 50 mL min^{-1} and then cooled down to 423 K. The sample was evacuated at 423 K for 1 h prior to the adsorption of NH_3. Approximately 2500 Pa of NH_3 contacted with the sample at 423 K for 10 min. Subsequently, the sample was evacuated to remove the weakly adsorbed NH_3 at the same temperature for 30 min. Finally, the sample was heated from 423 to 873 K at a ramping rate of 10 K min^{-1} in a He flow of 50 mL min^{-1}.

The high-resolution ^{27}Al MAS NMR and ^{29}Si MAS NMR spectra were obtained on a JEOL ECA-600 spectrometer (14.1 T) equipped with an additional 1 kW power amplifier. The ^{27}Al and ^{29}Si

chemical shifts were referenced to $AlNH_4(SO_4)_2 \cdot 12H_2O$ at -0.54 ppm and polydimethylsiloxane (PDMS) at -34.12 ppm, respectively. The samples were spun at 15 kHz by using a 4 mm ZrO_2 rotor.

4.2.4 Catalytic tests

4.2.4.1 Direct hydroxylation of benzene to phenol with H_2O_2 (BTP)

The BTP reaction was carried out in a 25 mL round-bottom flask equipped with a reflux condenser and a magnetic stirrer. In a typical run, 50 mg of catalyst was immersed in 10 mL of acetonitrile, 5 mmol of benzene and 10 mmol H_2O_2 was stirred at 333 K for 6 h [25]. After the reaction mixture was cooled down, the catalyst was removed. A certain amount of anisole as internal standard was added to the resultant liquid, resulting in the formation of a single-phase liquid for the GC analysis [26]. The remaining H_2O_2 concentration was quantified by standard titration method with 0.1 mol/L $Ce(SO_4)_2$ solution.

4.2.4.2 Direct conversion of methane to methanol with H_2O_2 (MTM)

The liquid-phase MTM reactions were carried out in a 100 ml PTFE autoclave. The CH_4 pressure was controlled by the pressure gage. The reactants were stirred vigorously by an agitator blade. In a typical run, 10 ml sulfolane, 50 mg catalyst and 27 mmol H_2O_2 were added to the autoclave and heated to 323 K. The sealed reactor was then purged with CH_4 to 3 Mpa. After reaction 2 h, the autoclave was cooled rapidly to 278 K in an ice bath to minimize any further chemical reaction and reduce loss of volatile products. After separation liquid phase and catalyst, the liquid-phase products were analyzed by ^1H NMR spectroscopy on JEOL ECA-600 spectrometer (14.1 T) equipped with an additional 1 kW power amplifier. Mesitylene and TMS/CD_3CN were used as the internal standard a chemical shift calibrator, respectively. The detectable products in the liquid phase were CH_3OH, HCOH, HCOOH and CH_3OOH. The amount of unconverted H_2O_2 was quantified by standard titration method with 0.1 mol/L $Ce(SO_4)_2$ solution.

4.3. Results and discussion

4.3.1 Characterization of catalysts

4.3.1.1 Physicochemical properties

Figure 4.1 show the XRD patterns of the as-synthesized FZ(T)*x* and FZ(TN)*y* zeolites. Both as-

synthesized Z(T) and Z(TN) showed good crystallinity. The crystallinity of all the Fe-ZSM-5 samples were decreased with the Si/Fe ratios decreased, indicating that too high Fe and Al contents were not conducive to form MFI structure zeolites. When the Si/Fe and Si/Al ratios both equaled to 25 in the synthesis gel, the crystallinity of as-FZ(TN)25 was very low but still maintained the MFI structure. However, it was amorphous for as-FZ(T)25. The possible reason was the limited positive charge provided by TPA cation. For all the highly crystallized Fe-ZSM-5 zeolites, no features belonging to large iron oxide particles were observed, indicating the high Fe dispersion in the as-synthesized zeolites.

The FE-SEM images of all the samples are shown in **Figure 4.2**. Z(T) displayed the cylindrical shape with protrusions on the side surface. The diameter of the cylinder was approximately 500 nm. For Z(TN), it was irregular sphere with the particle size of 200 nm. The FZ(T)*x* zeolites were spherical and the particle size was increased from 200 nm to 400 nm with the Fe content. However, the FZ(TN)*y* zeolites showed the irregular shape and the particle size was decreased from 300 nm to 50 nm with the Fe content increasing. In addition, some tiny particle was distributed on the surface of FZ(T)50 and FZ(TN)25, herein the lower crystallinity was displayed in XRD patterns.

The chemical composition and textural properties of the samples are listed in **Table 4.1**. The Si/Al ratios of the FZ(T)*x* and Z(T) were higher than FZ(TN)*y* and Z(TN), which was consistent with the results of our previous reports [1, 4], possible due to the limited positive charge proved by TPA cations for FZ(T)*x* and Z(T) zeolites. For all the samples, the actual Si/Fe ratios in the products were higher than those in the synthesis gels, especially FZ(T)100 and FZ(TN)100. Meanwhile, the actual Si/Fe ratios of FZ(T)*x* samples were higher than those of FZ(TN)*y*, possibly due to the less amount of positive charge provided by TPA cation for FZ(T)*x* than both TPA and Na cation for FZ(TN)*y*. The textural properties of all the samples are listed in **Table 4.1**. FZ(T)*x* zeolites showed the BET surface area (S_{BET}) of 408-379 m^2g^{-1} and external surface area (S_{EXT}) of 175-116 m^2g^{-1}, which were lower than FZ(TN)*y*, possibly due to the large particle size of FZ(T)*x*. All the Fe-containing MFI zeolite catalysts possessed the similar micropore volume (V_{micro}) of 0.14-0.16 cm^3g^{-1}.

4.3.1.2 Fe states

The Fe coordination of the Fe-containing MFI zeolite catalysts were studied by UV-vis spectroscopy, as shown in **Figure 4.3**. According to the reference [27], the multiple bands can adequately be fitted by using single bands corresponding to (1) framework Fe species (200-250 nm, λ1), (2) isolated and oligomeric extra framework Fe cations within the zeolite channels (250-350 nm, λ2), (3) larger Fe clusters (350-450 nm, λ3,) and finally (4) bulk Fe oxides on the surface of the zeolite

(>450 nm, λ4). The amount and proportion of different Fe species based on the relative peak areas are listed in **Table 4.2**. Similar to the results of FS(T)*x* zeolites in Chapter 3, the FZ(T)*x* zeolites contained every kind of Fe species even at a very low Fe content.

Connection with the character of TPA cation, it was considered that the framework Fe was distributed in or close to the intersection in the as-synthesized FZ(T) samples. Influenced by the charge amount and position, coordinated Fe species were preferentially distributed in close to the intersection. Because the intersection had larger void (8.9 Å) than the channels (ca. 5.5 Å), the extra framework Fe species were with different coordination after calcination. Thus the possibility of formation oligomer, cluster and aggregated Fe species after calcination for FZ(T)*x* were much higher than FZ(TN)*y*. In contrast, no bulk iron oxides appeared for FZ(TN)100, and the proportion of the other Fe species on the extra framework for FZ(TN)y samples were increased with the Fe content growing. The proportion of each kind of Fe species for FZ(TN) 50 and FZ(TN)25 were similar. It suggested that the proportion of each Fe species did not change when Fe content was increased continuously after the Fe species being evenly distributed.

4.3.1.3 Acidity

Figure 4.4 shows the NH_3-TPD profiles of the Fe-ZSM-5 zeolites with different locations of iron and aluminum. The profiles can be deconvoluted into three kinds of peaks at low (373-473 K), medium (473-573 K), and high temperature (573-873 K) (designated as LT, MT, and HT). The amounts of NH_3 adsorbed and the temperature of the maximum peak (T_{max}) are listed in **Table 4.3**. According to the references [28, 29], the LT peak corresponds to NH_3 adsorbed on the non-acidic-OH groups and NH_4^+ by hydrogen bonding, which was not related to the true acid site and excluded in the discussion. The MT peak corresponds to NH_3 adsorbed on the extra framework Fe or Al species (Lewis acid site), and the HT peak corresponds to NH_3 adsorbed on the bridged Si-O(H)-M (Brønsted acid site), which M means Fe and Al [29].

The acid amount for FZ(T)*x* zeolites were increased with the Fe content, but the increased amount was not much. Instead, the MT and HT were obviously increased from 539 K to 570 K and from 623 K to 673 K for FZ(T)100 and FZ(T)50, respectively, which indicating the different coordination states of Fe and Al. Meanwhile, the results were consistent with UV-vis of FZ(T)*x*, which contained each kind of acid site and the acid amount were slightly increased with Fe content increasing. It was clear to see that the acid amount of FZ(T)*x* zeolites were much weaker than Z(T), suggesting that the addition of Fe species affected the coordination state of aluminum in MFI zeolite. The acid amount of FZ(TN)*y*

were closed to each other with Fe content changing. Because there was no change in the amount of aluminum for FZ(TN)*y* zeolites that mainly providing the acid amount. However, compared with Z(TN), the intensity of peaks at around 540 K were increase with Fe content, and the intensity of peaks at around 650 K were decreased and migrated to the low temperature with Fe content. The possible reason was that Fe replaced or influenced part of Al in the framework thus decreased the acid amount at the high temperature. At the same time, part of Fe species appeared on the extra framework, as a results increased the intensity of peaks at around 540 K, although it did not reflect on **Table 4.3**.

4.3.1.4 The states of Si and Al in Fe-ZSM-5 zeolites

The ^{29}Si NMR spectra of the H-type MFI zeolites are shown in **Figure 4.5**. All the samples possessed a main resonance peak at around -111 ppm were assigned to the silicon atoms coordinated by four silicon atoms (Q4(0Al), $Si(OSi)_4$). And another obvious resonance was at -103 ppm due to the Q3 silicon atoms ($(OH)Si(OSi)_3$), which were mainly attributed to the surface silanol group, or Si(1Al) and Si(1Fe) for the FZ(T)*x* and FZ(TN)*y* zeolites [30]. There was a slightly increase in the spectral intensity at around -103 ppm for FZ(T)*x* and FZ(TN)*y* compared with Z(T) and Z(TN), respectively, possibly due to the increased amount of Si(1Fe) by addition of Fe. However, too much paramagnetic Fe species in FZ(T)50 affected the measurement and lead to the unsmooth curve.

Figure 4.6 shows the ^{27}Al NMR spectra of the MFI zeolites. The Al atoms were introduced into the structure in a tetrahedral form at ca. 56 ppm and existed at the extra framework in hexahedron form at ca. 0 ppm. Z(T) showed smooth curve and typical distribution at ca. 56 and 0 ppm, indicating that the vast majority of aluminum was in the form of tetra-coordination. The as-FZ(T)*x* contained relative higher intensity at ca. 56 ppm, suggesting that most of aluminum was in the framework as the form of tetra-coordination in the as-synthesized samples, but after calcination, the intensity of chemical shift at ca. 56 ppm for both FZ(T)100 and FZ(T)50 were greatly decreased. The phenomenon may be explain the low acid amount of FZ(T)*x* zeolites. Z(T) and FZ(TN)*y* displayed the similar spectra, indicating that most of the aluminum was in the framework as the tetrahedral form at ca. 56 ppm. It was also consistent with the results of acid amount of FZ(TN)*y*. Thus the distribution of Fe and Al in the MFI zeolite can be speculated. As shown in **Scheme 4.1**, the Fe and Al ions were distributed preferentially in and/or around the intersection, which was similar to the situation of ZSM-5 with TPAOH as OSDA in the absence of Na ions [1]. However, when the Na ions was presence in the

synthesis gel, the Fe and Al ions were distributed at both the intersection and channels due to the positive Na^+ and TPA^+ location.

4.3.2 Direct oxidation of benzene to phenol

The catalytic performances for the direct hydroxylation of benzene with H_2O_2 over Fe-containing MFI zeolite catalysts using TPAOH as OSDA without Na cations are detailed in **Table 4.4**. Z(T) achieved very low phenol yield (0.1%), indicating that ZSM-5 zeolite with the aluminum located in the intersection was no active or very low activity in BTP reaction with H_2O_2. However, Fe-containing MFI zeolites attained phenol yield of 1.4-3.6% with selectivity of higher than 98%, suggesting that the active site was Fe species, which has been discussed in Chapter 2. The FZ(T)*x* zeolites achieved higher phenol yield (2.2-3.6%) than FS(T)*x* (1.4-2.7%) with the selectivity of 98-99 % possibly due to the higher proportion of isolated and oligomeric Fe species on the extra framework for FZ(T)*x* zeolites.

Table 4.5 are listed the catalytic performances for the direct hydroxylation of benzene with H_2O_2 over Fe-containing MFI zeolite catalysts using TPAOH as OSDA with Na cations. Similarly to Z(T), Z(TN) displayed very low phenol yield (0.1%), indicating that ZSM-5 zeolite with the aluminum located in both the intersection and channels was no active or very low activity in BTP reaction with H_2O_2. However, Fe-containing MFI zeolites attained phenol yield of 1.4-3.7% with selectivity of more than 97%, suggesting that the active site was Fe species. The FZ(TN)*y* zeolites achieved higher phenol yield (1.5-3.7%) than FS(TN)*y* (1.4-3.2%) with the selectivity of 97-99 % possibly due to the higher proportion of isolated and oligomeric Fe species on the extra framework for FZ(TN)*y* zeolites .

Compared with the results in **Table 4.4** and **Table 4.5**, it was clear to see that FZ(T)*x* and FS(T)*x* attained higher phenol yield than FZ(TN)*y* and FS(TN)*y*. The larger reaction space in the intersection than the channels was one of the reasons. Besides, the activity of the formed Fe species in the intersection was different from the ones in the intersection and the channels. However, the specific kind of Fe species in the intersection and/ or the channels are still unknown.

4.3.3 Direct oxidation of methane to methanol

The catalytic performances for the direct hydroxylation of methane with H_2O_2 over Fe-containing MFI zeolite catalysts using TPAOH as OSDA without Na cations are detailed in **Table 4.6**. The FZ(T)*x*

zeolites achieved more methanol or total liquid products than FS(T)*x* possibly due to the higher proportion of isolated and oligomeric Fe species on the extra framework for FZ(T)*x* zeolites.

The catalytic performances for the direct hydroxylation of methane with H_2O_2 over Fe-containing MFI zeolite catalysts using TPAOH as OSDA with Na cations are detailed in **Table 4.7**. The FZ(TN)*y* zeolites achieved more methanol than FS(TN)*y* due to the higher proportion of isolated and oligomeric Fe species on the extra framework for FZ(TN)*y* zeolites .

Compared with the results in **Table 4.6** and **Table 4.7**, the different of catalytic performance in conversion of methane to methanol between FZ(T)*x* and FZ(TN)*y* were not obvious. One possible reason was no space limitation for methane and methanol in MFI zeolites. The H_2O_2 conversion of all the samples were between 4-15%, which was low due to the properties of sulfolane.

4.4. Conclusions

Fe-ZSM-5 zeolites were directly synthesized using TPAOH as OSDA with or without Na cations. The physicochemical properties, especially the states of Fe species were characterized by UV-vis and NH_3-TPD. Fe-ZSM-5 zeolites synthesized without Na cations displayed more uniform distribution for each kinds of Fe species. Fe-ZSM-5 zeolites synthesized with Na cations presented strong acidity, since most of aluminum located in the framework. Generally Fe-ZSM-5 zeolites synthesized without Na cations (FZ(T)*x*) showed better catalytic performance in BTP reaction than the ones with Na cations (FS(TN)*y*). The introduction of aluminum in FZ(T)*x* and FZ(TN)*y* zeolites increased the isolated and oligomeric Fe species on the extra framework compared with FS(T)*x* and FS(TN)*y*, respectively. Thus, the catalytic performance in BTP and MTM reactions were improved with the introduction of aluminum in the MFI zeolites.

References

[1] T. Yokoi, H. Mochizuki, T. Biligetu, Y. Wang, T. Tatsumi, Chem. Lett., 46 (2017) 798.
[2] J. Dedecek, V. Balgová, V. Pashkova, K. P. lein, B. Wichterlová, Chem. Mater., 24 (2012) 3231.
[3] T. Yokoi, H. Mochizuki, S. Namba, J. N. Kondo, T. Tatsumi, J. Phys. Chem. C, 119 (2015) 15303.
[4] T. Biligetu, Y. Wang, T. Nishitoba, R. Otomoa, S. Park, H. Mochizuki, J. N. Kondo, T. Tatsumi, T. Yokoi, J. Catal., 353 (2017) 1.
[5] A. B. Pinar, L. G. Hortiguela, J. P. Pariente, Chem. Mater., 19 (2007) 5617.
[6] A. B. Pinar, C. Márquez-Alvarez, R. García, M. Grande-Casas, J. Pérez-Pariente, Top Catal., 52 (2009) 1281.
[7] A. B. Pinar, L. Gomez-Hortiguela, F. Cora, J. Perez-Pariente, Chem. Commun. (Camb), 46 (2010) 2073.
[8] Y. R. Leshkov, M. Moliner, M. E. Davis, J. Phys. Chem. C, 115 (2011) 1096.
[9] L. Gómez-Hortigüela, A. B. Pinar, L. B. McCusker, J. Pérez-Pariente, Chem. Mater., 25 (2013) 3654.
[10] M. Liu, T. Yokoi, M. Yoshioka, H. Imai, J. N. Kondo, T. Tatsumi, Phys. Chem. Chem. Phys., 16 (2014) 4155.
[11] T. Nishitoba, N. Yoshida, J. N. Kondo, T. Yokoi, Ind. Eng. Chem. Res., 57 (2018) 3914.
[12] Z. Sobalik, J. Novakova, J. Dedecek, N. K. Sathu, E. Tabor, P. Sazama, P. Stastny, B. Wichterlova, Micropor. Mesopor. Mater., 146 (2011) 172.
[13] P. Sazama, B. Wichterlová, E. Tábor, P. Šťastný, K. S. Naveen, Z. Sobalík, J. Dědeček, S. Sklenák, P. Klein, A. Vondrová, J. Catal., 312 (2014) 123.
[14] M. A. C. Markovits, A. Jentys, M. Tromp, M. Sanchez-Sanchez, J. A. Lercher, Top Catal., 59 (2016) 1554.
[15] M. Iwamoto, H. Yahiro, Catal. Today, 22 (1994) 5.
[16] S. Brandenberger, O. Kröcher, A. Tissler, R. Althoff, Catalysis Reviews, 50 (2008) 492.
[17] I. Masakazu, H. Yahiro, K. Tanda, N. Mizuno, Y. Mine, S. Kagawat, J. Phys. Chem., 95 (1991) 3727.
[18] F. Kapteijn, J. R. Mirasol, J. A. Moulijn, Appl. Catal., B, 9 (1996) 25.
[19] P. C. Andrikopoulos, S. Sklenak, B. Boekfa, B. Jansang, J. Nováková, L. Benco, J. Hafner, T. Bucko, J. Dědeček, Z. Sobalík, J. Catal., 272 (2010) 262.
[20] K. A. Dubkov, N. S. Ovanesyan, A. A. Shteinman, E. V. Starokon, E. V. Starokon, G. I. Panov, J. Catal., 207 (2002) 341.
[21] P. Kubanek, B. Wichterlova, Z. Sobalik, J. Catal., 211 (2002) 109.
[22] M. H. Groothaert, P. J. Smeets, B. F. Sels, B. A. Jacobs, R. A. Schoonheydt, J. Am. Chem. Soc., 127 (2005) 1394.
[23] P. Vanelderen, R. G. Hadt, P. J. Smeets, E. I. Solomon, R. A. Schoonheydt, B. F. Sels, J. Catal., 284 (2011) 157.
[24] P. Sazama, J. Dedecek, V. Gabova, B. Wichterlova, G. Spoto, S. Bordiga, J. Catal., 254 (2008) 180.
[25] G. Wen, S. Wu, B. Li, C. Dai, D. Su, Angew. Chem. Int. Ed., 54 (2015) 4105
[26] M. Sasaki,Y. Sato, Y. Tsuboi, S. Inagaki, Y. Kubota, ACS Catal., 4 (2014) 2653.
[27] C. Hammond, I. Hermans, N. Dimitratos, N. Dimitratos, J. A. Lopez-Sanchez, R. L. Jenkins, G. Whiting, S. A. Kondrat, M. H. ab Rahim, M. M. Forde, A. Thetford, H. Hagen, E. E. Stangland, J. M.

Moulijn, S. H. Taylor, D. J. Willock, G. J. Hutchings, ACS Catal., 3 (2013) 1835.
[28] G. Wu, F. Hei, N. Zhang, N. Guan, L. Li, W. Grünert, Appl. Catal., A, 468 (2013) 230.
[29] R. Mohammad, Y. Fereydoon, Fuel, 181 (2016) 537.
[30] D. Freude, J. Kärger, Handbook of porous solids, 1 (2002) 465.

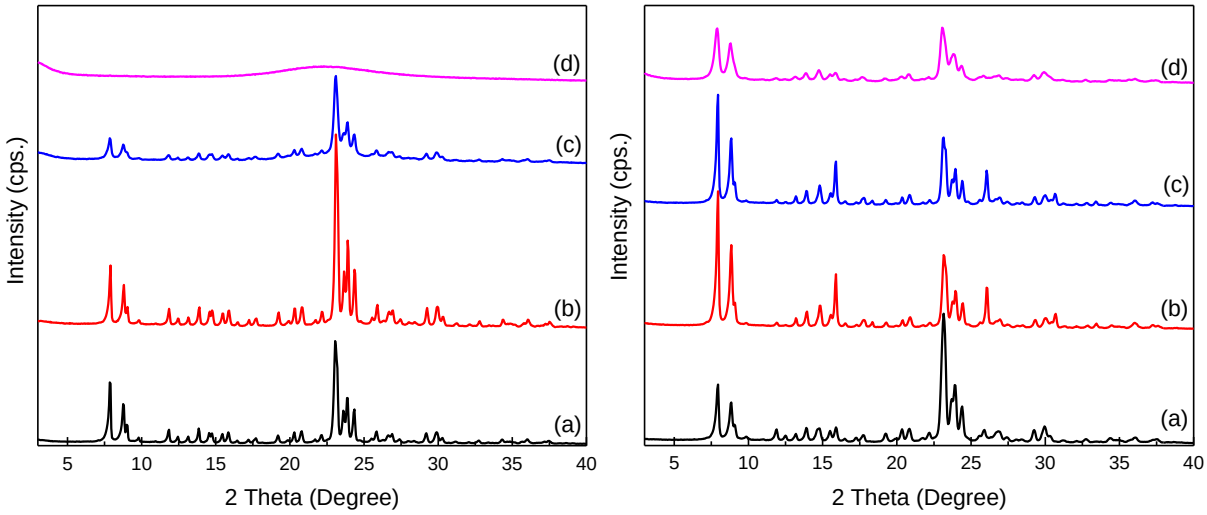

Figure 4.1 XRD patterns of the as-synthesized left: (a) Z(T), (b) FZ(T)100,(c) FZ(T)50, (d) FZ(T)25, right: (a) Z(TN), (b) FZ(TN)100,(c) FZ(TN)50, (d) FZ(TN)25.

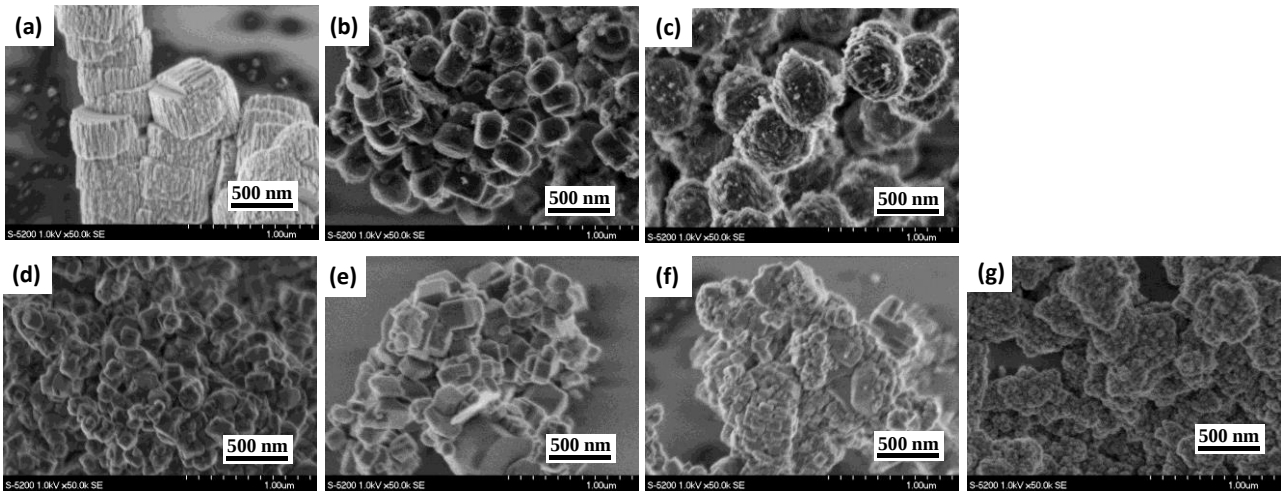

Figure 4.2 FE-SEM images of (a) Z(T), (b) FZ(T)100, (c) FZ(T)50, (d) Z(TN), (e) FZ(TN)100, (f) FZ(TN)50 and (g) FZ(TN)25.

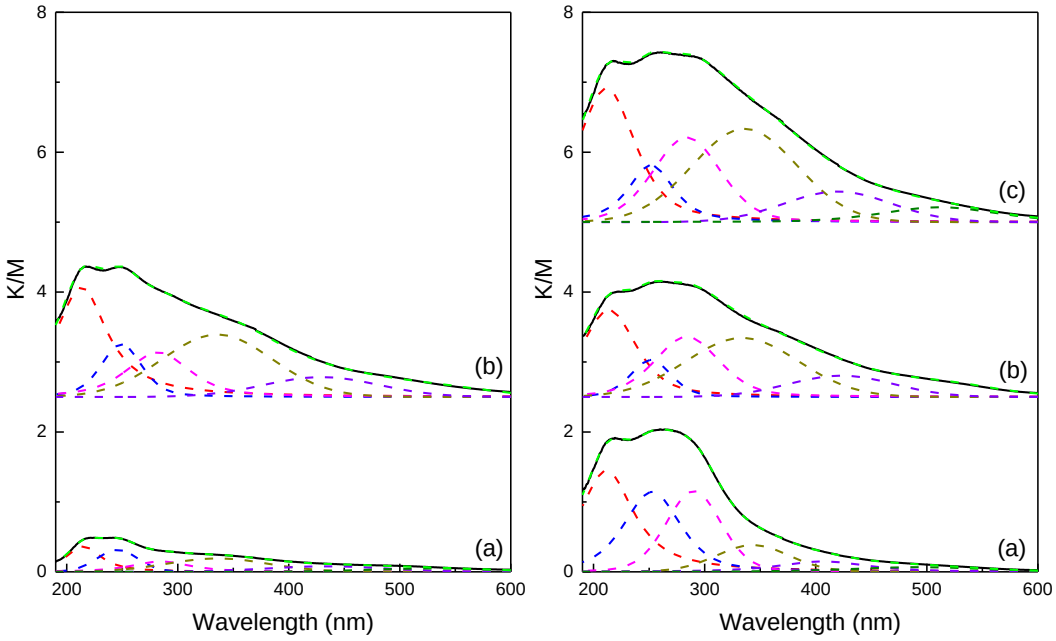

Figure 4.3 UV-vis spectra of left: (a) FZ(T)100,(b) FZ(T)50, right: (a) FZ(TN)100,(b) FZ(TN)50, (c) FZ(TN)25.

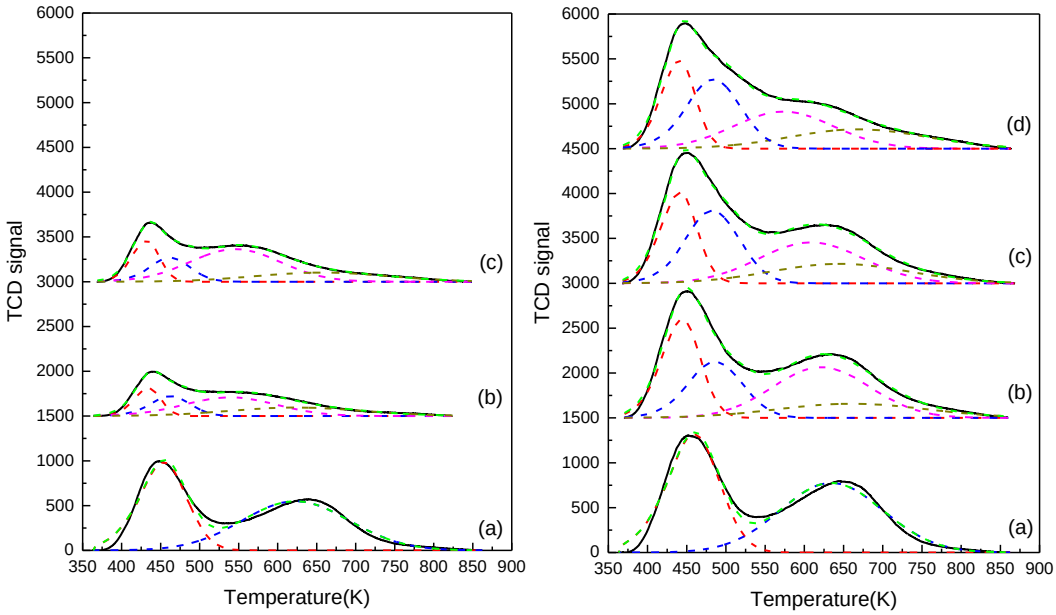

Figure 4.4 NH_3-TPD analyses of left: (a) Z(T), (b) FZ(T)100,(c) FZ(T)50, (d) FZ(T)25, right: (a) Z(TN), (b) FZ(TN)100,(c) FZ(TN)50, (d) FZ(TN)25.

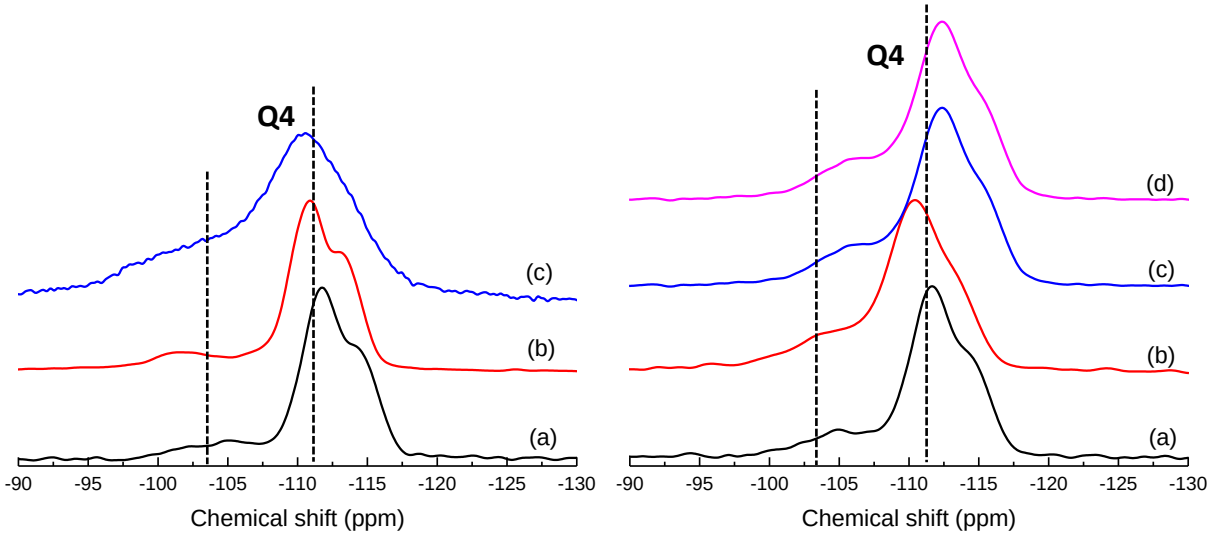

Figure 4.5 ^{29}Si MAS NMR spectra of left: (a) Z(T), (b) FZ(T)100, (c) FZ(T)50, right: (a) Z(TN), (b) FZ(TN)100, (c) FZ(TN)50, (d) FZ(TN)25.

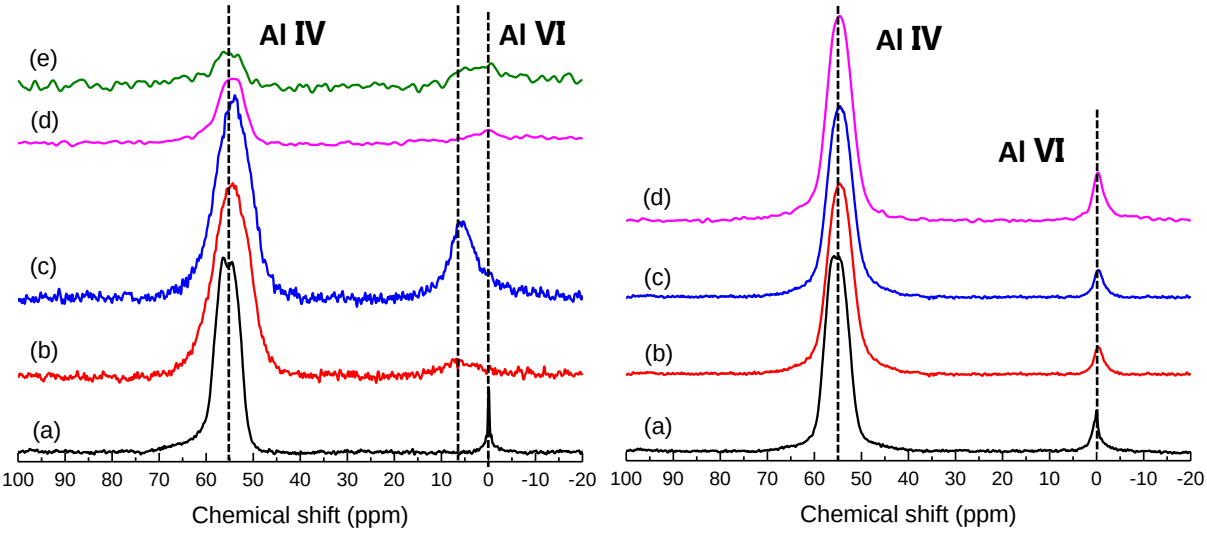

Figure 4.6 ^{27}Al MAS NMR spectra of left: (a) Z(T), (b) as-FZ(T)100, (c) as-FZ(T)50, (d) FZ(T)100, (e) FZ(T)50, right: (a) Z(TN), (b) FZ(TN)100, (c) FZ(TN)50, (d) FZ(TN)25.

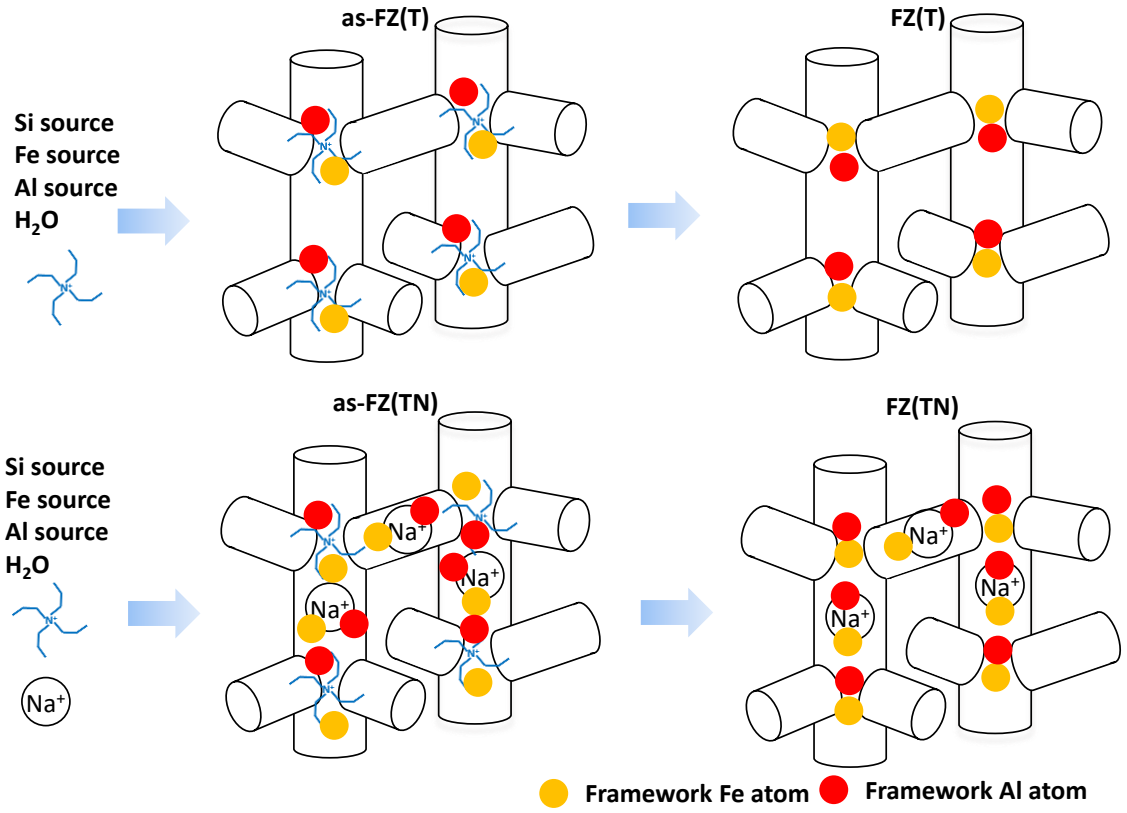

Scheme 4.1 Strategy for preferential distribution of the Fe and Al atoms in FZ(T)*x* and FZ(TN)*y* zeolites.

Table 4.1 Physicochemical characteristics of the Fe-containing MFI zeolite catalysts.

Sample	In gel		In product [a]			S_{BET}	S_{EXT}	V_{Total}	V_{Micro}
	Si/Al	Si/Fe	Si/Al	Si/Fe	Fe (wt.%)	(m^2g^{-1})[b]	(m^2g^{-1})[c]	(cm^3g^{-1})[d]	(cm^3g^{-1})[e]
Z(T)	25	-	27	-	-	462	126	0.41	0.15
FZ(T)100	25	100	28	241	0.4	408	175	0.50	0.14
FZ(T)50	25	50	28	66	1.3	379	116	0.35	0.14
Z(TN)	25	-	25	-	-	422	156	0.43	0.17
FZ(TN)100	25	100	23	133	0.6	450	212	0.48	0.16
FZ(TN)50	25	50	23	62	1.3	444	182	0.45	0.16
FZ(TN)25	25	25	24	28	3.1	470	251	0.61	0.16

[a] Si/Fe was determined by ICP-AES analysis.

[b] Specific surface areas of the catalysts were calculated using the Brunauer-Emmett-Teller (BET) equation on the N_2 adsorption isotherms.

[c] External surface area (S_{EXT}) of the catalysts were calculated by the *t*-plot method based on the adsorption isotherms.

[d] Total pore volumes of the catalysts were calculated based on BET equation on the N_2 adsorption isotherms.

[e] Micropore volumes of the catalysts were calculated by the *t*-plot method based on the adsorption isotherms.

Table 4.2 Percentage of sub-band areas (I_1:λ< 250 nm, I_2: 250 <λ< 350 nm, I_3: 350 <λ< 450 nm, and I_4: λ>450 nm) derived by deconvoluting UV-vis spectra and corresponding Fe species content for Fe-containing MFI zeolite catalysts.

Sample	Framework Fe		Isolated and Oligomeric Fe		Larger Fe clusters		Bulk Fe oxides	
	I_1(%)	wt.%	I_2(%)	wt.(%)	I_3(%)	wt.%	I_4(%)	wt.%
FZ(T)100	39.9	0.12	39.9	0.12	11.9	0.04	8.2	0.02
FZ(T)50	41.1	0.53	44.3	0.58	9.2	0.12	5.4	0.07
FZ(TN)100	60.8	0.36	30.4	0.18	8.8	0.05		
FZ(TN)50	38.5	0.50	46.5	0.60	9.1	0.12	5.9	0.08
FZ(TN)25	38.7	1.12	46.7	1.45	9.5	0.29	5.7	0.18

Table 4.3 NH_3 adsorbed amount of Fe-containing MFI zeolite catalysts.

Sample	NH_3 adsorbed amount (mmol/g) / T_{max} (K)			
	LT		MT	HT
Z(T)	0.27/434		0.36/622	
FZ(T)100	0.05/434	0.05/462	0.12/539	0.08/623
FZ(T)50	0.07/440	0.07/469	0.20/570	0.08/673
Z(TN)	0.34/458		0.48/633	
FZ(TN)100	0.19/432	0.16/486	0.25/620	0.11/660
FZ(TN)50	0.22/433	0.26/472	0.27/610	0.18/643
FZ(TN)25	0.19/440	0.25/484	0.25/573	0.18/668

Table 4.4 Catalytic results of Fe-containing MFI zeolite catalysts using TPAOH as OSDA without Na cations in the synthesis gel for the direct oxidation of benzene to phenol with H_2O_2.

Sample	Phenol Yield (%)[a]	Product Selectivity (%)[b]			H_2O_2 Conv.(%)[c]
		Phenol	HQ	CL	
Z(T)	0.1	100	0	0	2
FZ(T)100	2.2	99	1	0	40
FZ(T)50	3.6	98	1	1	53
FS(T)100	1.4	99	1	0	29
FS(T)50	2.7	98	1	1	48

Reaction conditions: 333 K, 10 mmol H_2O_2, 50 mg catalyst, 10 ml CH_3CN, 5 mmol Benzene, 6 h.

[a] Phenol yield = (moles of phenol produced)*100/(initial moles of benzene).

[b] Each product selectivity= (moles of each liquid product)*100/(moles of phenol + moles of HQ + moles of CL).

[c] H_2O_2 conversion = (moles of H_2O_2 after reaction)*100/(initial moles of H_2O_2).

Table 4.5 Catalytic results of Fe-containing MFI zeolite catalysts using TPAOH as OSDA with Na cations in the synthesis gel for the direct oxidation of benzene to phenol with H_2O_2.

Sample	Phenol Yield (%)[a]	Product Selectivity (%)[b]			H_2O_2 Conv.(%)[c]
		Phenol	HQ	CL	
Z(TN)	0.1	100	0	0	3
FZ(TN)100	1.5	98	2	1	48
FZ(TN)50	1.7	97	2	1	67
FZ(TN)25	3.7	99	1	0	90
FS(TN)100	1.4	99	1	0	55
FS(TN)50	2.5	98	1	1	63
FS(TN)25	3.2	97	2	1	78

Reaction conditions: 333 K, 10 mmol H_2O_2, 50 mg catalyst, 10 ml CH_3CN, 5 mmol Benzene, 6 h.

[a] Phenol yield = (moles of phenol produced)*100/(initial moles of benzene).

[b] Each product selectivity= (moles of each liquid product)*100/(moles of phenol + moles of HQ + moles of CL).

[c] H_2O_2 conversion = (moles of H_2O_2 after reaction)*100/(initial moles of H_2O_2).

Table 4.6 Catalytic results of Fe-containing MFI zeolite catalysts using TPAOH as OSDA without Na cations in the synthesis gel for the direct oxidation of methane to methanol with H_2O_2.

Sample	Liquid products				MeOH	H_2O_2	
	MeOH	HCOOH	HCOH	MeOOH	Sele.(%)[a]	Conv.(%)[b]	Eff. (%)[c]
FZ(T)100	131	44	114	0	45	7	16
FZ(T)50	250	6	187	0	56	10	10
FS(T)100	80	8	0	0	91	6	6
FS(T)50	266	30	83	0	70	7	9

Reaction conditions: 323 K, 27 mmol H_2O_2, 50 mg catalyst, 10 ml sulfolane, 3 Mpa CH_4, 2 h.

[a] Each product selectivity= (moles of each product)*100/(moles of total liquid products).

[b] H_2O_2 conversion = (moles of H_2O_2 after reaction)*100/(initial moles of H_2O_2).

[c] H_2O_2 efficiency = (moles of total liquid products)*100/(moles of H_2O_2 conversion).

Table 4.7 Catalytic results of Fe-containing MFI zeolite catalysts using TPAOH as OSDA with Na cations in the synthesis gel for the direct oxidation of methane to methanol with H_2O_2.

Sample	Liquid products				MeOH	H_2O_2	
	MeOH	HCOOH	HCOH	MeOOH	Sele.(%)[a]	Conv.(%)[b]	Eff. (%)[c]
FZ(TN)100	155	12	94	0	59	5	36
FZ(TN)50	245	9	189	36	51	11	17
FZ(TN)25	303	0	209	0	59	15	15
FS(TN)100	116	27	63	0	56	4	18
FS(TN)50	183	21	76	0	65	6	14
FS(TN)25	279	19	187	0	58	11	16

Reaction conditions: 323 K, 27 mmol H_2O_2, 50 mg catalyst, 10 ml sulfolane, 3 Mpa CH_4, 2 h.

[a] Each product selectivity= (moles of each product)*100/(moles of total liquid products).

[b] H_2O_2 conversion = (moles of H_2O_2 after reaction)*100/(initial moles of H_2O_2).

[c] H_2O_2 efficiency = (moles of total liquid products)*100/(moles of H_2O_2 conversion).

Chapter 5

Alkaline treatment on as-synthesized and calcined Fe-silicalite-1 and Fe-ZSM-5 zeolites for hydroxylation of benzene to phenol with H_2O_2

Abstract

The influence of desilication on as-synthesized and calcined Fe-ZSM-5 and Fe-silicalite-1 zeolites were investigated. Based on that, Fe-silicalite-1 and Fe-ZSM-5 zeolite were synthesized by in-situ method. The as-synthesized and calcined zeolites were modified by the same alkaline condition. N_2 adsorption and desorption was used to character the texture properties. The UV-vis spectroscopy was applied to evaluate the states of Fe species and the corresponding Fe species content derived by deconvoluting the sub-band areas. The ammonia adsorbed amount measured by NH_3-TPD was used to investigate the environment of iron and aluminum in the zeolites. Finally, the catalytic performance of thus prepared catalysts were estimated in hydroxylation of benzene to phenol with H_2O_2. Significant changes occurred in the calcined Fe-ZSM-5, both as-made and calcined Fe-silicalite-1 zeolites.

5.1. Introduction

Fe-containing zeolites have been widely used and revealed outstanding performance in various catalytic conversions related to environmental applications, such as direct N_2O decomposition [1-3], selective catalytic reduction of NO_x and N_2O [4, 5], selective oxidation of NH_3 to N_2 [6]; and in oxidative transformations of hydrocarbons, including benzene and phenol hydroxylation [7-9], propane oxidative dehydrogenation [2, 10-12], hydroxylation of methane to methanol [13-15] and so on.

The preparation method of Fe-containing zeolites strongly influences the nature and distribution of the resulting Fe species, which basically determine the catalytic performance. Extensive efforts have been dedicated to establishing reliable procedures for iron incorporation, including direct hydrothermal synthesis [4, 16, 17], ion exchange [18], impregnation [19, 20], chemical vapor deposition (CVD) [21, 22] and so on. Introduction of iron from the zeolite matrix is typically followed by high temperature calcination or steam treatment. The latter is crucial to yield active sites in isomorphously substituted zeolites by extraction of framework Fe to extra framework [23]. The positive effect of steaming has

also been reported for Fe/ZSM-5 zeolites prepared via CVD that were used in benzene hydroxylation with N_2O [21]. Besides, high temperature calcination on Fe-silicalite-1 and Fe-ZSM-5 was also reported to change the catalytic performance in aqueous phase methane oxidation, but the improvement only occurred on the Fe-silicalite-1[13].

Desilication has been reported to control the mesopore generation in zeolites with the ultimate aim of improving transport properties [24]. Adjustable mesoporosity has been achieved with preserved crystalline, microporous, and acidic properties, since the existence of template and aluminum in the zeolites have great influence. Several studies have showed that templates can be helpful for successful alkaline treatment. Pérez-Ramírez *et al.* reported that partial template followed by alkaline treatment can be used to tune the desilication process and that the addition of template molecules (TPA^+ or TBA^+) during desilication can be used as pore-growth moderators [25]. A study by Smirniotis *et al.* verified that templated ZSM-12 samples with Si/Al ratio up to 500 were protected from silicon extraction during alkaline treatment [26]. Perez-Ramirez and co-workers introduced that framework aluminium controlled the process of framework silicon extraction and made desilication selective towards intracrystalline mesopore formation [24]. Based on that, the hierarchical pore system can be controlled dependency on the initial Si/Al molar ratio in the zeolites [27, 28]. As a result, mild alkaline modification was applied to defragment zeolite crystals, and then iron was fully incorporated by liquid-phase ion exchange on zeolites, accordingly reducing agglomeration of Fe species, shorting diffusional path lengths and leading to improve activity [29, 30].

So far, desilication has not been directly applied to Fe-containing zeolites. Moreover, no open literature reported the effect of template and aluminum in Fe-ZSM-5 and Fe-silicalite-1 on desilication. In this study, Fe-ZSM-5 and Fe-silicalite-1 zeolites were alkaline treated in the absence or presence of OSDA. The structural textural properties, the states of Fe species and acid properties of the thus prepared samples were characterized. The effects of template and aluminum in Fe-ZSM-5 and Fe-silicalite-1 on desilication were discussed. Finally, the catalytic performance in BTP reaction was investigated to clarify the influence of alkaline treatment.

5.2. Experiments

5.2.1 Materials

Tetraethyl orthosilicate (TEOS), colloid silica (HS-40, 40 wt.%) and tetrapropylammonium hydroxide (TPAOH) (20-25% in water) were purchased from Tokyo Chemical Industry. NaOH, $Fe(NO_3)_3 \cdot 9H_2O$, $Al(NO_3)_3 \cdot 9H_2O$, H_2O_2 (30 wt.%), acetonitrile, benzene, acetone, acetonitrile and anisole were purchased from Wako. All of the reagents were used as received, without further purification.

5.2.2 Catalysts preparation

For the synthesis of Fe-ZSM-5 zeolites, TEOS was added into the mixed aqueous solution containing TPAOH, $Fe(NO_3)_3$, $Al(NO_3)_3$. The molar ratio of the gel compositions was as follows: 1 Si: 0.025 Al: 0.3 TPA: 0.01 Fe: 45 H_2O. After vigorous stirring at room temperature for 1 h, the resulting gel was transferred to a Teflon-lined autoclave and crystallized with 40 rpm at 443 K for 5 days. The solid products were filtered, washed, and dried. The as-made sample, which was noted as "as-FZ", was calcined at 823 K for 10 h, and then treated by 1 M NH_4NO_3 aqueous solution at 353 K for 3 h twice to obtain the NH_4^+-type ones. H-type sample was made from the NH_4^+-ones by calcination at 823 K for 5 h. Thus obtained product was denoted as "H-FZ".

The Fe-silicalite-1 zeolite was directly prepared with TPA cation in the absence of Na cation as follows. First, colloid silica was added to the solution containing water, TPAOH and Fe $(NO_3)_3 \cdot 9H_2O$. The gel with the molar composition of 1 Si: 0.067 Fe: 0.25 TPA: 20 H_2O was crystallized at 443 K for 7 days with 40 rpm after aging at 353 K for 24 h. Then, the solid product was collected by filtering, rinsing and drying. The as-synthesized material, noted as "as-FS", was calcined at 823 K for 10 h to remove TPA species and then treated by 1 M NH_4NO_3 aqueous solution at 353 K for 3 h twice to obtain the NH_4^+-type ones. H-type sample was made from the NH_4^+-ones by calcination at 823 K for 5 h. Thus obtained catalyst was designated as "H-FS"

The as-FZ and as-FS samples were treated in alkaline aqueous solution using 0.2 M NaOH at 353 K for 2 h. The resultant samples was calcined at 823 K for 10 h. In order to facilitate comparison, the alkaline treatment samples were NH_4^+-exchanged, then calcined at 823 K for 5 h. The final products were designated as "AAT-FZ" and "AAT-FS", respectively.

Similarly, the calcined Fe-ZSM-5 and Fe-silicalite-1 samples were treated in alkaline aqueous solution using 0.2 M NaOH at 353 K for 2 h and 1 h, respectively. The resultant samples were washed, dried overnight, NH_4^+-exchanged and calcined at 823 K for 5 h. The final products were designated as "CAT-FZ" and "CAT-FS".

5.2.3 Characterization of catalysts

XRD patterns were collected on a Rint-Ultima III (Rigaku) using a Cu Kα X-ray source (40 kV, 20 mA). Field-emission scanning electron microscopic (FE-SEM) images of the powder samples were obtained on S-5200 (Hitachi) microscope operating at 1 kV. Elemental analyses of the samples were performed on an inductively coupled plasma-atomic emission spectrometer (ICP-AES, Shimadzu ICPE-9000). Nitrogen adsorption and desorption measurements to obtain information on the micro- and meso-porosities were conducted at 77 K on a Belsorp-mini II (MicrotracBEL).

UV-vis diffuse reflectance spectra were recorded on a V-650DS spectrometer (JASCO). The diffuse reflectance spectra were converted into the absorption spectra using the Kubelka-Munk function.

Temperature-programmed ammonia desorption (NH_3-TPD) profiles were noted down on a Multitrack TPD equipment (Japan BEL). Normally, 25 mg catalyst was pretreated at 773 K for 1 h in a He flow of 50 mL min^{-1} and then cooled down to 423 K. The sample was evacuated at 423 K for 1 h prior to the adsorption of NH_3. Approximately 2500 Pa of NH_3 contacted with the sample at 423 K for 10 min. Subsequently, the sample was evacuated to remove the weakly adsorbed NH_3 at the same temperature for 30 min. Finally, the sample was heated from 423 to 873 K at a ramping rate of 10 K min^{-1} in a He flow of 50 mL min^{-1}.

5.2.4 Catalytic tests

The BTP reaction was carried out in a 25 mL round-bottom flask equipped with a reflux condenser and a magnetic stirrer. In a typical run, the mixture containing 50 mg of catalyst, 10 mL of acetonitrile, 5 mmol of benzene, and 10 mmol of H_2O_2 was stirred at 333 K for 6 h. After the reaction mixture was cooled down, the catalyst was removed. A certain amount of anisole as internal standard was added to the resultant liquid, and the products were fixed by exhaustive acetylation with excess $(CH_3CO)_2O$-K_2CO_3, the derivative products were analyzed by GC [28, 29]. The amount of unconverted H_2O_2 was quantified by standard titration method with 0.1 mol/L $Ce(SO_4)_2$ solution. The phenol yield was based on the amount of phenol produced per the initial amount of benzene. The product selectivity was based on phenol, hydroquinone and catechol.

5.3. Results and discussion

5.3.1 Characterization of the catalysts

5.3.1.1 Physicochemical properties

Figure 5.1 shows the XRD patterns of the different Fe-ZSM-5 and Fe-silicalite-1 catalysts. Both of as-synthesized Fe-ZSM-5 and Fe-silicalite-1 had the typical MFI structure, and after calcinaion the crystallinity of Fe-ZSM-5 and Fe-silicalite-1 were increased. However, the Fe-ZSM-5 has higher crystallinity than Fe-silicalite-1. For AAT-FZ and AAT-FS, the structure and crystallinity remained, indicating that alkaline treatment on the as-synthesized samples did not make seriously desilication. For CAT-FZ, the crystallinity was decreased, suggesting the severe desilication. As for CAT-FS, the crystallinity was not decreased. It was worth to note that the CAT-FS sample was treated in 0.2 M NaOH for only 1 h. The solid yield of CAT-FS was 69%. If the calcined Fe-silicalite-1 was treated for 2 h, the solid yield was only 9%, which topology structure was broken. The solid yield of AAT-FZ, CAT-FZ, AAT-FS were 90%, 27% and 62%, respectively.

Figure 5.2 shows the FE-SEM images of the samples. The Fe-ZSM-5 zeolite displayed the square structure and the flat surface with some tiny cuboids. The particle size of H-FZ was about 3 μm. The overall appearance of AAT-FZ has not changed, but some small pores was added to the flat surface, which produced by the alkaline treatment. In addition, the particle of a part of CAT-FZ was broken after alkaline treatment, indicating that the calcined sample was easily desilicated under the same condition, which was consistent with the result of XRD. The Fe-silicalite-1 zeolite showed the coffin shape with the particle size about 300 nm. No obvious pore on the zeolite was observed due to the small particle size and unsmooth surface. The overall shape of the CAT-FS particle was not destroyed since the the time of alkaline treatment on this sample was short.

The chemical composition of the samples are listed in **Table 5.1**. The actual Si/Al and Si/Fe ratios of H-FZ were higher than those in the synthesis gels, meaning that only part of iron was introduced into the zeolite. For AAT-FZ, the Si/Al and Si/Fe ratios were slightly increased, possibly due to the alkaline treatment on the as-made samples remove the alumina and iron oxide species on the extra framework. However, the Si/Al and Si/Fe ratios of CAT-FZ were much lower than those of H-FZ, suggesting that a large amount of silicon in the calcined sample was removed. For H-FS, the actual Si/Fe ratio was higher than those of AAT-FS and CAT-FS, which also indicated the removing of silicon from as-FS and calcined Fe-silicalite-1.

The N_2 adsorption desorption isotherms and BJH pore size distributions are depicted in **Figure 5.3**. The texture properties were listed in **Table 5.1**. The N_2 adsorption isotherm of the H-FZ sample was of type I with a plateau at higher relative pressures and no distinct hysteresis loop, typical for a microporous material without significant mesoporosity. The S_{BET} (432 m^2g^{-1}) of H-FZ was primarily a result of the presence of micropores, which was in accordance with Ma's results [31]. The N_2

adsorption isotherm of the AAT-FZ sample was similar to that of H-FZ, the S_{EXT}, V_{Total} and V_{Micro} were no much difference, except that the S_{BET} of AAT-FZ was slightly increased to 473 m^2g^{-1}. In the case of CAT-FZ, the isotherm can be ascribed to the type I isotherm with H4-shaped hysteresis loops, indicating the formation of considerable amount of mesopores (0.72 cm^3g^{-1}) accompanying with slight destruction of micropores (0.16 cm^3g^{-1}) after alkaline treatment [32]. Thereby, the S_{BET} and S_{EXT} of CAT-FZ were increased to 683 m^2g^{-1} and 366 m^2g^{-1}. The results of the pore size distribution reveal that H-FZ and AAT-FZ samples possess a narrow and sharp pore-size distribution in the micropore range, which is basically consistent with the pore size (0.53 nm×0.56 nm, IUPAC) of main channel in the ZSM-5 zeolite. The BJH model depending on the adsorption branch demonstrates the presence of mesopores in the CAT-FZ samples, a pronounced development of mesopores distributed at 5 and 12 nm was shown in **Figure 5.3(b)** [31].

Figure 5.4 shows the N_2 adsorption and desorption isotherms and BJH pore size distributions for the parent and alkali-treated Fe-silicalite-1 catalysts. The textural properties are also listed in **Table 5.1**. The S_{BET} of H-FS was 476 m^2g^{-1} and V_{total} was 0.55 cm^3g^{-1}, which were higher than H-FZ due to the smaller particle size. The S_{BET} of AAT-FS was increased to 551 m^2g^{-1}. The isotherms can be ascribed to the type I isotherm with H4-shaped hysteresis loops, indicating the formation of considerable amount of mesopores (1.02 cm^3g^{-1}) accompanying with very low micropores (0.05 cm^3g^{-1}) after alkaline treatment. Among the mesopores, a part of constructional void porosity was contained due to the sharp risen at the p/p0 over 0.9. The CAT-FS showed closed S_{BET} (536 m^2g^{-1}) compared with AAT-FS. But there was no constructional void porosity observed, thus the measured mesopores (0.78 cm^3g^{-1}) was lower than that of AAT-FS. But CAT-FS had mesopores distributed at 13 nm.

5.3.1.2 Fe states

The UV-vis spectra of the Fe-ZSM-5 samples are shown in **Figure 5.5**, which were deconvoluted into sub-bands by applying Gauss functions, as listed in **Table 5.2**. According to the references [33, 34], the bands at about 210 nm should be ascribed to the isolated Fe in tetrahedral coordination and 250 nm assigned to the higher coordination. Generally, the bands below 250 nm were assigned to framework Fe species, the bands between 250-350 nm were ascribed to isolated and oligomeric Fe species on the extra framework (e.g., dimeric, trimeric, and tetrameric Fe species), the bands between 350-450 nm were ascribed to iron oxide clusters, and the bands above 450 nm were ascribed to bulk iron oxide particles less or larger than 2 nm. The bands for as-FZ sample mainly located at 209 nm and 256 nm. The high proportion of 83.5% indicated that most of Fe was introduced into the framework during the crystallization. The remaining 16.5% Fe species mainly concentrated at the bands below

350 nm, indicating small amount of isolated and oligomeric Fe species on the extra framework. For H-FZ, the proportion of bands from 250 nm to 350 nm was increased from 16.5 to 42.8%, indicating that a large amount of Fe in the framework immigrated to the extra framework. What interesting was the composition of Fe species for the AAT-FZ sample, the proportion of isolated and oligomeric Fe species on the extra framework were lower than that of H-FZ, possibly due to part of Fe and Al species on the extra framework being removed after alkaline treatment. The distinct difference of CAT-FZ was the severe aggregated degree of Fe species, isolated and oligomeric Fe species on the extra framework were increased to 47.6%, large Fe species and bulk iron oxide were increased to 11.5% and 7.2%, respectively. Because framework silicon was extracted from the calcined Fe-ZSM-5, the iron and aluminum in the framework were more easily to migrate to the extra framework after calcination due to the defects formed during the alkaline treatment.

Figure 5.6 shows the UV-vis spectra of the different form of Fe-silicalite-1 zeolites, which were deconvoluted into several bands by applying Guass functions. The amount and proportion of different Fe species based on the relative peak areas are listed in **Table 5.2**. The as-FS zeolite took a strong sharp peak at 210 nm with shoulder at 250 nm, assignment to tetrahedral coordination and octahedral coordination. The broad peak at 320 nm was ascribed to oligomeric Fe species on the extra framework, due to the high Fe content in the synthesis gel, part of the Fe species existed on the surface of the zeolite during the crystallization. After calcination, part of Fe species in the framework migrate to the extra framework, thus the intensity of band from 350 to 600 nm was increased. Alkaline treatment on as-FS made the proportion of bands from 300 to 600 nm further increased compare with that of H-FS. Similarly, the proportion of aggregated Fe species for CAT-FS was increased compared with H-FS, but it was not obvious to compare with AAT-FS.

5.3.1.3 Acidity

The acidity measured by NH_3-TPD revealed the Fe environment to a certain degree. **Figure 5.7(a-c)** show the NH_3-TPD profiles of the H-FZ, AAT-FZ and CAT-FZ. Most of the profiles can be deconvoluted into three kinds of peaks at low (373-473 K), medium (473-573 K), and high temperature (573-773 K) (designated as LT, MT, and HT). The amounts of NH_3 adsorbed of the samples are listed in **Table 5.3**. According to the references [11, 35], the LT peak corresponds to NH_3 adsorbed on the non-acidic-OH groups and NH_4^+ by hydrogen bonding, which was not related to the true acid site and excluded in the discussion. The MT peak corresponds to NH_3 adsorbed on the extra framework Fe and Al species (Lewis acid site), and the HT peak corresponds to NH_3 adsorbed on the bridged Si-O(H)-Fe and Si-O(H)-Al (Brønsted acid site) [35].

The acid amount on MT for AAT-FZ was decrease from 0.21 to 0.15 mmol/g compared with H-

FZ, which indicated the decrease Fe species on the extra framework. It was consistent with the result of UV-vis, which showed that the isolated and oligomeric Fe species on the extra framework were reduced for AAT-FZ due to the same reason. The acid amount on HT for AAT-FZ was slightly increased from 0.06 to 0.08 mmol/g compared with H-FZ. The reason was the slight desilication on as-FZ, which slightly decreased the Si/Fe and Si/Al ratios. However, the acid amount on both MT and HT for CAT-FZ were greatly increased due to the decreased Si/Fe and Si/Al ratios and the increased proportion of isolated and oligomeric Fe species on the extra framework after desilication, which were consistent with the results of ICP and UV-vis.

The NH_3-TPD profiles of the H-FS, AAT-FS and CAT-FS are presented in **Figure 5.7(d-f).** The amounts of NH_3 adsorbed of the Fe-silicalite-1 are listed in **Table 5.3**. For both AAT-FS and CAT-FS, the acid amount on MT showed no obvious difference compared with H-FS. However, the acid amount on HT for AAT-FS and CAT-FS were slightly increased. Note that, although the proportion of Fe species for AAT-FS and CAT-FS were similar in UV-vis spectra, the specific states of Fe species may be different. Meanwhile, the acid amount on MT and HT for CAT-FS were slightly higher than AAT-FS.

5.3.2. Direct oxidation of benzene to phenol with H_2O_2 (BTP)

The catalytic performances for the direct hydroxylation of benzene with H_2O_2 over different form of Fe-ZSM-5 and Fe-silicalite-1 are detailed in **Table 5.4**. H-FZ achieved only 0.6% yield with 100% selectivity to phenol, demonstrating the low activity. After alkaline treatment on as-FZ, the phenol yield of AAT-FZ was only increased to 0.8% due to the almost unchanged Fe species and amount. However, after alkaline treatment on calcined Fe-ZSM-5, the phenol yield of CAT-FZ was dramatically increased to 5.3% with 98% phenol selectively. The results were greatly depended on the increased Fe content, which increased the active site. Another possible reason was the function of mesopores, leading the decrease of mass transfer resistance (**Scheme 5.1**).

For Fe-silicalite-1 zeolites, H-FS displayed phenol yield of 5.0% with selectivity of 96%, demonstrating the high activity, which was related to the high Fe content. After alkaline treatment on as-FS, the phenol yield of AAT-FS was also increased to 6.4% with selectivity of 95% due to the increased amount of isolated and oligomeric Fe species, the surface area and the pore size. Similarly, after desilication on calcined Fe-silicalite-1, the phenol yield of CAT-FS was also increased to 7.5% with phenol selectively of 91%. Note that the content of isolated and oligomeric Fe species for CAT-FS was close to AAT-FS, but the states of Fe species was somewhat different, which has been discussed in the acidity. Besides, the textual properties may be another reason, AAT-FS possessed high V_{Meso} (1.02 cm^3g^{-1}), but containing part of constructional void porosity. CAT-FS hold a definite V_{Meso} of 0.78

cm^3g^{-1} and mesopores distributed at 13 nm, which was larger than AAT-FS (**Scheme 5.2**).

5.4. Conclusions

The influence of desilication on as-synthesized and calcined Fe-ZSM-5 and Fe-silicalite-1 zeolites were investigated. Both template and aluminum can prevent desilication and protect the crystal structure. While the introduction of iron in the zeolite did not avoid desilication to a large extent. Thus alkaline treatment on Fe-ZSM-5 and Fe-silicalite-1 is an effective post modification method that affected both the porosity of the zeolite and the nature of Fe species. The increased porosity and surface area can improve the transport properties, reduce diffusion resistance and well disperse of Fe species. After alkaline treatment the phenol yield for Fe-ZSM-5 and Fe-silicalite-1 were increased from 0.6% (H-FZ) to 5.3% (CAT-FZ) and from 5.0% (H-FS) to 7.5% (CAT-FS), respectively.

References

[1] B. Wichterlová, P. Sazama, E. Tábor, P. Šťastný, K. S. Naveen, Z. Sobalík, J. Dědeček, S. Sklenák, P. Klein, A. Vondrová, J. Catal., 312 (2014) 123.
[2] N. K. Sathu, P. Sazama, E. Tabor, B. Wichterlová, S. Sklenák, Z. Sobalík, J. Catal., 299 (2013) 188.
[3] K. Sun, H. Xia, Z. Liu, Z. Feng, P. Ying, C. Li, J. Catal., 270 (2010) 103.
[4] G. Wu, E. Yuan, W. Dai, N. Guana, L. Li, Catal. Sci. Technol., 7 (2017) 3036.
[5] C. Shi, L. Xu, B. Chen, Q. Zhao, Y. Zhu, H. Gies, F. S. Xiao, D. De Vos, T. Yokoi, X. H. Bao, U. Kolb, M. Feyen, S. Maurer, A. Moini, U. Müller, W. Zhang, Micropor. Mesopor. Mater., 236 (2016) 211.
[6] R. T. Yang, G. Qi, Appl. Catal., A, 287 (2005) 25.
[7] L. Meng, X. Zhu, E. J. M. Hensen, ACS Catal., 7 (2017) 2709.
[8] A. Badiei, M. Jourshabani, Z. Shariatinia, N. Lashgari, G.M. Ziarani, Ind Eng Chem Res, 55 (2016) 3900.
[9] Q. Meng, L. Li, J. Wen, J. Wang, G. Tu, C. Xu, F. Zhang, Y. Zhong, W. Zhu, Q. Xiao, Micropor. Mesopor. Mater., 227 (2016) 252.
[10] R. D. Armstrong, V. Peneau, G. Shaw, J. Xu, R. L. Jenkins, D. J. Morgan, N. Dimitratos, S. H. Taylor, H. W. Zanthoff, S. Peitz, G. Stochniol, Q. He, C. J. Kiely, G. J. Hutchings, ChemCatChem, 9 (2017) 642.
[11] G. Wu, F. Hei, N. Zhang, N. Guan, L. Li, W. Grünert, Appl. Catal., A, 468 (2013) 230.
[12] G. Wu, F. Hei, N. Guan, L. Li, Catal. Sci. Technol., 3 (2013) 1333.
[13] C. Hammond, I. Hermans, N. Dimitratos, N. Dimitratos, J. A. Lopez-Sanchez, R. L. Jenkins, G. Whiting, S. A. Kondrat, M. H. ab Rahim, M. M. Forde, A. Thetford, H. Hagen, E. E. Stangland, J. M. Moulijn, S.H. Taylor, D. J. Willock, G. J. Hutchings, ACS Catal., 3 (2013) 1835.
[14] C. Hammond, N. Dimitratos, R. L. Jenkins, J. A. Lopez-Sanchez, S. A. Kondrat, M. H. ab Rahim, M. M. Forde, A. Thetford, S. H. Taylor, H. Hagen, E. E. Stangland, J. H. Kang, J. M. Moulijn, D. J. Willock, G. J. Hutchings, ACS Catal., 3 (2013) 689.
[15] C. Hammond, M. M. Forde, R. Rahim, A. Thetford, Q. He, R. L. Jenkins, N. Dimitratos, J. A. Lopez-Sanchez, N. F. Dummer, D. M. Murphy, A. F. Carley, S. H. Taylor, D. J. Willock, E. E. Stangland, H. Hagen J. Kang, C. J. Kiely, G. J. Hutchings, Angew. Chem. Int. Ed., 51 (2012) 5129.
[16] H. Zhang, L. Chu, Q. Xiao, L. Zhu, C. Yang, X. Meng, F. S. Xiao, J. Mater. Chem. A, 1 (2013) 3254.
[17] H. Liu, Y. Yue, P. Yuan, C. Yu, X. Bao, Scientific Reports, 5 (2015) 9270.
[18] J. Szanyi, F. Gao, J. H. Kwak, M. Kollar, Y. Wang, C. H. Peden, Phys. Chem. Chem. Phys., 18 (2016) 10473.
[19] R. T. Yang, D. Zhang, Energy Fuel, 32 (2018) 2170.
[20] A. Zhang, C. Dai, L. Luo, Z. Zhang, M. Liu, J. Wang, X. Guo, C. Song, Catal. Today, 297 (2017) 335.
[21] E. J. M. Hensen, Q. Zhu, M. M. R. M. Hendrix, A. R. Overweg, P. J. Kooyman, M. V. Sychev, R. A. van Santena, J. Catal., 221 (2004) 560.
[22] R. M. V. Teeffelen, Q. Zhu, R. A. V. Santen, E. J. M. Hensen, J. Catal., 221 (2004) 575.
[23] F. Kapteijn, J. Pérez-Ramírez, J. C. Groen, A. Doménech, G. Mul, J. A. Moulijn, J. Catal., 214 (2003) 33.
[24] L. A. Peffer, J. C. Groen, J. A. Moulijn, J. Perez-Ramirez, Chemistry, 11 (2005) 4983.

[25] D. Verboekend, J. Pérez-Ramírez, A. Bonilla, S. Abelló, Adv Funct Mater, 19 (2009) 3972.
[26] P. G. Smirniotis, X. Wei, Micropor. Mesopor. Mater., 97 (2006) 97.
[27] A. G. Machoke, W. Schwieger, T. Weissenberger, A. Inayat, T. Selvam, M. Klumpp, A. Inayat, Chem. Soc. Rev., 45 (2016) 3353.
[28] J. C. Groen, J. C. Jansen, J. A. Moulijn, J. Perez-Ramı´rez, J. Phys. Chem. B, 108 (35) (2004) 13062.
[29] I. Melián-Cabrera, S. Espinosa, J. C. Groen, B. Linden, F. Kapteijn, J. A. Moulijn, J. Catal., 238 (2006) 250.
[30] J. Groen, A. Bruckner, E. Berrier, L. Maldonado, J. Moulijn, J. P. Ramirez, J. Catal., 243 (2006) 212.
[31] J. Ma, D. Weng, X. Wu, Z. Si, Z. Wu, Prog. Nat. Sci., 23 (2013) 493.
[32] D. H. Choi, J. W. Park, J. H. Kim, Y. Sugi, G. Seo, Polym. Degrad. Stab., 91 (2006) 2860.
[33] P. Sazama, R. Pilar, L. Mokrzycki, A. Vondrova, D. Kaucky, J. Plsek, S. Sklenak, P. Stastny, P. Klein, Appl. Catal., B, 189 (2016) 65.
[34] I. Yuranov, D. Bulushev, A. Renken, L. Kiwiminsker, J. Catal., 227 (2004) 138.
[35] R. Mohammad, Y. Fereydoon, Fuel, 181 (2016) 537.

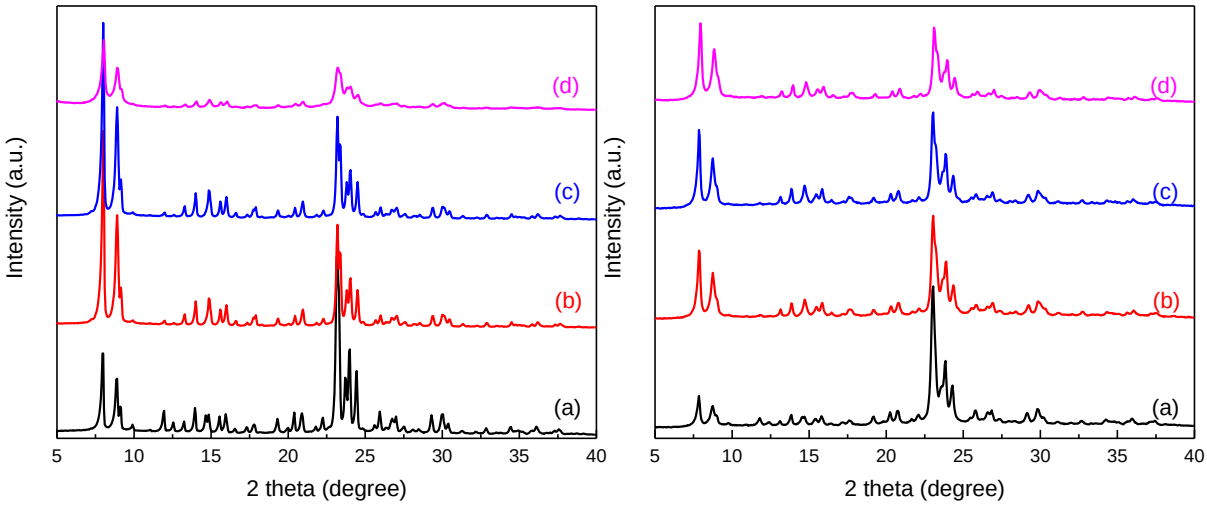

Figure 5.1 XRD patterns of left: (a) as-FZ, (b) H-FZ, (c) AAT-FZ and (d) CAT-FZ and right: (a) as-FS, (b) H-FS, (c) AAT-FS and (d) CAT-FS.

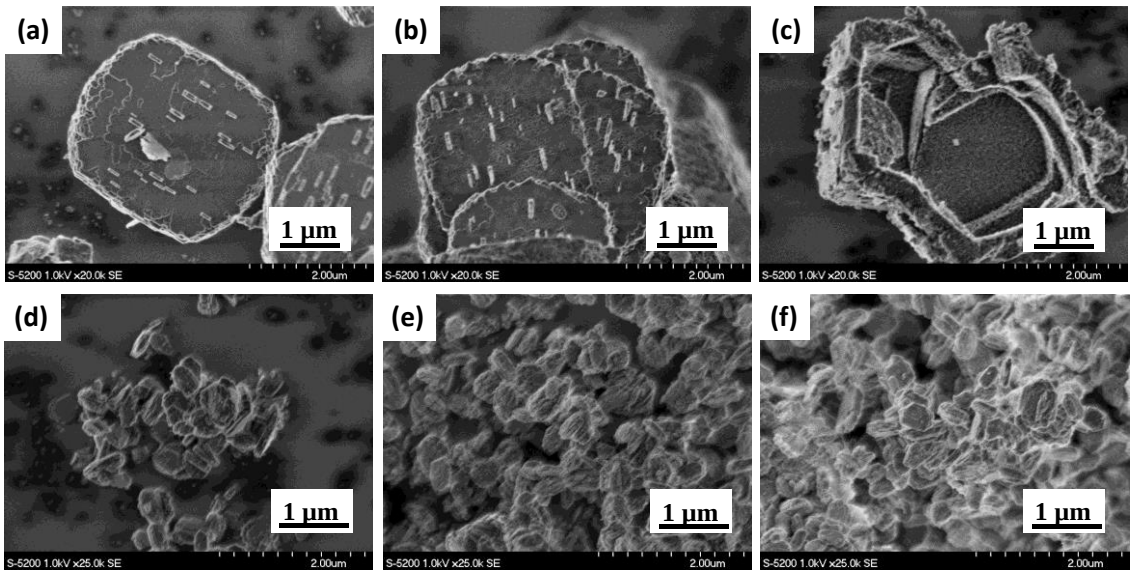

Figure 5.2 FE-SEM images of (a) H-FZ, (b) AAT-FZ, (c) CAT-FZ, (d) H-FS, (e) AAT-FS and (f) CAT-FS.

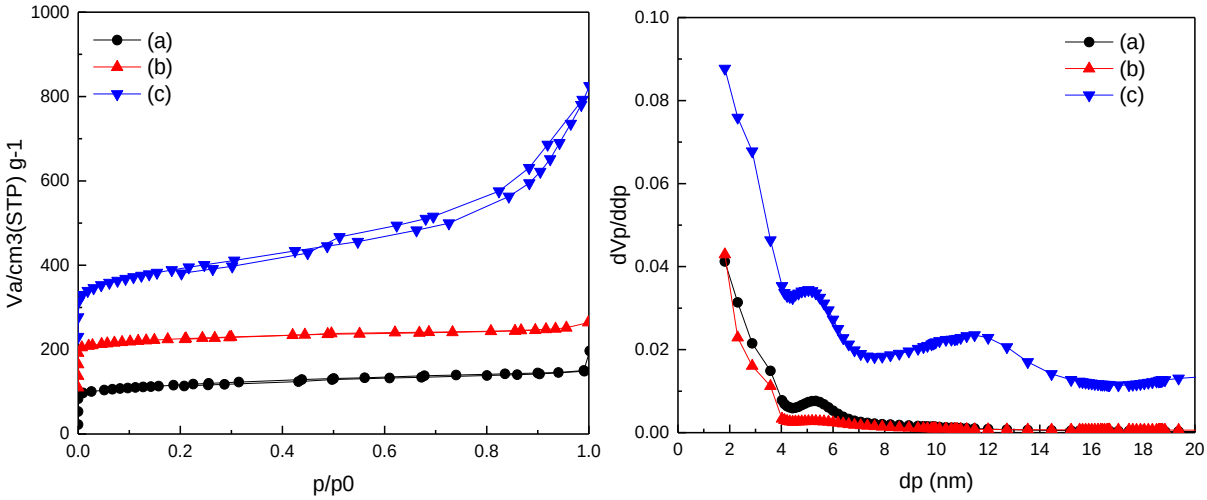

Figure 5.3 Left: N_2 adsorption desorption isotherms and right: BJH pore size distributions of the (a) H-FZ, (b) AAT-FZ and (c) CAT-FZ zeolite.

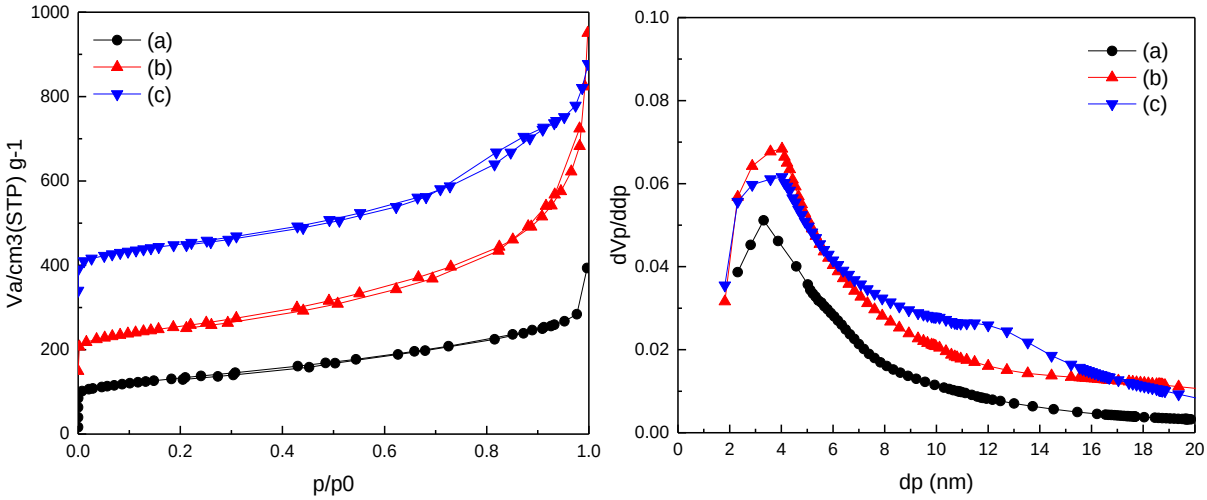

Figure 5.4 Left: N_2 adsorption desorption isotherms and right: BJH pore size distributions of the (a) H-FS, (b) AAT-FS and (c) CAT-FS zeolite.

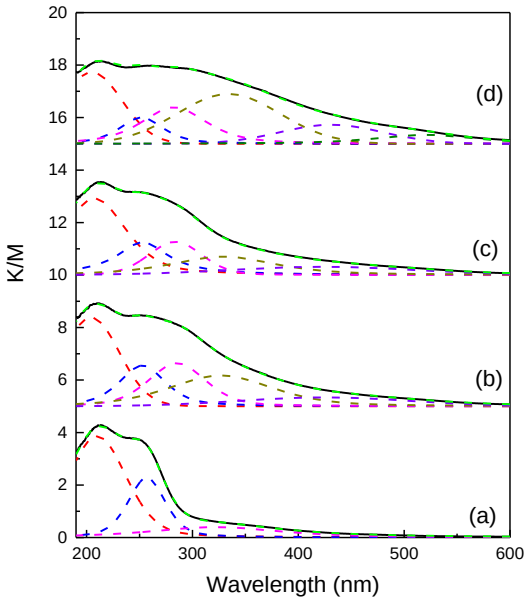

Figure 5.5 UV-vis spectra of (a) as-FZ, (b) H-FZ, (c) AAT-FZ, (d) CAT-FZ.

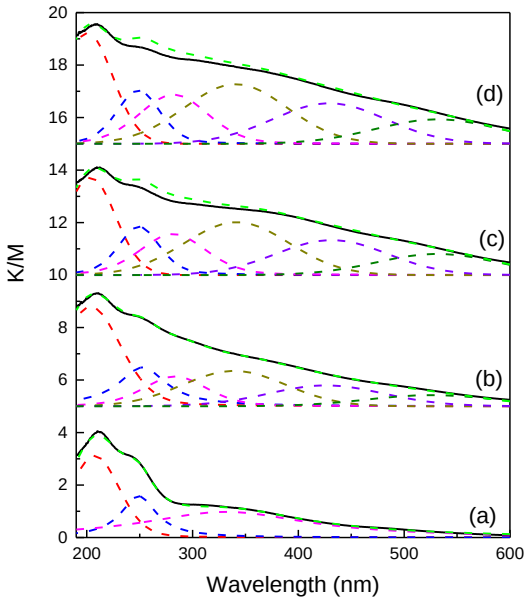

Figure 5.6 UV-vis spectra of (a) as-FS, (b) H-FS, (c) AAT-FS, (d) CAT-FS.

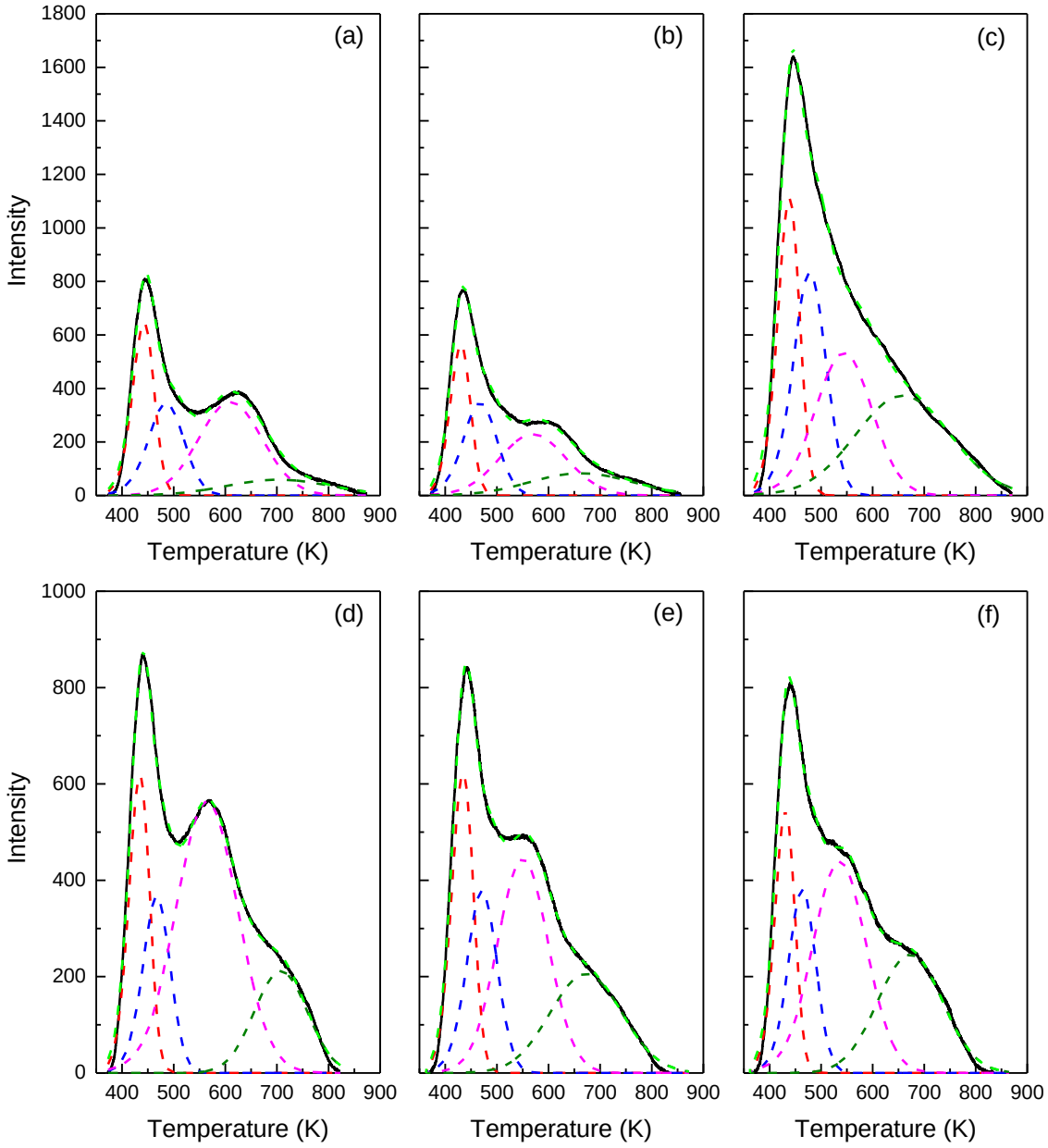

Figure 5.7 NH_3-TPD spectra of (a) H-FZ, (b) AAT-FZ, (c) CAT-FZ, (d) H-FS, (e) AAT-FS and (f) CAT-FS.

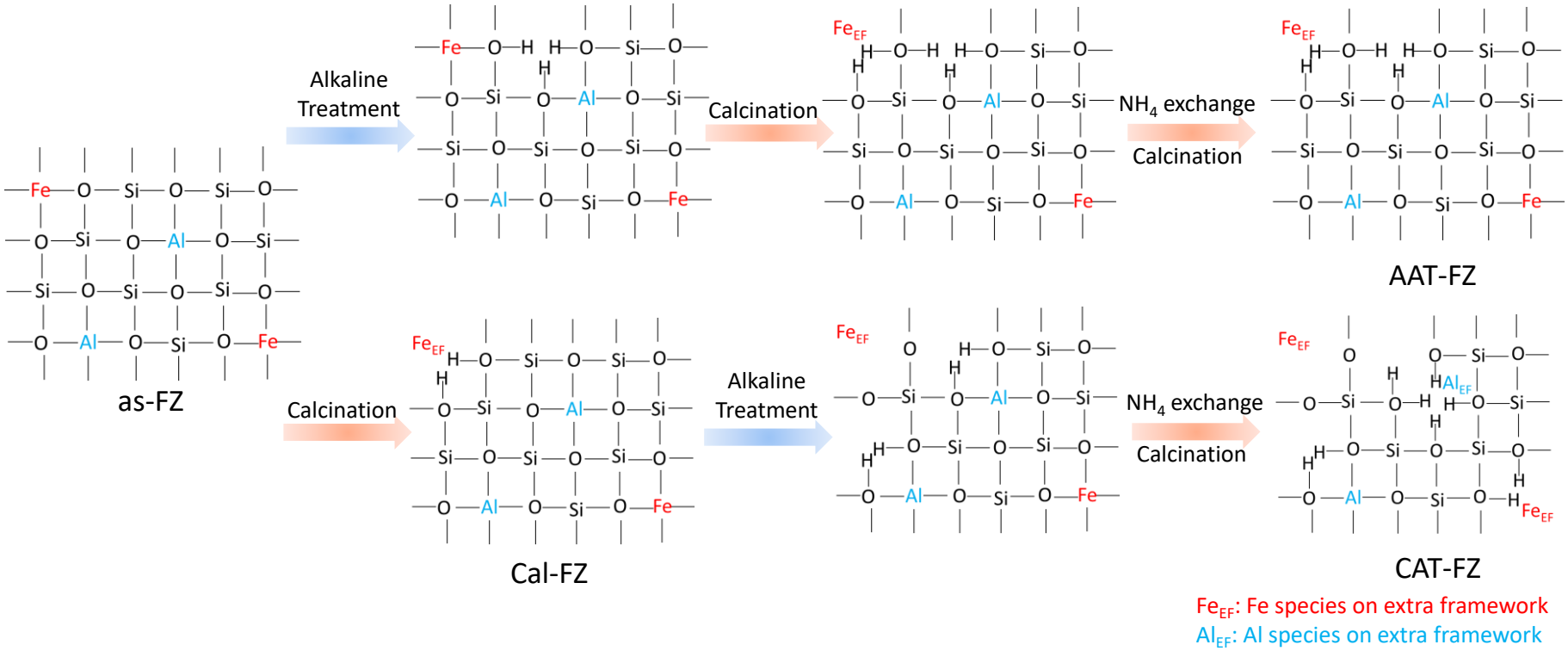

Scheme 5.1 Schematic diagram about the formation of calcined, AAT and CAT type from Fe-ZSM-5 zeolite.

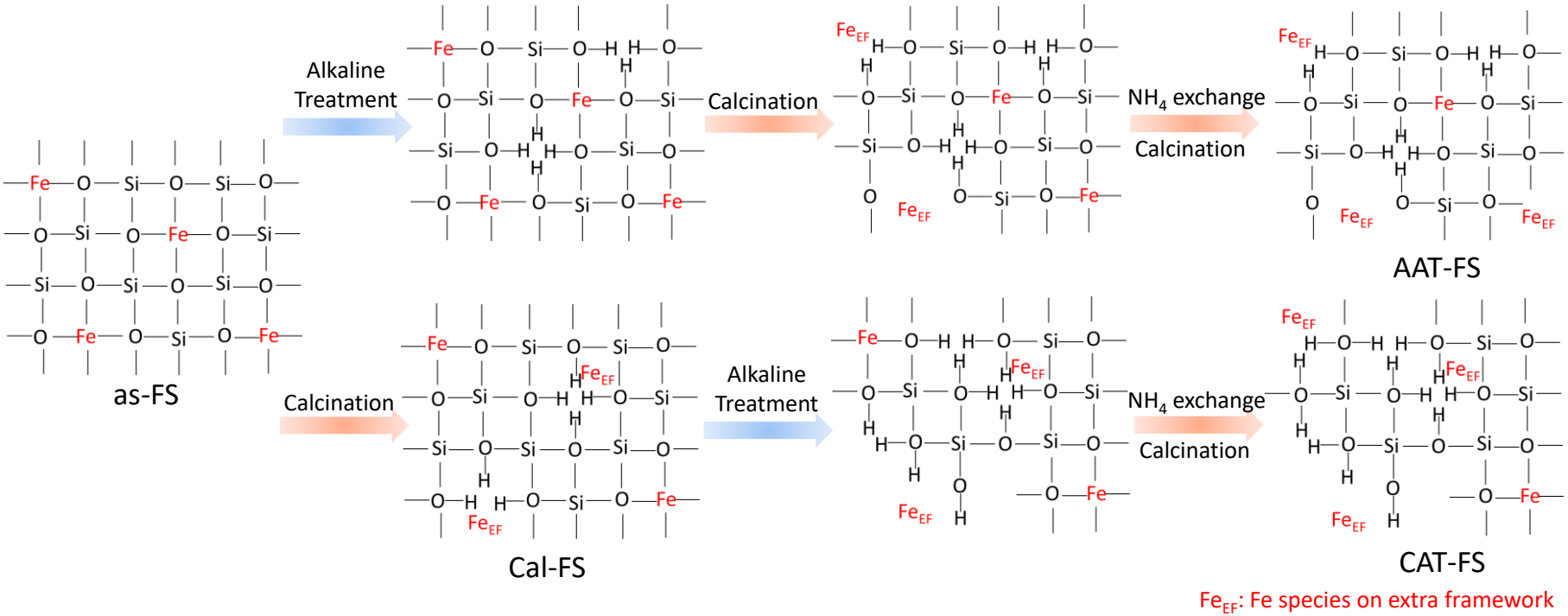

Scheme 5.2 Schematic diagram about the formation of calcined, AAT and CAT type from Fe-silicalite-1 zeolite.

Table 5.1 Physicochemical characteristics of the alkaline modified Fe-ZSM-5 and Fe-silicalite-1 zeolites.

Sample	Alkaline treatment condition	Solid yield (%)[a]	In product [b]			S_{BET} (m^2g^{-1})[c]	S_{EXT} (m^2g^{-1})[d]	V_{Total} (cm^3g^{-1})[e]	V_{Micro} (cm^3g^{-1})[f]	V_{Meso} (cm^3g^{-1})[g]
			Si/Al	Si/Fe	Fe (wt.%)					
H-FZ	-	-	63	184	0.5	432	40	0.23	0.18	0.05
AAT-FZ	0.2 M, 353K, 2h	90	68	202	0.4	473	41	0.25	0.19	0.06
CAT-FZ	0.2 M, 353K, 2h	27	14	50	1.6	683	366	0.92	0.16	0.72
H-FS	-	-	-	19	4.7	476	223	0.55	0.14	0.41
AAT-FS	0.2 M, 353K, 2h	62	-	14	6.5	551	429	1.07	0.05	1.02
CAT-FS	0.2 M, 353K, 2h	9	-	-	-	-	-	-	-	-
CAT-FS	0.2 M, 353K, 1h	69	-	14	6.5	536	416	0.83	0.05	0.78

[a] solid yield = mass after alkaline treatment*100/initial mass.

[b] Si/Fe was determined by ICP-AES analysis, Fe content was calculated by Si/Fe.

[c] Specific surface areas of the catalysts were calculated using the Brunauer-Emmett-Teller (BET) equation on the N_2 adsorption isotherms.

[d] External surface area (S_{EXT}) of the catalysts were calculated by the *t*-plot method based on the adsorption isotherms.

[e] Total pore volumes of the catalysts were calculated based on BET equation on the N_2 adsorption isotherms.

[f] Micropore volumes of the catalysts were calculated by the *t*-plot method based on the adsorption isotherms.

[g] Mesopore volumes = total pore volumes - micropore volumes.

Table 5.2 Percentage of sub-band areas (I_1:λ< 250 nm, I_2: 250 <λ< 350 nm, I_3: 350 <λ< 450 nm, and I_4: λ>450 nm) derived by deconvoluting UV-vis spectra and corresponding Fe species content for Fe-containing MFI zeolite catalysts.

Sample	Framework Fe		Isolated and Oligomeric Fe		Larger Fe clusters		Bulk Fe oxides	
	I_1(%)	wt.%	I_2(%)	wt.(%)	I_3(%)	wt.%	I_4(%)	wt.%
as-FZ	83.5	0.42	16.5	0.08	-	-	-	-
H-FZ	47.6	0.24	42.8	0.21	9.7	0.05	-	-
AAT-FZ	58.1	0.23	30.6	0.12	11.3	0.06	-	-
CAT-FZ	33.7	0.54	47.6	0.76	11.5	0.18	7.2	0.12
as-FS	50.2	2.36	49.8	2.34	-	-	-	-
H-FS	49.1	2.31	30.4	1.43	13.1	0.62	7.5	0.35
AAT-FS	32.7	2.13	38.5	2.50	17.5	1.14	11.4	0.74
CAT-FS	32.1	2.09	38.0	2.47	17.9	1.16	11.9	0.77

Table 5.3 Ammonia adsorbed amount of H-type, AAT and CAT form Fe-ZSM-5 and Fe-silicalite-1 zeolite catalysts

Sample	**Ammonia adsorbed amount (mmol/g)/ T_{max} (K)**			
	LT		**MT**	**HT**
H-type	0.12/443	0.11/485	0.21/612	0.06/695
AAT-FZ	0.10/439	0.11/478	0.15/544	0.08/658
CAT-FZ	0.21/431	0.25/467	0.28/570	0.33/661
H-FS	0.08/435	0.07/467	0.23/563	0.08/707
AAT-FS	0.11/430	0.10/463	0.20/536	0.13/672
CAT-FS	0.09/435	0.09/471	0.22/550	0.15/672

Table 5.4 Catalytic results for the H-type, AAT and CAT form of Fe-ZSM-5 and Fe-silicalite-1 zeolite catalysts for the direct oxidation of benzene to phenol with H_2O_2.

Sample	Phenol Yield (%)[a]	Product Selectivity (%)[b]			H_2O_2 Conv. (%)[c]
		Phenol	HQ	CL	
H-FZ	0.6	100	0	0	46
AAT-FZ	0.8	100	0	0	45
CAT-FZ	5.3	98	1	1	78
H-FS	5.0	96	3	1	96
AAT-FS	6.4	95	3	2	75
CAT-FS	7.5	91	8	1	75

Reaction conditions: 333 K, 10 mmol H_2O_2, 50 mg catalyst, 10 ml CH_3CN, 5 mmol Benzene, 6 h.

[a] Phenol yield = (moles of phenol produced)*100/(initial moles of benzene).

[b] Each product selectivity= (moles of each liquid product)*100/(moles of phenol + moles of HQ + moles of CL).

[c] H_2O_2 conversion = (moles of H_2O_2 after reaction)*100/(initial moles of H_2O_2).

Chapter 6

Direct synthesis of Fe-containing MWW zeolite for direct hydroxylation of benzene to phenol and methane to methanol with H_2O_2

Abstract

Fe-containing MWW zeolite catalysts (i.e. Fe-MWW and Fe,Al-MWW) were directly synthesized. The physiochemical properties, especially the states of Fe species was characterized by using UV-vis and NO adsorbed FT-IR. Fe-MWW showed better performance than Fe,Al-MWW in both MTM and BTP reaction with H_2O_2. The effect of calcination temperature on the catalytic performance in BTP reaction has been studied in detail. Relatively high temperature calcination in the first step to remove OSDA was beneficial to produce more isolated and oligomeric Fe species on the extra framework for Fe-MWW, thus activate the catalytic performance but not good for Fe,Al-MWW. However, increasing the second step calcination temperature to prepare H-type zeolite from NH_4^+-type made more seriously Fe aggregation and reduce the terminal hydroxyl (Fe-OH and/or Al-OH on the extra framework) for both Fe-MWW and Fe,Al-MWW, thus decrease the catalytic performance. The best results were achieved by FW-1023-823, displaying phenol yield of 8.3% with selectivity of 93% in BTP reaction and 855.8 μmol methanol yield with 70% selectivity in MTM reaction with H_2O_2.

6.1. Introduction

C-H activation has become a hot topic in the recent decades due to the huge economic and sustainable value [1]. An early and continuing aspiration of C-H activation is the possibility of methane conversion to useful partial oxidation products such as MeOH [1]. Of course, it also includes the light olefins such as ethylene, propylene, and benzene conversion to high-density energy sources or high value-added chemicals [2]. However, the cleavage of high energy C-H bond (≈440 kcal·mol^{-1}) typically requires harsh reaction conditions resulting in limited substrate scope and low functional group tolerance [3]. As such, C-H activation has not yet found widespread applications in the late stage functionalization of complex molecules, which often contain many functionalities not tolerant of harsh reaction conditions. Substantial efforts have been made to develop an efficient method to activate C-H. Bao *et al.* cover the area of direct conversion of methane to value-added chemicals with their review

of heterogeneous catalytic reactions in gas phase [2]. Direct oxidation of methane to methanol (MTM) and benzene to phenol (BTP) in liquid phase with heterogeneous catalysts, especially zeolite catalysts, are the tiny but popular aspects [4-7]. As a result, the catalytic reaction system with mild reaction condition and decent performance are exactly what the field needs.

MWW structure zeolite is a kind of layered zeolite with high surface area, complex porosity and containing both medium and large pores [8, 9]. The structural complexity derives from the presence of two independent pore systems accessible through 10-ring openings. One of these systems is defined by two-dimensional sinusoidal channels, maintaining an effective 10-ring diameter throughout the structure. The second one includes large supercages with 12-ring openings defined by inner diameter of 7.1 Å and inner length of 18.2 Å [8, 10]. This material is particularly interesting as a considerably higher amount of Fe can be introduced in the T sites of its framework [8]. It is important to mention that ion exchange or impregnation of MWW with Fe-salts in various ways results in poor Fe states, mainly because of the more extensive agglomeration of iron [11]. A simple but reproducible approach to highly active Fe-containing zeolite catalysts is persistently pursued, but it is always hindered by the intrinsic complexity of Fe species [12]. Hence, this work is devoted to the study of Fe-containing MWW zeolite catalysts prepared by isomorphous insertion, i.e. in-situ synthesized. Comparison with the post-synthesis, in-situ synthesized method introduces Fe ions in the framework by mixture Fe-salt in the synthesis gel, and the Fe species including isolated, oligomer, aggregated cluster and iron oxide particles are formed by calcination in air [13]. Hence, the state of Fe ions in the framework in the as-synthesized sample and the conditions of calcination are the key factors for influence the state of Fe species and improving the catalytic activity.

The presence or absence of aluminum in the framework of Fe-containing **MWW** zeolite catalysts is one of the most important factors to affect the Fe state in the framework. According to Hammond *et al.*[14], the function of aluminum in the Fe-containing **MFI** zeolite catalysts are (1) assist the extraction of Fe from the framework to the extra framework and hence increase the formation of the active Fe species and (2) provide an associated negatively charged framework, which is capable of stabilizing and maintaining the dispersion of the cationic Fe species on the extra framework responsible for catalytic activity in direct oxidation of methane to methanol with H_2O_2. In addition, Hensen *et al*. pointed out that an extra framework Fe-Al-O species stabilized in the zeolite micropores was the active

component in the benzene oxidation with nitrous oxide [15-17]. Meanwhile, Hensen's group suggested that the large difference in activity of Fe-silicalite-1 and Fe-ZSM-5 should not be ascribed to a higher active site density in Fe-ZSM-5 but to the chemical difference of Fe species in the Fe-O-Al and Fe-O-Fe adducts [18]. Centi *et al.* indicated that the presence of Al in the zeolite framework is beneficial to reduce the rate of deactivation with respect to Fe-silicalite-1 samples, probably due to the different position of the sites responsible for phenol synthesis and further conversion inside the zeolite channels [19]. Indeed, the presence of aluminum can influence the state of Fe species due to the effect of charge. However, the specific effect of Al on the catalytic performance of Fe-containing **MWW** has not been investigated in the published literatures.

Besides, the calcination temperature and sequence for Fe-MWW and Fe,Al-MWW samples should make a huge impact on the Fe species and catalytic performance. According to Berlier, increase the activation temperature is a general increase in integrated band intensities for Fe-silicalite-1 zeolite [20]. Meanwhile, Hensen *et al.* thought that high-temperature treatments increased the disordered nature of the iron oxide aggregates rather than the presence of an abundant fraction of binuclear iron clusters in Fe-ZSM-5 zeolite [21]. The direct oxidation of methane to methanol with H_2O_2 in liquid phase reported by Hammond *et al.* just verified the abovementioned points, increase the pretreatment temperature with a certain range could increase the catalytic performance of Fe-silicalite-1 but decrease that of the Fe-ZSM-5 [14]. Furthermore, calcination at different stages have different function, such as removing the template, preparing the proton-type sample and activation the catalysts before reaction. Thus, temperature at different calcination stages makes different effects.

To our best knowledge, the influence of the presence of Al, calcination temperature and sequence in the Fe-containing **MWW** zeolite catalysts have not been investigated, let alone the application in hydroxylation of benzene to phenol and methane to methanol with H_2O_2 in liquid phase. In this study, Fe-containing MWW-type zeolite catalysts were prepared by in-situ synthesized method. The effects of aluminum in the synthesis gel, the calcination temperature and sequence on the BTP and MTM reaction with H_2O_2 were investigated in details.

6.2. Experiments

6.2.1 Materials

Fumed silica (Cab-O-Sil M5, Cabot), sodium aluminate (53.1% Al_2O_3, 32.3% Na_2O, Koso Chemical Co., Ltd.), NaOH (97%, Wako), $Fe(NO_3)_3 \cdot 9H_2O$ (99%, Wako), hexamethyleneimine (HMI) (99%, Acros Organics). NH_4NO_3, H_2O_2 (30%), benzene, acetone, acetonitrile, anisole, sulfolane, mesitylene, tetramethylsilane (TMS) and CD_3CN were purchased from Wako. Methane (99.99%) gas was provided by Taiyo Nippon Sanso Co., Ltd.. All of the reagents were used as received, without further purification.

6.2.2 Catalysts preparation

The Fe,Al-MWW lamellar precursor was hydrothermal synthesized with fumed silica, sodium aluminate, NaOH, $Fe(NO_3)_3 \cdot 9H_2O$, hexamethyleneimine (HMI) and deionized water according to the literature [10]. Firstly, 1.62 g $Fe(NO_3)_3 \cdot 9H_2O$, 0.43 g $NaAlO_2$ and 1.03 g NaOH were dissolved in 81 g deionized water and stirred for 10 min. Then, 8.91 g HMI was added and stirred for 1 h. Finally, 6 g fumed silica and 0.3 g DeB-MWW zeolite (5% weight based on the weight of SiO_2), the detail prepared method refer literature [22], were added and further stirred for 1 h to obtain a gel with a molar composition of 1 SiO_2: 0.15 Na_2O: 0.016 Al_2O_3: 0.02 Fe_2O_3: 0.9 HMI: 45 H_2O. The hydrothermal treatment was carried out in a Teflon-lined stainless steel autoclave at 423 K for 5 d under tumbling conditions. The Fe-MWW lamellar precursor was hydrothermal synthesized by the same method without sodium aluminate.

In order to investigate the influence of calcination temperature (K) on the catalytic performance, the first step calcination temperature for removing OSDA was noted as T1, and the second step for preparation H-type sample form NH_4^+-type was donated as T2. The samples were filtered, washed, and dried at 373K to produce the Fe,Al-MWW and Fe-MWW precursors. The as-synthesized samples were calcined in air at T1 for 10 h resulted in the product with the 3D MWW structure. Thus obtained Na-type samples were converted to the H-type one by treating it with 1 M NH_4NO_3 twice at 353K for 3 h then by calcination at T2 for 5 h in air. Thus prepared H-form Fe,Al-MWW and Fe-MWW zeolites were denoted by FAW-T1-T2 and FW-T1-T2.

6.2.3 Characterization of catalysts

XRD patterns were collected on a Rint-Ultima III (Rigaku) using a Cu Kα X-ray source (40 kV, 20 mA). Field-emission scanning electron microscopic (FE-SEM) images of the powder samples were

obtained on S-5200 (Hitachi) microscope operating at 1 kV. The samples for FE-SEM observations were mounted on a carbon-coated microgrid (Okenshoji Co.) without any metal coating. Elemental analyses of the samples were performed on an inductively coupled plasma-atomic emission spectrometer (ICP-AES, Shimadzu ICPE-9000). Nitrogen adsorption and desorption measurements to obtain information on the micro- and meso-porosities were conducted at 77 K on a Belsorp-mini II (Microtrac BEL).

UV-vis diffuse reflectance spectra were recorded on a V-923DS spectrometer (JASCO). The diffuse reflectance spectra were converted into the absorption spectra using the Kubelka-Munk function. FT-IR spectra were obtained by a JASCO FT-IR 4100 spectrometer equipped with a triglycine sulfate (TGS) detector. For FT-IR observation, the sample was pressed into a self-supporting disk (20 mm diameter, ca. 30 mg) and placed in an IR cell attached to a closed gas-circulation system. After the sample was pretreated by evacuation at 773 K for 2 h, then adsorbed 5-1000 Pa NO at ambient temperature. The IR spectra resulting from the subtraction of the background spectra from those with NO adsorbed are shown unless otherwise noted.

Temperature-programmed ammonia desorption (NH_3-TPD) profiles were noted down on a Multitrack TPD equipment (Japan BEL). Normally, 25 mg catalyst was pretreated at 773 K for 1 h in a He flow of 50 mL min^{-1} and then cooled down to 423 K. The sample was evacuated at 423 K for 1 h prior to the adsorption of NH_3. Approximately 2500 Pa of NH_3 contacted with the sample at 423 K for 10 min. Subsequently, the sample was evacuated to remove the weakly adsorbed NH_3 at the same temperature for 30 min. Finally, the sample was heated from 423 to 873 K at a ramping rate of 10 K min^{-1} in a He flow of 50 mL min^{-1}.

The high-resolution ^{27}Al MAS NMR and ^{29}Si MAS NMR spectra were obtained on a JEOL ECA-600 spectrometer (14.1 T) equipped with an additional 1 kW power amplifier. The ^{27}Al and ^{29}Si chemical shifts were referenced to $AlNH_4(SO_4)_2 \cdot 12H_2O$ at -0.54 ppm and polydimethylsiloxane (PDMS) at -34.12 ppm, respectively. The samples were spun at 15 kHz by using a 4 mm ZrO_2 rotor.

6.2.4 Catalytic tests

6.2.4.1 Direct hydroxylation of benzene to phenol (BTP)

The BTP reaction was carried out in a 25 mL round-bottom flask equipped with a reflux condenser

and a magnetic stirrer. In a typical run, 50 mg of catalyst was immersed in 10 mL of acetonitrile, 5 mmol of benzene and 10 mmol H_2O_2 was stirred at 333 K for 6 h. After the reaction mixture was cooled down, the catalyst was removed. A certain amount of anisole as internal standard was added to the resultant liquid, and the products were fixed by exhaustive acetylation with excess $(CH_3CO)_2O$-K_2CO_3, the derivative products were analyzed by GC [23]. The remaining H_2O_2 concentration was quantified by standard titration method with 0.1 mol/L $Ce(SO_4)_2$ solution.

6.2.4.2 Direct conversion of methane to methanol (MTM)

The liquid-phase MTM reaction was carried out in a 100 ml PTFE autoclave. The CH_4 pressure was controlled by the pressure gage. The reactants were stirred vigorously by an agitator blade. In a typical run, 10 ml sulfolane, 50 mg catalyst and 27 mmol H_2O_2 were added to the autoclave and heated to 323 K. The sealed reactor was then purged with CH_4 to 3 Mpa. After reaction 2 h, the autoclave was cooled rapidly to 278 K in an ice bath to minimize any further chemical reaction and reduce loss of volatile products. After separation liquid phase and catalyst, the liquid-phase products were analyzed by ^1H NMR spectroscopy on JEOL ECA-600 spectrometer (14.1 T) equipped with an additional 1 kW power amplifier. Mesitylene and TMS/CD_3CN were used as the internal standard and chemical shift calibrator, respectively. The detectable products in the liquid-phase were CH_3OH, HCOH, HCOOH and CH_3OOH. The amount of unconverted H_2O_2 was quantified by standard titration method with 0.1 mol/L $Ce(SO_4)_2$ solution.

6.3. Results and discussion

6.3.1 Characterization of catalysts

6.3.1.1 Physicochemical properties

The XRD patterns of FW and FAW samples calcined at different temperatures are shown in **Figure 6.1**. The diffraction pattern of all the samples were consistent with those reported by Rubin and Chu [24], indicating that they were well-crystallized MWW-type zeolites. No change was observed among the samples after calcination at different temperatures, meaning good thermal stability for the FW and FAW catalysts. Besides, the diffraction peaks ascribed to bulk iron oxides were not observed in both FW and FAW, indicating the Fe species dispersed well in the samples.

Figure 6.2 shows the SEM images of FW and FAW zeolites, revealing that both Fe-MWW and Fe,Al-MWW samples were composed of very thin flake-like crystals.

Table 6.1 lists the composition and textual properties of the Fe-containing MWW zeolites. The Fe content of Fe,Al-MWW was higher than that of Fe-MWW possibly due to the existence of aluminum in the framework providing some attachment points for Fe species.

Figure 6.3 displays the N_2 adsorption and desorption isotherms of the FW and FAW zeolites calcined at different temperatures. The additional N_2 uptakes at around $0.8 < p/p_0 < 1.0$ were due to the inter particle voids of the flake-like crystals. The average pore diameters displayed no difference between FW and FAW zeolites after calcined at different temperatures (ca. 2.3 nm). Pore size distribution data demonstrate that the MWW zeolites contain uniform mesopores, these mesopores may originate from voids between the zeolite crystals, as shown in **Figure 6.4**. Meanwhile, the peak of the pore size distribution for FW zeolites were higher those of the FAW zeolites, indicating that the uniformity of mesopores for FW zeolites was higher than that of FAW zeolites. As listed in **Table 6.1**, the BET (S_{BET}) and external (S_{EXT}) surface areas of FW were slightly higher than those of FAW zeolite calcined at different temperatures. Besides, FW and FAW samples possessed the same micropore volumes (V_{Micro}) and pretty high total pore volumes (V_{Total}) (0.73-1.15 cm^3g^{-1}). The V_{Total} of FW were decreased a little (1.15 to 0.99 cm^3g^{-1}) with calcination temperature increase, possibly due to the formation of the iron oxide on the pores.

6.3.1.2 Fe states

The coordination state and extent of aggregation of iron in Fe-containing MWW zeolite were investigated by UV-vis spectroscopy. Generally, the bands below 250 nm are assigned to framework Fe species, the bands between 250-350 nm are ascribed to the isolated and oligomeric extra framework Fe species, the bands between 350-450 nm are assigned to aggregated iron oxide, and the bands above 450 nm are ascribed to bulk iron oxide particles [11, 14].

Figure 6.5 shows the UV-vis spectra of FW and FAW zeolites calcined at different temperatures, which were deconvoluted into several bands by applying Guass functions. The amount and proportion of different Fe species based on the relative peak areas are listed in **Table 6.2**. The intensity of bands at high wavenumber for both FW and FAW zeolites were increased with calcination temperature

increase, indicating the formation of more Fe species on the extra framework. Comparison with the directly synthesized Fe-containing **MFI-type** zeolite catalysts, Fe species in the Fe-containing MWW zeolite did not easily aggregate, probable due to the high surface area and big pore size for MWW zeolite [25]. Note that the degree of Fe aggregation after the second step calcination for both FW and FAW were weaker than those of the first step calcination, because most of iron in the framework have already been moved outside in the process of the first calcination. Meanwhile, it was interesting to find that the degree of Fe aggregation for FW was more seriously than that of FAW. Possibly because the existence of aluminum in FAW could separate and stabilize Fe, which has been reported in the literature [14].

The in-situ FT-IR spectroscopy technique using NO as probe molecule was applied to investigate the coordinated unsaturated Fe states on the extra framework. **Figure 6.6** shows the NO-adsorbed FT-IR spectra of FW and FAW samples calcined at different temperatures. For FW catalysts, the asymmetrical peaks at 1862 cm^{-1} with shoulder at 1840 cm^{-1} achieved when the NO pressure was 5 Pa. While the FAW catalysts showed symmetrical peaks at 1867 cm^{-1}, which was assigned to $Fe^{2+}(NO)$. Upon increasing NO pressure, peaks at 1900 cm^{-1} and 1815 cm^{-1} for FW appeared and the intensity enhanced until saturated, the two peaks were both assigned to $Fe^{2+}(NO)_3$. However, for FAW samples, the corresponding peaks at 1900 cm^{-1} and 1815 cm^{-1} slightly right migrated to 1898 cm^{-1} and left shifted to 1819 cm^{-1} and the intensity enhanced along with pressure increase.

For FW samples calcined at higher temperature, the peaks position were basically unchanged while the intensity of these bands were seriously decreased comparison FW-1023-823 and FW-823-823 samples, especially the adsorptions at around 1862 cm^{-1} dropped almost half. The intensity of bands for FW-1023-1023 was decreased one third compared with FW-1023-823, meaning that the increase of the second step calcination temperature was conducive to aggregate, but the degree of Fe aggregation was weaker than that of the first step calcination. Peaks position for FAW were shifted to higher wavenumbers with calcination temperature increase and the intensity of bands at 1898, 1867, 1819 and 1790 cm^{-1} were decreased. Note that the bands at 1867 cm^{-1} of FAW-1023-823 and FAW-1023-1023 migrated left to 1875 cm^{-1}, possibly indicating the formation of Fe-O-Al oligomers [26]. The reduced ratios between FAW-1023-823 and FAW-823-823, FAW-1023-823 and FAW-1023-1023 were less than those of FW. It suggested that the presence of aluminum was prone to disperse Fe and

form the unsaturated Fe species [26]. The different intensity between FW and FAW also indicated the different responsible values for NO adsorbed FT-IR just like that aluminum can provide higher acidity than iron in NH_3-TPD.

Summarize the above characterization results, the influence of calcination temperature on FW and FAW can be displayed in Scheme. 1. For FW, calcination made Fe in the framework migrate to the extra framework and form the abundant Fe species, such as isolated Fe cations, oligomeric cationic Fe complexes, and neutral Fe-oxide clusters (Fe_xO_y) as well as larger Fe-oxide aggregates. High temperature calcination made the migration seriously and caused more severe aggregated between Fe species. However, owing to the high surface area and large pore size provided by the MWW zeolite, it was not easy to aggregate for Fe species compared with MFI or other zeolites. The proportion of isolated Fe and oligomer Fe species were increased. Nevertheless, for FAW, calcination, especially high temperature calcination migrated not only Fe but also Al to the extra framework and formed clustered FeO_x species and $FeAlO_x$ species.

6.3.1.3 Acidity

The ammonia adsorbed amount actually reflect the environment of Fe in the zeolite. **Figure 6.7** shows the NH_3-TPD profiles of Fe-MWW and Fe,Al-MWW zeolite catalysts calcined at different temperatures. The peaks at 373-473 K are denoted as physically adsorption and 573-873K are assigned to strongly adsorbed ammonia on Brønsted and/or Lewis acid sites [27, 28]. The peak at 473-573 K may be due to ammonia weakly adsorbed on the extra framework Fe and/or Al [29]. The ammonia adsorbed amount calculated according to the peak area at 373-473 K, 473-573 K and 573-873 K are demonstrated in **Table 6.3**. It was clear to see that the ammonia adsorbed amount of FW zeolites were much lower than those of FAW on account of aluminum [30].

When the first step calcination temperature was increased from 823 to 923 K, the decreased degree of the ammonia adsorbed amount for both FW and FAW were low, indicating that the amount of the Fe immigration from framework to the extra framework was small. While increasing the first step calcination temperature from 923 to 1023 K, the decreased amount of ammonia adsorbed amount on the Brønsted and/or Lewis acid sites for both FW and FAW were higher than those of increasing the first step calcination temperature from 823 to 923 K. Note that the ammonia adsorbed amount on

the extra framework Fe and/or Al and the Brønsted and/or Lewis acid sites for both FW and FAW were decreased by increasing the second step calcination temperature from 823 to 1023 K. It implied that increasing the second step calcination temperature was not only immigration Fe and /or Al to the extra framework but also affect the coordination and saturation of the Fe and Al species on the extra framework.

The hydroxyl vibrations regions measured by FT-IR can also reflect the Fe states of Fe-containing MWW zeolite catalysts. **Figure 6.8** shows the hydroxyl vibrations regions of FW and FAW samples calcined at different temperatures. The peak at 3746 cm^{-1} is assigned to isolated and terminal silanols. Both FW and FAW samples presented sharp and high peaks at 3746 cm^{-1}, indicating the catalysts with large amount of hydroxyl. The bands at about 3637 cm^{-1} for FW zeolites were ascribed to OH groups bridged between framework Si and Fe atoms. The bands were decreased with the increase of the first and second step calcination temperature. The related bands for FAW samples appeared at around 3621 cm^{-1} correlation with the framework Si, Fe and Al, which were also decreased with calcination temperature increase. Meanwhile the peaks area of FAW samples were larger than those of FW catalysts at 3620-3640 cm^{-1}, which was consistent with the results of NH_3-TPD due to the similar reason. The bands at around 3670 cm^{-1} assigned t to the terminal hydroxyl like Fe-OH and Al-OH were decreased with calcination temperature increasing [31]. The area of the terminal hydroxyl for FW zeolites were slightly higher than those of FAW. According to the reference [32], the binuclear Fe species on the extra framework with the hydroxyl presented higher activity than the ones without hydroxyl.

6.3.1.4 The states of Si and Al in Fe-containing MWM zeolites

The ^{29}Si NMR spectra of the H-type FW and FAW zeolites calcined at different temperatures are shown in **Figure 6.9(a)**. All the samples possessed a main resonance peak at around -111 ppm were assigned to the silicon atoms coordinated by four silicon atoms (Q^4(0Al), $Si(OSi)_4$). And another obvious resonance was at -103 ppm due to the Q^3 silicon atoms ($(OH)Si(OSi)_3$), which were mainly attributed to the surface silanol group, or Si(1Al) or Si(1Fe) for Fe-MWW and Fe,Al-MWW [33]. There was a slightly increase in the spectral intensity between -95 and -105 ppm for FAW compared with FW zeolites. And the substantial broadening of the resonances belonged to Q^3 defect sites by

breaking Si-O-Si bonds, or Si(1Al) and Si(1Fe) due to the presence of Al atom in the FAW zeolites [34]. There was an apparent peaks at -105 ppm for both FW-1023-823 and FAW-1023-823, possibly due to the defect sites by breaking Si-O-Si bonds under high temperature calcination [35]. **Figure 6.9** does not show any fine structure due to the presence of paramagnetic Fe(III) species, which lead to line broadening [36].

Figure 6.9(b) shows the ^{27}Al NMR spectra of FAW-823-823 and FAW-1023-823 zeolite. The Al atoms were introduced into the structure in a tetrahedral form at ca. 56 ppm and existed at the extra framework in hexahedron form at ca. 0 ppm. The same to the ^{29}Si NMR spectra, the curve of the ^{27}Al NMR spectra was not smooth influenced by the paramagnetic Fe(III) species. The peaks area for the tetra-coordinated and hexa-coordinated Al of FAW-1023-823 were smaller than those of FAW-823-823. The possible reason was that high temperature calcination migrated Al in the framework to extra framework and formed alumina or other non-coordinated aluminum species [33, 37].

6.3.2 Direct oxidation of benzene to phenol with H_2O_2 (BTP)

The catalytic performances for the direct hydroxylation of benzene with H_2O_2 over FW and FAW zeolite catalysts calcined at different temperatures are detailed in **Table 6.4**. FW catalysts achieved higher phenol yield than FAW. The result was different from the literatures, which reported that the presence of Al in Fe-containing MFI zeolite catalysts was benefit to the dispersion of Fe on the zeolite thus increasing the catalytic performance [38]. However, the significantly low degree of aggregation for Fe in FW and FAW zeolites demonstrated that even without the presence of Al, Fe could be well dispersed, possibly due to the high surface area, large pore size and the different T sites of MWW from MFI zeolite.

For FW catalysts, the phenol yield was increased with the first step calcination temperature increase from 823 to 1023 K, while it was decreased when the second step calcination temperature was enhanced from 823 to 1023 K. The possible reason was the severe Fe aggregation, especially for the Fe species on the extra framework under the second step calcination. In addition, the reduced terminal hydroxyl produced by the Fe species on the extra framework under high temperature may be another reason. However, the phenol yield of FAW catalysts were decreased with increase the temperature for both the first and second step calcination. The Fe aggregation was one possible reason, but the degree

was not as serious as FW, thus the reason may be the formation of $FeAlO_x$ on the extra framework, which possess low activity [37]. Besides, the deceased terminal hydroxyl perhaps involved. In addition, the phenol selectivity of FW zeolites were at the range of 93-95%, which were lower than those of FAW (95-99%). It implied that the presence of aluminum can improve the selectivity in BTP reaction with H_2O_2.

The phenol yield of FW and FAW were higher than those of Fe-MFI catalysts under the same Si/Fe ratio in the synthesis gel [BTP1]. One of the possible reasons was the well dispersion of Fe on the FW and FAW zeolites due to the higher surface area and larger pore size of MWW zeolite than MFI zeolite. Another reason was the larger reaction space of MWW than MFI zeolite. It was also possible that the abovementioned reasons common caused the different Fe species thus the different catalytic performance in BTP reaction with H_2O_2.

Turnover number (TON) was used to display the catalytic performance, normally the total Fe content on the used catalyst was took to calculate the value, which was noted as TON1. There was no doubt that the TON1 for all the catalysts were a little low due to the high Fe amount and low phenol yield. However, in our research the Fe content of the isolated and oligomeric Fe species on the extra framework was used to calculate the TON2, because the active site was a part of the isolated and oligomeric Fe species on the extra framework, TON2 was closer to the true value. Obviously, FW achieved the highest TON among the Fe-containing zeolite catalysts.

To further clarify the importance of the isolated and oligomeric Fe species on extra framework, **Figure 6.10** displays the change in the phenol yield and TON2 as function of the content of isolated and oligomeric Fe species on extra framework for the FW and FAW catalysts. The phenol yield was proportional to the content of isolated and oligomeric Fe species on extra framework for FW catalyst. But the TON was inversely proportional to the corresponding content, indicating that the increase of phenol yield can not keep up with the increase of analogous Fe content. The relationship of FAW between phenol yield and Fe content was different from that of FW, decrease with the Fe content, which suggesting that the migration of Al from the framework to the extra framework was not beneficial to the catalytic performance or the existence of Al in FAW prevented the movement of Fe from the framework to the extra framework and the formation of active Fe species. Similarly, the TON and the Fe content for FAW showed the same relationship.

6.3.3 Direct oxidation of methane to methanol with H_2O_2 (MTM)

The essential features of the reaction pathways for the benzene-phenol and methane-methanol conversions are identical, especially in bonding characters [39]. Thus, the catalytic performance are the similar to each other theoretically. The influence of the presence of Al in the Fe-containing MWW zeolite, i.e. FW and FAW, and the calcination temperature on catalytic performance were investigated, the detail results as shown in **Table 6.5**. Not surprisingly, FW-823-823 and FW-1023-823 achieved higher methanol yield than FAW-823-823 and FAW-1023-823, respectively. The methanol selectivity for FW-823-823 and FW-1023-823 maintained above 70%, while those of FAW-823-823 and FAW-1023-823 were only 40%. The presence of aluminum in MWW zeolites decreased the selectivity of methanol, which was different from the results of BTP reaction but consistent with the results of Hammond [14]. Meanwhile, high temperature calcination improved the catalytic performance in MTM reaction for FW catalyst, but reduced the catalytic performance for FAW. The results were a little consistent with the paper of Hammond *et al.*[14]. In Hammond's paper, the catalytic performance of Fe-slicalite-1 zeolite in MTM reaction with H_2O_2 was increased with the activation temperature increasing, while the performance of Fe-ZSM-5 was decreased. In addition, the H_2O_2 conversion for FW and FAW were in the range of 25-53%, which were much higher than that of Fe-silicalite-1 catalyst in the same reaction conditions. Meanwhile, the methanol yield of FW-823-823 and FAW-823-823 were higher than those of Fe-silitalite-1 catalysts under the same Si/Fe ratio in the synthesis gel in Chapter 3. As for the reasons, the particle size of methane and the products were smaller than 0.4 nm, which was smaller than the reaction space in MWW (ca.0.5 nm), so as to the higher activity of Fe species in the MWW zeolites was the reason.

6.4. Conclusions

Fe-containing MWW zeolites (i.e. Fe-MWW and Fe,Al-MWW) were synthesized by direct method and extensively characterized, especially the states of Fe species and the acidity of catalysts. Fe-MWW showed better performance than Fe,Al-MWW in both MTM and BTP reaction with H_2O_2. The effect of calcination temperature on the catalytic performance has been studied in detail. Relatively high temperature calcination in the first step to remove OSDA was beneficial to produce more isolated

and oligomeric Fe species on the extra framework for Fe-MWW, thus activate the catalytic performance. But the presence of aluminum in Fe,Al-MWW dispersed iron and high temperature calcination produced the FeAlOx species, which may be not beneficial to the catalytic performance. In addition, increasing the second step calcination temperature to prepare H-type zeolite from NH_4^+-type made more seriously Fe aggregation and reduce the terminal hydroxyl (Fe-OH and/or Al-OH on the extra framework) for both Fe-MWW and Fe,Al-MWW, thus decrease the catalytic performance. The best results were achieved by FW-1023-823, phenol yield of 8.3% with selectivity of 93% in BTP reaction and 855.8 μmol methanol yield with 70% selectivity in MTM reaction with H_2O_2. Both Fe-MWW and Fe,Al-MWW realized considerable and better catalytic performance comparison with Fe-MFI zeolite in BTP and MTM reactions.

References

[1] R. H. Crabtree, A. Lei, Chem. Rev., 117 (2017) 8481.
[2] P. Schwach, X. Pan, X. Bao, Chem. Rev., 117 (2017) 8497.
[3] T. Gensch, M. N. Hopkinson, F. Glorius, J. Wencel-Delord, Chem. Soc. Rev., 45 (2016) 2900.
[4] B. Daniele, B. Luigi, B. Rossella, D. Rino, R. Marco, S. Guido, T. Roberto, T. Cristina, U. Raffaele, Adv. Synth. Catal., 349 (2007) 979.
[5] T. Jiang, W. Wang, B. Han, New J. Chem., 37 (2013) 1654.
[6] C. Hammond, M. M. Forde, R. Rahim, A. Thetford, Q. He, R. L. Jenkins, N. Dimitratos, J. A. Lopez-Sanchez, N. F. Dummer, D. M. Murphy, A. F. Carley, S. H. Taylor, D. J. Willock, E. E. Stangland, H. Hagen J. Kang, C. J. Kiely, G. J. Hutchings, Angew. Chem. Int. Ed., 51 (2012) 5129.
[7] S. Al-Shihri, C. J. Richard, D. Chadwick, ChemCatChem, 9 (2017) 1276.
[8] G. Berlier, M. Pourny, S. Bordiga, G. Spoto, A. Zecchina, C. Lamberti, J. Catal., 229 (2005) 45.
[9] M. Rutkowska, U. Díaz, A. E. Palomares, L. Chmielarz, Appl. Catal., B, 168-169 (2015) 531.
[10] Y. Wang, T. Yokoi, S. Namba, J. N. Kondo, T. Tatsumi, J. Catal., 333 (2016) 17.
[11] L. Meng, X. Zhu, E. J. M. Hensen, ACS Catal., 7 (2017) 2709.
[12] E. Yuan, G. Wu, W. Dai, N. Guana, L. Li, Catal. Sci. Technol., 7 (2017) 3036.
[13] A. Zecchina, M. Rivallan, G. Berlier, C. Lamberti, G. Ricchiardi, Phys. Chem. Chem. Phys., 9 (2007) 3483.
[14] C. Hammond, I. Hermans, N. Dimitratos, N. Dimitratos, J. A. Lopez-Sanchez, R. L. Jenkins, G. Whiting, S. A. Kondrat, M.H. ab Rahim, M. M. Forde, A. Thetford, H. Hagen, E. E. Stangland, J. M. Moulijn, S. H. Taylor, D. J. Willock, G. J. Hutchings, ACS Catal., 3 (2013) 1835.
[15] E. J. M. Hensen, Q. Zhu, R.A. van Santen, J. Catal., 220 (2003) 260.
[16] E. J. M. Hensen, Q. Zhu, R. A. J. Janssen, P. C. M. M. Magusin, P. J. Kooyman, R. A. van Santen, J. Catal., 233 (2005) 123.
[17] E. J. M. Hensen, Q. Zhu, R.A. vanSanten, J. Catal., 233 (2005) 136.
[18] E. J. M. Hensen, Q. Zhu, P. Liu, K. Chao, R. Vansanten, J. Catal., 226 (2004) 466.
[19] S. Perathoner, F. Pinoa, G. Centi, G. Giordano, A. Katovic, J. B. Nagy, Top Catal., 23 (2003) 125.
[20] G. Berlier, C. Lamberti, M. Rivallan, G. Mul, G. Spoto, S. Bordiga, G. Ricchiardi, P. Fisicaro, A. Zecchina, I. Rossetti, E. Selli, L. Forni, E. Giamello, C. Lamberti, J. Catal., 208 (2002) 64.
[21] E. J. M. Hensen, Q. Zhu, M. M. R. M. Hendrix, A. R. Overweg, P. J. Kooyman, M. V. Sychev, R. A. van Santena, J. Catal., 221 (2004) 560.
[22] Y. Wang, T. Yokoi, S. Namba, J. N. Kondo, T. Tatsumi, Appl. Catal., A, 504 (2015) 192.
[23] M. Sasaki, Y. Sato, Y. Tsuboi, S. Inagaki, Y. Kubota, ACS Catal., 4 (2014) 2653.
[24] M. K. Rubin, P. Chu, Composition of synthetic porous crystalline material, its synthesis and use, U.S. Patent United States 1990.
[25] Y. Yue, H. Liu, P. Yuan, C. Yu, X. Bao, Scientific Reports, 9 (2015) 9270.
[26] G. Berlier, A. Zecchina, G. Spoto, G. Ricchiardi, S. Bordiga, C. Lambert, J. Catal., 215 (2003) 264.
[27] I. Hwang, L. J. Lobree, J. A. Reimer, A. T. Bell, J. Catal., 186 (1999) 242.
[28] N. Y. Topsøe, K. Pedersen, E. G. Derouane, J. Catal., 70 (1981) 41.
[29] A. Ayten, H. Christopher, G. Alexandre, Appl. Catal., A, 441-442 (2012) 30.
[30] L. Meng, X. Zhu, B. Mezari, R. Pestman, W. Wannapakdee, E. J. M. Hensen, ChemCatChem, 9 (2017) 3942.

[31] D. J. Wang, J. H. Lunsford, M. P. Rosynek, J. Catal., 169 (1997) 347.
[32] M. He, J. Zhang, X. L. Sun, B. H. Chen, Y. G. Wang, J. Phys. Chem. C, 120 (2016) 27422.
[33] D. Freude, J. Kärger, Handbook of porous solids, 1 (2002) 465.
[34] H. Xu, L. Fu, J. Jiang, M. He, P. Wu, Micropor. Mesopor. Mater., 189 (2014) 41.
[35] S. Choi, J. Coronas, E. Jordan, W. Oh, S. Nair, F. Onorato, D. F. Shantz, M. Tsapatsis, Angew. Chem. Int. Ed. Engl, 47 (2008) 552.
[36] F. Testa, F. Crea, G. D. Diodati, L. Pasqua, R. Aiello, G. Terwagne, P. Lentz, J. B. Nagy, Micropor. Mesopor. Mater., 30 (1999) 187.
[37] F. Gao, M. Kollár, R. K. Kukkadapu, N. M. Washton, Y. Wang, J. Szanyi, C. H. F. Peden, Appl. Catal., B, 164 (2015) 407.
[38] K. Sun, H. Xia, Z. Feng, R. Vansanten, E. J. M. Hensen, C. Li, J. Catal., 254 (2008) 383.
[39] K. Yoshizawa, Y. Shiota, T. Yumura, T. Yamabe, J. Phys. Chem. B, 104 (2000) 734.

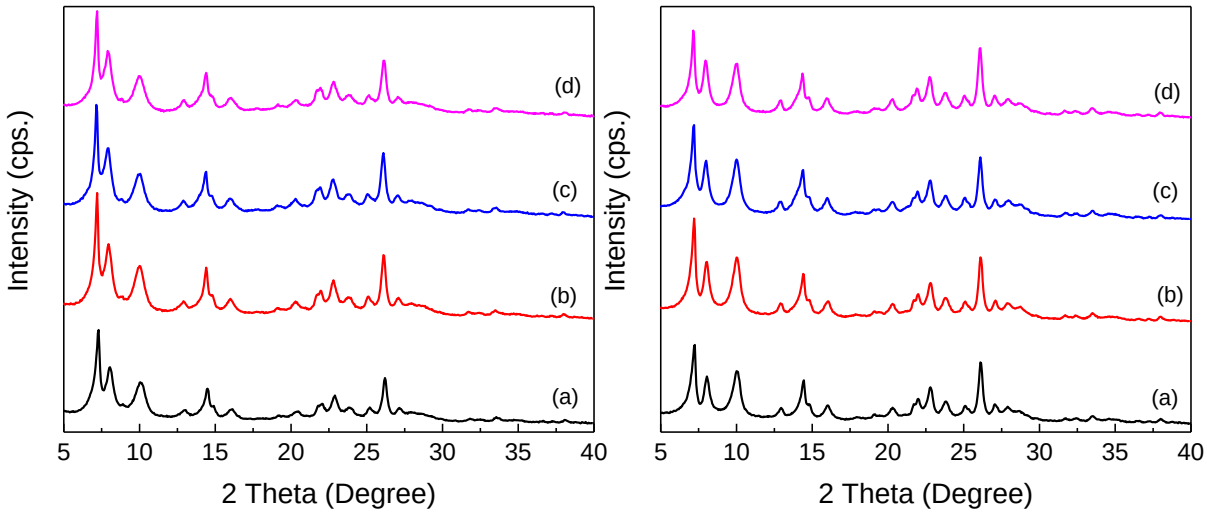

Figure 6.1 XRD patterns of left: (a) FW-823-823, (b) FW-923-823, (c) FW-1023-823 and (d) FW-1023-1023, right: (a) FAW-823-823, (b) FAW-923-823, (c) FAW-1023-823 and (d) FAW-1023-1023.

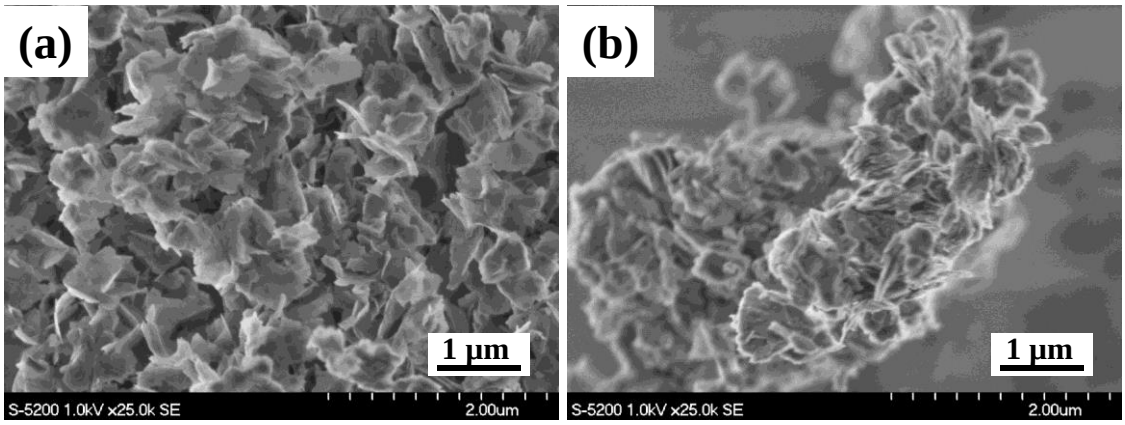

Figure 6.2 FE-SEM images of as-synthesized (a) FW and (b) FAW.

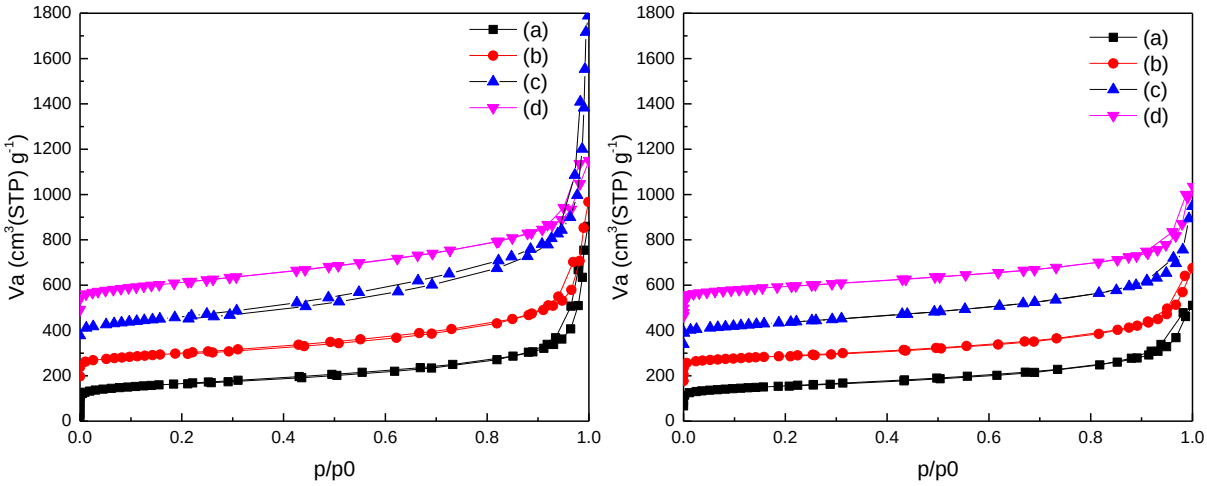

Figure 6.3 N_2 adsorption and desorption isotherms of left: (a) FW-823-823, (b) FW-923-823, (c) FW-1023-823 and (d) FW-1023-1023, right: (a) FAW-823-823, (b) FAW-923-823, (c) FAW-1023-823 and (d) FAW-1023-1023.

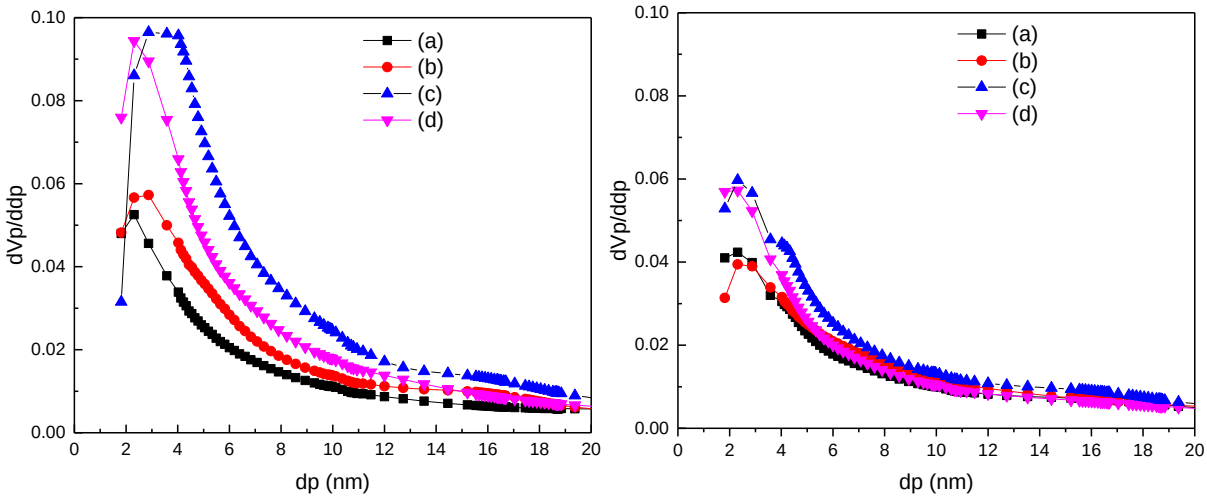

Figure 6.4 Pore size distribution of left: (a) FW-823-823, (b) FW-923-823, (c) FW-1023-823 and (d) FW-1023-1023, right: (a) FAW-823-823, (b) FAW-923-823, (c) FAW-1023-823 and (d) FAW-1023-1023.

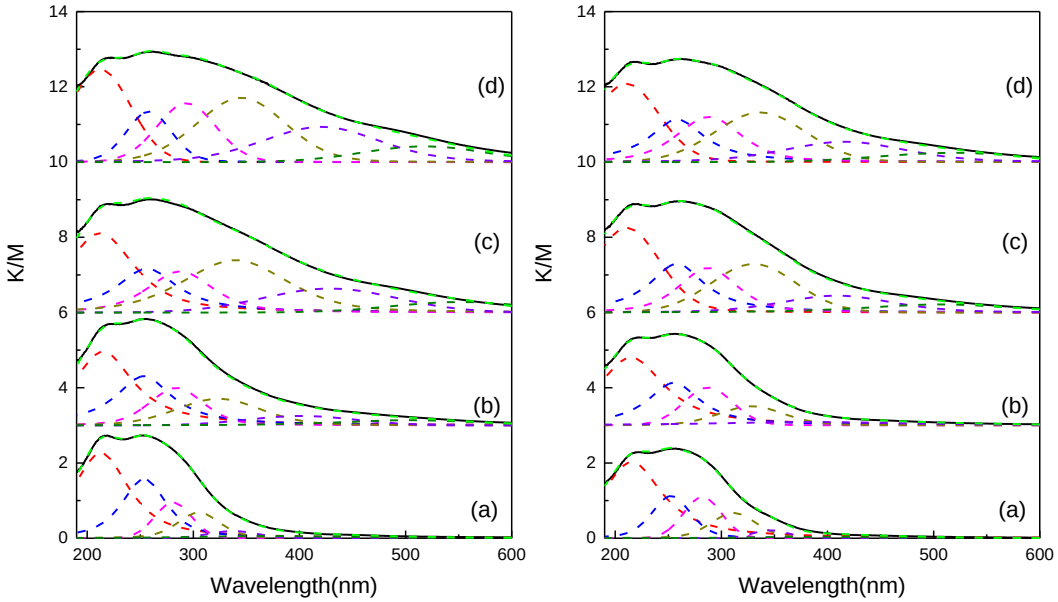

Figure 6.5 UV-vis spectra of left: (a) FW-823-823, (b) FW-923-823, (c) FW-1023-823, (d) FW-1023-1023, and right: (a) FAW-823-823, (b) FAW-923-823, (c) FAW-1023-823, (d) FAW-1023-1023.

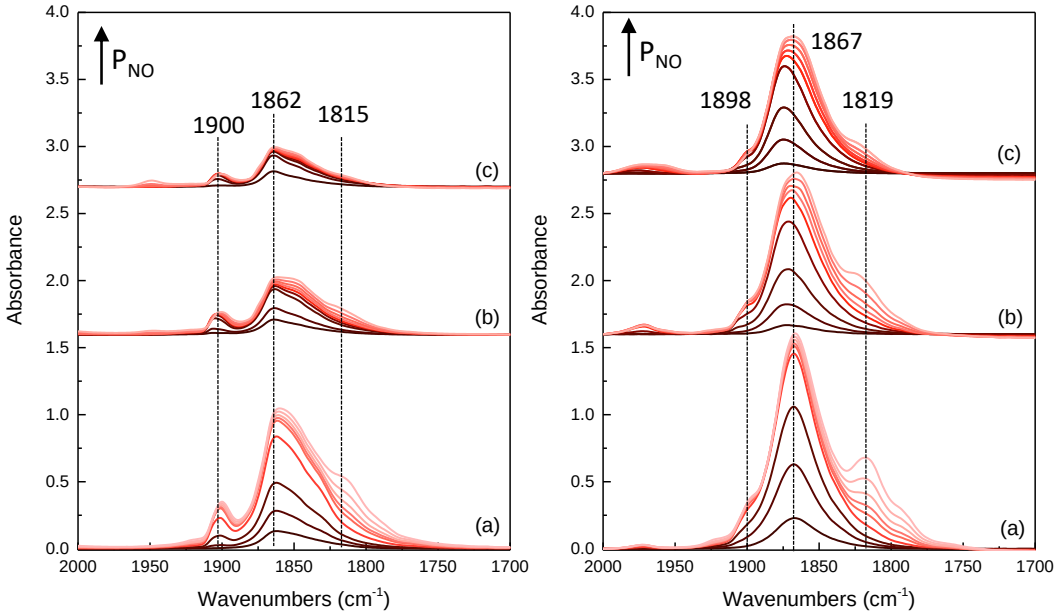

Figure 6.6 NO adsorbed FT-IR spectra (increasing P_{NO} from 5 Pa to 1000 Pa) at room temperature on left: (a) FW-823-823, (b) FW-1023-823, (c) FW-1023-1023, and right: (a) FAW-823-823, (b) FAW-1023-823, (c) FAW-1023-1023.

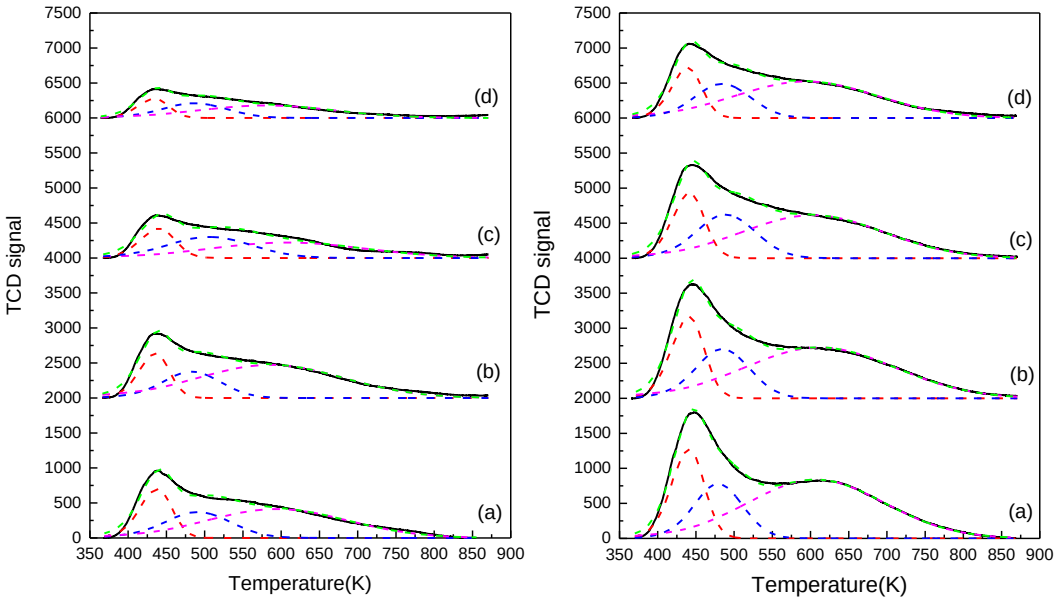

Figure 6.7 NH_3-TPD spectra of left: (a) FW-823-823, (b) FW-923-823, (c) FW-1023-823, (d) FW-1023-1023, and right: (a) FAW-823-823, (b) FAW-923-823, (c) FAW-1023-823, (d) FAW-1023-1023.

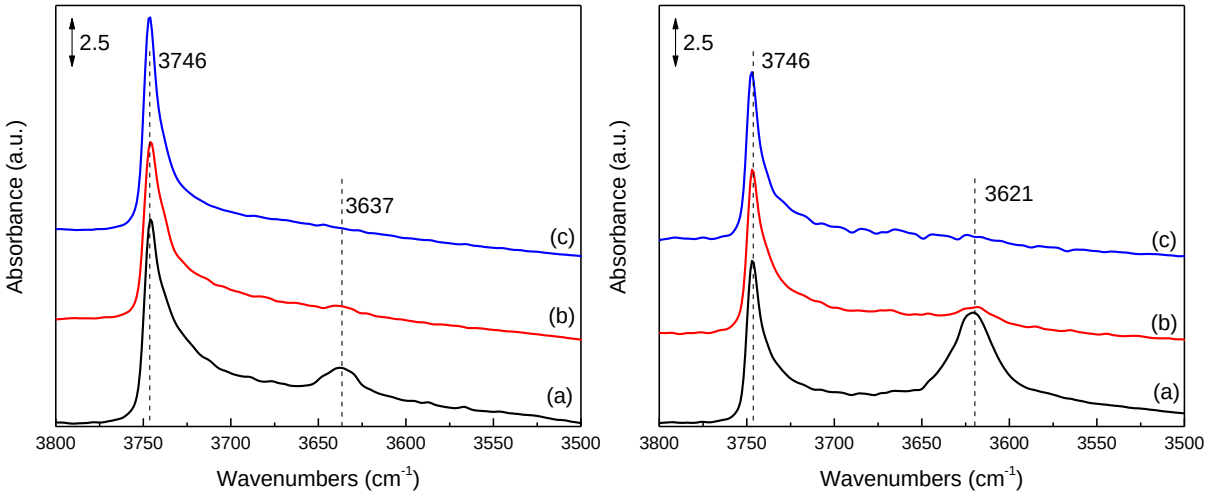

Figure 6.8 FT-IR spectra in the *ν*(OH) vibrations regions of left: (a) FW-823-823, (b) FW-1023-823, (c) FW-1023-1023, and right: (a) FAW-823-823, (b) FAW-1023-823, (c) FAW-1023-1023.

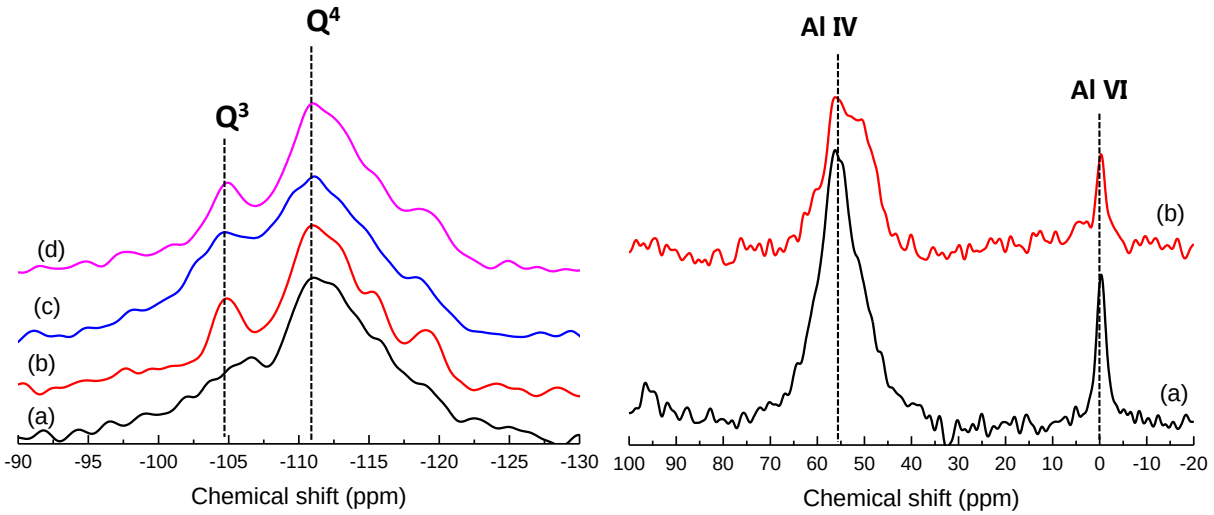

Figure 6.9 Left: ^{29} Si MAS NMR spectra of (a) FW-823-823, (b) FW-1023-823, (c) FAW-823-823, (d) FAW-1023-823; right: ^{27}Al MAS NMR spectra of (a) FAW-823-823 and (b) FAW-1023-823 zeolite catalysts.

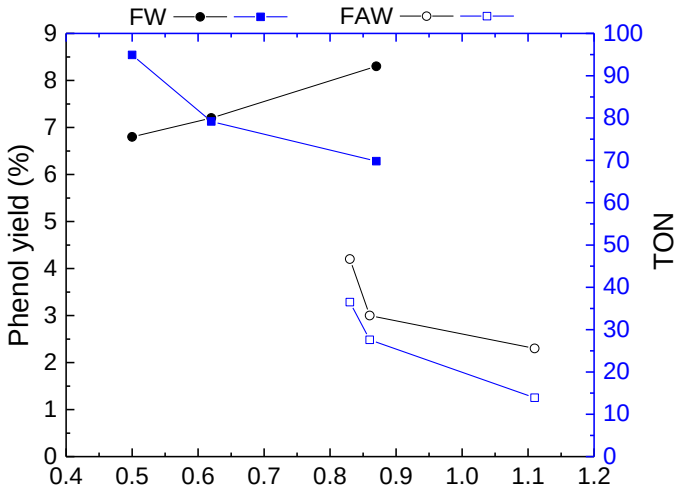

Figure 6.10 Change in the phenol yield and TON as function of the content of isolated and oligomeric Fe species on the extra framework for the FW and FAW zeolite catalysts. Reaction conditions: 50 mg catalyst, 10 ml CH_3CN, 5 mmol Benzene, H_2O_2/Benzene=2, 333 K, 6 h. Phenol yield = (moles of phenol produced)*100/(initial moles of benzene). TON = (moles of phenol + moles of HQ + moles of CL+ moles of p-BQ)*100/(moles of the used Fe content for the isolated and oligomeric Fe species on the extra framework).

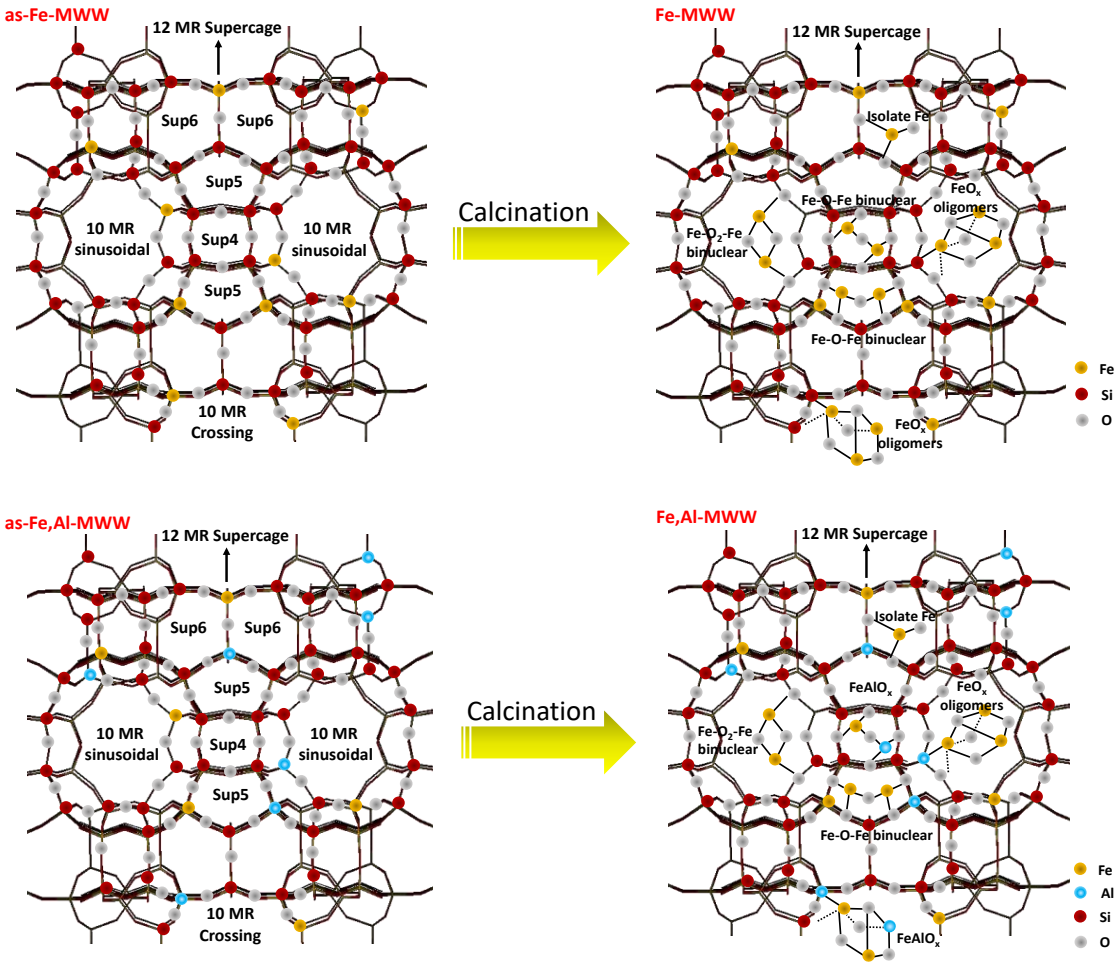

Scheme 6.1. Schematic representation the formation of Fe species for the directly synthesized Fe-MWW and Fe,Al-MWW after calcination.

Table 6.1 Physicochemical characteristics of the FW and FAW zeolite catalysts calcined at different temperatures.

Sample	Si/Al[a]	Si/Fe[a]	Fe (wt.%)[a]	S_{BET} (m^2g^{-1})[b]	S_{EXT} (m^2g^{-1})[c]	V_{Total} (cm^3g^{-1})[d]	V_{Micro} (cm^3g^{-1})[e]
FW-823-823	-	40	2.3	601	264	1.15	0.16
FW-923-823				534	266	1.09	0.17
FW-1023-823				573	342	1.65	0.27
FW-1023-1023				517	385	0.99	0.15
FAW-823-823	31	26	3.2	569	225	0.73	0.16
FAW-923-823				501	214	0.73	0.15
FAW-1023-823				485	276	0.86	0.13
FAW-1023-1023				512	248	0.83	0.14

[a] Si/Fe was determined by ICP-AES analysis, Fe content was calculated by Si/Fe.
[b] Specific surface areas of the catalysts were calculated using the Brunauer-Emmett-Teller (BET) equation on the N_2 adsorption isotherms.
[c] External surface area (S_{EXT}) of the catalysts were calculated by the *t*-plot method based on the adsorption isotherms.
[d] Total pore volumes of the catalysts were calculated based on BET equation on the N_2 adsorption isotherms.
[e] Micropore volumes of the catalysts were calculated by the *t*-plot method based on the adsorption isotherms.

Table 6.2 Numerical analysis of UV-vis spectra of FW and FAW zeolite catalysts calcined at different temperatures. Percentage of the sub-bands (I_1: $\lambda < 250$ nm, I_2: $250 < \lambda < 350$ nm, I_3: $350 < \lambda < 450$ nm, I_4: $\lambda > 450$ nm) and wt.% Fe of the corresponding species.

Sample	Framework Fe		Isolate and oligomer Fe		Aggregated iron oxide		Bulk iron oxide	
	I_1(%)	wt.%	I_2(%)	wt.(%)	I_3(%)	wt.%	I_4(%)	wt.%
FW-823-823	75.5	1.74	21.7	0.50	2.7	0.06	-	-
FW-923-823	63.6	1.46	27.1	0.62	5.8	0.13	5.0	0.12
FW-1023-823	44.2	1.02	38.0	0.87	12.3	0.39	5.5	0.13
FW-1023-1023	33.6	0.77	39.4	0.91	18.8	0.43	8.1	0.19
FAW-823-823	72.4	2.32	25.8	0.83	1.9	0.06	-	-
FAW-923-823	67.6	2.16	26.8	0.86	5.6	0.18	-	-
FAW-1023-823	47.2	1.51	34.8	1.11	10.2	0.33	7.2	0.23
FAW-1023-1023	41.8	1.34	38.7	1.24	13.2	0.42	6.4	0.20

Table 6.3 Ammonia adsorbed amount of FW and FAW zeolite catalysts calcined under different temperatures.

Sample	Ammonia adsorbed amount (mmol/g)/T_{max} (K)		
	LT	**MT**	**HT**
FW-823-823	0.13/438	0.15/492	0.36/590
FW-923-823	0.11/435	0.15/484	0.34/589
FW-1023-823	0.09/440	0.16/508	0.21/610
FW-1023-1023	0.05/435	0.08/489	0.15/579
FAW-823-823	0.24/440	0.23/479	0.70/605
FAW-923-823	0.22/442	0.24/489	0.65/608
FAW-1023-823	0.18/439	0.23/486	0.54/591
FAW-1023-1023	0.12/441	0.17/485	0.46/611

Table 6.4 Catalytic results of FW and FAW zeolite catalysts under different temperatures calcination for the direct oxidation of benzene to phenol with H_2O_2.

Sample	Phenol Yield (%)[a]	Product Selectivity (%)[b]				H_2O_2 Conv. (%)[c]	TON1[d]	TON2[e]	Refer.
		Phenol	HQ	CL	p-BQ				
FW-823-823	6.8	94	5	1	0	88	20.6	94.9	
FW-923-823	7.2	95	4	1	0	91	21.4	70.2	
FW-1023-823	8.3	93	5	2	0	88	26.4	69.8	
FW-1023-1023	5.0	95	3	1	1	82	15.6	39.5	This
FAW-823-823	4.2	95	5	0	0	98	9.5	36.5	Chapter
FAW-923-823	3.0	97	3	0	0	98	6.5	27.6	
FAW-1023-823	2.3	97	3	0	0	95	4.8	13.9	
FAW-1023-1023	1.2	99	1	0	0	98	2.5	6.6	
FMD25	3.7	97	2	1	0	76	6.3	16.3	Chapter
FZP2.5	3.0	99	1	0	0	44	3.9	19.3	2

Reaction conditions: 333 K, 10 mmol H_2O_2, 50 mg catalyst, 10 ml CH_3CN, 5 mmol Benzene, 6 h.

[a] Phenol yield = (moles of phenol produced)*100/(initial moles of benzene).

[b] Each product selectivity = (moles of each liquid product)*100/(moles of phenol + moles of HQ + moles of CL+ moles of p-BQ).

[c] H_2O_2 conversion = (moles of H_2O_2 after reaction)*100/(initial moles of H_2O_2).

[d] TON1=(moles of phenol + moles of HQ + moles of CL+ moles of p-BQ)*100/(moles of the total Fe content used).

[e] TON2=(moles of phenol + moles of HQ + moles of CL+ moles of p-BQ)*100/(moles of the used Fe content for the isolated and oligomeric Fe species on the extra framework).

Table 6.5 Catalytic performance for Fe-containing MWW zeolite catalysts using sulfolane as reaction solvent for the direct oxidation of methane to methanol with H_2O_2.

Catalyst	Product Amount (μmol)				MeOH Selec.(%)	H_2O_2		Refer.
	MeOH	HCOOH	HCOH	MeOOH		Conv. (%)[b]	Eff. (%)[c]	
FW-823-823	729	91	115	0	78	25	16	
FAW-823-823	552	151	500	0	46	53	8	This
FW-1023-823	856	179	144	49	70	43	11	Chapter
FAW-1023-823	339	273	96	80	43	38	8	
FMD25	209	15	115	0	55	7	22	Chapter 2

Reaction conditions: 323 K, 27 mmol H_2O_2, 50 mg catalyst, 10 ml sulfolane, 3 Mpa CH_4, 2 h.

[a] Each product selectivity= (moles of each product)*100/(moles of total liquid products).

[b] H_2O_2 conversion = (moles of H_2O_2 after reaction)*100/(initial moles of H_2O_2).

[c] H_2O_2 efficiency = (moles of total liquid products)*100/(moles of H_2O_2 conversion).

Chapter 7

Iron- and copper-exchanged Beta zeolite catalysts for hydroxylation of benzene to phenol and methane to methanol with H_2O_2

Abstract

Fe-exchanged, Cu-exchanged and Fe-Cu bimetallic exchanged Beta catalysts were prepared by the aqueous ion-exchange method with the loading of metal varied. The metallic states were investigated by UV-vis, NO adsorbed FT-IR and NH_3-TPD. The influence of the reaction conditions in BTP reaction on the catalytic performance on Fe and/or Cu-containing Beta zeolite catalysts were studied in details. The stability in the BTP reaction of the Fe and/or Cu-containing Beta zeolite catalysts were investigated. Fe-Cu bimetallic exchanged Beta catalyst showed a dramatically high catalytic activity in both the BTP and MTM reaction comparison with the Fe/Beta and Cu/Beta zeolites, the highest phenol yield of 10.5 % with the selectivity of 90 %, and the highest MeOH yield of 720 μmol with the selectivity 57% were achieved.

7.1. Introduction

Direct hydroxylation of benzene to phenol (BTP reaction) and methane to methanol (MTM) have attracted increasing attention in recent decades because of the economic outlook, environmental friendliness and technical difficulty [1-3]. However, take BTP reaction as an example, direct introduction of hydroxyl functionality into benzene is still full of challenging. Almost all the developed catalytic systems in the gas phase require an elevated temperature and suffer from low conversion because of the notoriously low reactivity of aromatic C−H bonds [4-5]. Moreover, in liquid phase phenol is easily over-oxidized to produce by-products such as catechol (CL), hydroquinone (HQ), benzoquinones (*p*-BQ), and tars, which makes the low selectivity [6]. Substantial efforts have been made to develop an efficient method to direct hydroxylation of benzene to phenol with H_2O_2.

Bianchi and co-workers used titanium silicalite (TS-1) as catalyst, obtaining 4.5% of benzene conversion with 43% of phenol selectivity in acetonitrile [7]; when they applied TS-1B, which modified with NH_4HF_2 and H_2O_2, the benzene conversion of 8.6% with phenol selectivity of 94% was achieved in sulfolane [8]. CuAPO-5 zeolite was applied in the BTP reaction, 5.9% benzene conversion

with 68% phenol selectivity was attained [9]. Besides, the BTP reaction was executed on Fe/TS-1 mixture, a reasonable phenol yield of 7.6% with selectivity of 15% was obtained [10]. It is clear to see that the Fe, Cu, Ti and so on are widely used in the oxidation of benzene to phenol with H_2O_2 but the Fe-Cu bimetallic composite zeolite catalysts are rarely reported.

In addition, studies have shown that the reaction intermediates and the transition states in this reaction pathway of benzene to phenol are quite similar to those in the methane-methanol conversion pathway with respect to essential bonding characters [11]. Benzene and methane, especially methane is recognized as one of the most stable hydrocarbons due to its perfectly symmetrical tetrahedron structure [12]. The dissociation energy of the methane C-H bond is 440 $kJ \cdot mol^{-1}$ and hence its activation may require harsh conditions [12]. Typically, the products of direct conversion methane to methanol are trace and high requirement on the equipment [13]. It seems that the benzene-phenol process is slightly easy compared to the methane-methanol process, judging from the published papers concerning the hydroxylation of methane and benzene [14]. Besides, the products of benzene-phenol process are easier to detect [15]. Hence, benzene to phenol process can be selected as the screening reaction to investigate the catalytic performance in this research. The catalysts with good catalytic performance are then applied in the methane-methanol process.

Beta zeolite has large 12-membered-ring pores with three-dimensional interconnection, is thermally stable, and can be easily obtained with a varied range of Si/Al ratio. Meanwhile its open crystalline structure decreases the diffusion path of reactants [16]. Fe-exchanged Beta zeolite has been widely used in the selective catalytic reduction (SCR) of NO_x [17-18], N_2O decomposition [19-20], hydroxylation of benzene to phenol with N_2O and so on [21], but it is rarely reported in direct oxidation of benzene to phenol with H_2O_2.

Moreover, the introduction of Fe and Cu cations together by ion-exchanged has been established in other fields. Gao *et al.* studied on Fe- and Cu-exchanged Beta for NH_3-SCR, a clear synergetic effect between Fe and Cu species was found [22]. Hammond and co-workers have reported that the Cu-Fe/ZSM-5 catalyst used as an efficient heterogeneous catalyst for the direct oxidation of methane to methanol with H_2O_2 under mild reaction conditions, and the presence of Cu cation maintain the high selectivity to alcohol [23]. However, no published paper involve in both Fe- and Cu-exchanged Beta for the BTP reaction in liquid-phase with H_2O_2. Besides, the influence of the Fe and/or Cu contents on

the catalytic performance has not fully been investigated.

In the study, Fe and/or Cu Beta zeolite catalysts with different metal contents were prepared. The states of the Fe and Cu species were investigated by UV-vis, NO adsorbed FT-IR, and NH_3-TPD. The influence of metallic type and content on the hydroxylation of benzene to phenol and methane to methanol with H_2O_2 were studied. Meanwhile, the effects of reaction conditions on the catalytic performance of Fe and/ or Cu-containing Beta zeolite catalysts in BTP reaction were investigated.

7.2. Experiments

7.2.1 Materials

NH_4^+-Beta (Si/Al=12) was provided by Zeolyst. $Fe(NO_3)_3 \cdot 9H_2O$, $Cu(NO_3)_2 \cdot 3H_2O$, H_2O_2 (30 wt.%), benzene, acetonitrile, sulfolane, mesitylene, anisole, 1,4-dioxane, tetramethylsilane (TMS), and CD_3CN were purchased from Wako. Methane (99.99%) gas was purchase from Taiyo Nippon Sanso Co., Ltd.. All of the reagents were used as received, without further purification.

7.2.2 Catalyst preparation

The Fe/Beta and Cu/Beta catalysts were prepared by aqueous ion exchange of NH_4^+-Beta (Zeolyst, Si/Al=12) with $Fe(NO_3)_3$ or $Cu(NO_3)_2$ solutions at 353 K. After stirring 24 h, the suspension was vacuum filtered, washed, dried at 373 K overnight and calcined in air at 823 K for 5 h. The obtained products were denoted as "*x*Fe/Beta" or "*y*Cu/Beta", where *x* and *y* were the inputting Fe and Cu content (wt.%), respectively (based on the zeolite). The Fe and Cu bimetallic exchanged Beta zeolite catalysts were prepared by adding $Fe(NO_3)_3$ and $Cu(NO_3)_2$ aqueous solutions together to NH_4^+-Beta. The other steps were the similar to those of Fe/Beta. The obtained products were denoted as "*x*Fe-*y*Cu/Beta", where *x* and *y* were the inputting Fe and Cu content (wt.%), respectively.

7.2.3 Characterization of catalysts

XRD patterns were collected on a Rint-Ultima III (Rigaku) using a Cu Kα X-ray source (40 kV, 20 mA). Elemental analyses of the samples were performed on an inductively coupled plasma-atomic emission spectrometer (ICP-AES, Shimadzu ICPE-9000).

UV-vis diffuse reflectance spectra were recorded on a V-650DS spectrometer (JASCO). The

diffuse reflectance spectra were converted into the absorption spectra using the Kubelka-Munk function. Fourier Transform Infrared (FT-IR) spectra were obtained by a JASCO FT-IR 4100 spectrometer equipped with a triglycine sulfate (TGS) detector. For FT-IR observation, the sample was pressed into a self-supporting disk (20 mm diameter, ca. 30 mg) and placed in an IR cell attached to a closed gas-circulation system. After the sample was pretreated by evacuation at 773 K for 2 h, then adsorbed 5-1000 Pa NO at ambient temperature. The IR spectra resulting from the subtraction of the background spectra from those with NO adsorbed are shown unless otherwise noted.

Temperature-programmed ammonia desorption (NH_3-TPD) profiles were noted down on a Multitrack TPD equipment (Japan BEL). Normally, 25 mg catalyst was pretreated at 773 K for 1 h in a He flow of 50 mL min^{-1} and then cooled down to 423 K. The sample was evacuated at 423 K for 1 h prior to the adsorption of NH_3. Approximately 2500 Pa of NH_3 contacted with the sample at 423 K for 10 min. Subsequently, the sample was evacuated to remove the weakly adsorbed NH_3 at the same temperature for 30 min. Finally, the sample was heated from 423 to 873 K at a ramping rate of 10 K min^{-1} in a He flow of 50 mL min^{-1}.

7.2.4 Catalytic tests

7.2.4.1 Direct conversion of benzene to phenol with H_2O_2 (BTP)

The BTP reaction was carried out in a 25 mL round-bottom flask equipped with a reflux condenser and a magnetic stirrer. In a typical run, the mixture containing 50 mg of catalyst, 10 mL of acetonitrile, 5 mmol of benzene, and 10 mmol of H_2O_2 was stirred at 333 K for 6 h. After the reaction mixture was cooled down, the catalyst was removed. A certain amount of anisole as internal standard was added to the resultant liquid, and the products were fixed by exhaustive acetylation with excess $(CH_3CO)_2O$-K_2CO_3, the derivative products were analyzed by GC [24]. The amount of unconverted H_2O_2 was quantified by standard titration method with 0.1 mol/L $Ce(SO_4)_2$ solution.

7.2.4.2 Direct conversion of methane to methanol with H_2O_2 (MTM)

The liquid-phase MTM reactions were carried out in a 100 ml PTFE autoclave. The CH_4 pressure was controlled by the pressure gage. The reactants were stirred vigorously by an agitator blade. Aqueous hydrogen peroxide (30 wt.%) was used as oxidant. In a typical run, 10 ml sulfolane, 50 mg

catalyst and 27 mmol H_2O_2 were added to the autoclave and heated to 323 K. The sealed reactor was then purged with CH_4 to 3 Mpa. After reaction 2 h, the autoclave was cooled rapidly to 278 K in an ice bath to minimize any further chemical reaction and reduce loss of volatile products. After separation liquid phase and catalyst, the liquid-phase products were analyzed by ^1H NMR spectroscopy on JEOL ECA-600 spectrometer (14.1 T) equipped with an additional 1 kW power amplifier. Mesitylene was used as the internal standard and TMS/CD_3CN was took as chemical shift calibrator, respectively. The detectable products in the liquid-phase were CH_3OH, HCOH, HCOOH and CH_3OOH. The amount of unconverted H_2O_2 was quantified by standard titration method with 0.1 mol/L $Ce(SO_4)_2$ solution.

7.3. Results and discussion

7.3.1 Characterization of catalysts

7.3.1.1 Physicochemical properties

Figure 7.1 shows the XRD patterns of the catalysts, indicating that all the samples had the typical **BEA** structure. No obvious iron and copper oxide particles were observed, suggesting that the Fe and Cu species were highly dispersed on the Beta zeolite.

Figure 7.2 shows the SEM image of the parent Beta zeolite. It was clear that the zeolite composed of tiny particles.

The elemental compositions of the zeolites as determined by ICP elemental analysis are listed in **Table 7.1**. An increase in the Si/Al ratio was observed in all the catalysts after the ion-exchange due to the leaching of Al under low pH during the ion-exchange process, as well as the isomorphic substitution of Al by Fe and/or Cu on the octahedral network [25]. The output Fe and Cu contents were considerably different under the same ion-exchange conditions. The output Fe content was regularly increased with the input Fe content in both Fe/Beta and Fe-Cu/Beta catalysts. The output Cu content in Cu/Beta was also increased along with the input Cu content (1.3-1.8 wt.%). However, the output Cu content in Fe-Cu/Beta catalysts was much lower than the input ones (0.2-0.3 wt.%), suggesting that NH_4^+ cations on the Beta zeolites were more easily exchanged with Fe cations rather than Cu ones under such competitive conditions.

Figure 7.3 displays the N_2 adsorption and desorption isotherms of the zeolites. The isotherm risen

sharply at low relative pressure where the micropore filling occurs in the precapillary condensation range. A sharp risen at the p/p_0 over 0.9 indicated the existence of constructional void porosity so that the total pore volumes for some samples were higher than 1.0 cm^3g^{-1}, as listed in **Table 7.1**. The BET surface area of all the samples were around 600-700 cm^2g^{-1} and the external surface were 200-300 cm^2g^{-1} due to the tiny particles. Besides, different metal species and amount loading on the Beta zeolite did not change the textural properties. It was concluded that micropores were present along with some mesopores.

7.3.1.2 The states of Fe and Cu species

Figure 7.4 shows the UV-vis spectra of the Fe/Beta, Cu/Beta and Fe-Cu/Beta products with proton form. For Fe/Beta samples, a shoulder band at 215 nm was related to the electron transfer from O to isolated ferric ions in tetrahedral coordination. The band around 270 nm was derived from isolated mononuclear Fe^{3+} species in octahedral coordination, whereas the bands ranging from 300 to 400 nm were assigned to octahedral Fe^{3+} species in small oligomeric Fe_xO_y clusters, and the bands above 400 nm are ascribed to bulk iron oxide particles less or larger than 2 nm [25]. The Cu/Beta samples show a sharp band below 350 nm. The maximum band at about 209 nm was attributed to monomeric Cu^{2+} ions interacting with oxygen of the zeolite structure, and the maximum band at about 267 nm was ascribed to oligomeric [Cu^{2+}-O^{2-}-Cu^{2+}] species [20, 26-27]. The spectra of Fe-Cu/Beta catalysts were basically the same to those of the Fe/Beta samples, possibly due to a high contribution of the Fe species.

Because the UV-vis spectra can not distinguish the Fe/Beta and Fe-Cu/Beta zeolites, meanwhile NO adsorbed FT-IR technology can be applied to investigate the states of Fe and Cu species on the extra framework [28]. The left parts of **Figures 7.5(a-c)** present the NO adsorbed FT-IR spectra for the Fe/Beta samples with different Fe loadings at 298 K. At the lowest NO pressure (5 Pa), the band at 1875 cm^{-1} was assigned to Fe^{2+}(NO) on Fe^{2+}-O-Al species or oligomer Fe species of the extra framework [17, 29-30]. The intensity of the band was dramatic increased along with NO pressure, indicating the existence of a large amount of Fe^{2+}-O-Al species or oligomeric Fe species. Meanwhile the intensity of the bands were increased along with the Fe content, suggesting that the amount of Fe^{2+}-O-Al species or oligomeric Fe species were increased with the total Fe content. The high loading of NO led to the appearance of a broad band centered at around 1820 cm^{-1}, assigned to $Fe^{2+}(NO)_3$ on isolated ferrous ions, which was highly coordinatively unsaturated [31-32]. Note that the intensity of

the bands at 1820 cm^{-1} were not increased along with the Fe content. 3Fe/Beta zeolite displayed the highest intensity at 1820 cm^{-1}, implying the highest proportion of highly coordinatively unsaturated Fe species in the Fe/Beta catalysts. The middle parts of **Figures 7.5(a-c)** show the NO adsorbed FT-IR spectra of the Cu/Beta samples. The band at 1802 cm^{-1} with a weak shoulder at 1818 cm^{-1} assigned to Cu^{+}(NO) were observed at the lowest NO pressure [32]. The intensity of these bands were increased and then decreased with increasing the NO pressure. Meanwhile, some new bands at 1913 and 1950 cm^{-1} attributed to Cu^{2+}(NO) appeared [33]. With increasing Cu content, the intensity of bands at 1913 cm^{-1} and 1802 cm^{-1} were increased and then maintained. However, the bands at 1913 cm^{-1} migrated to lower wavenumber with Cu content increase possibly due to the change of coordinatively unsaturated degree for Cu species. For the Fe-Cu/Beta samples (the right parts of **Figures 7.5(a-c)**), the intensity of bands at 1875 cm^{-1} were increased with the metal content increase. But the intensity of Fe-Cu/Beta zeolites were lower than Fe/Beta under the similar Fe content, indicating that the states of Fe species in the Fe-Cu/Beta zeolite were influenced by the introduction of Cu. Compared with the spectra of Fe/Beta zeolites, the bands at 1815 cm^{-1} for Fe-Cu/Beta samples shifted to lower wavenumber with ca. 5 cm^{-1} possibly due to the introduction of Cu. The intensity of the band at 1815 cm^{-1} of Fe-Cu/Beta were increased along with metal content, and higher than those of Fe/Beta zeolites. It greatly illustrated the more highly coordinatively unsaturated Fe species for Fe-Cu/Beta than Fe/Beta zeolites. Among them, 6Fe-6Cu/Beta presented the highest intensity. A weak band at 1808 cm^{-1} appeared, which was attributed to Cu^{+}(NO). The existence of Cu was also reflected on the band at 1912 cm^{-1}, even though the intensity was very weak due to the low Cu content in the Fe-Cu/Beta catalysts.

7.3.1.3 Acidity

NH_3-TPD can also reflect the condition of the metal species in the zeolites. **Figure 7.6** shows the NH_3-TPD profiles of the catalysts. All the profiles can be deconvoluted into three peaks at low, medium, and high temperatures (designated as LT, MT, and HT). The amounts of NH_3 adsorbed and the temperature of the maximum peak (T_{max}) are listed in **Table 7.2**. According to the references [34-35] , the LT peak, which corresponds to NH_3 adsorbed on the non-acidic OH groups and NH_4^+ by hydrogen bonding, was not related to the true acid site and excluded in the discussion. The MT and HT peaks correspond to NH_3 adsorbed on the extra framework metal species (Lewis acid site), and to NH_3 adsorbed on the bridged Si-O(H)-M species (Brønsted acid site) (M means Fe, Cu and Al),

respectively.

The introduction of iron species to the Beta zeolite by ion exchange results in a distinct decrease in the amount at the Brønsted acid sites due to the replacement of protons in Brønsted acid hydroxyl groups by cationic iron species (**Figure 7.6(a)**). It can also be noted that the amount of Brønsted acid sites in Fe/Beta were gradually decreased with the accumulative of Fe content, which should be ascribed to the continuous dealumination in the Beta framework [35]. Meanwhile the HT reached the maximum value for 3Fe/Beta (576 K), meaning that the Brønsted acid site of 3Fe/Beta was a little different from those of 1.5Fe/Beta and 6Fe/Beta. Besides, the NH_3 adsorbed amount on the extra framework metal species displayed interesting phenomenon. It was not increased with the Fe content, but reached the maximum value on 3Fe/Beta (0.23 mmol/g), demonstrating that the NH_3 adsorbed amount on the extra framework metal species was related to the states instead of the amount of metal species. In addition, incorporation of Cu into Beta zeolite increased strong acid sites from 0.46 to 0.54 mmol/g, which was consistent with the Sultana's report [36]. But the HT was decreased from 568 to 549 K with the increase of Cu content from 0 to 1.8 wt.%, illustrating the changed strength of the acid site. The NH_3 adsorbed amount on the extra framework metal species for Cu/Beta was decreased with the Cu content, which was different from Fe/Beta. For Fe-Cu/Beta, the NH_3 adsorbed amount was the joint effect of Fe and Cu species. The amount of both Brønsted acid site and Lewis acid site were decreased with Fe and Cu content increase. One possible reason was the severe dealumination, which was verified by the ICP result. Another reason was that the presence of Fe influenced the state of Cu species and cannot increase the strong acid sites, consequently influence the condition of Brønsted acid sites.

7.3.2 Direct oxidation of benzene to phenol with H_2O_2 (BTP)

Table 7.3 lists reaction results in the BTP reaction with H_2O_2. H-Beta exhibited 0.9% phenol yield with 100% selectivity to phenol, no significant but higher than H-ZSM-5 in Chapter 2. The phenol yield was in the following order: Fe-Cu/Beta > Fe/Beta > Cu/Beta. For the Fe/Beta catalysts, the phenol yield was increased from 4.6% to 5.1% with an increase in the Fe content from 0.8 to 2.1 wt.%, and then it was decreased to 4.4% with Fe content continuously increase to 5.6 wt.%. It indicated that the phenol yield was not only related to Fe content but also to the Fe state, since the 3Fe/Beta containing

the highest amount of highly coordinatively unsaturated Fe species. For Cu/Beta, the highest phenol yield was achieved on 1Cu/Beta, the increase of Cu content resulted in the decrease of phenol yield, signifying that high Cu content was not beneficial to the phenol production. It may be related to the change of coordinatively unsaturated condition of Cu species. However, it is still unknown for the specific influence of Cu state on the catalytic performance. Fe-Cu/Beta catalysts showed dramatically high catalytic activity compared with both Fe/Beta and Cu/Beta catalysts. The phenol yield was increased from 7.4 to 10.5% along with the Fe content, since the Cu contents were maintained at 0.2-0.3 wt.%. The improvement would be due to the synergetic effect, which could be explained by cooperation between Fe and Cu cations, *i.e.*, so-called "Fenton-like" reaction mechanism [37,38]. Especially 6Fe-6Cu/Beta achieved the highest phenol yield, which could be related to the highest isolated Fe ions. The high activity in partial oxidation reactions of isolated Fe ions has also been reported the by Berlier *et al.* [39].

The phenol selectivity of the catalysts exhibited the following order: Fe/Beta > Fe-Cu/Beta > Cu/Beta. Fe/Beta zeolites achieved 89-96% phenol selectivity. In contrast, Cu/Beta catalysts presented a low phenol selectivity, 84-78%, since the by-product *p*-BQ was much produced. For the Fe-Cu/Beta catalysts, the phenol selectivity was higher than that of Cu/Beta but lower than that of Fe/Beta. The Cu species in the Beta would show a high activity for not only the hydroxylation of benzene but also the successive reaction of phenol, resulting in the low yield and selectivity. Actually, the liquid product for Cu/Beta catalysts were always black, indicating the formation of tar as by-product, which cannot be analyzed by GC. On the other hand, the Fe species exhibited a high phenol selectivity. For comparison, the results over other zeolite catalysts reported in the literatures were listed in **Table 7.3**. It was clear to show that the higher phenol yield for Fe-Cu/Beta zeolites were achieved.

In order to investigate the influence of reaction time, molar ratio of H_2O_2/benzene, and reaction temperature on the reaction performance, 6Fe/Beta, 6Cu/Beta and 6Fe-6Cu/Beta zeolites were used as the typical catalysts.

As shown in **Figure 7.7**, the phenol yield of 6Cu/Beta was increased from 1.9 to 2.7% with time prolonging from 0.33 to 2 h, and then maintained at 2.7% by extending reaction time from 2 to 10 h. Because H_2O_2 conversion was up to 85% when reacting for 2 h. The HO· produced from H_2O_2 was limited after 2 h, thus the phenol yield maintained at 2.7%. Meanwhile, the phenol selectivity of

Cu/Beta was decreased from 89 to 78% with time changing from 0.33 to 2 h, and maintained at 78% by prolonging reaction time from 2 to 10 h. The increased benzene conversion of 6Cu/Beta indicated the formation of undetectable by-products. For 6Fe/Beta, except the result of reaction 6 h, the basic trend was similar to 6Fe-6Cu/Beta. The phenol yield and benzene conversion gave a massive growth firstly and then slowly increase. It was also related to the H_2O_2 conversion. When reaction time increased from 0.33 to 6 h, the H_2O_2 conversion was increased from around 20 to 90%, which produced a large number of HO·. However, when the reaction time prolonging to 10 h, the H_2O_2 conversion showed no significant changes. In short, long reaction time was beneficial to the benzene conversion and phenol yield, but limited by the H_2O_2 conversion.

Figure 7.8 displays the reaction results under different molar ratios of H_2O_2/benzene, the benzene amount was fixed at 5 mmol. For the three samples, the phenol yield and benzene conversion were both increased with the molar ratio varying from 2 to 8. But the increased rate of phenol yield was not significant. The phenol selectivity for the three samples were maintained, except the result of 6Fe/Beta attaining at molar ratio equal to 2. The results were involved to the sufficient HO· provided by the H_2O_2. Although, the H_2O_2 conversion were decreased with H_2O_2 amount increase, the consumed H_2O_2 amount were increased. In a word, high molar ratios of H_2O_2/benzene was conducive to the reaction under the catalytic systems, but high price of H_2O_2 was worth considering.

The influence of reaction temperature on the catalytic performance are presented in **Figure 7.9**. The benzene conversion and phenol yield for the three samples were increased with temperature raising from 313 to 333 K due to the dramatically increased H_2O_2 conversion. Continuing to increase temperature to 353 K, the benzene conversion of the three samples, the phenol yield of 6Fe/Beta and 6Cu/Beta were increased, while the phenol yield for 6Fe-6Cu/Beta was decreased to from 10.5 to 9.4%. The phenol selectivity of 6Fe-6Cu/Beta and 6Fe/Beta were reduced by 6%, while that of 6Cu/Beta was increased by 12%. Note that the reaction systems were boiling when the reaction temperature was 353K. Thus the H_2O_2 conversion were up to 90% for the three samples at 333 and 353K. Overall, properly increasing the reaction temperature favored the catalytic performance. However, too high reaction temperature did not improve the performance, but increased the energy consumption.

Besides, from the results of 0.33 h for 6Cu/Beta in **Figure 7.7,** molar ratio of H_2O_2/Benzene for 2 in **Figure 7.8**, and 313K in **Figure 7.9**, we found that high H_2O_2 conversion with low phenol

selectivity were achieved for 6Cu/Beta under the mild conditions. It implied that Cu/Beta could easily and quickly react with H_2O_2 to produce HO· and HO_2·, thus the detectable by-products like HQ and undetectable products like tar were produced. That may be the reason of low phenol selectivity provided by Cu/Beta.

The stability of the Fe and/or Cu-containing Beta zeolite catalysts and the catalytic performance of other composite bimetallic catalysts were investigated, showing in **Table 7.4**. The catalytic performance of the used and calcined 6Cu/Beta was reduced by 48%, and 6Fe-6Cu/Beta was reduced 38%, due to the severe leaching of Cu species. In contrast, the Fe species was so stable to maintain the phenol yield for 6Fe/Beta catalyst. The catalytic performance of 25mg 6Fe/Beta plus 25mg 6Cu/Beta was better than 50mg 6Fe/Beta and 50 mg 6Cu/Beta, but worse than 6Fe-6Cu/Beta, indicating that the synergistic effect was influenced by the states and content of metals. Besides, the reaction result of imp-6Fe-6Cu/Beta was much worse than both 6Fe-6Cu/Beta and 6Fe/Beta+6u/Beta, though the highest Fe and Cu content were contained, which confirmed the above statement.

7.3.3 Direct oxidation of methane to methanol with H_2O_2 (MTM)

3Fe/Beta, 1.5Cu/Beta and 6Fe-6Cu/Beta as the catalysts achieved the highest phenol yield in Fe/Beta, Cu/Beta and Fe-Cu/Beta catalysts, respectively, were applied in the direct oxidation of methane to methanol, as a contrast the H/Beta catalyst was also investigated , the results are displayed in **Table 7.5**. Similarity to the results of direct oxidation of benzene to phenol, 6Fe-6Cu/Beta catalyst achieved the highest methanol amount which was double times than that of 3Fe/Beta, four times than that of 1.5Cu/Beta and almost thirteen times than that of H/Beta. Meanwhile, 3Fe/Beta attained the highest total liquid product amount and 57% methanol selectivity. The H_2O_2 conversion of the catalysts ranged from 4% to 22%, which was not very high affected by the aprotic solvent sulfolane. In addition, the H_2O_2 efficiency was determined by the liquid product amount and H_2O_2 conversion, 6Fe-6Cu/Beta realized the highest H_2O_2 efficiency 43%. Meanwhile, the methanol yield of 3Fe/Beta and 6Fe-6Cu/Beta were higher than Fe-MFI catalyst. The more active Fe species provided by the large surface area and pore size for Beta zeolites maybe the reason.

7.4. Conclusions

In conclusion, Fe and/ or Cu exchanged Beta catalysts with varied metal content were investigated in hydroxylation of benzene to phenol with H_2O_2. The states of Fe and Cu species were characterized by UV-vis and NO adsorbed FT-IR. The influence of the reaction conditions in BTP reaction on the catalytic performance of Fe and/or Cu-containing Beta zeolite catalysts were studied in details. The stability of the Fe and/or Cu-containing Beta zeolite catalysts in the BTP reaction were investigated. The synergetic effect was influenced by the states of the metals instead of the content. Fe-Cu/Beta catalysts showed dramatically high catalytic activity due to the synergetic effect. 6Fe-6Cu/Beta achieved the highest phenol yield of 10.5 % in BTP reaction and MeOH yield of 720 μmol in MTM reaction, which was related to the highest isolated Fe species influenced by the introduction of Cu. Thus, we successfully found that the incorporation of Fe and Cu cation species together into zeolite is a promising method for improving catalytic performance in the BTP and MTM reaction, and such synergetic effect by attaining the introduction of different metal cation species will be applicable to other applications.

References

[1] A. R. Kulkarni, Z. J. Zhao, S. Siahrostami, J. K. Nørskov, F. Studt, Catal. Sci. Technol., 8 (2018), 114.
[2] N. J. Gunsalus, A. Koppaka, S. H. Park, S. M. Bischof, B. G. Hashiguchi, R. A. Periana, Chem. Rev., 117 (2017) 8521.
[3] M. Li, X. Zhu, E. J. M. Hensen, ACS Catal., 7 (2017) 2709.
[4] D. Wang, M. Wang, Z. Li, ACS Catal., 5 (2015) 6852.
[5] C. I. Herrerı´as, X. Yao, Z. Li, C. Li, Chem. Rev., 107 (2007) 2546.
[6] J. Piera, J. E. Backvall, Angew. Chem. Int. Ed., 47 (2008) 3506.
[7] L. Balducci, D. Bianchi, R. Bortolo, R. D'Aloisio, M. Ricci, R. Tassinari, R. Ungarelli, Angew. Chem. Int. Ed., 115 (2003) 5087.
[8] D. Bianchi, L. Balducci, R. Bortolo, R. D'Aloisio, M. Ricci, G. Spanò, R. Tassinari, C. Tonini, R. Ungarelli, Adv. Synth. Catal., 349 (2007) 979.
[9] X. Qi, J. Li, T. Ji, Y. Wang, L. Feng, Y. Zhu, X. Fan, C. Zhang, Micropor. Mesopor. Mater., 122 (2009) 36.
[10] X. Ye, Y. Cui, X. Qiu, X. Wang, Appl. Catal., B, 152 (2014) 383.
[11] K. Yoshizawa, Y. Shiota, Y. Kagawa, T. Yamabe, J. Phys. Chem. A, 104 (2000) 2552.
[12] M. Ravi, M. Ranocchiari, J. A. van Bokhoven, Angew. Chem. Int. Ed., 2017.
[13] C. Hammond, M. M. Forde, R. Rahim, A. Thetford, Q. He, R. L. Jenkins, N. Dimitratos, J. A. Lopez-Sanchez, N. F. Dummer, D. M. Murphy, A. F. Carley, S. H. Taylor, D. J. Willock, E. E. Stangland, J. Kang, H. Hagen, C. J. Kiely, G. J. Hutchings, Angew. Chem. Int. Ed., 51 (2012) 5129.
[14] K. Yoshizawa, Y. Shiota, T. Yumura, T. Yamabe, J. Phys. Chem. B, 104 (2000) 734.
[15] M. Sasak, Y. Sato, Y. Tsuboi, S. Inagaki, Y. Kubota, ACS Catal., 4 (2014) 2653.
[16] S. Song, G. Wu, W. Dai, N. Guan, L. Li, Catal. Sci. Technol., 6 (2016) 8325.
[17] P. Sazama, R. Pilar, L. Mokrzycki, A. Vondrova, D. Kaucky, J. Plsek, S. Sklenak, P. Stastny, P. Klein, Appl. Catal., B, 189 (2016) 65.
[18] A. Wang, Y. Wang, E. D. Walter, R. K. Kukkadapu, Y. Guo, G. Lu, R. S. Weber, Y. Wang, R. H. F. Peden, F. Gao, J. Catal. 358 (2018)199.
[19] M. Rutkowska, Z. Piwowarska, E. Micek, L. Chmielarz, Micropor. Mesopor. Mater., 209 (2015) 54.
[20] I. Yuranov, D. A. Bulushev, A. Renken, L. Kiwi-Minsker, Appl. Catal., A, 319 (2007) 128.
[21] A. Wang, Y. Wang, E. D. Walter, N. M. Washton, Y. Guo, G. Lu, C. H. F. Peden, F. Gao, Catal. Today 2017.
[22] C. Hammond, R. L. Jenkins, N. Dimitratos, J. A. Lopez-Sanchez, M.H. ab Rahim, M. M. Forde, A. Thetford, D. M. Murphy, H. Hagen, E. E. Stangland, J. M. Moulijn, S. H. Taylor, D. J. Willock, G. J. Hutchings, Chemistry, 18 (2012) 15735.
[23] G. Wen, S. Wu, B. Li, C. Dai, D. Su, Angew. Chem. Int. Ed., 54 (2015) 4105
[24] Y. S. M. Sasaki, Y. Tsuboi, S. Inagaki, Y. Kubota, ACS Catal., 4 (2014) 2653.
[25] S. A. Yashnik, Z. R. Ismagilov, V. F. Anufrienko, Catal. Today, 110 (2005) 310.
[26] F. Gao, M. Kollár, R. K. Kukkadapu, N.M. Washton, Y. Wang, J. Szanyi, C. H. F. Peden, Appl. Catal., B, 164 (2015) 407.
[27] G. Wu, F. Hei, N. Guan, L. Li, Catal. Sci. Technol., 3 (2013) 1333.
[28] G. Wu, F. Hei, N. Zhang, N. Guan, L. Li, W. Grünert, Appl. Catal., A, 468 (2013) 230.

[29] T. Cheung, S. K. Bhargava, M. Hobday, K. Foger, J. Catal., 158 (1996) 301.
[30] G. Berlier, G. Spoto, S. Ricchiardi, S. Bordiga, C. Lamberti, A. Zecchina, J. Mol. Catal. A, 182 (2002) 359.
[31] Y. Wang, H. Zhao, G. Zhao, Appl. Catal., B, 164 (2015) 396.
[32] F. Giordanino, P. N. Vennestrom, L. F. Lundegaard, F. N. Stappen, S. Mossin, P. Beato, S. Bordiga, C. Lamberti, Dalton T., 42 (2013) 12741.
[33] T. Cheung, S. K. Bhargava, M. Hobday, K. Foger, J. Catal., 158 (1996) 301.
[34] I. H. L. J. Lobree, J. A. Reimer, A. T. Bell, J. Catal., 186 (1999) 242.
[35] G. Wu, F. Hei, N. Guan, L. Li, Catal. Sci. Technol., 3 (2013) 1333.
[36] A. Sultana, M. Sasaki, K. Suzuki, H. Hamada, Catal. Commun., 41 (2013) 21.
[37] E. G. Garrido-Ramírez, J. F. Marco, N. Escalona, M. S. Ureta-Zañartu, Micropor. Mesopor. Mater., 225 (2016) 303.
[38] G. Berlier, G. Spoto, G. Ricchiardi, S. Bordiga, C. Lamberti, A. Zecchina, J. Mol. Catal. A, 182 (2002) 359.
[39] G. Berlier, A. Zecchina, G. Spoto, G. Ricchiardi, S. Bordiga, C. Lamberti, J. Catal., 215 (2003) 264.

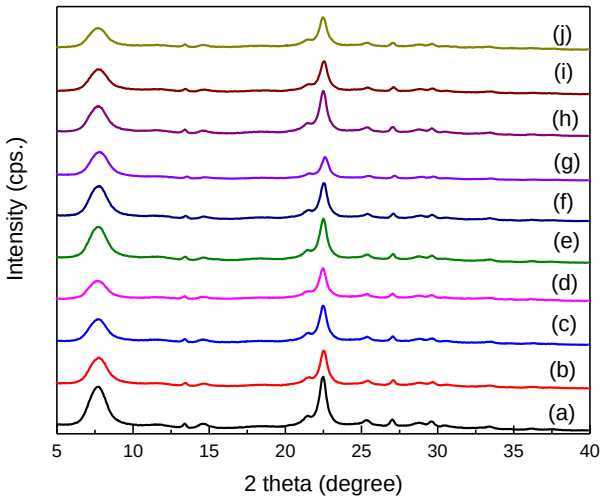

Figure 7.1 XRD patterns of the (a) H-Beta, (b)1.5Fe/Beta, (c) 3Fe/Beta, (d) 6Fe/Beta, (e) 1.5Cu/Beta, (f) 3Cu/Beta, (g) 6Cu/Beta, (h) 1.5Fe-1.5Cu/Beta, (i) 3Fe-3Cu/Beta, (j) 6Fe-6Cu/Beta.

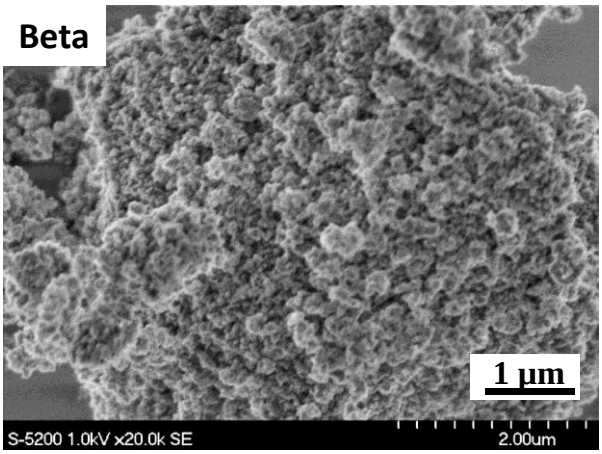

Figure 7.2 SEM image of the parent Beta zeolite.

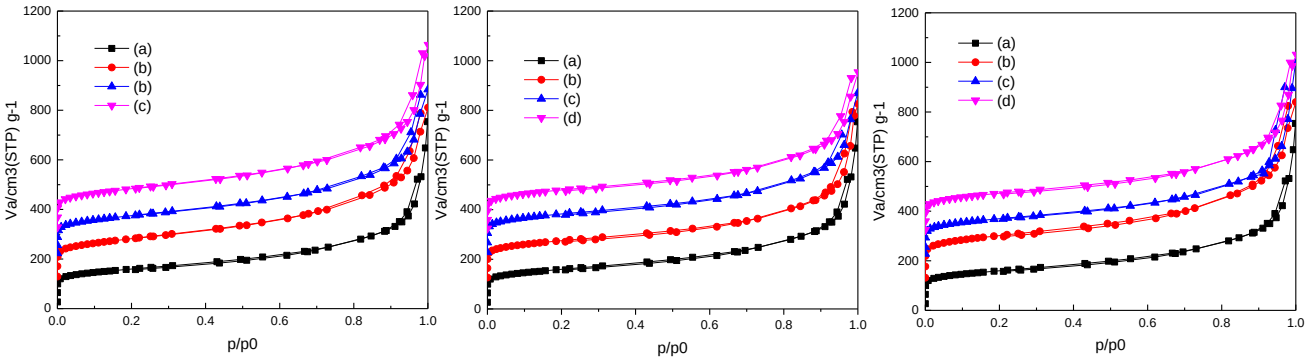

Figure 7.3 N_2 adsorption and desorption isotherms of left: (a) H/Beta, (b) 1.5Fe/Beta, (c) 3Fe/Beta, (d) 6Fe/Bea; middle: (a) H/Beta, (b) 1.5Cu/Beta, (c) 3Cu/Beta, (d) 6Cu/Bea; right: (a) H/Beta, (b) 1.5Fe-1.5Cu/Beta, (c) 3Fe-3Cu/Beta, (d) 6Fe-6Cu/Bea.

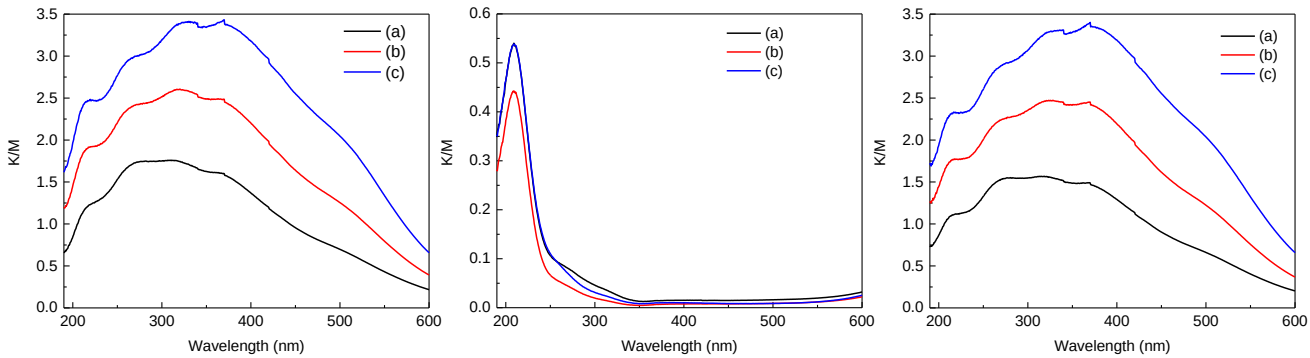

Figure 7.4 UV-vis spectra of left: (a) H/Beta, (b) 1.5Fe/Beta, (c) 3Fe/Beta, (d) 6Fe/Bea; middle: (a) H/Beta, (b) 1.5Cu/Beta, (c) 3Cu/Beta, (d) 6Cu/Bea; right: (a) H/Beta, (b) 1.5Fe-1.5Cu/Beta, (c) 3Fe-3Cu/Beta, (d) 6Fe-6Cu/Bea.

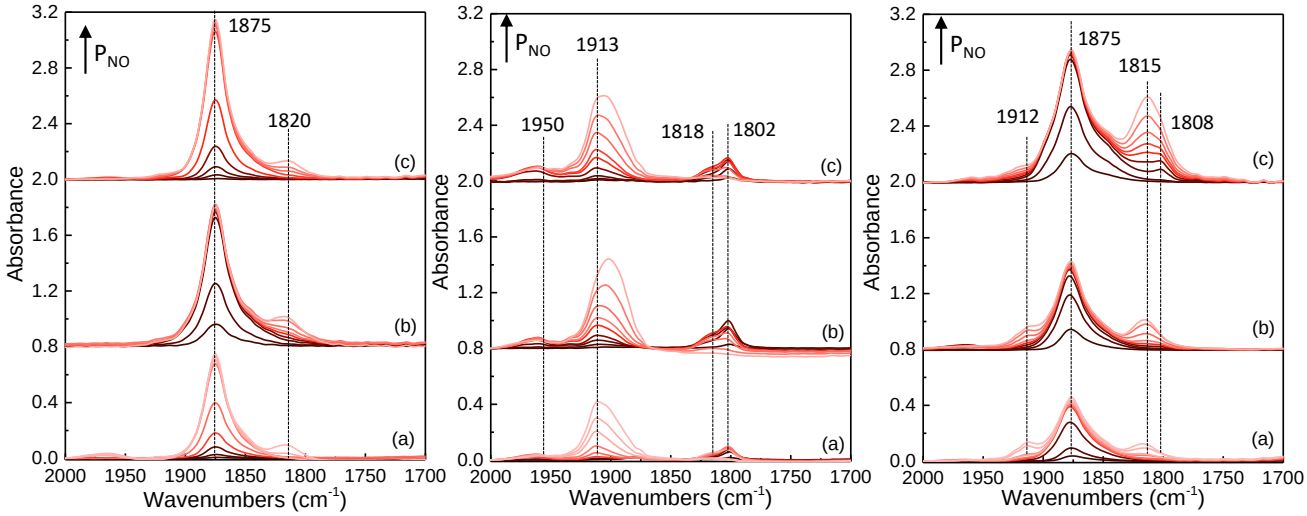

Figure 7.5 NO-adsorbed FT-IR spectra of left: (a) H/Beta, (b) 1.5Fe/Beta, (c) 3Fe/Beta, (d) 6Fe/Bea; middle: (a) H/Beta, (b) 1.5Cu/Beta, (c) 3Cu/Beta, (d) 6Cu/Bea; right: (a) H/Beta, (b) 1.5Fe-1.5Cu/Beta, (c) 3Fe-3Cu/Beta, (d) 6Fe-6Cu/Bea.

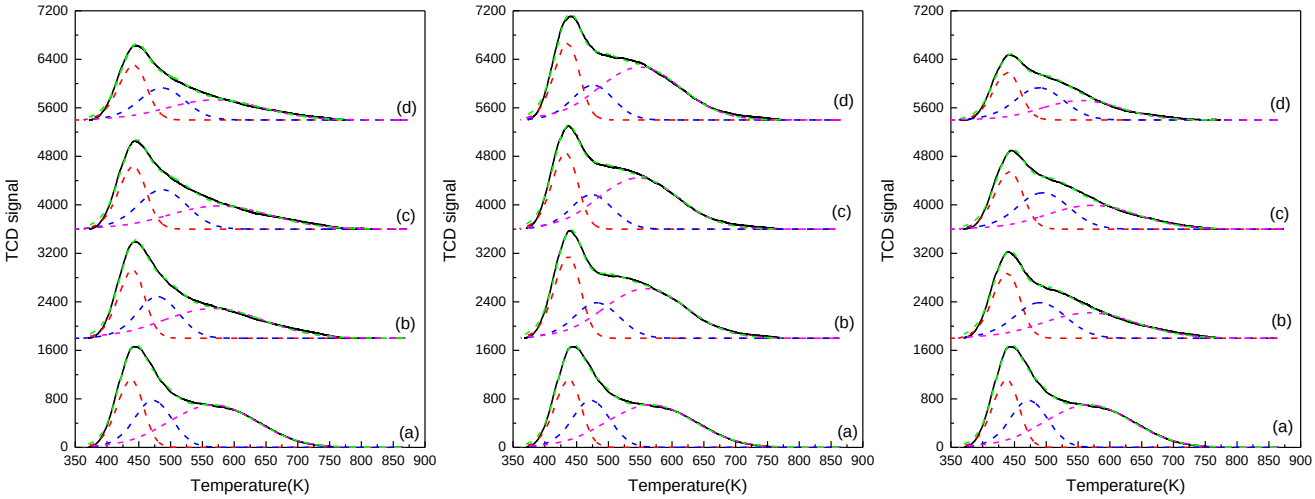

Figure 7.6 NH_3-TPD spectra of left: (a) H/Beta, (b) 1.5Fe/Beta, (c) 3Fe/Beta, (d) 6Fe/Bea; middle: (a) H/Beta, (b) 1.5Cu/Beta, (c) 3Cu/Beta, (d) 6Cu/Bea; right: (a) H/Beta, (b) 1.5Fe-1.5Cu/Beta, (c) 3Fe-3Cu/Beta, (d) 6Fe-6Cu/Bea.

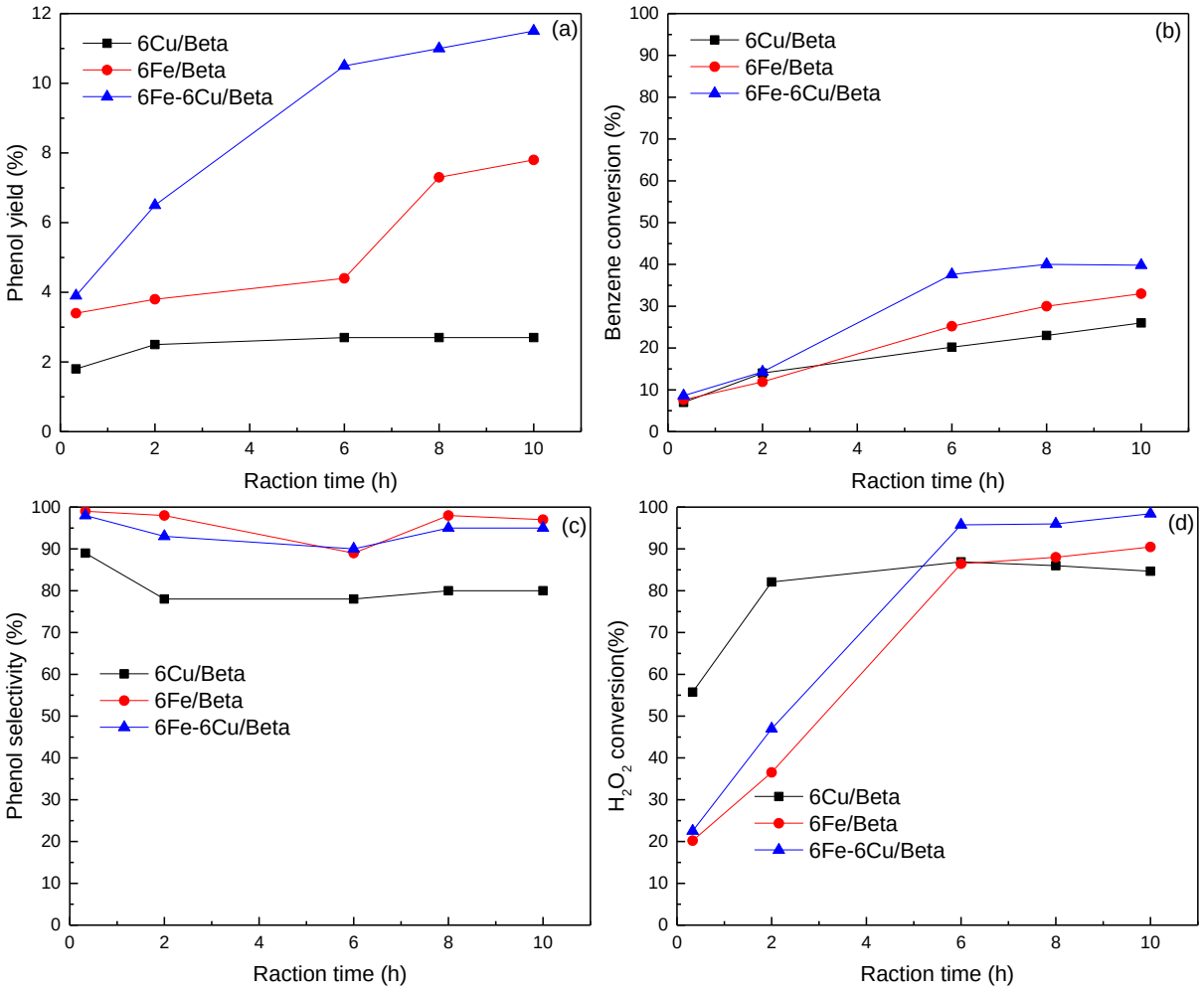

Figure 7.7 Changes of (a) phenol yield, (b) benzene conversion, (c) phenol selectivity and (d) H_2O_2 conversion over Fe and/ or Cu containing Beta zeolite catalysts as a function of reaction time. Reaction conditions: 50 mg catalyst, 10 ml CH_3CN, 5 mmol Benzene, 333 K. [a] Phenol yield = (moles of phenol produced)*100/(initial moles of benzene). [b] Benzene conversion = (moles of benzene consumed)*100/(initial moles of benzene). [c] Phenol selectivity = (moles of each liquid product)*100/(moles of phenol + moles of HQ + moles of CL+ moles of p-BQ). [d] H_2O_2 conversion = (moles of H_2O_2 consumed)*100/(initial moles of H_2O_2).

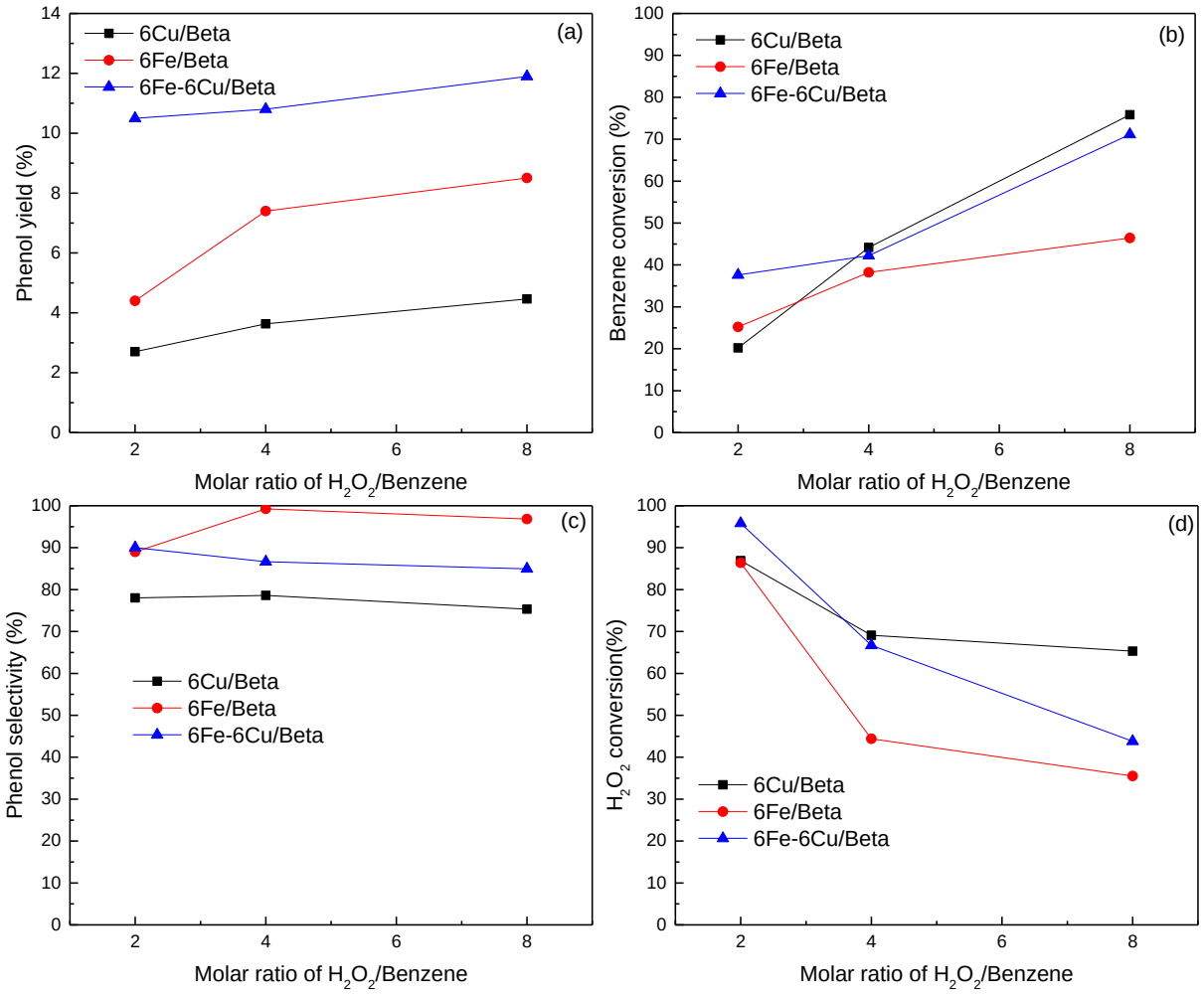

Figure 7.8 Changes of (a) phenol yield, (b) benzene conversion, (c) phenol selectivity and (d) H_2O_2 conversion over Fe and/ or Cu containing Beta zeolite catalysts as a function of molar ratio of H_2O_2/Benzene. Reaction conditions: 50 mg catalyst, 10 ml CH_3CN, 5 mmol Benzene, 333 K, 6 h. [a] Phenol yield = (moles of phenol produced)*100/(initial moles of benzene). [b] Benzene conversion = (moles of benzene consumed)*100/(initial moles of benzene). [c] Phenol selectivity = (moles of each liquid product)*100/(moles of phenol + moles of HQ + moles of CL+ moles of p-BQ). [d] H_2O_2 conversion = (moles of H_2O_2 consumed)*100/(initial moles of H_2O_2).

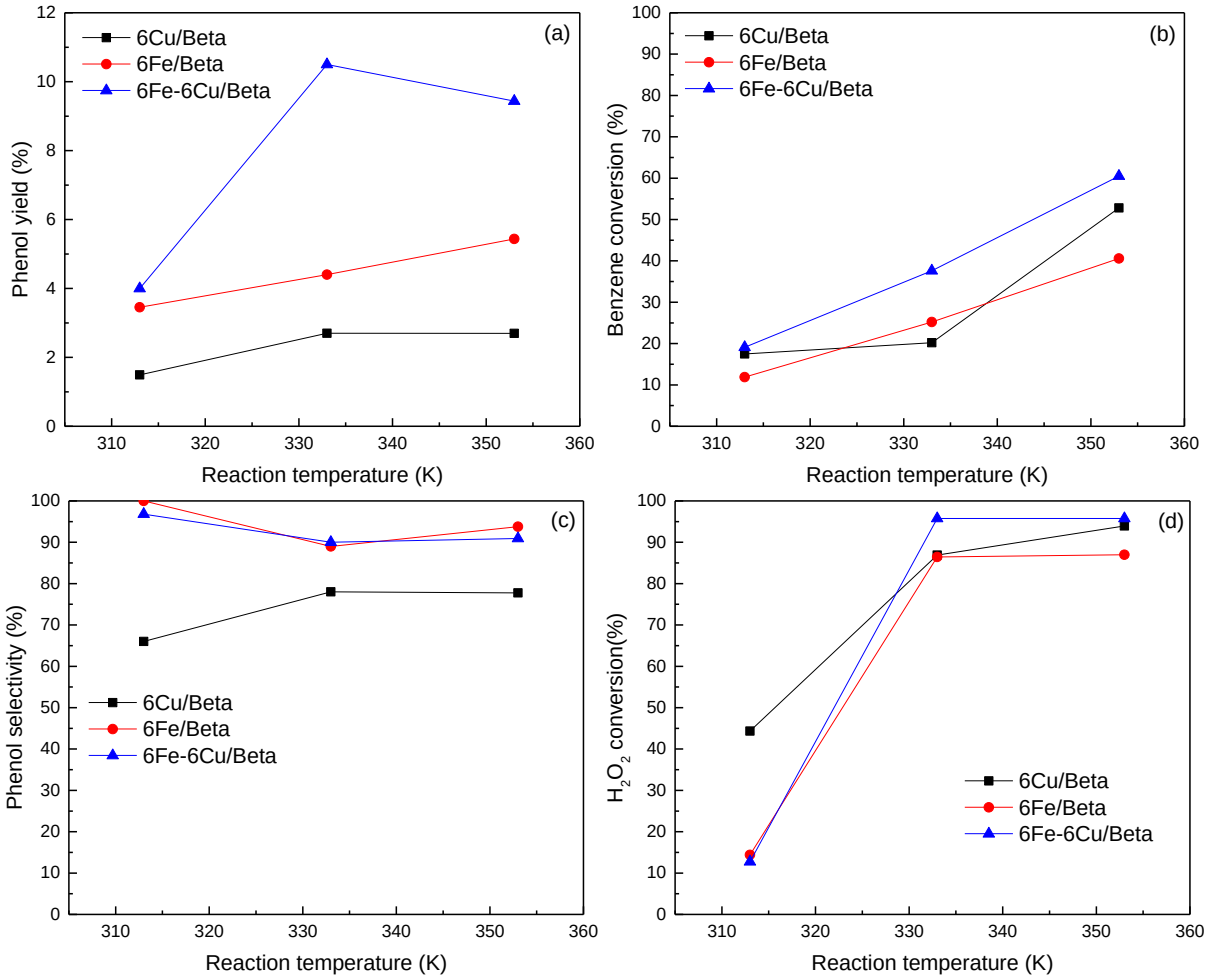

Figure 7.9 Changes of (a) phenol yield, (b) benzene conversion, (c) phenol selectivity and (d) H_2O_2 conversion over Fe and/ or Cu containing Beta zeolite catalysts as a function of reaction temperature. Reaction conditions: 50 mg catalyst, 10 ml CH_3CN, 5 mmol Benzene, 10 mmol H_2O_2, 6 h. [a] Phenol yield = (moles of phenol produced)*100/(initial moles of benzene). [b] Benzene conversion = (moles of benzene consumed)*100/(initial moles of benzene). [c] Phenol selectivity = (moles of each liquid product)*100/(moles of phenol + moles of HQ + moles of CL+ moles of p-BQ). [d] H_2O_2 conversion = (moles of H_2O_2 consumed)*100/(initial moles of H_2O_2).

Table 7.1 Composition and texture properties of Fe/Beta, Cu/Beta and Fe-Cu/Beta zeolite catalysts.

Sample	Input (wt.%)		Output (wt.%) [a]		S_{BET} (m^2g^{-1})[b]	S_{EXT} (m^2g^{-1})[c]	V_{Total} (cm^3g^{-1})[d]	V_{Micro} (cm^3g^{-1})[e]
	Fe	Cu	Fe	Cu				
1.5Fe/Beta	1.5	-	0.8	-	641	286	1.02	0.24
3Fe/Beta	3.0	-	2.1	-	616	264	0.98	0.23
6Fe/Beta	6.0	-	5.6	-	647	275	1.09	0.25
1.5Cu/Beta	-	1.5	-	1.3	629	241	1.05	0.22
3Cu/Beta	-	3.0	-	1.6	657	244	0.95	0.23
6Cu/Beta	-	6.0	-	1.8	645	240	0.93	0.23
1.5Fe-1.5Cu/Beta	1.5	1.5	0.9	0.3	726	310	1.07	0.23
3Fe-3Cu/Beta	3.0	3.0	2.1	0.2	608	237	1.08	0.23
6Fe-6Cu/Beta	6.0	6.0	5.5	0.3	618	242	1.05	0.24

[a] Si/Fe was determined by ICP-AES analysis, Fe content was calculated by Si/Fe.
[b] Specific surface areas of the catalysts were calculated using the Brunauer-Emmett-Teller (BET) equation on the N_2 adsorption isotherms.
[c] External surface area (S_{EXT}) of the catalysts were calculated by the *t*-plot method based on the adsorption isotherms.
[d] Total pore volumes of the catalysts were calculated based on BET equation on the N_2 adsorption isotherms.
[e] Micropore volumes of the catalysts were calculated by the *t*-plot method based on the adsorption isotherms.

Table 7.2 NH_3 adsorbed amount of the Fe/Beta, Cu/Beta and Fe-Cu/Beta zeolite catalysts.

Samples	NH_3 adsorbed amount (mmol/g) / T_{max} (K)		
	LT	MT	HT
H-Beta	0.21/437	0.22/472	0.46/568
1.5Fe/Beta	0.21/441	0.21/476	0.37/568
3Fe/Beta	0.19/441	0.23/486	0.28/576
o6Fe/Beta	0.18/441	0.18/487	0.23/570
1.5Cu/Beta	0.24/437	0.20/481	0.50/559
3Cu/Beta	0.31/431	0.18/472	0.52/551
6Cu/Beta	0.22/435	0.18/476	0.54/549
1.5Fe-1.5Cu/Beta	0.21/439	0.23/489	0.30/569
3Fe-3Cu/Beta	0.19/439	0.23/495	0.26/570
6Fe-6Cu/Beta	0.15/439	0.19/489	0.19/553

Table 7.3 Direct oxidation of benzene to phenol results using Fe or/and Cu-containing Beta catalysts with H_2O_2.

Sample	Phenol Yield (%)[a]	Product Selectivity (%)[b]				H_2O_2 Conv. (%)[c]	Refer.
		Phenol	HQ	CL	*p*-BQ		
H-Beta	0.9	100	0	0	0	19	This Chapter
1.5Fe/Beta	4.6	95	4	1	0	84	
3Fe/Beta	5.1	96	4	1	0	80	
6Fe/Beta	4.4	89	10	1	0	86	
1.5Cu/Beta	3.4	84	8	1	7	85	
3Cu/Beta	2.8	80	10	2	8	92	
6Cu/Beta	2.7	78	11	3	7	87	
1.5Fe-1.5Cu/Beta	7.4	92	3	4	0	65	
3Fe-3Cu/Beta	9.4	94	4	2	0	61	
6Fe-6Cu/Beta	10.5	90	7	2	0	96	
TS-1B	8.1	94	-	-	-	97	[7]
CuAPO-5	7.9	62	11	27	0	-	[8]
TS-1	1.9	43	13	12	-	93	[9]
Fe/TS-1	7.6	15	-	-	-	96	[10]

Reaction conditions: 333 K, 10 mmol H_2O_2, 50 mg catalyst, 10 ml CH_3CN, 5 mmol Benzene, 6 h.

[a] Phenol yield = (moles of phenol produced)*100/(initial moles of benzene).

[b] Product selectivity = (moles of each liquid product)*100/(moles of phenol + moles of HQ + moles of CL+ moles of p-BQ)

[c] H_2O_2 conversion = (moles of H_2O_2 consumed)*100/(initial moles of H_2O_2).

Table 7.4 Direct oxidation of benzene to phenol results using Fe or/and Cu-containing Beta catalysts with H_2O_2.

Catalyst	Type	Fe (mg)	Cu (mg)	Phenol Yield (%)[a]	Product Selectivity (%)[b]				H_2O_2 Conv. (%)[c]
					Phenol	HQ	CL	*p*-BQ	
6Cu/Beta	Fresh	-	0.9	2.7	78	11	3	7	87
	Refresh [d]	-	0.3	1.4	94	5	1	0	4
6Fe/Beta	Fresh	2.8	-	4.4	89	10	1	0	86
	Refresh [d]	2.6	-	4.3	99	1	0	0	43
6Fe-6Cu/Beta	Fresh	2.8	0.2	10.5	90	7	2	0	96
	Refresh [d]	2.6	-	6.5	99	1	0	0	27
6Fe/Beta+6Cu/Beta [e]	Fresh	1.4	0.5	5.1	97	1	2	0	89
imp-6Fe-6Cu/Beta [f]	Fresh	3.0	3.0	2.0	66	13	1	20	92

Reaction conditions: 333 K, 10 mmol H_2O_2, 50 mg catalyst, 10 ml CH_3CN, 5 mmol Benzene, 6 h.

[a] Phenol yield = (moles of phenol produced)*100/(initial moles of benzene).

[b] Product selectivity = (moles of each liquid product)*100/(moles of phenol + moles of HQ + moles of CL+ moles of p-BQ).

[c] H_2O_2 conversion = (moles of H_2O_2 consumed)*100/(initial moles of H_2O_2).

[d] Catalysts were used in BTP, washed using Ethanol, dried overnight, calcined at 823K for 5h.

[e] 25 mg 6Fe/Beta and 25 mg 6Cu/Beta.

[f] Prepared by impregnation.

Table 7.5 Direct oxidation of methane to methanol results using Fe or/and Cu Beta catalysts with H_2O_2.

Sample	Products(μmol)			MeOH	H_2O_2	
	MeOH	HCOOH	HCOH	Selec.(%)[a]	Conv. (%)[b]	Eff.(%)[c]
H/Beta	57	-	27	68	4	9
3Fe/Beta	437	51	396	49	22	15
1.5Cu/Beta	174	0	133	57	4	29
6Fe-6Cu/Beta	720	77	472	57	12	43
FMD25	209	15	115	55	7	22

Reaction conditions: 323 K, 28 mmol H_2O_2, 50 mg catalyst, 10 ml solfulane, 3Mpa CH_4 pressure, 2 h.
[a] Each product selectivity= (moles of each product)*100/(moles of total liquid products).
[b] H_2O_2 conversion = (moles of H_2O_2 after reaction)*100/(initial moles of H_2O_2).
[c] H_2O_2 efficiency = (moles of total liquid products)*100/(moles of H_2O_2 conversion).

Chapter 8

Summary

Chapter 2 explored Fe-containing MFI zeolite catalysts including Fe-silicalite-1 and Fe-ZSM-5 by direct or post-synthesized method and post-modification by acid or alkaline treatment. In the BTP reaction with H_2O_2, direct-synthesized Fe-silicalite-1 achieved much higher phenol yield than the post-synthesized ones at similar Fe content. Based on the specific characterizations, we successfully clarified that the formation of isolated and oligomeric Fe species on the extra framework in **MFI** zeolites were critical for achieving high phenol yield. Among isolated and oligomeric extra framework Fe species, low nuclear oligomeric Fe species would be more active. Moreover, alkaline treatment was found to be advantageous to the formation of oligomeric Fe species, and as a result, 7.6% of phenol yield with 92% selectivity was attained. Our findings would contribute to the improvement of catalytic activity of Fe-containing zeolite catalysts, and also the development of the catalytic process for direct production of phenol from benzene.

Chapter 3 investigated the Fe-silicalite-1 zeolites directly synthesized using TPAOH as OSDA with or without Na cations in the synthesis gel. The physicochemical properties, especially the states of Fe species was characterized. Fe-silicalite-1 zeolites synthesized without Na cations displayed more uniform distribution for each kinds of Fe species and higher proportion of framework Fe than those synthesized with Na cations. The impact of solvent on the reaction performance was investigated. We firstly found that sulfolane was the best one among the solvents used in terms of the improvement in the production of methanol and its stability during the reaction. Finally, the effects of various reaction parameters, such as reaction temperature, CH_4 pressure, reaction time, catalyst amount and the amount of H_2O_2 were optimized. Furthermore, the use of mixture of sulfolane-water solvent with an appropriate proportion led to an extremely high methanol production with a high selectivity. Generally Fe-silicalite-1 zeolites synthesized using TPAOH as OSDA without Na cations (FS(T)*x*) showed better catalytic performance than those with Na cations (FS(TN)*y*). Under the optimal condition, FS(T)15 zeolite displayed the highest methanol yield of 947.8 μmol with the selectivity of 85% in the aqueous sulfolane solvent.

Chapter 4 discussed the Fe-ZSM-5 zeolites directly synthesized using TPAOH as OSDA with or without Na cations. The physicochemical properties, especially the states of Fe species were

characterized by UV-vis and NH_3-TPD. Fe-ZSM-5 zeolites synthesized without Na cations displayed more uniform distribution for each kinds of Fe species. Fe-ZSM-5 zeolites synthesized with Na cations presented strong acidity, since most of aluminum located in the framework. Generally Fe-ZSM-5 zeolites synthesized without Na cations (FZ(T)*x*) showed better catalytic performance in BTP reaction than the ones with Na cations (FS(TN)*y*). The introduction of aluminum in FZ(T)*x* and FZ(TN)*y* zeolites increased the isolated and oligomeric Fe species on the extra framework compared with FS(T)*x* and FS(TN)*y*, respectively. Thus, the catalytic performance in BTP and MTM reactions were improved with the introduction of aluminum in the MFI zeolites.

Chapter 5 researched the influence of desilication on as-synthesized and calcined Fe-ZSM-5 and Fe-silicalite-1 zeolites. Both template and aluminum can prevent desilication and protect the crystal structure. While the introduction of iron in the zeolite did not avoid desilication to a large extent. Thus alkaline treatment on Fe-ZSM-5 and Fe-silicalite-1 is an effective post modification method that affected both the porosity of the zeolite and the nature of Fe species. The increased porosity and surface area can improve the transport properties, reduce diffusion resistance and well disperse of Fe species. After alkaline treatment the phenol yield for Fe-ZSM-5 and Fe-silicalite-1 were increased from 0.6% (H-FZ) to 5.3% (CAT-FZ) and from 5.0% (H-FS) to 7.5% (CAT-FS), respectively.

Chapter 6 discovered Fe-containing MWW zeolites (i.e. Fe-MWW and Fe,Al-MWW) directly synthesized and extensively characterized, especially the states of Fe species and the acidity of catalysts. Fe-MWW showed better performance than Fe,Al-MWW in both MTM and BTP reaction with H_2O_2. The effect of calcination temperature on the catalytic performance has been studied in detail. Relatively high temperature calcination in the first step to remove OSDA was beneficial to produce more isolated and oligomeric Fe species on the extra framework for Fe-MWW, thus activate the catalytic performance. But the presence of aluminum in Fe,Al-MWW dispersed iron and high temperature calcination produced the FeAlOx species, which may be not beneficial to the catalytic performance. In addition, increasing the second step calcination temperature to prepare H-type zeolite from NH_4^+-type made more seriously Fe aggregation and reduce the terminal hydroxyl (Fe-OH and/or Al-OH on the extra framework) for both Fe-MWW and Fe,Al-MWW, thus decrease the catalytic performance. The best results were achieved by FW-1023-823, phenol yield of 8.3% with selectivity of 93% in BTP reaction and 855.8 μmol methanol yield with 70% selectivity in MTM reaction with

H_2O_2. Both Fe-MWW and Fe,Al-MWW realized considerable and better catalytic performance comparison with Fe-MFI zeolite in BTP and MTM reactions.

Chapter 7 included Fe and/ or Cu exchanged Beta catalysts with varied metal content for hydroxylation of benzene to phenol with H_2O_2. The states of Fe and Cu species were characterized by UV-vis and NO adsorbed FT-IR. The influence of the reaction conditions in BTP reaction on the catalytic performance of Fe and/or Cu-containing Beta zeolite catalysts were studied in details. The stability of the Fe and/or Cu-containing Beta zeolite catalysts in the BTP reaction were investigated. The synergetic effect was influenced by the states of the metals instead of the content. Fe-Cu/Beta catalysts showed dramatically high catalytic activity due to the synergetic effect. 6Fe-6Cu/Beta achieved the highest phenol yield of 10.5 % in BTP reaction and MeOH yield of 720 μmol in MTM reaction, which was related to the highest isolated Fe species influenced by the introduction of Cu.

List of publications

Journal articles

1. Peipei Xiao, Yong Wang, Junko N. Kondo, Toshiyuki Yokoi, Iron- and Copper-exchanged Beta Zeolite Catalysts for Hydroxylation of Benzene to Phenol with H_2O_2, Chemistry Letters, 2018, 47(9). (Chapter 7)
2. Peipei Xiao, Yong Wang, Junko N. Kondo, Toshiyuki Yokoi, Direct synthesis of phenol by hydroxylation of benzene with hydrogen peroxide over Fe-containing MFI zeolite catalysts, Catalysis Science & Technology, submission preparation. (Chapter 2)
3. Peipei Xiao, Yong Wang, Toshiki Nishitoba, Junko N. Kondo, Toshiyuki Yokoi, Dramatic impacts of the location of Fe species in Fe-silicalite-1 zeolites and solvent on liquid-phase methane conversion to methanol with H_2O_2, in preparation. (Chapter 3)
4. Peipei Xiao, Yong Wang, Junko N. Kondo, Toshiyuki Yokoi, Direct synthesis of Fe-containing MWW zeolite for direct hydroxylation of benzene to phenol with H_2O_2, in preparation. (Chapter 6)

Presentations

1. Peipei Xiao, Yong Wang, Masato Yoshioka, Ryoichi Otomo, Junko N. Kondo, Toshiyuki Yokoi, Direct conversion of Methane to Methanol over Fe-containing zeolites/H_2O_2 system, the 21 st JPIJS, May 25-26, 2016, Funabori, Tokyo. *Poster presentation.*
2. Peipei Xiao, Yoshihiko Kimura, Yong Wang, Junko N. Kondo, Toshiyuki Yokoi, Direct conversion Methane to Methanol over Fe-containing zeolites/H_2O_2 system, the 16th international congress on catalyst (ICC16), July 3-8, 2016, Beijing, China. *Poster presentation.*
3. Peipei Xiao, Junko N. Kondo, Toshiyuki Yokoi, Direct conversion of methane to methanol in solvent/H_2O_2 system using Fe-containing MFI catalyst prepared by newly developed direct method, 2016 Zeolite Joint Study Group, December 17-18, 2016, Hakone, Tokyo. *Oral presentation.*
4. Peipei Xiao, Yong Wang, Junko N. Kondo, Toshiyuki Yokoi, Direct conversion of Methane to Methanol over Fe-containing zeolites/H_2O_2 system, The 3rd Euro-Asia Zeolite Conference, January 22-25, 2017, Bali, Indonesia. *Poster presentation.*
5. Peipei Xiao, Junko N. Kondo, Toshiyuki Yokoi, Direct hydroxylation of benzene to phenol using H_2O_2 as an oxidant over Fe- or Cu-containing zeolite catalysts, the 16 th Korea-Japan Symposium on Catalysis, May 15-17, 2017, Sapporo, Japan. *Poster presentation.*
6. Peipei Xiao, Toshiki Nishitoba, Junko N. Kondo, Toshiyuki Yokoi, Direct conversion of Methane to Methanol over Fe-containing zeolites/H_2O_2 system, the 22 nd JPIJS, May 23-24, 2017, Funabori, Japan, *Poster presentation.*
7. Peipei Xiao, Ryota Osuga, Yoshihiko Kimura, Junko N. Kondo, Toshiyuki Yokoi, Effect of Al distribution in the MFI framework on the catalytic performance in the CH_4 conversion, the 25th North American Meeting of the Catalysis Society, June 4-9, 2017, Colorado, American. *Poster presentation.*
8. Peipei Xiao, Junko N. Kondo, Toshiyuki Yokoi, Fe or/ and Cu- Beta catalysts: preparation, characterization and catalytic performance in oxidation of benzene to phenol, 2017 International Conference on Nanospace Materials, August 24-28, 2017, Shanghai, China. *Poster presentation.*

9. Peipei Xiao, Junko N. Kondo, Toshiyuki Yokoi, One-pot synthesized Fe-containing MWW zeolite for hydroxylation of methane to methanol with H_2O_2, the International CLS Forum on Photo and Catalytic Science for Sustainable Society, March 3-4, 2018, Tokyo, Japan. *Poster presentation.*
10. Peipei Xiao, Junko N. Kondo, Toshiyuki Yokoi, The effect of Fe site location in Fe-MFI zeolite catalysts on the performance of hydroxylation of benzene to phenol with H_2O_2, 255th ACS National Meeting, March 18-22, 2018, New Orleans, LA, America. *Poster presentation.*

Acknowledgement

The doctoral thesis was conducted at Nomura & Yokoi group, Laboratory for Chemistry and Life Science & Nanospace Catalysis Unit, Institute of Innovative Research, Tokyo Institute of Technology during 2015.10-2018.8. I sincerely appreciate all the members in our laboratory, my friends and family.

I am grateful to Assoc. Prof. Junko N. Kondo, Assoc. Prof. Keigo Kamata, Assoc. Prof. Ken Motokura, Assoc. Prof. Yoshiaki Shoji, and Assoc. Prof. Toshiyuki Yokoi for taking time to review my thesis.

Firstly, I would like to express my deepest gratitude to Assoc. Prof. Junko N. Kondo and Assoc. Prof. Toshiyuki Yokoi for providing me such an excellent opportunity to carry out my Ph.D. research in the laboratory.

Nomura-sensei, you always gave me sincere help when I need. I am grateful for your guidance, constructive suggestion, and encouragement throughout my studies. Thank you very much.

Yokoi-sensei, your tolerance, generosity and humor have always affected me. You supported me with so many opportunities to attend the international and domestic academic conferences. You helped me to modify the manuscripts over and over again. Thank you very much.

The financial support from Japan Student Services Organization (JASSO) and the Asahi Glass Scholarship are highly appreciated.

Wang-san, you have put forward a lot of good suggestions for my research. You taught me to use the NH_3-TPD, FT-IR, TG, N_2 adsorption and desorption about zeolite measurements. You helped me to modify each chapter of the doctoral thesis, each academic manuscript and conference paper. Every seminar you know my progress and point out my shortcomings. You and your wife have given me a lot of help and encouragement, invited me in the reunion days, who was far from home. Thank you very much.

Yunan-san, you carefully taught me to synthesize mesoporous silicon materials and mesoporous carbon materials in the days when I first came to the lab. You taught me to use the FE-SEM (SU9000), XRD, UV-vis, N_2 adsorption and desorption about mesoporous materials measurements. You provided me a lot of help in the daily life, I still use the rice cooker that you gave me three years ago. Thank you very much.

Kunitake-san and Osuga-san, when I met trouble in the experiments and instruments, you guys can always help me to solve the problems quickly and effectively. Thank you very much. Kunitake-kun, the AEI zeolite you provided me, has applied in the BTP and MTM reactions with H_2O_2, which proved that the small pore zeolite was not suitable for these two reactions. Osuga-san, the NO and CH_4 adsorbed FT-IR on Cu/MFI(TPA) and Cu/MFI(PET+Na) zeolite catalysts that you helped me to measure, they were the start that I researched on the influence of aluminum distribution on the states of the transition metals. Although, the two parts of work were not written in the doctoral thesis, I believe that they can be published in the future. Thank you very much.

I am also appreciate Otomo-san, Bili-san, Kimura-kun and Fuji-kun who have already graduated from our laboratory. In the old days, you offered me tremendous help and joy. Thank you very much.

Nakamura-sensei, I always admire your colorful life. You are so harmony, optimism and easy-going that make you just a senior friend in our lab.

Nishitoba-san, you are the very hard working person in our lab. Every time I did the experiments late, only you were still in the lab. Congratulations on your PhD graduate. In the aspect of solid ^{29}Si MAS NMR and ^{27}Al MAS NMR, and liquid H-NMR, incredible support have been provided by

Nakamura-sensei and Nishitoba-san. Thank you very much.

Raquel-san, thank you very much to give me a worthy suggestion in terms of testing the type of leaching Fe species, and it has been reported in Chapter 2. You have also set an example for me in the aspect of publishing paper. It is a kind of driving force for me to make progress. Thank you very much.

Park-san, you have made great efforts to maintain the normal operation of the laboratory. Thank you very much.

Thanks to all the young members in Nomura &Yokoi laboratory and the secretaries, Hirose-san and Furuzono-san, thank you very much for maintaining such a harmonious laboratory.

I would like to express heartfelt thanks to my former supervisors, Dr. Chuyi Zeng and Assoc. Prof. Hong Zhao. You are my advisors and friends. You always encouraged me to pursue my dreams bravely and you also help me greatly. There is no doubt that I can not be here today without your encouragement and help. Thank you very much.

My dear friends, who climbed the Mount Fuji together, we have experienced the hardest climb, as well as enjoyed the most beautiful meteor shower, sunrise and sea of clouds.

I greatly appreciate my boyfriend, Dai Xin. Thank you for making delicious food for me in every weekend, which can be proved by my double chin. Thank you for walking outside with me in weekend, for example taste pickled vegetables in Kamakura, I think Yokoi-sensei can be the witness. You always tell me to relax and then inviting me to watch variety show, anime, World Cup and play Nintendo games, even at the last day of the deadline. Thank you for taking me so many photos, then I have a stack of goofy photos. All of these makes every routine day colorful.

Thanks uncle Dai Fuming and aunt Zhu Aimei. Thank you for sending me new clothes, comfortable shoes, and a variety of homemade food. You are so attentive about our healthy and daily life that makes us feel to be concerned about all the time. Thank you very much.

Special thanks to my family, Papa, Mama, Dabo, Xiaobo, Jingge and Ma Diandian, thank you for your understanding, support and encouragement. On my way of studying these years, my family is always the warmest haven, let me fill with the anticipation to the future. It is my greatest wish that my family will always be healthy and happy!

Aug 21, 2018
Xiao Peipei